JAERI-M
90-083

ANALYSIS OF SCTF/CCTF COUNTERPART TEST RESULTS

June 1990

Tsutomu OKUBO, Makoto SOBAJIMA, Takamichi IWAMURA
Akira OHNUKI, Yutaka ABE, Hiromichi ADACHI
and Yoshio MURAO

日本原子力研究所
Japan Atomic Energy Research Institute

JAERI-Mレポートは，日本原子力研究所が不定期に公刊している研究報告書です。
入手の問合わせは，日本原子力研究所技術情報部情報資料課（〒319－11茨城県那珂郡東海村）あて，お申しこしください。なお，このほかに財団法人原子力弘済会資料センター（〒319-11茨城県那珂郡東海村日本原子力研究所内）で複写による実費頒布をおこなっております。

JAERI-M reports are issued irregularly.
Inquiries about availability of the reports should be addressed to Information Division, Department of Technical Information, Japan Atomic Energy Research Institute, Tokai-mura, Naka-gun, Ibaraki-ken 319-11, Japan.

編集兼発行　日本原子力研究所
印　　刷　日立高速印刷株式会社

JAERI-M 90-083

Analysis of SCTF/CCTF Counterpart Test Results

Tsutomu OKUBO, Makoto SOBAJIMA+, Takamichi IWAMURA
Akira OHNUKI, Yutaka ABE, Hiromichi ADACHI and Yoshio MURAO

Department of Reactor Engineering
Tokai Research Establishment
Japan Atomic Energy Research Institute
Tokai-mura, Naka-gun, Ibaraki-ken

(Received May 7, 1990)

Slab Core Test Facility (SCTF) and Cylindrical Core Test Facility (CCTF) are large scale experimental facilities of Japan Atomic Energy Research Institute (JAERI) for the investigation of reflooding behavior during a postulated loss-of-coolant accident (LOCA) in PWRs. Although the flow area scaling ratios of both facilities to a 1,000 MWe class PWR are the same and 1/21.4, the SCTF has the same core width as the radius of the reference PWR while the CCTF has a 1/4.5 times shorter core radius. Therefore, a few SCTF/CCTF counterpart tests were conducted in order to investigate the difference in core reflooding behavior between in the SCTF and CCTF tests as well as the effect of core radial length on core two-dimensional thermo-hydrodynamic behavior. This report present the test results and an analysis on them. Major results obtained are:

(1) Taking account of the differences in test conditions and facility design, core reflooding behavior is considered to be similar between the SCTF and the CCTF tests. Main difference of the facility design is in the effective core flow area and this is considered to result in the difference in core water accumulation behavior.

(2) The effect of core radial length on core two-dimensional thermo-hydrodynamic behavior has been observed to be significant and heat transfer enhancement or degradation in radial direction is more significant for the longer radius core.

+ Department of Fuel Safety Research

(3) In addition, where the core power varies significantly in the radial direction, significant heat transfer enhancement has been observed in the higher power bundle during the LPCI period. Also, in the peripheral region, heat transfer degradation has been observed more significantly in the outer bundle even they have the same bundle power.

(4) Magnitude of these heat transfer enhancement or degradation was larger at the higher elevation than the midplane level in the SCTF test, whereas smaller in the CCTF test.

Keywords: Reactor Safety, LOCA, ECCS, PWR, Reflooding, Two-phase Flow, Heat Transfer, SCTF Core-II, Tow-dimensional Core Behavior

ＳＣＴＦ／ＣＣＴＦ対照試験結果の解析

日本原子力研究所東海研究所原子炉工学部
大久保　努・傍島　　真[+]・岩村　公道・大貫　　晃
阿部　　豊・安達　公道・村尾　良夫

（1990年5月7日受理）

平板炉心試験装置（ＳＣＴＦ）および円筒炉心試験装置（ＣＣＴＦ）は，ＰＷＲの仮想的な冷却材喪失事故（ＬＯＣＡ）時の再冠水挙動を検討するための日本原子力研究所の大型実験装置である。1,000MWe級ＰＷＲに対する両装置の流路面積のスケール割合はともに1／21.4であるものの，ＳＣＴＦは参照ＰＷＲの半径と同じ炉心幅を有するのに対し，ＣＣＴＦは1／4.5倍の短い炉心半径を有している。そこで，数回のＳＣＴＦ／ＣＣＴＦ対照試験を実施して，ＳＣＴＦおよびＣＣＴＦ試験の間の炉心再冠水挙動の差および炉心の2次元的な熱水力学的挙動に与える炉心半径長さの効果を検討した。本報告書は，その試験結果とそれに対する解析をまとめたものである。得られた主要な結果は以下の通りである。

(1) ＳＣＴＦ試験とＣＣＴＦ試験の間の試験条件の差と両装置の設計に於ける相違を考慮すれば，両試験に於ける再冠水挙動は類似のものであると考えられる。両装置間に於ける設計上の主要な相違は炉心の実効流路面積の相違で，これにより炉心の蓄水挙動に相違が生じたと考えられる。

(2) 炉心の半径長さがその2次元的な熱水力学的挙動に及ぼす効果は大きいことが見い出され，それが炉心半径の長い程顕著に現れることが分った。

(3) 更に，半径方向に大きな出力の変化がある場合には，その高出力側のバンドルに於いてＬＰＣＩ注水期に著しい熱伝達率の増加が観測された。また，炉心の周辺領域では，同一のバンドル出力であるにも係らず外周側のバンドル程熱伝達率の低減が大きいことが見い出された。

(4) これらの熱伝達の増加および低減は，ＳＣＴＦ試験では中央高さ位置より高い位置でより大きかったが，ＣＣＴＦ試験では逆により小さかった。

東海研究所：〒319－11　茨城県那珂郡東海村白方字白根2－4
+　燃料安全工学部

Contents

目　　次

List of Tables

List of Figures

1. Introduction

Thermo-hydrodynamic behavior during the reflood phase of a loss-of-coolant accident (LOCA) in a pressurized water reactor (PWR) has been investigated at the Japan Atomic Energy Research Institute (JAERI) by using the Slab Core Test Facility (SCTF)[1],[2] as well as the Cylindrical Core test Facility (CCTF)[1]. They are large scale experimental facilities with the flow area scaling ratio of 1/21 to a 1,100 MWe class PWR. The major objective for the SCTF tests is to investigate two-dimensional thermo-hydrodynamic behavior in the core. For this purpose, the SCTF simulates a full-radius slab section of the PWR with eight heater rod bundles arranged in a raw. On the other hand, the CCTF cylindrically simulates the core and simulates the primary loop system as closely as possible, since the major objective for the CCTF tests is to investigate system thermo-hydrodynamic behavior during the reflood phase. The system simulation of the SCTF is not as good as that of the CCTF, whereas the SCTF simulates the actual core radius, which is 4.6 times larger than the CCTF. Therefore, it is important and of interest to perform a SCTF/CCTF counterpart tests and investigate the difference of thermo-hydrodynamic behavior between the facilities, including the effects of core radial length on two-dimensional core thermo-hydrodynamic behavior, which is the major objective of the SCTF as mentioned above. Accordingly, three SCTF/CCTF counterpart tests, *i.e.* Tests S2-07, S2-14[3] and S2-18, have been performed with SCTF Core-II facility simulating as closely as possible the initial and boundary core conditions of corresponding CCTF tests, *i.e.* Tests C2-05[4] and C2-06[5].

This report presents an analysis of those SCTF tests by using the corresponding CCTF test results together. In Appendix A, a brief description of the SCTF Core-II facility is presented. Some selected data of Tests S2-07 and S2-18 are presented in Appendices B and C, respectively, for the better understanding of those test results. Data of S2-14 are already presented in Reference [3] and are not repeated here.

2. Test Description

2.1 Test Facility[2]

A schematic diagram of SCTF is shown in Fig. 2.1. The primary coolant loops consist of a hot leg, which is equivalent to four actual hot legs, a steam/water separator corresponding to four actual steam generators, an intact cold leg, which is equivalent to three intact cold legs, a broken cold leg on the pressure vessel side, and a broken cold leg on the steam/water separator side. These two broken cold legs are individually connected to two containment tanks, which are connected to each other by a pressure equalizing pipe. The flow area scaling ratio of SCTF components is 1/21 to a 1,100 MWe class PWR, whereas height of each component is preserved.

Figure 2.2 shows the vertical cross section of the pressure vessel. The pressure vessel includes the simulated core, the upper plenum with internals, the lower plenum, the core baffle and the downcomer. The SCTF pressure vessel simulates a full radius slab section of a 1,100 MWe class PWR. The core and the upper plenum are enveloped by honeycomb thermal insulators with wall plates to minimize the wall thermal effects.

The simulated core consists of 8 bundles arranged in a row with full radial length. Each bundle consists of 234 heater rods and 22 non-heated rods arranged in 16 x 16 square array. Outer diameter and heated length of the heater rod are 10.7 mm and 3660 mm, respectively. Dimensions and arrangement pitch of the rods are based on those for a 15 x 15 fuel rod bundle of a Westinghouse type PWR.

The emergency core cooling system (ECCS) consists of an accumulator (Acc) system and a low pressure coolant injection (LPCI) system. Injection ports for the Acc and LPCI systems are usually the lower plenum and the intact cold leg, respectively.

More detailed information of the SCTF is available in reference [2] and a brief description is presented in Appendix A.

2.2 Test Conditions

The tests referred to in this report are Test S2-07 (slant radial power profile and cold leg injection), Test S2-14 (flat radial power profile and lower plenum injection) and Test S2-18 (slant radial power profile and lower plenum injection). Major test conditions for these three

tests are listed in Table 2.1. BOCREC (bottom of core recovery) in Table 2.1 represents the time when the ECC water reaches the bottom of heated part of heater rods.

Test S2-07 was performed under the cold leg injection, whereas Tests S2-14 and S2-18 were performed under the forced feed lower plenum injection, i.e. the downcomer was blocked up by inserting a plate at the bottom. Tests S2-07 and S2-18 were intended to simulate the core cooling behavior of CCTF Test C2-5[4], whereas Test S2-14 was intended to simulate Test C2-6[5]. Test S2-18 was performed repeatedly, because the simulation for Test C2-5 achieved by Test S2-07 was judged to be unsatisfactory due to mismatch in core water accumulation rate.

The ECC water injection rates for the SCTF Tests S2-14 and S2-18 were determined to simulate as closely as possible the core water accumulation behavior in the concerned CCTF tests rather than the ECC water injection rate itself, especially during the Acc injection period. This is because the effective core flow area of the SCTF Core-II is 1.24 ~ 1.35 times larger than the real one and this is expected to change the effective core flooding rate, and hence the core water accumulation behavior. As described in reference [2], there is large excess flow area of 0.061 ~ 0.091 m^2 surrounding the real core area of 0.259 m^2, *i.e.* rod assembly area, in the SCTF Core-II. The ECC injection rate for Test S2-18 was set to be the same as for Test S2-14. Water accumulated in the upper plenum was extracted from side nozzles in Test S2-14 in order to avoid the influence of water level distribution on core thermal-hydrodynamic behavior.

2.3 Test Procedure

The test procedure for these three tests was almost the same and is as follows. After establishing the initial pressure and temperature conditions, core heating was initiated. In order to achieve the same initial stored energy, the Acc injection into the lower plenum was initiated, at the time when four cladding temperatures exceeded 1053 K, 910 K and 1053 K for Tests S2-07, S2-14 and S2-18, respectively. The initial level of saturation water in the lower plenum was 0.14 m below the bottom of heated part. After keeping the core power constant during the specified time after Acc injection initiation, core power decay simulation started simulating the reactor transient from 40 s after shutdown. The decay curve

was based on the 1.02 x (ANS standard + Actinides). The injection location was changed from the lower plenum to the intact cold leg at 47 s after the Acc injection initiation in Test S2-07. At this time, Acc injection was terminated and LPCI injection was initiated. At 900 s after the initiation of LPCI injection, the test was terminated. In Tests S2-14 and S2-18, the ECC water was injected only into the lower plenum throughout the transient. The ECC water injection was performed by using the other Acc injection system, *i.e.* UT (UCSP water supply tank)-1 and UT-2, controlling water flow rate and temperature as specified. The injection duration was 500 s for both the tests, and then the tests were terminated.

Chronologies of major events for these three tests are summarized in Table 3.1 of the next chapter.

Table 2.1 Test conditions for Tests S2-07, S2-14 and S2-18

	Test S2-07	Test S2-14	Test S2-18
Initial system pressure (MPa)	0.2	0.2	0.2
Initial total power (MW)	7.12	7.12	7.12
Maximum rod temperature at BOCREC (K)	1073	922	1073
Injection location	Cold leg	Lower plenum (Forced feed)	Lower plenum (Forced feed)
Acc injection conditions			
Flow rate (kg/s)	24.5	26.2 (max.)	26.2 (max.)
Temperature (K)	363	368	368
Duration (s)	40	40	40
LPCI injection conditions			
Flow rate (kg/s)	5.41	8.51 ∿ 4.84	8.51 ∿ 4.84
Temperature (K)	350	368 ∿ 393	368 ∿ 393
Upper plenum water extraction time (s)	None	77 ∿ 377	None
Radial power ratio	Slant profile	Flat profile	Slant profile
Bundle 1	1.360	1.0	1.360
Bundles 2, 3, 4	1.200	1.0	1.200
Bundles 5, 6, 7, 8	0.760	1.0	0.760
Decay curve	1.02 × (ANS + Actinides), 40 s after scram		

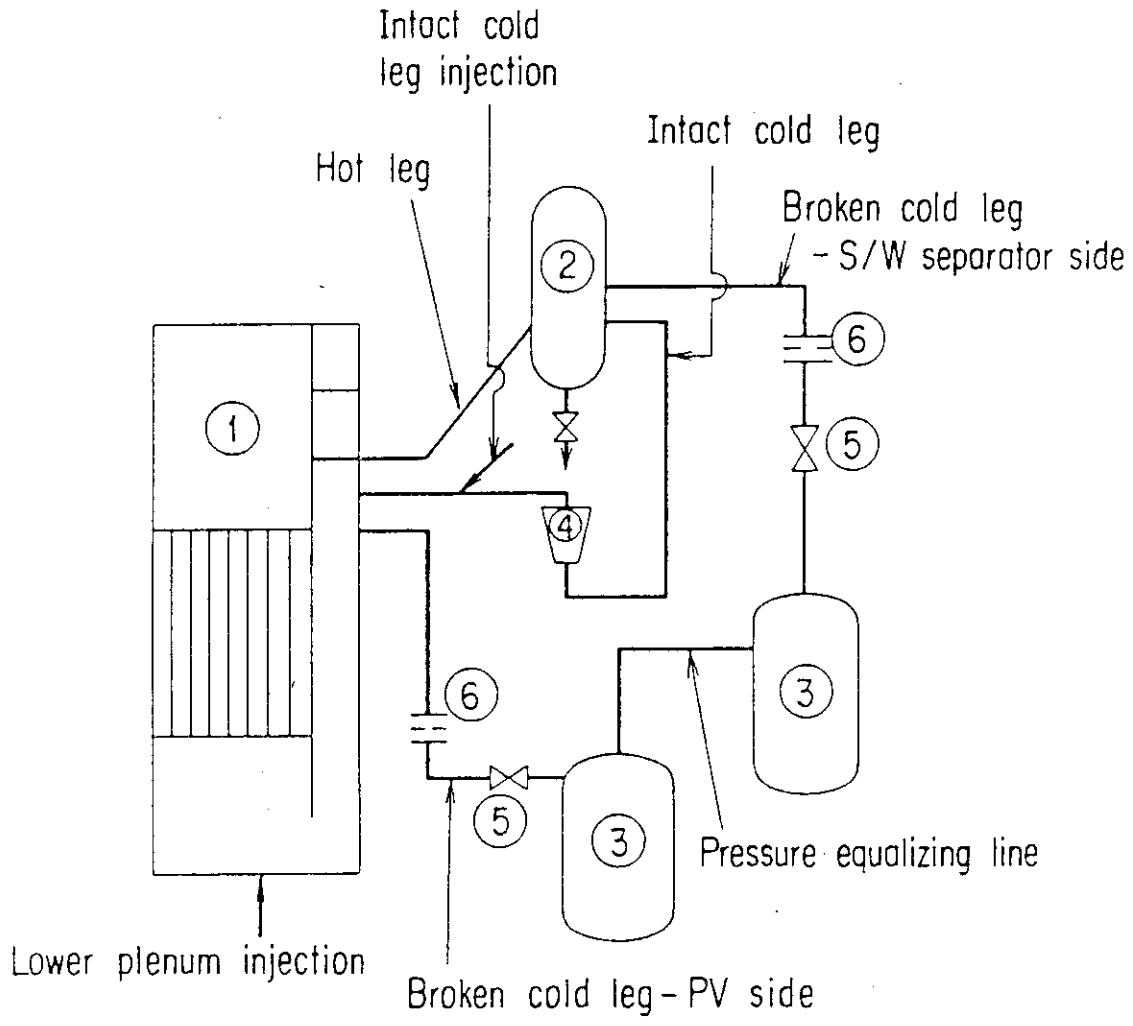

① Pressure vesel
② Steam / water separator
③ Containment tanks
④ Pump simulator
⑤ Break valves
⑥ Flow resistance simulators

Fig. 2.1 Schematic diagram of SCTF

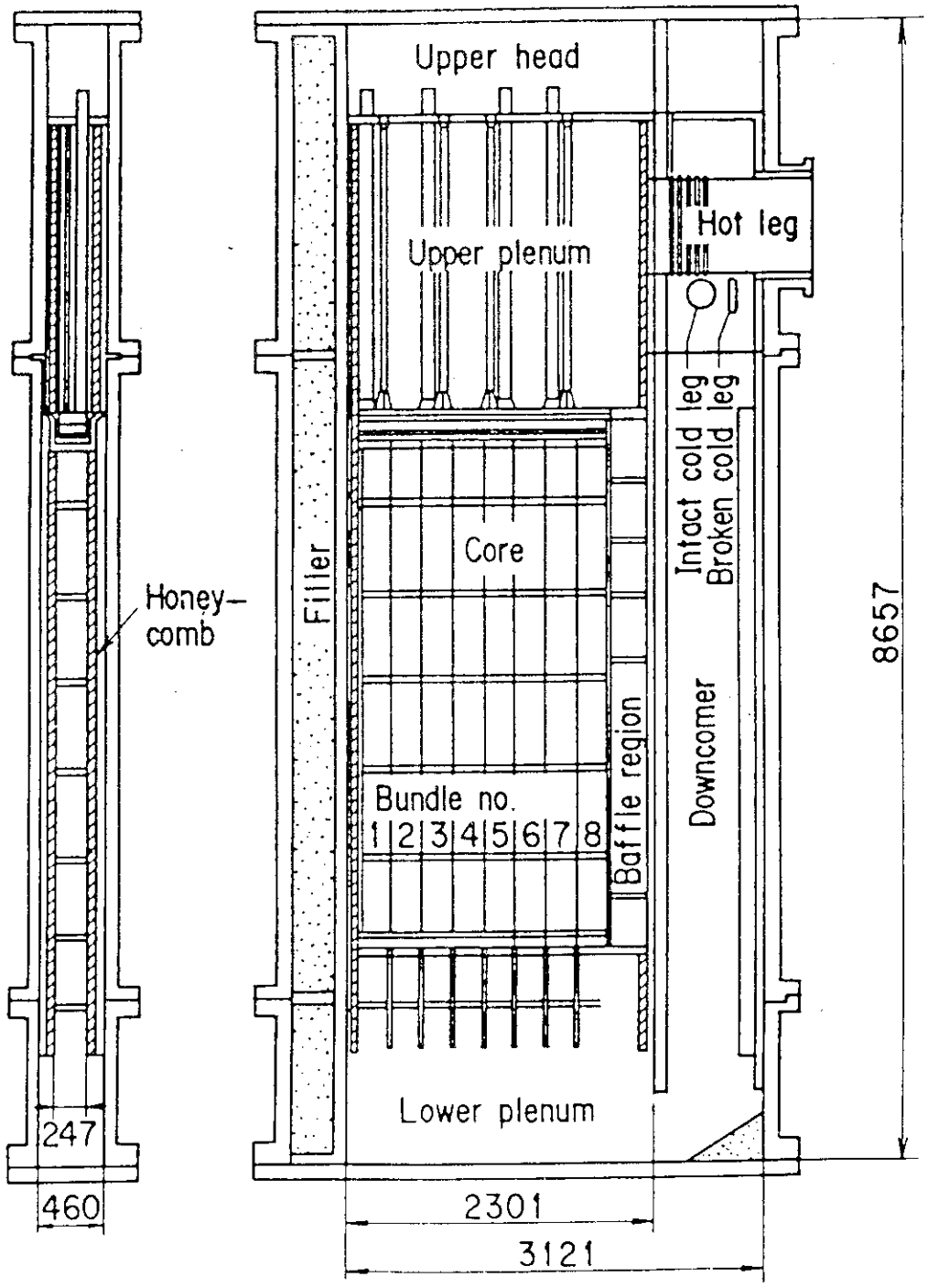

Fig. 2.2 Vertical cross section of pressure vessel

3. Test Results and Discussion

The tests concerned in this report are divided into two groups. That is, Test S2-14 was performed under the flat radial power and initial temperature profile, whereas Tests S2-07 and S2-18 were performed under the slant radial power and initial temperature profile. Therefore, the analysis of Test S2-14 together with Test C2-6[5] is appropriate to investigate the difference of the thermo-hydrodynamic behavior in the pressure vessel between the SCTF and the CCTF, and the analysis of Tests S2-07 and S2-18 together with Test C2-5[4] is appropriate to investigate effects of the core radial length on two-dimensional core thermo-hydrodynamic behavior. In the following, the analysis of Test S2-14 is presented in Sec. 3.1 and the analysis of Tests S2-07 and S2-18 is presented in Sec. 3.2. Chronologies of major events for the three SCTF tests are presented in Table 3.1.

3.1 Results and Discussion for Test S2-14

Test S2-14 was performed under the flat core radial power profile and the forced feed lower plenum injection. The conditions for this test was set as close as possible to those of CCTF Test C2-6[5], except for the upper plenum water level. In Test S2-14, the upper plenum water level was controlled to be flat by using a upper plenum water extraction system, whereas not in Test C2-6.

3.1.1 Achieved Major Test Conditions

Major test conditions achieved in Test S2-14 are presented in this section being compared with those in Test C2-6. They form the basis for the discussion in the following sections.

The core flooding rates are compared in Fig. 3.1. They were evaluated by the mass balance calculation. This figure shows that the core flooding rates are not identical between the two tests and the value for the present test is much larger until about 200 s. This is for compensation of the larger effective core flow area of the SCTF, in order to simulate the same core water accumulation behavior as mentioned in Sec. 2.2. The average core flooding rates are almost the same after about 200 s. The data for the present test experiences an unexpected transient or oscillation around

300 s. This is considered to be caused by the air trapped in the ECC water injection system. However, the average value is almost the same as the specified value as recognized from Fig. 3.1(b), which gives time-integrated values.

The core inlet water temperature and the upper plenum pressure are compared in Figs. 3.2 and 3.3, respectively. The temperature for the present test is higher for 30 through 240 s and lower during the initial 30 s and after 260 s. The difference is 20 K at most. The upper plenum pressure is lower in the present test after 30 s and the maximum difference is 35 kPa. The effect of difference in core inlet subcooling on core water accumulation is investigated in the next section.

3.1.2 Hydrodynamic Behavior in Pressure Vessel

The total core differential pressure is compared in Fig. 3.4. The data are almost the same on the average during the initial 30 s as intended. The data for Test C2-6 shows the large oscillation, which is the U-tube type one between the downcomer and the core. After this period, the value is lower for 30 through 200 s, although the core flooding rate is larger in the present test. However, it becomes larger after 250 s in the present test. It should be noted that the increasing rate of the data is much larger in the present test after 150 s, in spite of the nearly identical core flooding rate mentioned above (Fig. 3.1). This suggests that the core water accumulation characteristic or the core carry-over characteristic is different between these two tests. The core carry-over ratio is defined as

$$\frac{\text{Core outlet fluid mass flow rate}}{\text{Core inlet water mass flow rate}}$$

and is compared in Fig. 3.5. This shows that in Test C2-6 the carry-over ratio is almost unity on the average after 100 s, whereas in Test S2-14 it is smaller and about 0.4 on the average through the whole transient.

Main reason for this is considered to be the larger effective core flow area in the SCTF. As presented in Reference [2], the effective core flow area of the SCTF is 0.32 ~ 0.35 m^2, whereas the real core flow area in the rod assemblies is 0.259 m^2. Iguchi and Murao[6] examined influence of

the effective core flow area on core water accumulation using a reflood analysis code REFLA[7] and showed larger effective core flow area resulted in more core water accumulation under the same core flooding rate. Although they did not explain the reason for this, it is considered to be smaller steam velocity due to larger core flow area. Smaller steam velocity is considered to affect the core water accumulation in the regions above and below the quench front in the opposite way. That is, smaller steam velocity is considered to result in lower void fraction below the quench front, whereas higher void fraction above the quench front due to smaller water entrainment. This explains the smaller carry-over ratio or the larger core water accumulation in the present test.

In order to confirm the discussion above, core water accumulation behavior has been investigated by using the REFLA code. Since the core boundary conditions, such as core flooding rate, system pressure and core inlet fluid temperature were somewhat different between Tests S2-14 and C2-6 as presented in Sec. 3.1.1, the effects of them on the core water accumulation behavior should also be taken into account in addition to the effect of the core effective flow area. Calculations with the REFLA code is useful for this purpose, and hence several REFLA calculations have been performed varying the effective core flow area under the measured core boundary conditions for the concerned experiments. Figure 3.6(a) shows a comparison of core differential pressure for Test C2-6 between the calculation and the experiment. The calculated results give a excellent agreement with the measured except for 20 ~ 50 s. The difference during this period is considered to be caused by the evaluated lower core flooding rate. Anyway, this figure indicates the REFLA code can be used for analyses of the CCTF. Figure 3.6(b) shows a comparison of core differential pressure of two calculations. One is for the CCTF Test C2-6 and the other is for the same core geometry as for Test C2-6 but with the boundary conditions for the SCTF Test S2-14. Agreement between them is excellent except for 20 ~ 60 s. The difference during this period is attributed to the difference in evaluated core flooding rate shown in Fig. 3.1. By Fig. 3.6(b) it is found that the effects of the differences in the core boundary conditions on core water accumulation behavior is very little except for 20 ~ 60 s.

Figure 3.6(c) shows a comparison of core differential pressure among three calculations in order to see the effect of core flow area on core water accumulation. These calculations were performed under the same core

boundary conditions but with different core flow area from each other: Broken line with plus marks gives calculational results with the same core flow area as the CCTF under the same boundary conditions as in Test S2-14. This is called "base case" hereafter. Dotted line with triangle marks gives ones with 1.2 times larger core flow area than in the base case. Solid line with circle marks gives ones with 1.4 times larger core flow area than in the base case. It is clear from this figure that larger core flow area gives larger increasing rate of core water accumulation after 40 s. As previously mentioned, the SCTF has 1.24 ~ 1.35 times lager effective core flow area than the CCTF and the increasing rate of core water accumulation in Test S2-14 is much larger than that in Test C2-6.

In order to examine quantitative agreement of the increasing rate between the experiment and the calculation, one more comparison of core water accumulation is presented in Fig. 3.6(d). The average increasing rate of the experimental data is about 22.6 Pa/s between 100 s and 300 s. The values of calculated results are about 16.7 and 19.6 Pa/s for 1.2 and 1.4 times cases, respectively. This means that the calculated increasing rate corresponds to about 80 % of the observed in the experiment. Therefore, the larger effective core flow area of the SCTF is considered to be the main cause of the larger increasing rate of core water accumulation in Test S2-14.

Figures 3.7(a) through (f) show core sectional void fractions. They are obtained from the differential pressure data neglecting accelerational and frictional pressure losses. Although measured sections are not exactly the same between the SCTF and the CCTF, they are close enough to be compared directly. From these figures it is recognized that void fractions are higher in Test S2-14 before 250 s except for the top section.

Upper plenum differential pressure is compared in Fig. 3.8(a). Data of both tests were obtained by measurement above the baffle region. The value for Test S2-14 is about 0.0010 to 0.0015 MPa until about 400 s due to the control of the water level on the UCSP using the extraction system as mentioned at the beginning of this Section 3.1. The planned value is 10 to 13 cm of water head. The water level control began at 77 s and ended at 377 s as presented in Tables 2.1 and 3.1. On the other hand, the data for Test C2-6, which was conducted without water extraction, increases slowly and gradually through the whole transient.

Figure 3.8(b) shows a comparison of water level on the UCSP above some

bundles and the baffle in Test S2-14. The data above Bundles 1, 2 and 3 are almost identical to those above Bundles 4, 5 and 6. This figure shows that the water levels above Bundles 7 and 8 and the baffle are higher than others by about 80% until about 270 s. It has been already observed[8] that the water levels above the UCSP are higher above Bundles 7 and 8 and the baffle, even when the core power and initial heater rod temperature distributions are radially flat. This is considered to be a geometrical effect. That is, the hot leg is connected on the baffle side.

Figures 3.9(a) and (b) show core horizontal differential pressures at 2.57 and 3.235 m, respectively. Data at 2.57 m (Fig. 3.9(a)) indicate the differential pressure is almost zero on the average until about 400 s, when the upper plenum water levels started to increase rapidly as shown in Fig. 3.8. Data at 1.905 m, which are not presented here, show the same tendency. Therefore, it can be said that the core hydrodynamic behavior is radially flat at least up to about 2.6 m elevation, when core initial and boundary conditions are radially flat, and a little difference in the upper plenum water level does not influence the core horizontal differential pressure. Figure 3.9(b) shows, however, that the horizontal differential pressures at 3.235 m are slightly in the negative value through the most period of the transient. This means that the pressure in the Bundle 8 side is higher and this is attributed to the higher upper plenum water level in Bundle 8 side shown in Fig. 3.8(b). Comparing Figs. 3.9(b) with 3.8(b), it is recognized that there is a clear coincidence in the transient between the horizontal differential pressure and the upper plenum water level. Therefore, in the top region of the core, the core horizontal differential pressure is influenced by the radial distribution of upper plenum water level.

3.1.3 Core Thermal Behavior

Figures 3.10(a) through (c) show temperature histories of the heater rod surface at the axial peak power or midplane section in core central, intermediate and core peripheral regions, respectively. They show the good agreement between the SCTF and the CCTF experiments. A comparison at the higher elevation is given in Fig. 3.10(d). This shows the same tendency as at the midplane level (Fig. 3.10(a)).

Figures 3.11 and 3.12 show comparisons in the radial direction for

temperature and corresponding heat transfer coefficient histories at the peak power section, respectively. As shown in Figs. 3.11(a) and 3.12(a), the core thermal behavior is radially uniform in Test S2-14, whereas there is small difference in Test C2-6 as shown in Figs. 3.11(b) and 3.12(b). In Test C2-6, the heat transfer is slightly worse in the peripheral region. Although the SCTF results show no difference of the heat transfer in the radial direction, the CCTF results show some difference. There are two possible reasons for the difference. One is the geometrical effect. That is, the wall exists only in the peripheral region in the CCTF, whereas in the SCTF every bundle faces the wall at two or three faces out of four. Incidentally, the initial wall temperature is almost the same as the saturation temperature for the initial pressure. The other is the effect of the upper plenum water level distribution. Although it has not been measured in the CCTF tests, it is likely that there exists upper plenum water level distribution judging from the SCTF test results mentioned before.

The heat transfer coefficients of the two tests at the peak power section are compared in Fig. 3.13. Figure 3.13(b) shows plots against the distance from quench front. These figures show the heat transfer coefficient is higher in Test C2-6 except for the period just before the quenching. As presented in previous sections, the core water accumulation and the core pressure are lower, and the core inlet fluid temperature is higher in Test S2-14 during major time period up to 200 s. According to many previous experimental results[9], all these situations tend to result in the worse core cooling in Test S2-14 comparing to Test C2-6. Therefore, the experimental results shown in Fig. 3.13 are qualitatively consistent with the previous results. However, the better core cooling just before quenching and resultant earlier quenching can not be explained based on the previous results. Although the reason for this has not been clarified yet, a possible reason for this is possible better wettability of the SCTF heater rods than of the CCTF. It has been confirmed the heat up transients are almost identical between the heater rods of the two facilities, although the material of the heater rods are not the same between the facilities.

Figures 3.14(a) and (b) show the quench front envelopes of Test S2-14 and C2-6, respectively. In both tests, the quench front envelopes are almost identical in the radial direction up to about 2.5 m elevation from the bottom and above 2.5 m elevation there appear a little difference. Figure

3.15 shows the comparison between the two tests up to 3 m elevation in the last quenched bundle. Test S2-14 shows the faster quench than Test C2-6. This earlier quenching in Test S2-14 has already discussed above. Figure 3.15 also shows the time-scaled CCTF data, which are set to have the same quench time as the SCTF at 3 m elevation. As shown in the Figure, they are in good agreement. This indicates the quench front propagation characteristic, *i.e.* heat release characteristic in axial direction of heater rods, is almost same in both the facilities.

3.1.4 Thermo-hydrodynamic Behavior in Primary Loop

Although the thermo-hydrodynamic behavior comparison in the primary coolant loops between the SCTF and the CCTF tests is not one of the major objectives here, the intact loop differential pressure is compared in Fig. 3.16. This is because the intact loop differential pressure has a strong contribution to the upper plenum pressure and there observed some difference in the upper plenum pressure between the two tests as shown in Fig. 3.3. Figure 3.16 shows the differential pressure is higher in Test C2-6 by the magnitude of 10 to 20 kPa, which is corresponding to the difference in the upper plenum pressure (Fig. 3.3). Figure 3.17 shows a comparison of the core outlet steam mass flow rate evaluated by a core energy balance calculation. From this figure and Fig. 3.16, it is recognized that although the core outlet steam mass flow rates are close to each other during about 100 through 300 s, the intact loop differential pressures are different from each other. This suggests the intact loop flow resistance is different between the SCTF and the CCTF.

3.1.5 Summary

Summarizing the above results and discussion the following conclusions are obtained for the flat radial core power distribution case:

(1) Although there observed some differences between the SCTF and CCTF test results due to the differences in the test conditions and the test facility design, the overall core thermo-hydrodynamic behavior was not significantly different from each other. The differences observed were explainable by the differences in the test conditions and the facility design as in the following.

(2) Although the core heat transfer was radially uniform in Test S2-14,

there observed a little difference in Test C2-6. In Test C2-6, the heat transfer was worse in the periphery. The possible reasons for this are the geometrical effects, *i.e.* the wall effect and the upper plenum water level distribution effect.

(3) The core water accumulation characteristic was found to be different between the SCTF and the CCTF. Major part of this difference is quantitatively explained to be caused by the difference in the effective core flow area.

(4) Core heat transfer was slightly lower in Test S2-14 except for the short period just before quenching. The difference is reasonably explained with the different achieved boundary conditions for the core. Only just before quenching, the heat transfer was better in Test S2-14 resulting in the faster quench front propagation. The reason for this is still under investigation.

3.2 Results and Discussion for Tests S2-18 and S2-07

Tests S2-18 and S2-07 were performed under the slant core radial power profile. As mentioned before, although Test S2-07 was performed under the cold leg injection, achieved simulation for Test C2-5 was judged to be unsatisfactory due to the significant difference in core water accumulation during the Acc period. Therefore, Test S2-18 was performed under the forced feed lower plenum injection based on the information obtained from tests performed after Test S2-07. Accordingly, in the following, the results of Test S2-18 will be mainly presented and discussed.

As mentioned at the beginning of this chapter, the main purpose of this section is to investigate the effects of the core radial length on two-dimensional core thermo-hydrodynamic behavior.

3.2.1 Achieved Major Test Conditions

Figure 3.18 shows a comparison of the core flooding rate. They were evaluated by the mass balance calculation. Figure 3.18(a) shows a comparison between Tests S2-18 and C2-6. Since the core differential pressure for Test C2-5 showed significant zero-shift during about initial 100 s[4], core differential pressure and core flooding rate for Test C2-6 are presented instead of those for Test C2-5 in this section. According to the investigation in Reference [5], the core differential pressures and the

core flooding rate are judged to be nearly identical between those tests. The transient for Test S2-18 is the same as planned but is a little different from that for Test C2-6 up to about 150 s. As previously mentioned (Sec. 2.2), simulation of the core water accumulation transient was intended rather than the core flooding rate itself for better coupling of core thermo-hydrodynamic behavior. Figure 3.18(b) shows a comparison between Tests S2-07 and C2-6. The data for Test S2-07 experiences the significant oscillation during the Acc period. There was a significant difference in the core water accumulation and core cooling behaviors as is shown later. Figure 3.18(c) shows a comparison of the time-integrated core flooding rate, gradient of which gives the average core flooding rate.

Figure 3.19 shows the core inlet fluid temperature. There observed difference up to 15 K between Tests S2-18 and C2-5. The upper plenum pressures are compared in Fig. 3.20. There is a difference up to 35 kPa between Tests S2-18 and C2-5.

3.2.2 Hydrodynamic Behavior in Pressure Vessel

The core differential pressures are compared in Fig. 3.21 among the three tests. Since the core differential pressure measurements were judged[4] to be unreliable for Test C2-5 during the initial 100 s, the data for Test C2-6 are presented here instead of those for Test C2-5 as mentioned above. After 100 s, however, The data were in good agreement[5] between Tests C2-5 and C2-6 in spite of the difference in the core radial power profile. The core water accumulation behavior is significantly different between Tests S2-07 and C2-6 during about initial 150 s, whereas the agreement between Tests S2-18 and C2-6 is satisfactory until about 250 s which covers the crucial time period for reflooding.

The core carry-over ratio is compared in Fig. 3.22. Although the value for Test C2-6 is almost unity on the average after 100 s, the average value for Test S2-18 is about 0.6. This difference between the two facilities is also observed in the flat core radial power distribution case (Fig. 3.5).

Figures 3.23(a) through (f) show the sectional core void fraction comparison between Tests S2-18 and C2-6. The same water accumulation characteristics as described in Sec. 3.1.2 is observed.

Figure 3.24 shows a comparison of the upper plenum differential pressure above the core baffle region between Tests S2-18 and C2-5. The value

for Test S2-18 is larger after 20 s, especially after 300 s. The rapid increase after 300 s is judged to be caused by the water flow reversal to the upper plenum at the hot leg bottom part. This is confirmed by the negative drag force value in the hot leg bottom region shown in Fig. 3.25. The higher differential pressure in Test S2-18 during 20 through 300 s shown in Fig. 3.24 is considered to be caused mainly by the effect of upper plenum structures on the water accumulation. Iguchi *et al.*[10] showed the upper plenum structure has a significant effect on upper plenum water carry-over and the existence of the structure such as the control rod guide tube reduces the carry-over water mass due to its de-entrainment effect. Since the radial dimensions are different between SCTF and CCTF, there is a possibility of larger de-entrainment in SCTF upper plenum. Horizontal distribution of water level is presented in Fig. 3.26. Water levels above Bundles 4, 5 and 6 are almost the same. The data above Bundles 1, 2 and 3 are almost the same as those above Bundles 4, 5 and 6. However, the water levels above Bundles 7 and 8 and the core baffle are higher than the others by about 40 to 60 percent. It should be noted that although the power and initial rod temperature distributions are the same in Bundles 5 through 8, the water level on the UCSP is higher only above Bundles 7 and 8, suggesting the geometrical effect.

Figure 3.27 shows the horizontal differential pressures in Test S2-18 at 1.905 m elevation between Bundles 1 and 4 and between Bundles 4 and 8. The quenching of heater rods at this elevation varies from 170 through 240 s as shown in Fig. 3.35(a) later. This time period is corresponding to the timing when the horizontal differential pressure decreases and then changes from the positive value to the negative. Before quenching the differential pressures are in the positive value, *i.e.* the flow direction is from Bundle 1 side to Bundle 8 side. After quenching, however, the flow direction becomes opposite. That is, the water flows from the lower power side to the higher power side below the quench front. The value between Bundles 4 and 8 is 1.5 through 2.0 times larger than that between Bundles 1 and 4. This suggests the cross flow is larger in the low power peripheral region.

3.2.3 Core Thermal Behavior

Figure 3.28(a) shows a temperature history comparison at the maximum power location. The data for Test S2-18 are close to those for Test C2-5,

whereas Test S2-07 shows significantly worse core cooling than the others. These are corresponding to the fact that the core water accumulation up to about 250 s is in good agreement between Tests S2-18 and C2-5 but not between Tests S2-07 and C2-5 as shown in Fig. 3.21. Comparisons in the medium and lowest power bundles at their highest power locations are shown in Figs. 3.28(b) and (c), respectively. Heat transfer coefficients corresponding to the temperatures shown in Figs. 3.28(a) through (c) are presented in Figs. 3.29(a) through (c), respectively. Except for the times around 25 s and just before quenching, heat transfer coefficients are larger in Test C2-5 than in Test S2-18. This is consistent with the differences in core inlet water temperature, core pressure and core water accumulation shown in Figs. 3.19 through 3.21. The better core cooling in Test S2-18 around 25 s is corresponding to its larger core water accumulation (Fig. 3.21). A possible reason for the better core cooling in the SCTF test just before quenching is the same as presented in Sec. 3.1.3.

Comparisons in the radial direction for Tests S2-18 and C2-5 are shown in Figs. 3.30(a) and (b), respectively. Comparisons of heat transfer coefficient in the radial direction are shown in Figs. 3.31(a) and (b), corresponding to Figs. 3.30(a) and (b), respectively. In both tests the higher power region shows higher heat transfer coefficient. This tendency is consistent with the other SCTF tests results[8].

Figures 3.32(a) and (b) show the heat transfer coefficients plotted against the distance from quench front for Tests S2-18 and C2-5, respectively. Figure 3.32(a) shows the heat transfer coefficient is higher in the higher power bundle during the Acc period. The CCTF results shown in Fig. 3.32(b) shows the same tendency as this through the whole transient. However, during the LPCI period, the value for Bundle 4 becomes the highest in Test S2-18. The characteristic like this has not been observed previously even in the SCTF tests. The reason for this is a large step in the bundle power between Bundles 4 and 5, and will be investigated later. Another point, which is recognized from Fig. 3.32(a), is although each bundle power is the same in the low power bundles (Bundles 5 through 8), the heat transfer coefficient is lower in the outer bundle (Bundle 8 side). In order to know the degree of enhancement or degradation, the heat transfer coefficients for Tests S2-14 and S2-18 are plotted together in Fig. 3.32(c). The bundle power for Test S2-14 is corresponding to the average bundle power for Test S2-18. The bundle power ratios in Test S2-18 to the

average are 1.357 : 1.203 : 0.759 for the high (Bundle 1), medium (Bundles 2, 3, 4) and low (Bundles 5, 6, 7, 8) power bundles, respectively. The data for Test S2-14 are almost in between the data for the medium power bundles and the low power bundles where the average bundle power for Test S2-18 exists. Therefore, this result suggests the heat transfer coefficient is higher or lower than the average power bundle value, corresponding to its higher or lower bundle power than the average, respectively.

As recognized in Fig. 3.32(a), the heat transfer enhancement in Bundle 4 is observed after the distance from the quench front becomes less than about 1.1 m, *i.e.* after about 60 s (Fig. 3.35). Since the maximum clad temperature is observed by 20 s as shown in Fig. 3.29(a), this heat transfer enhancement dose not reduce the maximum clad temperature but it is interesting to investigate this special behavior. Until 20 s, when the maximum clad temperature is observed, the heat transfer coefficient is higher in the higher power bundle as shown in Fig. 3.32(a). The ratio of the heat transfer coefficient for each bundle to that for the highest power bundle is tabulated at two different distances from the quench front in Table 3.2. In Test C2-5 and in the early period (*i.e.* at 1.6 m) of Test S2-18, the ratios of the heat transfer coefficient are roughly in good agreement with the power ratios. However, in the LPCI period (*i.e.* at 0.7 m) of Test S2-18, these ratios are not in good agreement. Bundle 4 gives a significantly high ratio and the outer bundle gives the lower ratio even in the same low power bundles (Bundles 5 through 8).

In order to investigate the reason for the highest heat transfer coefficient in Bundle 4 mentioned above, the horizontal differential pressures at 1.905 m elevation are compared in Fig. 3.33. Figure 3.33(a) shows the original differential pressures and Fig. 3.33(b) shows the differential pressure per one bundle length since the measurement distances are different among them. As recognized from Fig. 3.33(b), the differential pressure between Bundles 4 and 6 is the largest. The reason is considered to be as follows : There is a large step in the power between Bundles 4 and 5. Accordingly, there also exists a large difference in quench front elevation between them. Under this situation, accumulated water below the higher quench front in Bundle 5 is considered to fall on the lower quench front in Bundle 4. This suggests the horizontal flow is most significant in this area resulting in the highest heat transfer coefficient in Bundle 4.

Figures 3.34(a) and (b) show comparisons of the heat transfer coeffi-

cient in the radial direction at higher elevation than the midplane level (Fig. 3.32). The heat transfer ratios are given in Fig. 3.34(c) at both the midplane and higher elevations. These are the ratios of the heat transfer coefficients for the slant radial core power profile tests (Test S2-18 and C2-5) to those for the flat radial core power profile tests (Tests S2-14 and C2-6). From Fig. 3.34(c) or comparing Figs. 3.34(a) and (b) with Figs. 3.32(c) and (b), it is recognized the degree of the heat transfer enhancement and degradation is larger at the higher elevation in Test S2-18, whereas smaller at the higher elevation in Test C2-5. Therefore, the core two dimensional effect has a different tendency against the elevation between the SCTF and CCTF tests. One possible reason for this is as follows : In the SCTF tests, the heat transfer difference along the radial direction is mainly produced by the effect of the upper plenum water level difference during the LPCI period[8], and hence, the effect is expected more significant at higher elevation, which is closer to the upper plenum. On the other hand, since the radius of the CCTF core is much less than in the SCTF and the geometry of the CCTF pressure vessel is symmetrical, the upper plenum water level in the CCTF is expected to be rather uniform along the radius. Therefore, the upper plenum water level effect is expected to be much smaller, and hence, degree of difference in heat transfer coefficient is inferred to be less at higher elevation in the CCTF tests due to the cosine-shape axial power distribution. A comparison of the clad surface temperature at the higher elevation is shown in Fig. 3.34(d) for the highest power bundle. This shows core cooling in Test S2-18 is better and is a different tendency from that at midplane level (Fig. 3.28(a)).

Figures 3.35(a) and (b) show the quench front envelopes of Tests S2-18 and C2-5, respectively. In the low power bundles of Test S2-18, the difference is only a little. In the medium power bundles, Bundle 4 gives the shortest quench time as shown in Fig. 3.35(a). Figure 3.35(c) shows the comparison between Tests S2-18 and C2-5. The quench time is shorter in Test S2-18 everywhere. As shown in Fig. 3.29(a) through (c), the heat transfer is better in Test S2-18 just before quenching, although until then the heat transfer is better in Test C2-5. This is the same tendency as observed in the flat radial power profile case presented in Sec. 3.1.3.

3.2.4 Summary

Summarizing the above results and discussion, the following conclusions are obtained for the slant radial core power and initial clad temperature distribution case:

(1) The core water accumulation characteristics were different between the SCTF and the CCTF, but showed the same tendency as found in the flat core radial power distribution case.

(2) Upper plenum water accumulation was found to be larger in the SCTF test. There also observed significant radial directional differences in the upper plenum water accumulation in Test S2-18.

(3) In Test C2-5 the heat transfer coefficient was higher in higher power region. In test S2-18, although the heat transfer coefficient was also higher in higher power region during the Acc period, it became the highest in Bundle 4, where there is significant difference in bundle power from neighboring Bundle 5, during the LPCI period. Furthermore, even in the low power bundles with the same power, the heat transfer coefficient was lower in the periphery side.

(4) The heat transfer enhancement or degradation was more significant in the SCTF test than in the CCTF test. This is considered to be caused by the difference in the core radial length.

(5) The degree of the heat transfer enhancement or degradation was larger at the higher elevation than the midplane level in the SCTF test, whereas smaller in the CCTF test. This is also considered to be caused by the large difference in the upper plenum water accumulation distribution.

Table 3.1 Chronologies of major events for Tests S2-07, S2-14 and S2-18

(1) Test S2-07

	Time after BOCREC(s)
Core power "ON"	- 119
Acc injection initiation	- 3
BOCREC	0
Maximum containment tank-II pressure (0.226 MPa)	14
Maximum core temperature (1140 K)	21
Core power decay initiation	35
Switching of injection location from lower plenum to cold leg and from Acc to LPCI	44
Maximum core pressure (0.273 MPa)	44
Whole core quench	435

(2) Test S2-14

	Time after BOCREC(s)
Core power "ON"	- 114
Acc injection initiation	- 3
Core power decay initiation	- 3
BOCREC	0
Maximum core temperature (965 K)	10
Maximum containment tank-II pressure (0.22 MPa)	23
Maximum core pressure (0.266 MPa)	28
Initiation of liquid level control on UCSP	77
Whole core quench	368
Termination of liquid level control on UCSP	377

(3) Test S2-18

	Time after BOCREC(s)
Core power "ON"	- 115.5
Acc injection initiation	- 2.0
Core power decay initiation	0
BOCREC	0
Maximum core temperature (1116 K)	9.5
Maximum containment tank-II pressure (0.224 MPa)	23.5
Maximum core pressure (0.277 MPa)	31
Whole core quench	384.5

Table 3.2 Ratio of heat transfer coefficient for each bundle to that for highest power bundle at midplane level

(a) Test S2-18

Bundle	Power ratio	Heat transter coefficient ratio	
		At 1.6 m*	At 0.7 m**
1	1	1	1
2	0.883	0.797	0.921
3	0.883	0.891	0.944
4	0.883	0.875	1.18
5	0.559	0.437	0.775
6	0.559	0.437	0.719
7	0.559	0.437	0.517
8	0.559	0.375	0.483

(b) Test C2-5

Power region	Power ratio	Heat transfer coefficient ratio	
		At 1.6 m*	At 0.7 m**
High	1	1	1
Medium	0.883	0.914	0.903
Low	0.559	0.571	0.532

* The distance from the quench front corresponding to the time when the maximum clad temperature is observed

** The distance from the quench front corresponding to the typical time in the LPCI period

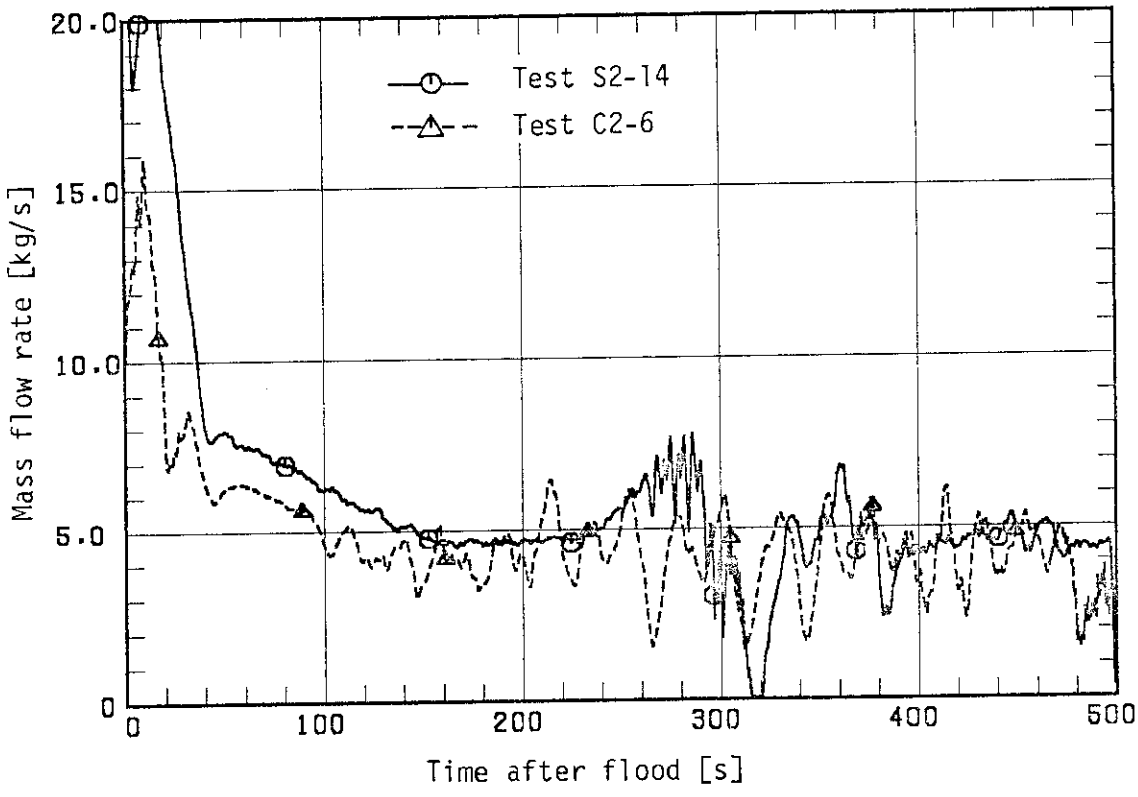

Fig. 3.1(a) Core flooding rate (evaluated value)

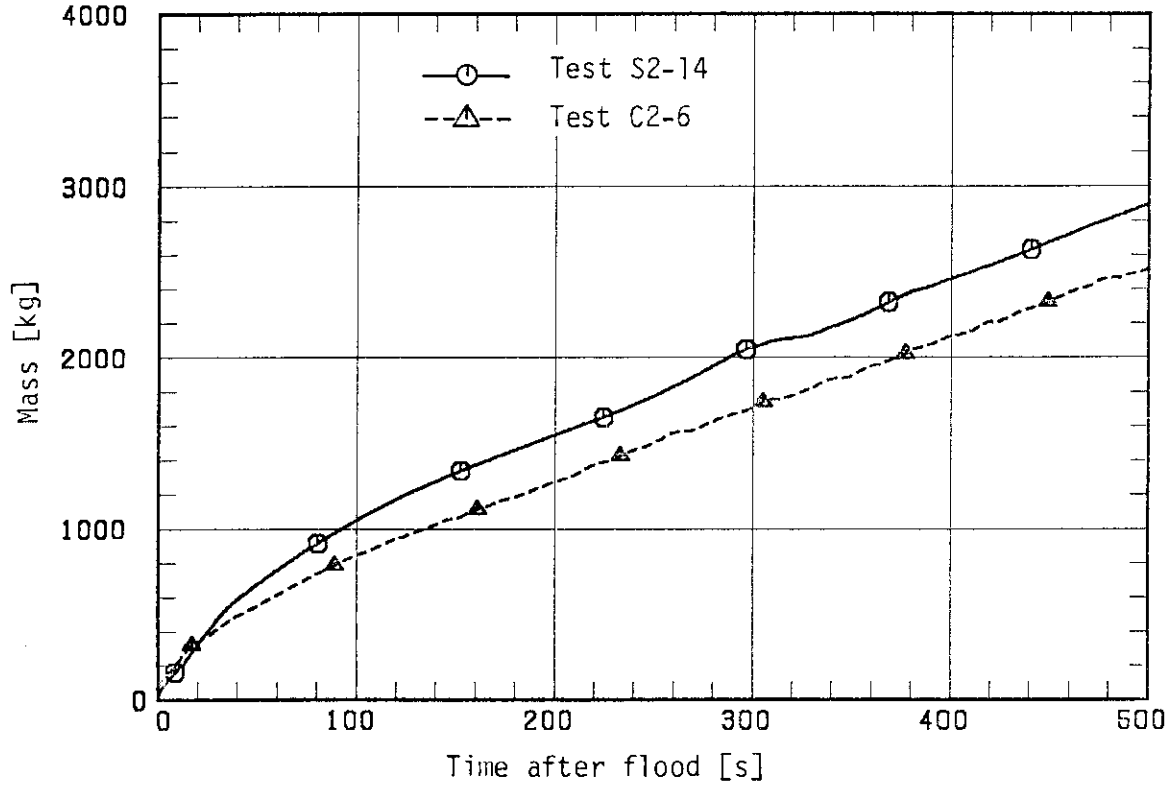

Fig. 3.1(b) Time-integration of core flooding rate

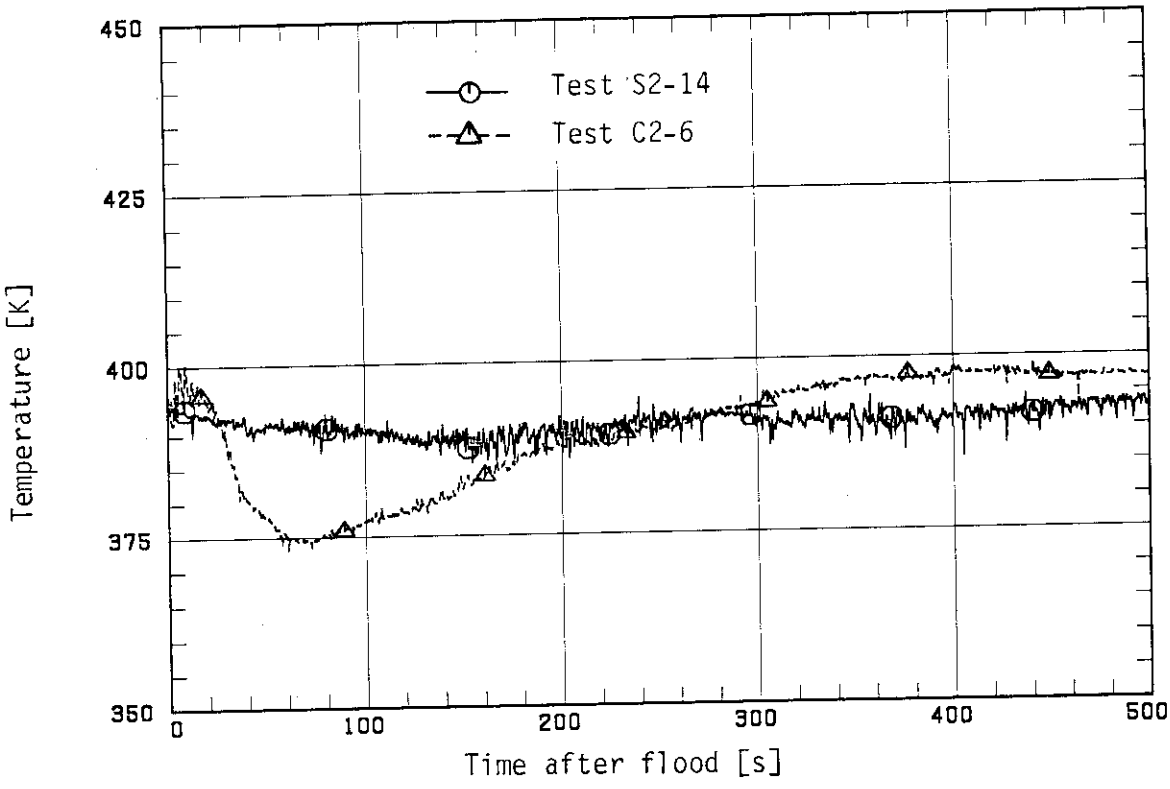

Fig. 3.2 Core inlet fluid temperature

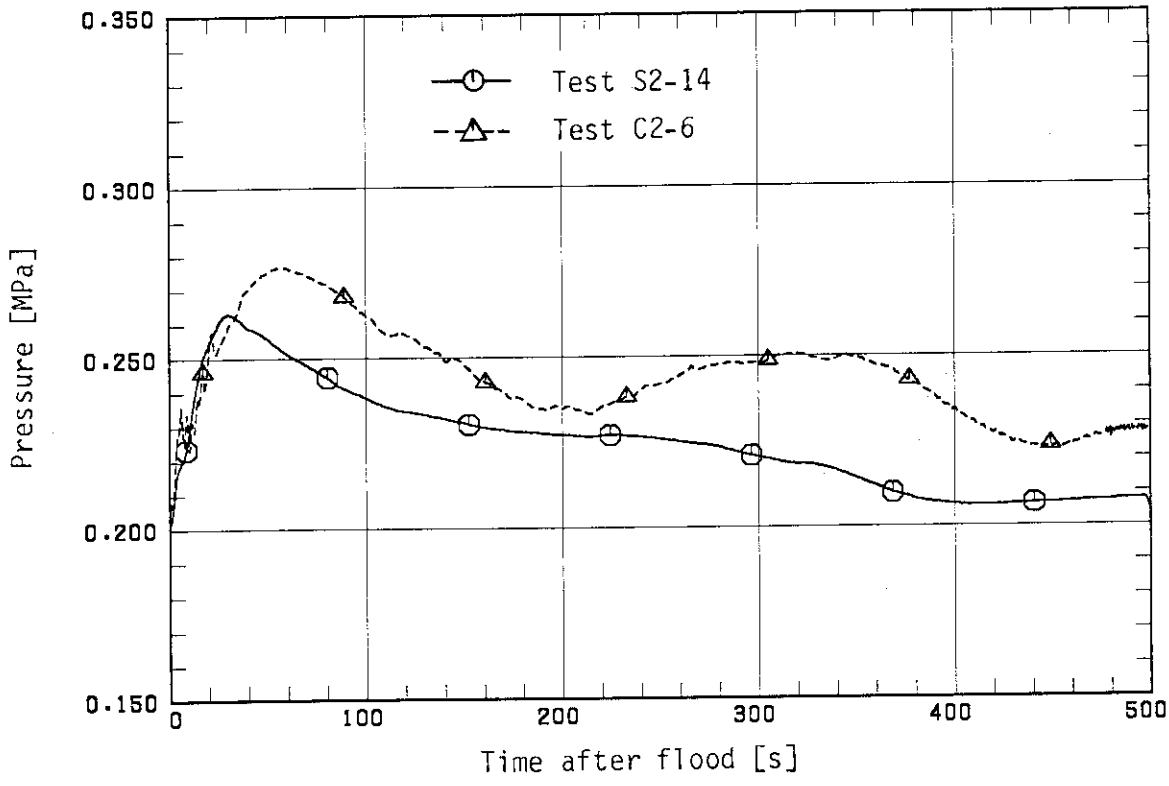

Fig. 3.3 Upper plenum pressure

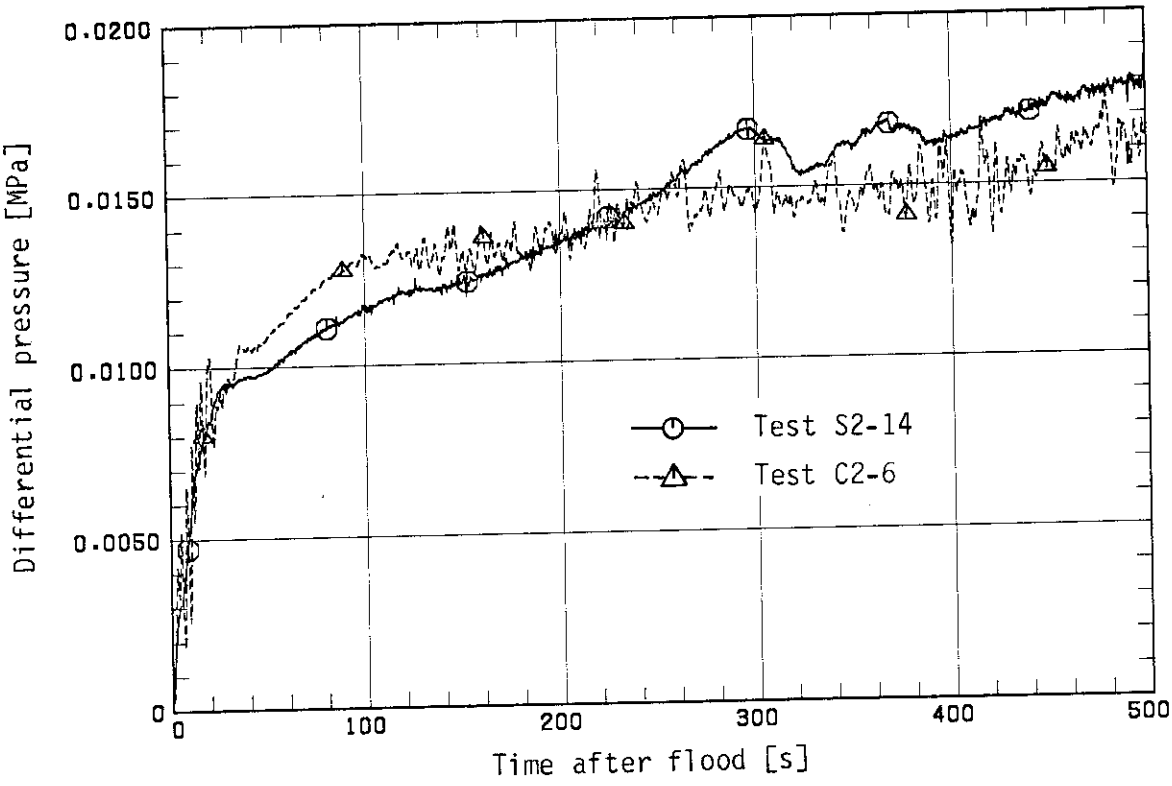

Fig. 3.4 Core differential pressure

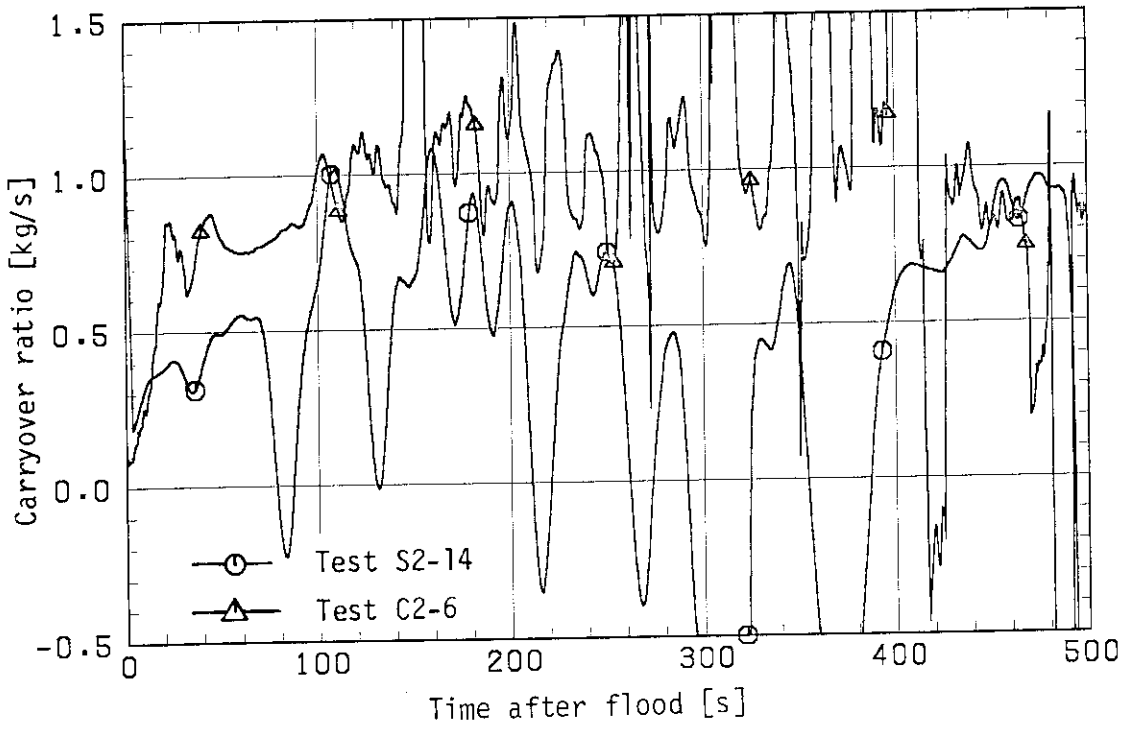

Fig. 3.5 Core carry over ratio

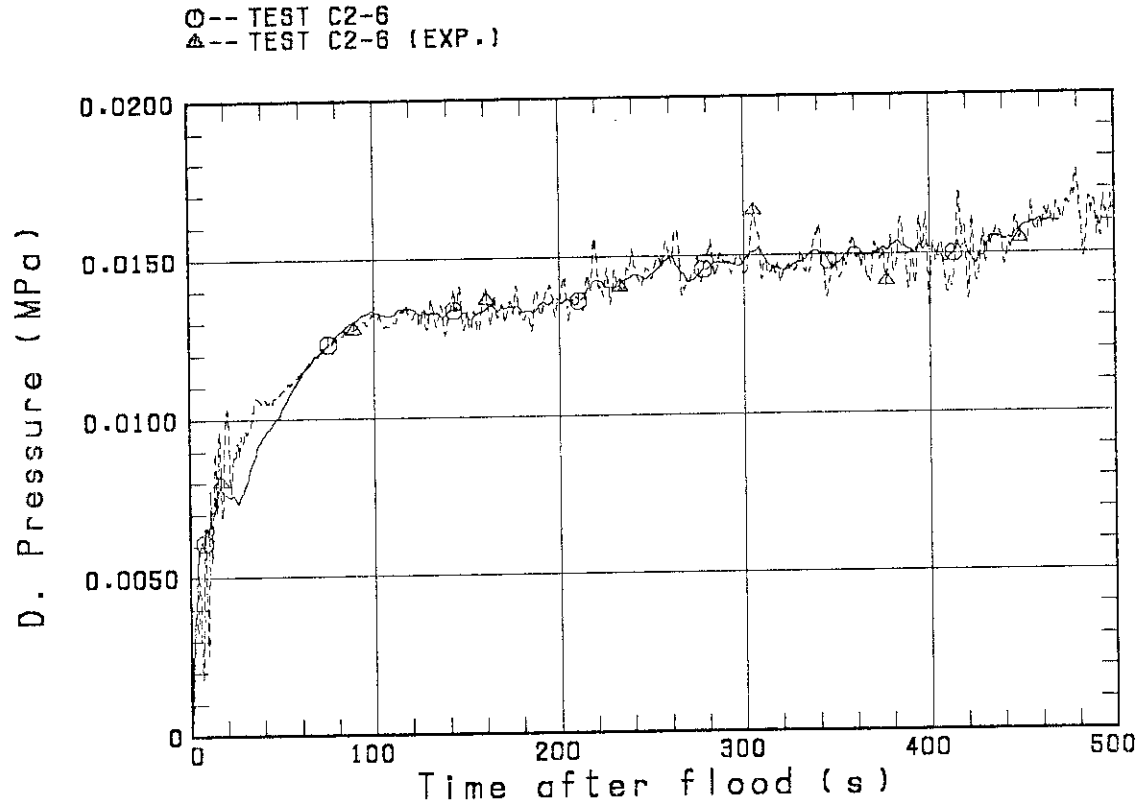

Fig. 3.6(a) Comparison of core differential pressure between calculation and experiment for Test C2-6

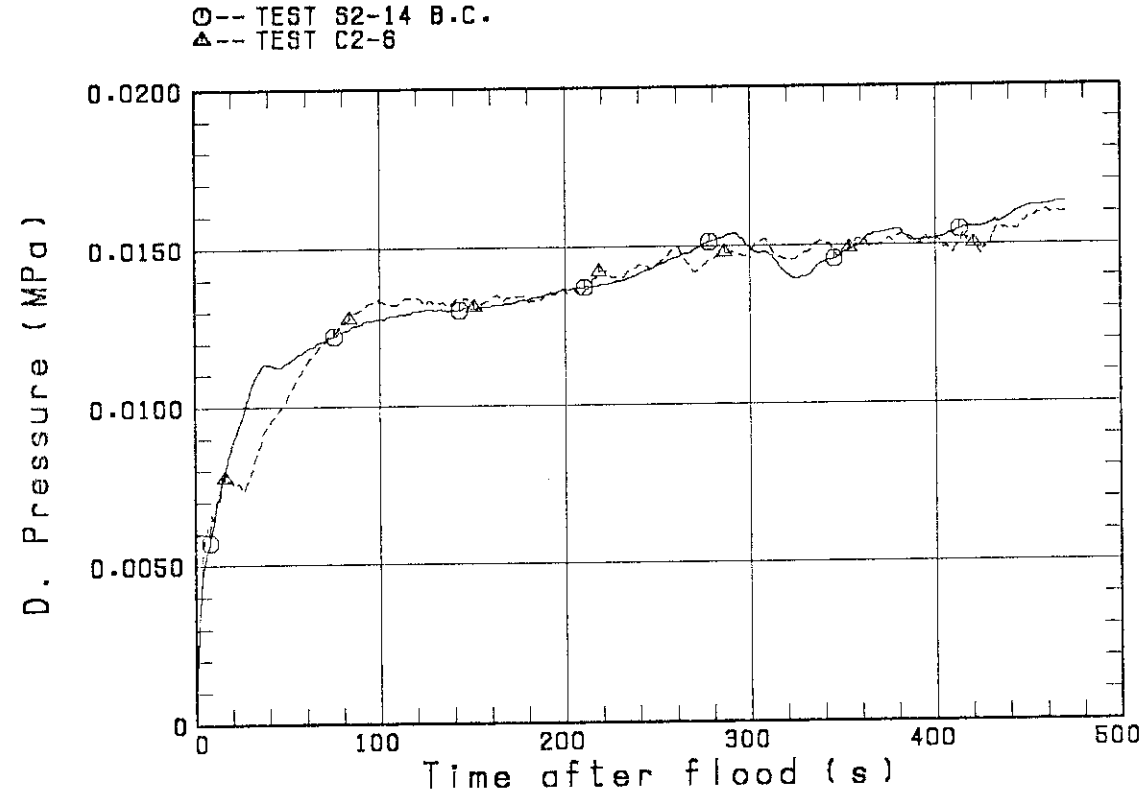

Fig. 3.6(b) Comparison of calculated core differential pressure for Test C2-6 under different core boundary conditions

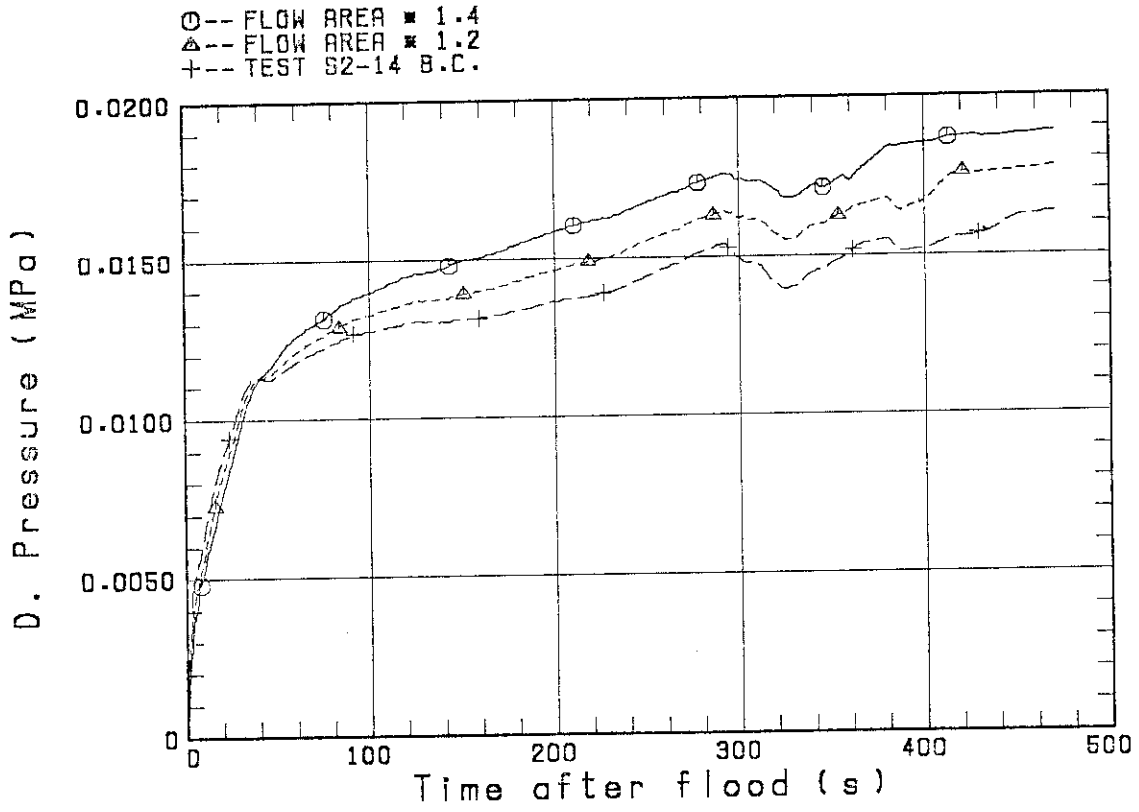

Fig. 3.6(c) Comparison of calculated core differential pressure for three different core flow area under same core boundary conditions

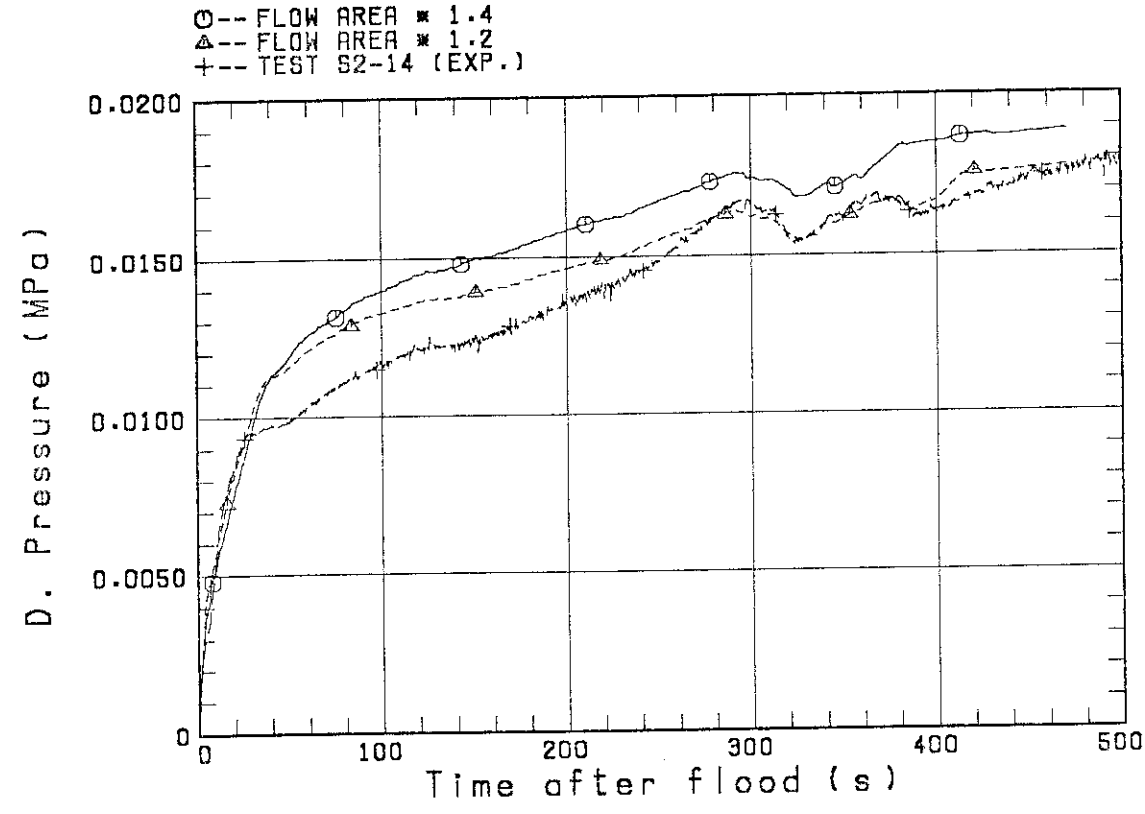

Fig. 3.6(d) Comparison of core differential pressure between calculations with different core flow area and experiment for Test S2-14

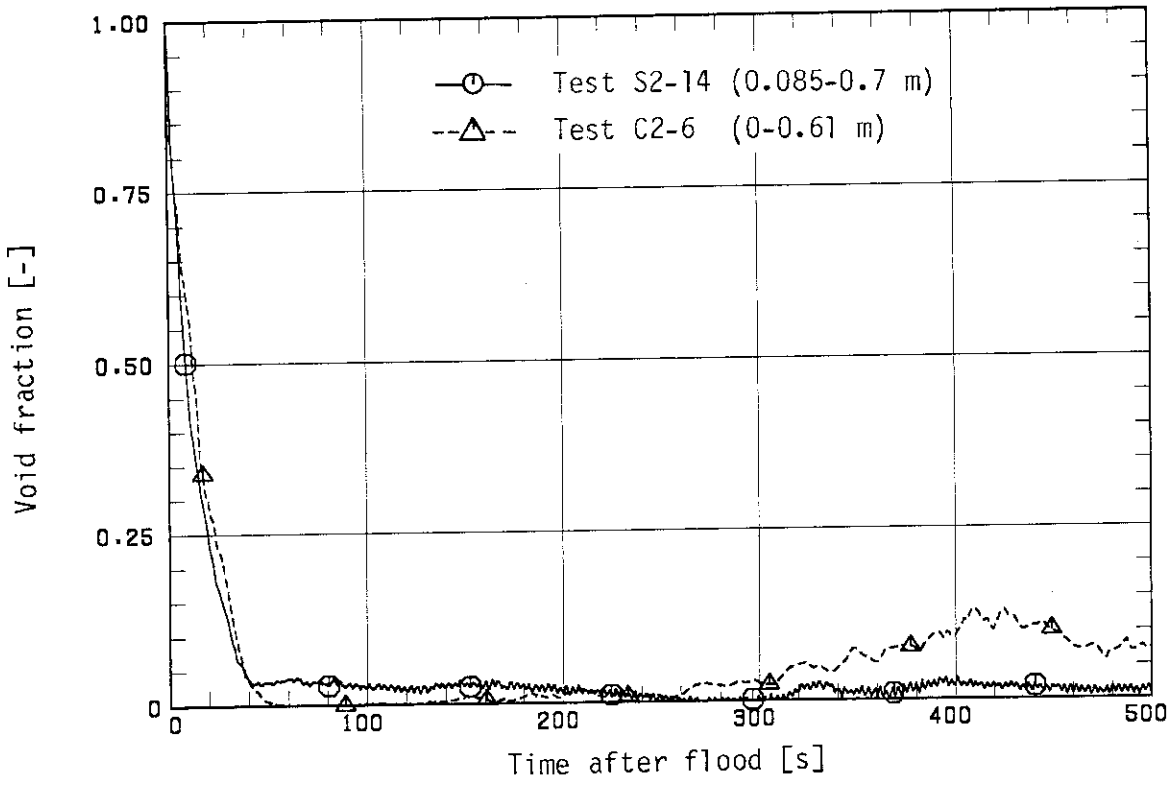

Fig. 3.7(a) Core void fraction (1)

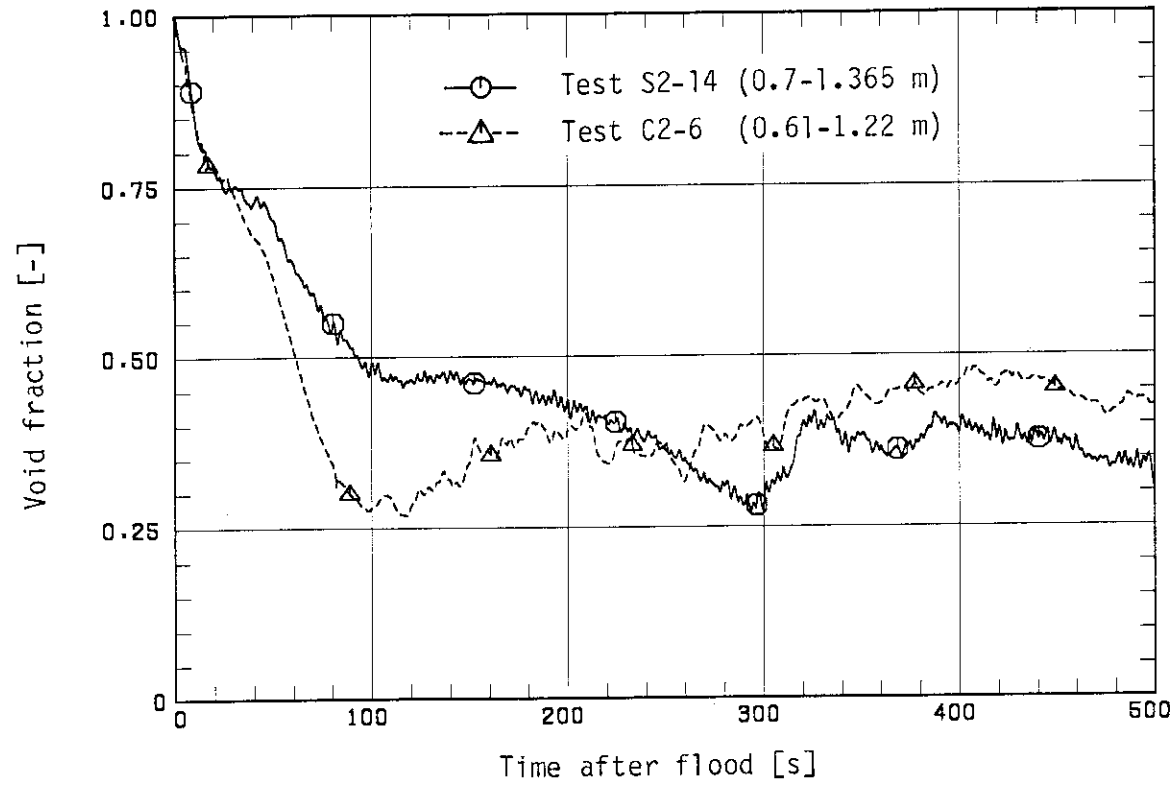

Fig. 3.7(b) Core void fraction (2)

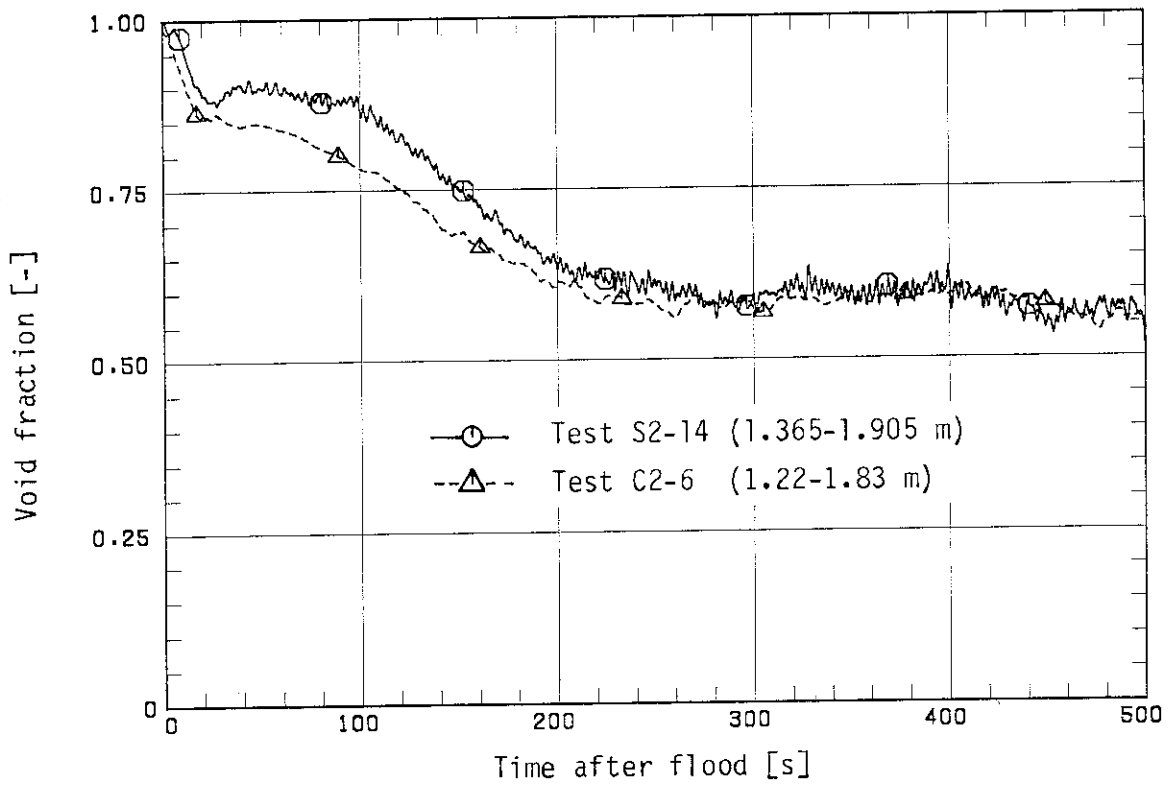

Fig. 3.7(c) Core void fraction (3)

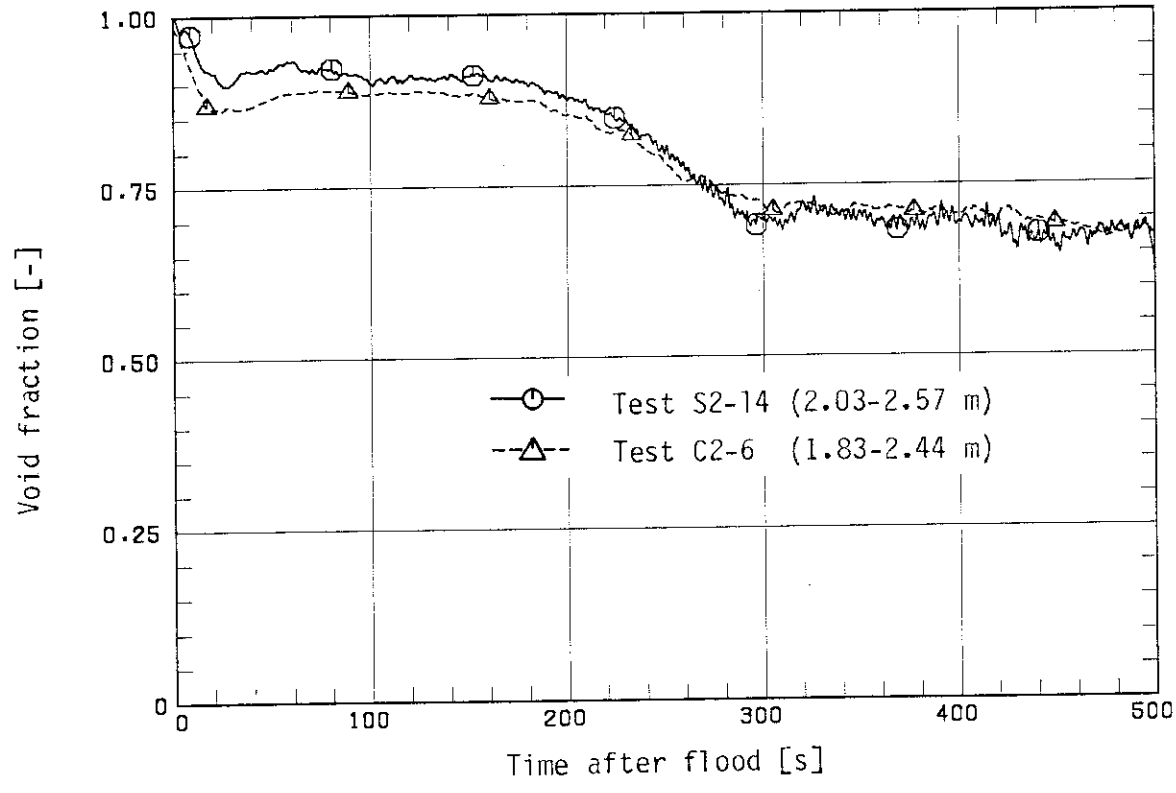

Fig. 3.7(d) Core void fraction (4)

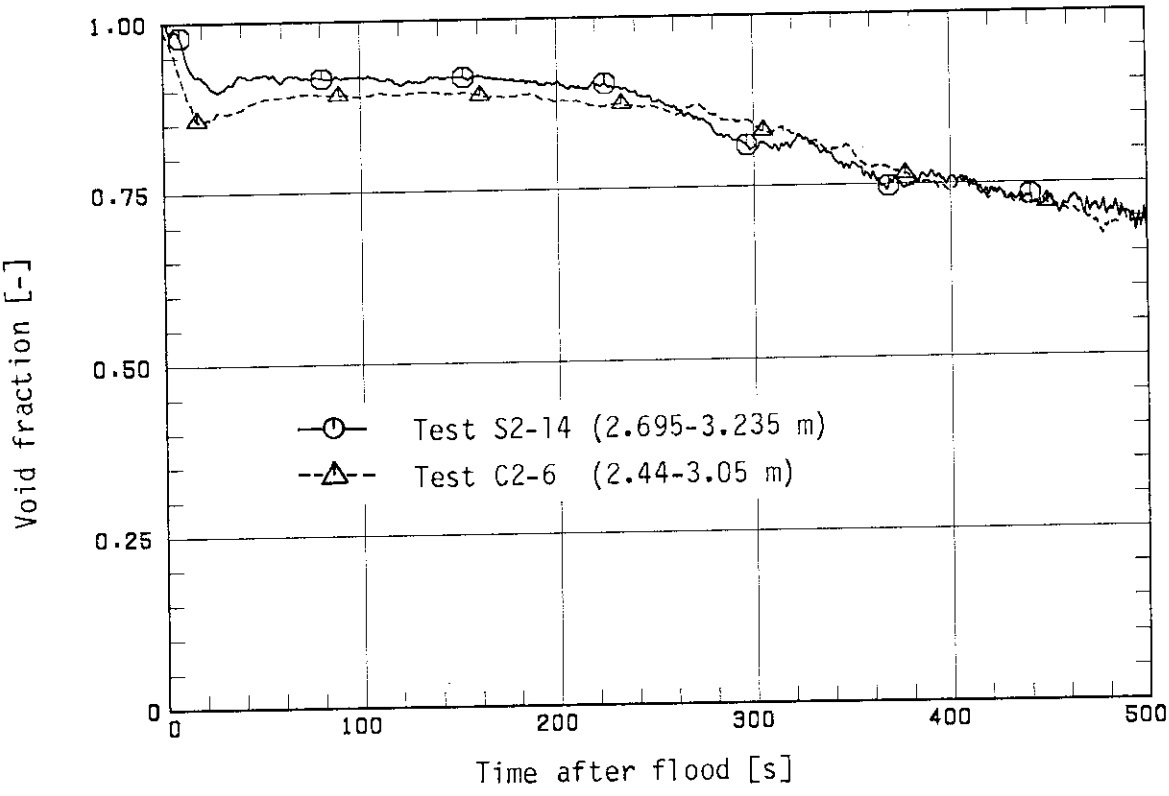

Fig. 3.7(e) Core void fraction (5)

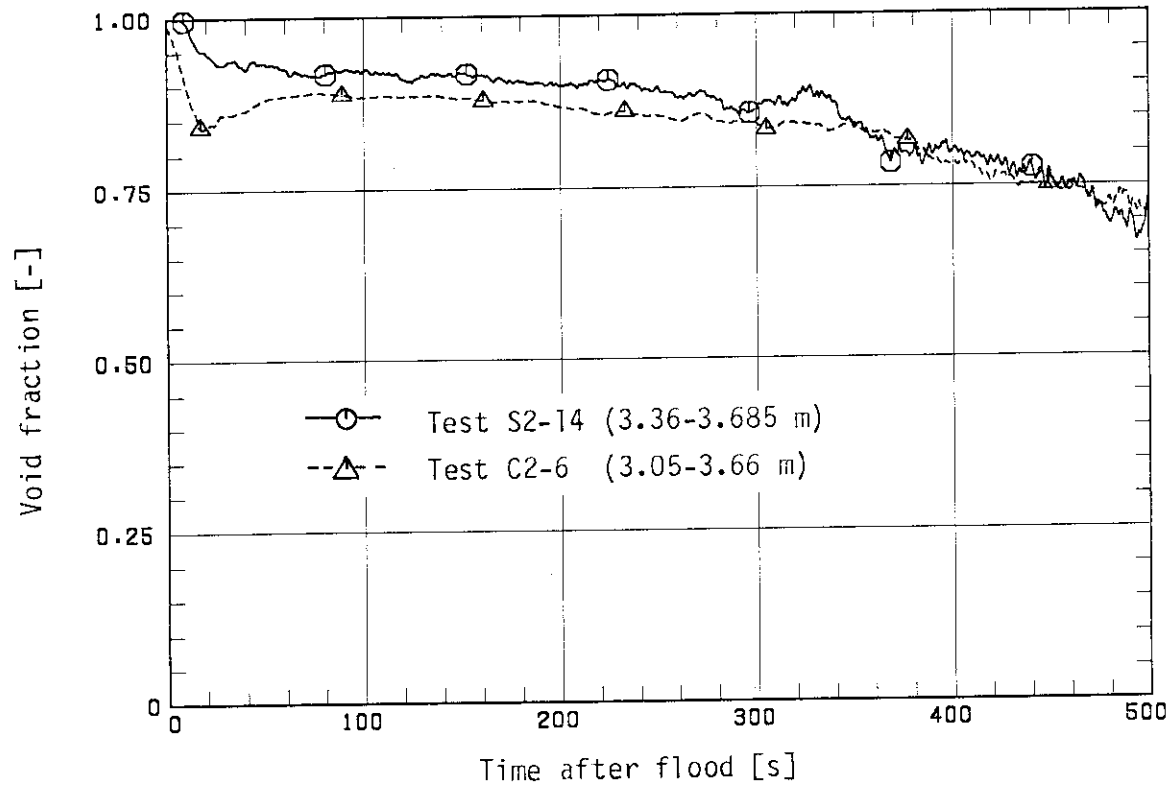

Fig. 3.7(f) Core void fraction (6)

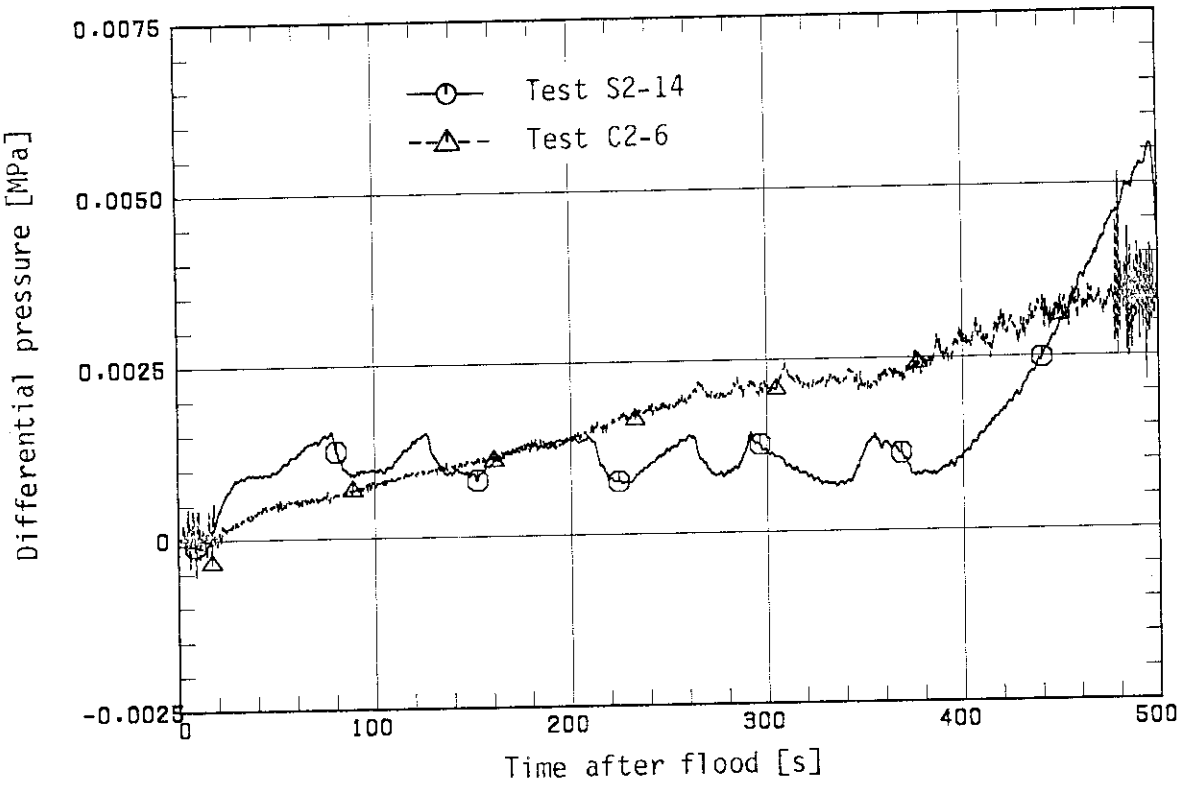

Fig. 3.8(a) Upper plenum differential pressure

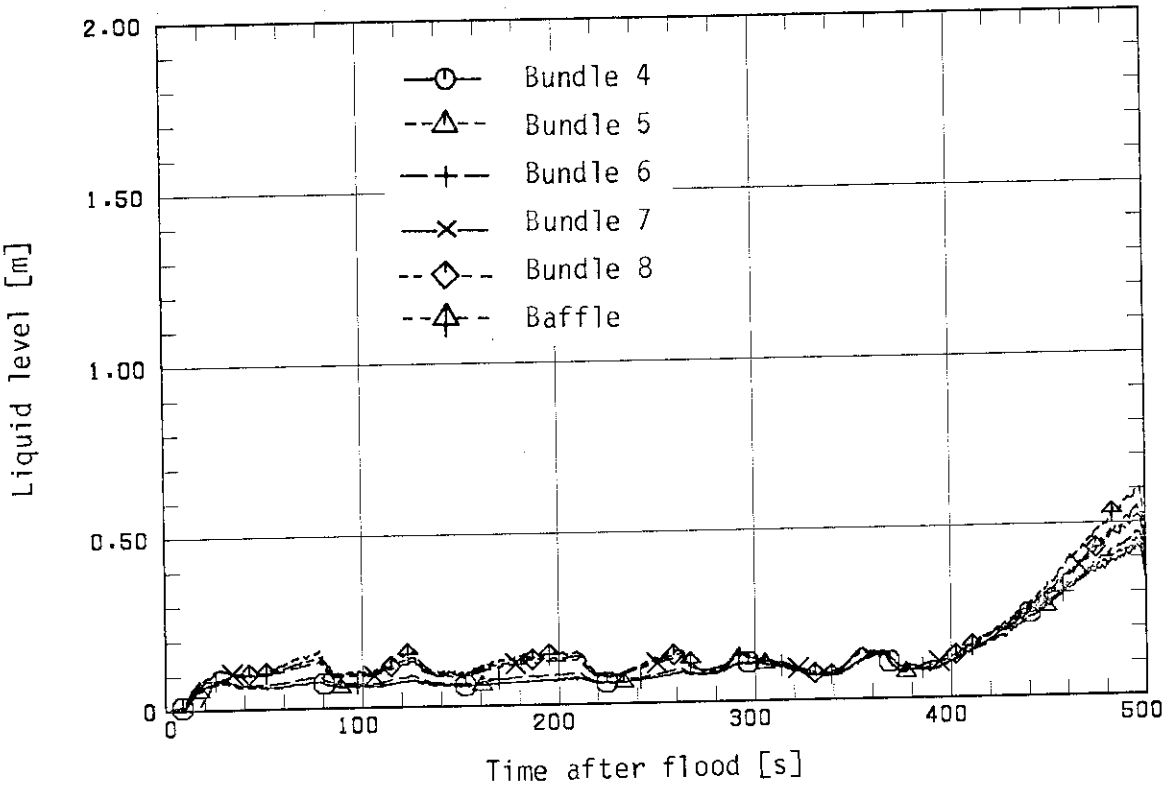

Fig. 3.8(b) Upper plenum water level above UCSP

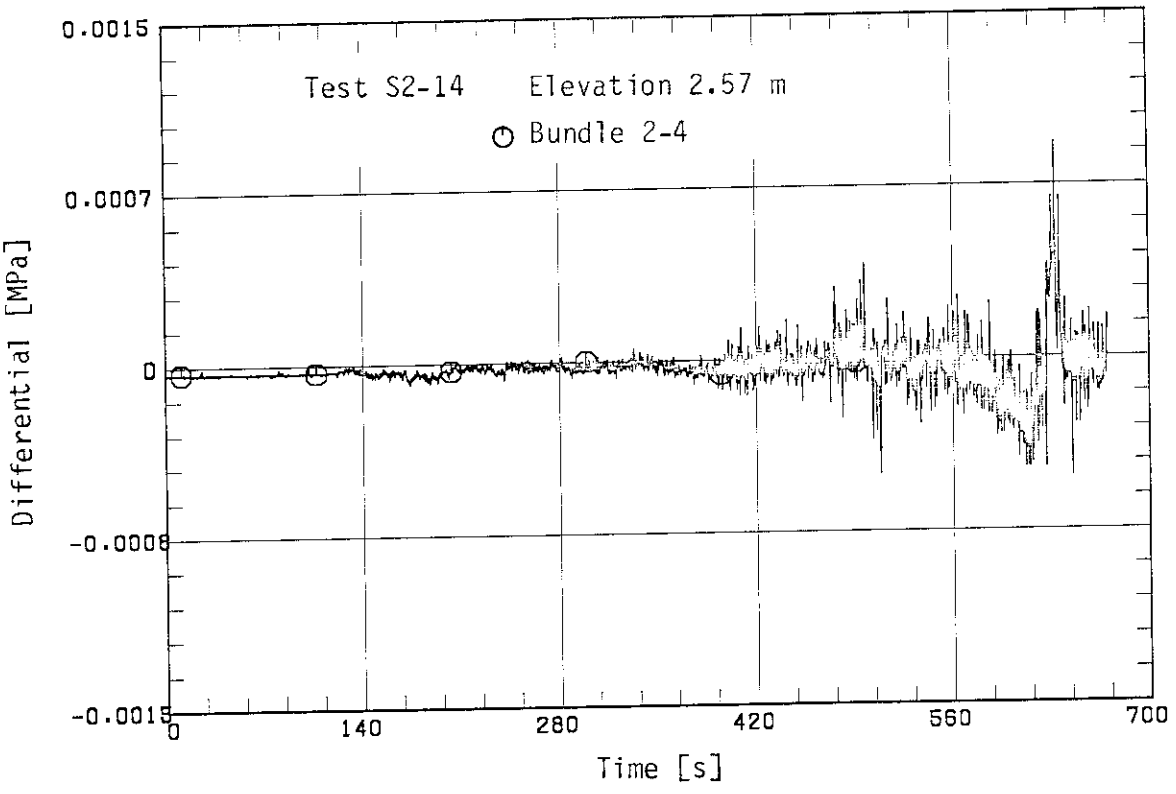

Fig. 3.9(a) Core horizontal differential pressure at 2.57 m elevation in Test S2-14

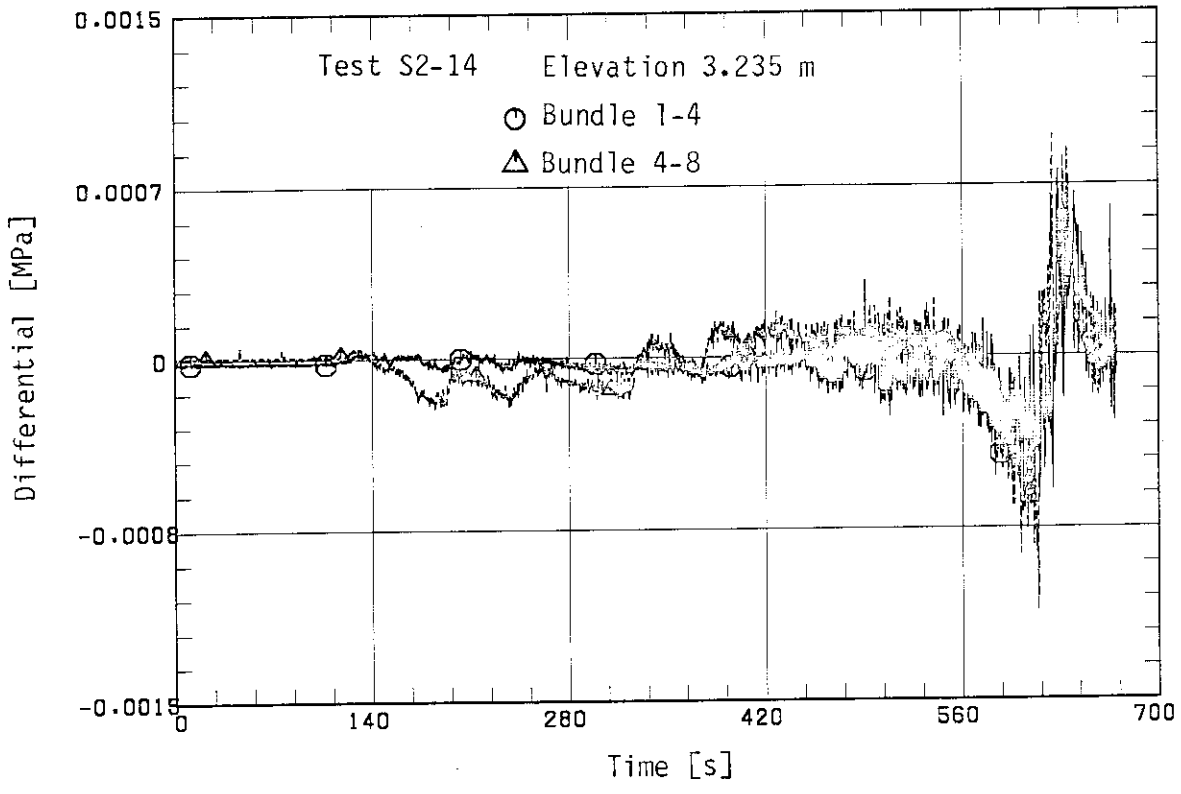

Fig. 3.9(b) Core horizontal differential pressure at 3.235 m elevation in Test S2-14

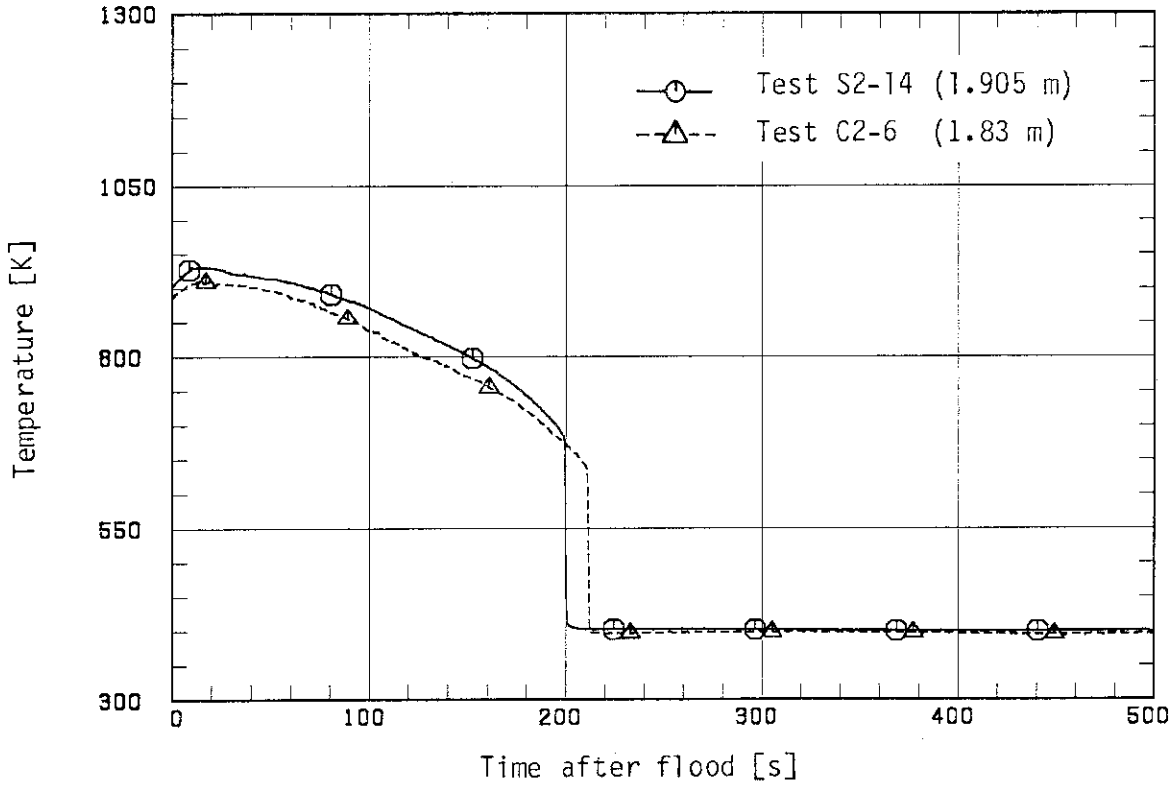

Fig. 3.10(a) Heater rod surface temperature history in core central side region at midplane level

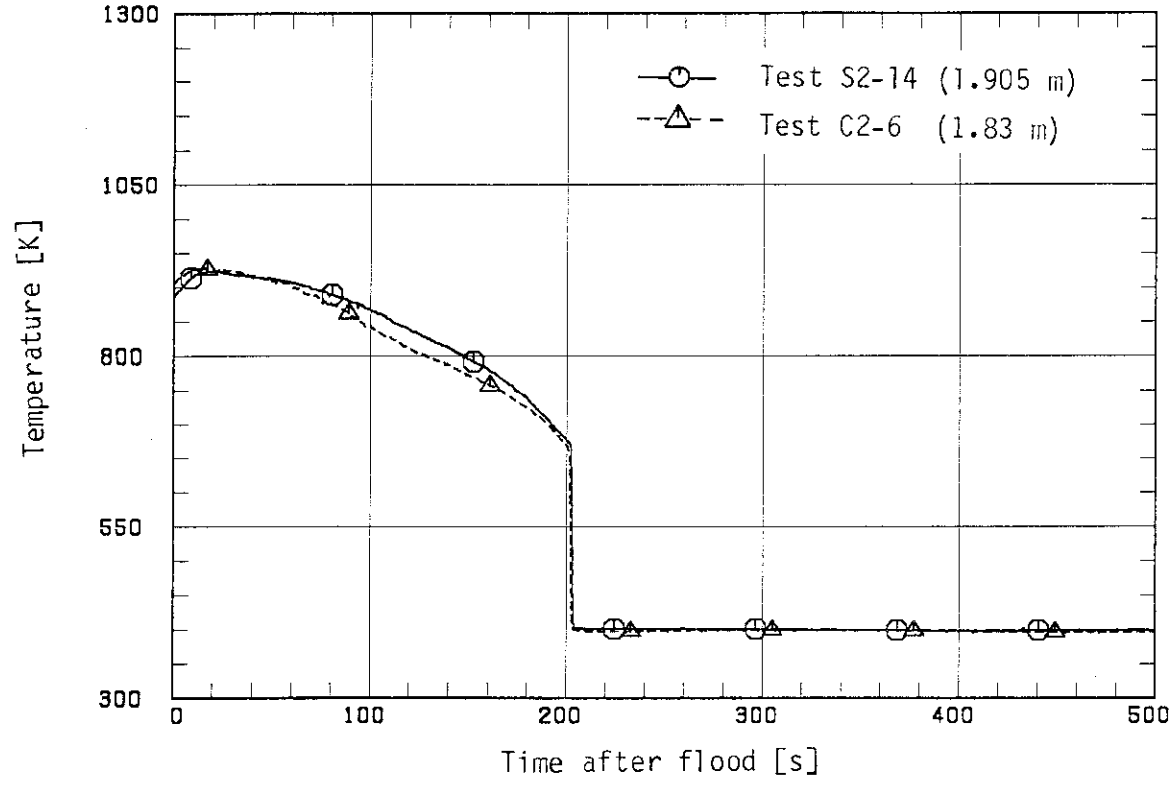

Fig. 3.10(b) Heater rod surface temperature history in intermediate region at midplane level

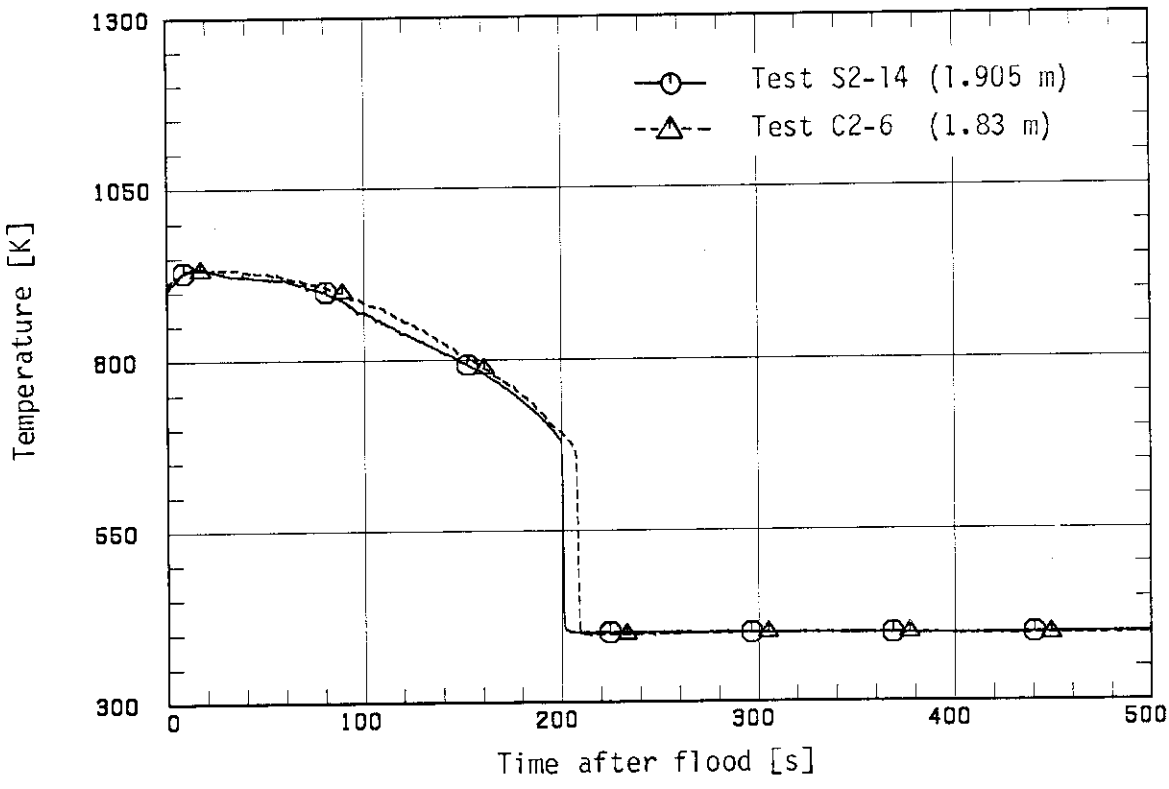

Fig. 3.10(c) Heater rod surface temperature history in core peripheral region at midplane level

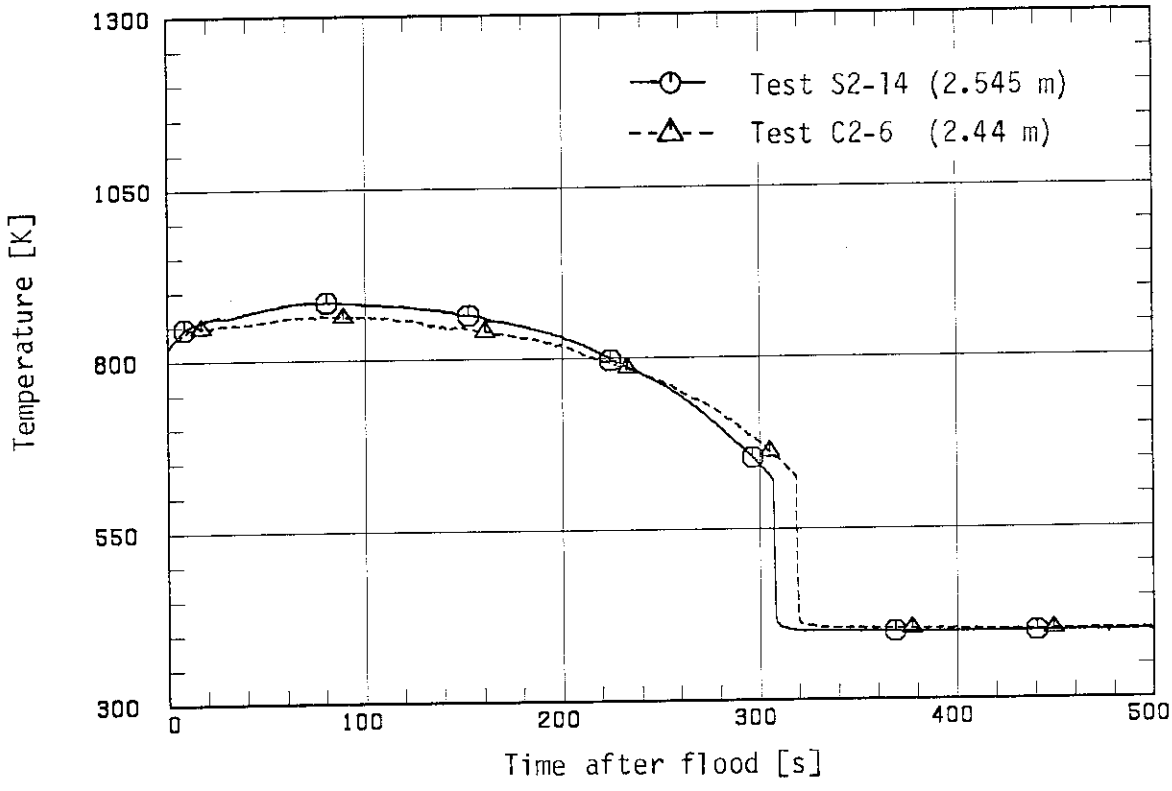

Fig. 3.10(d) Heater rod surface temperature history in central side region at higher elevation than midplane level

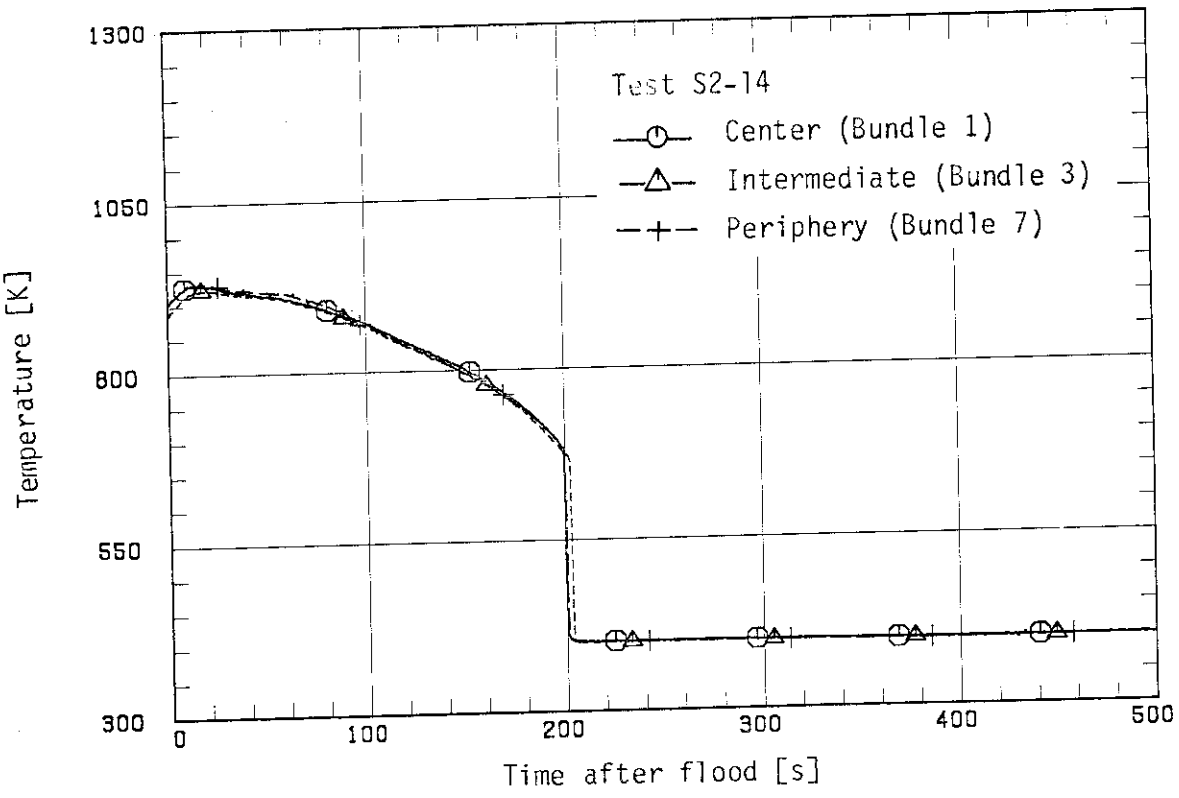

Fig. 3.11(a) Heater rod surface temperature history comparison in radial direction for Test S2-14 at 1.905 m elevation

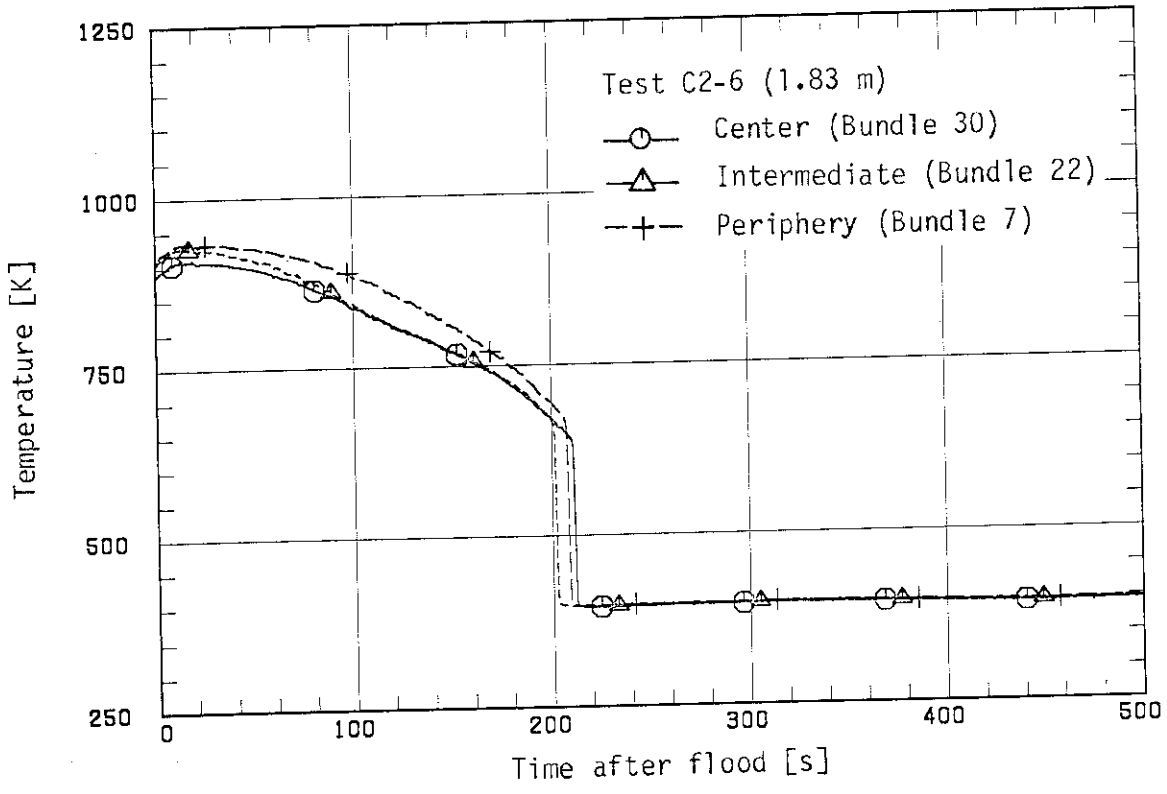

Fig. 3.11(b) Heater rod surface temperature history comparison in radial direction for Test C2-6 at 1.83 m elevation

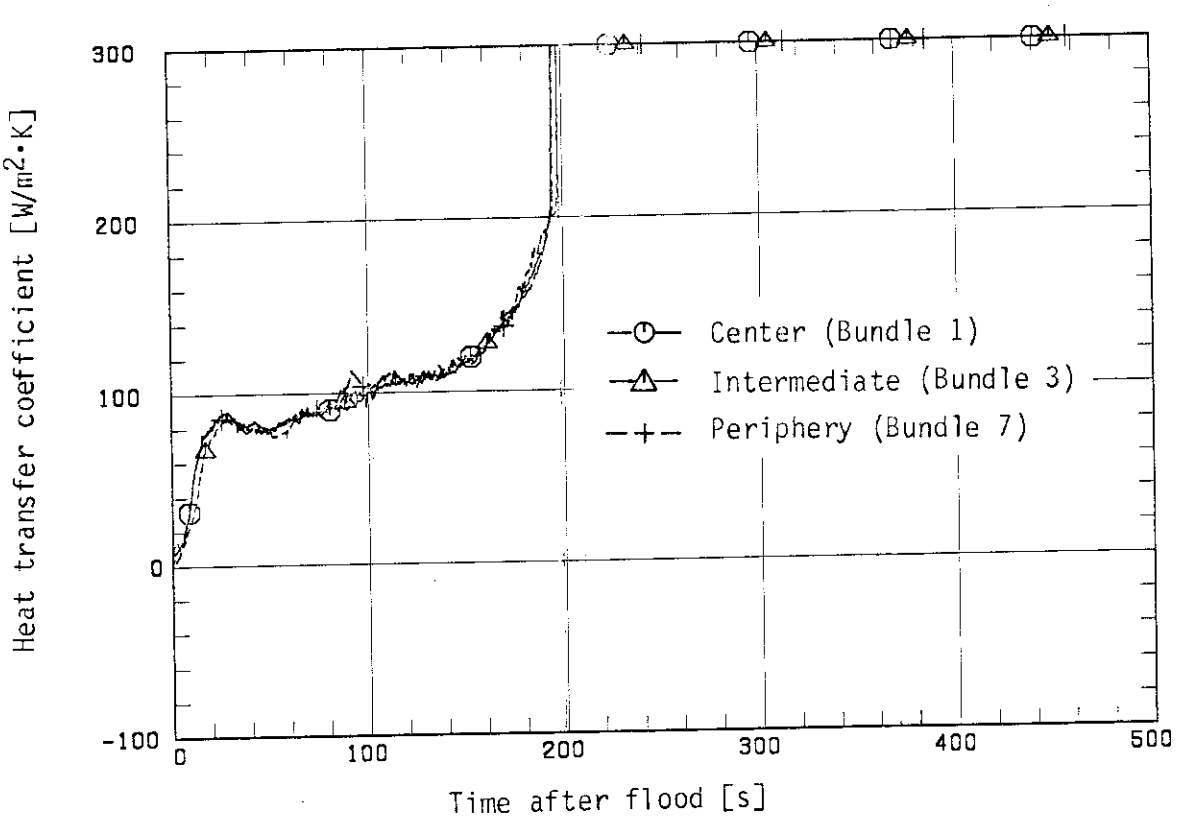

Fig. 3.12(a) Heat transfer coefficient history comparison in radial direction for Test S2-14 at 1.905 m elevation

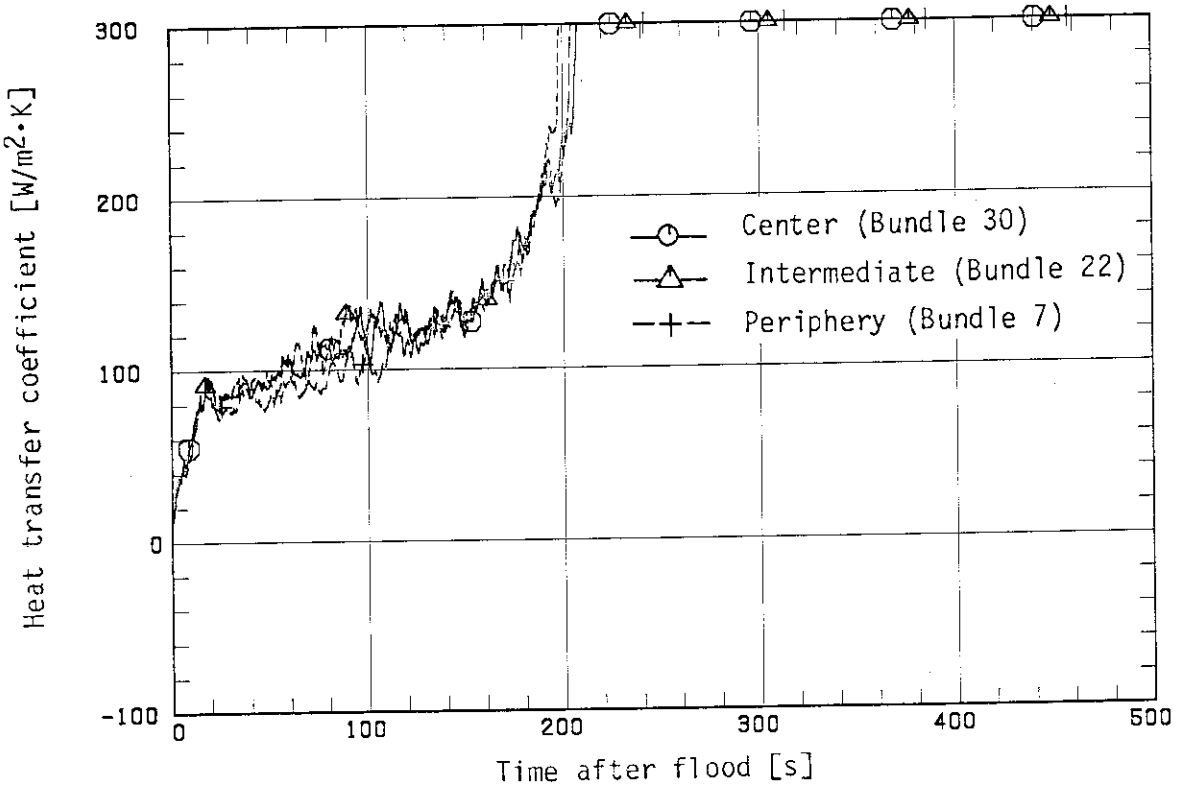

Fig. 3.12(b) Heat transfer coefficient history comparison in radial direction for Test C2-6 at 1.83 m elevation

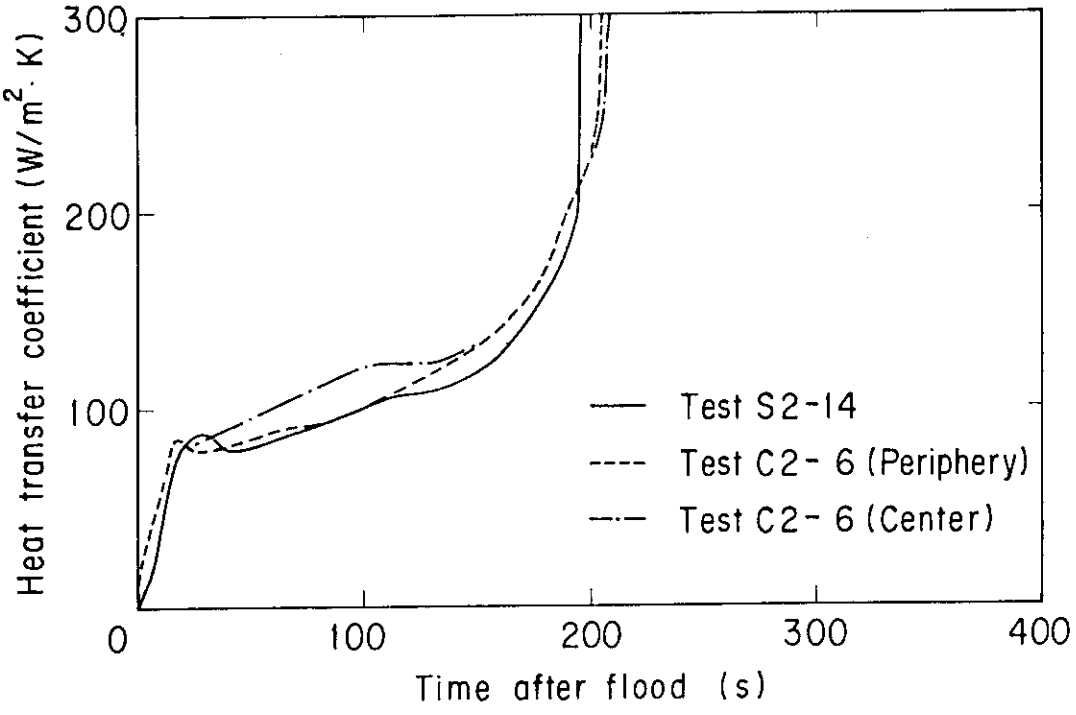

Fig. 3.13(a) Heat transfer coefficient history at midplane level

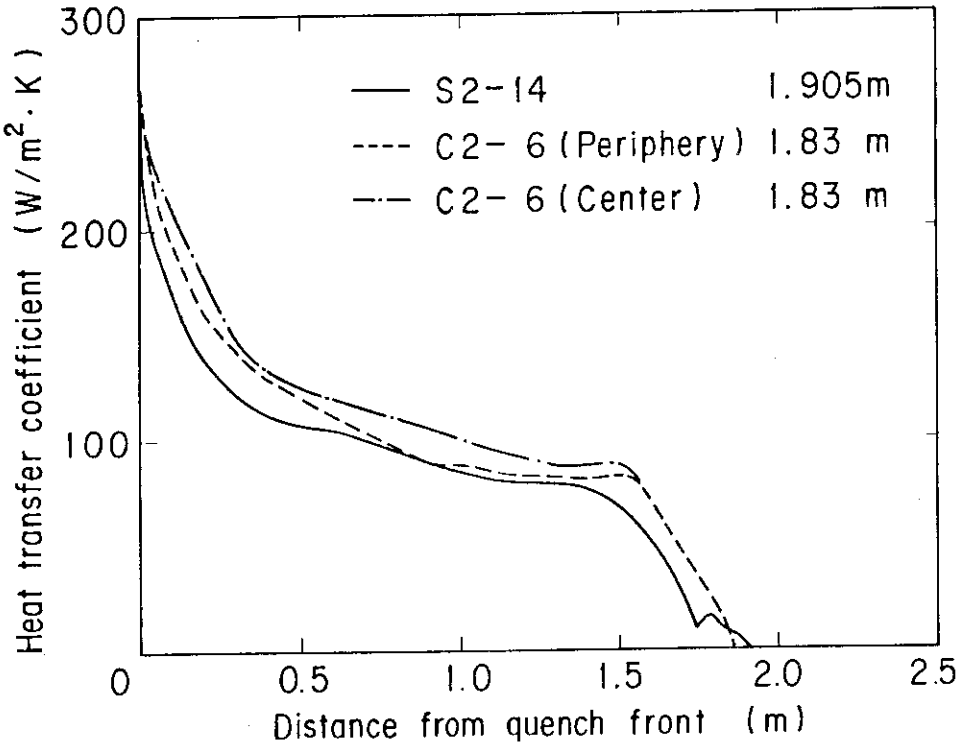

Fig. 3.13(b) Heat transfer coefficient history plotted against distance from quench front at midplane level

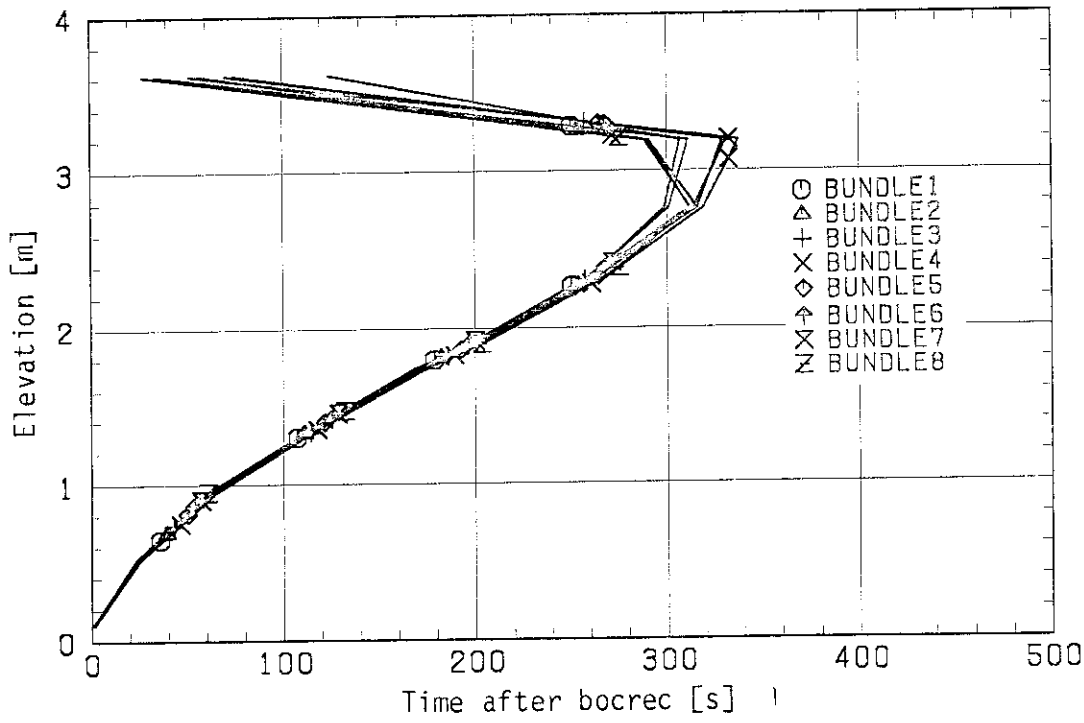

Fig. 3.14(a) Quench front envelope comparison in radial direction for Test S2-14

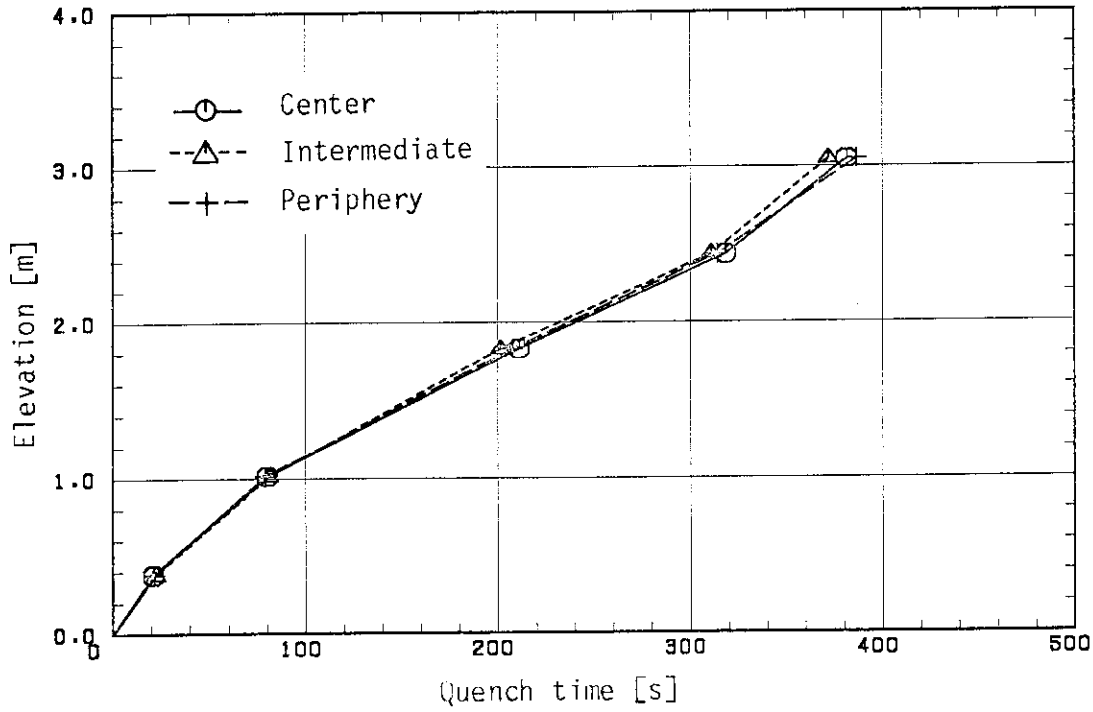

Fig. 3.14(b) Quench front envelope comparison in radial direction for Test C2-6

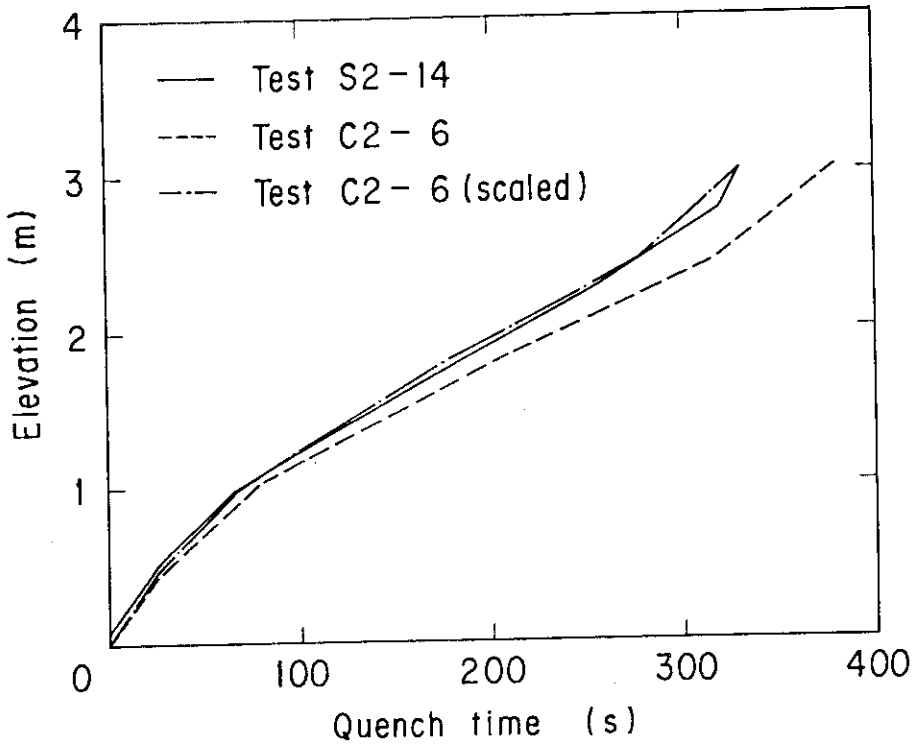

Fig. 3.15 Quench front envelope

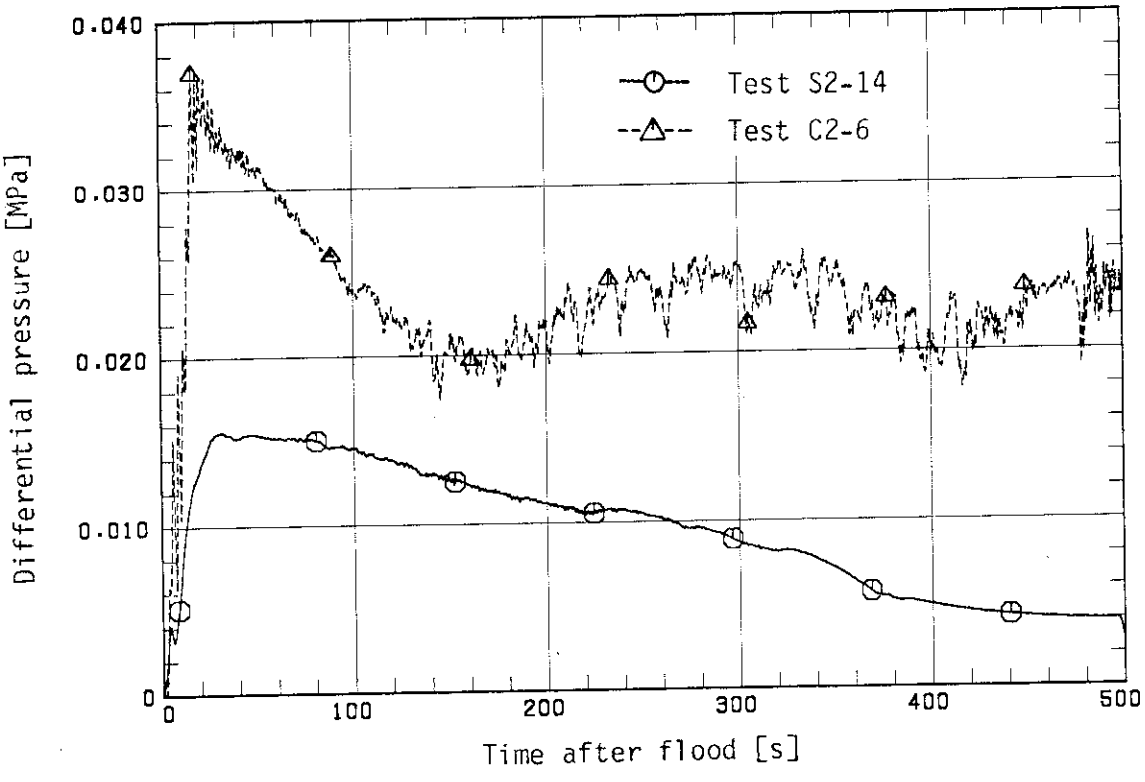

Fig. 3.16 Intact loop differential pressure

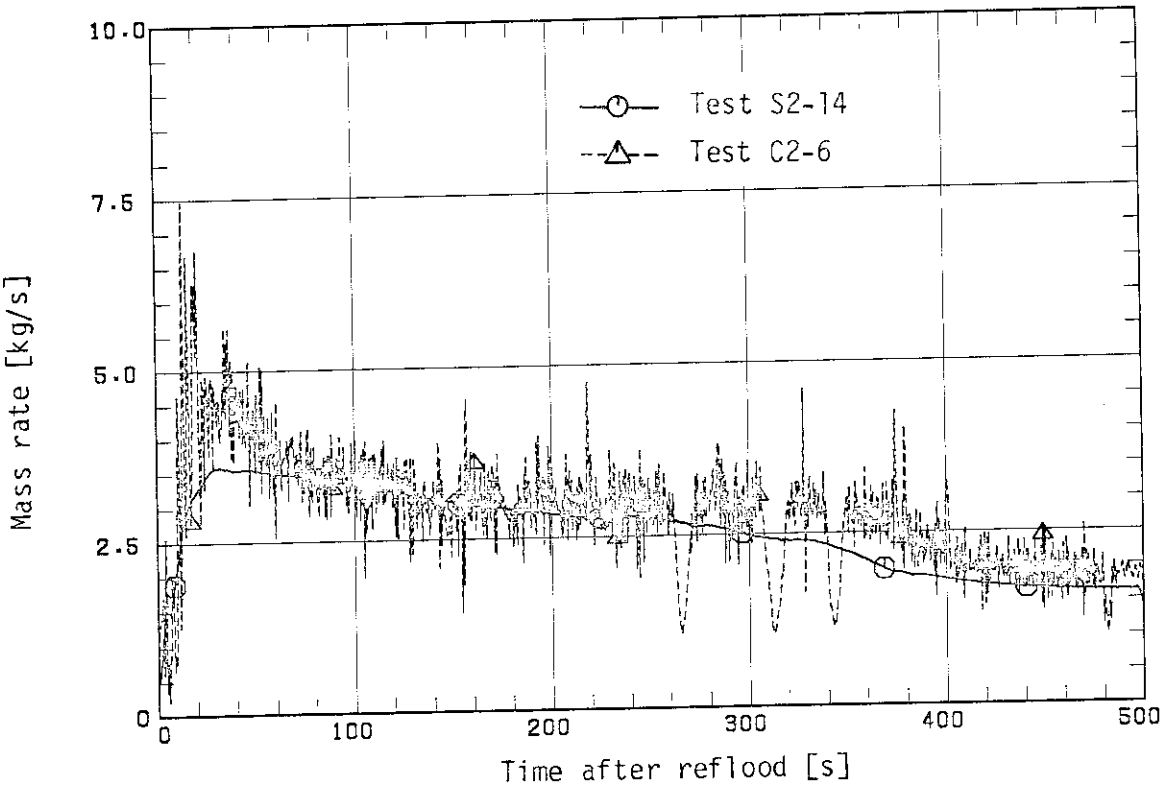

Fig. 3.17 Core outlet steam flow (evaluated value)

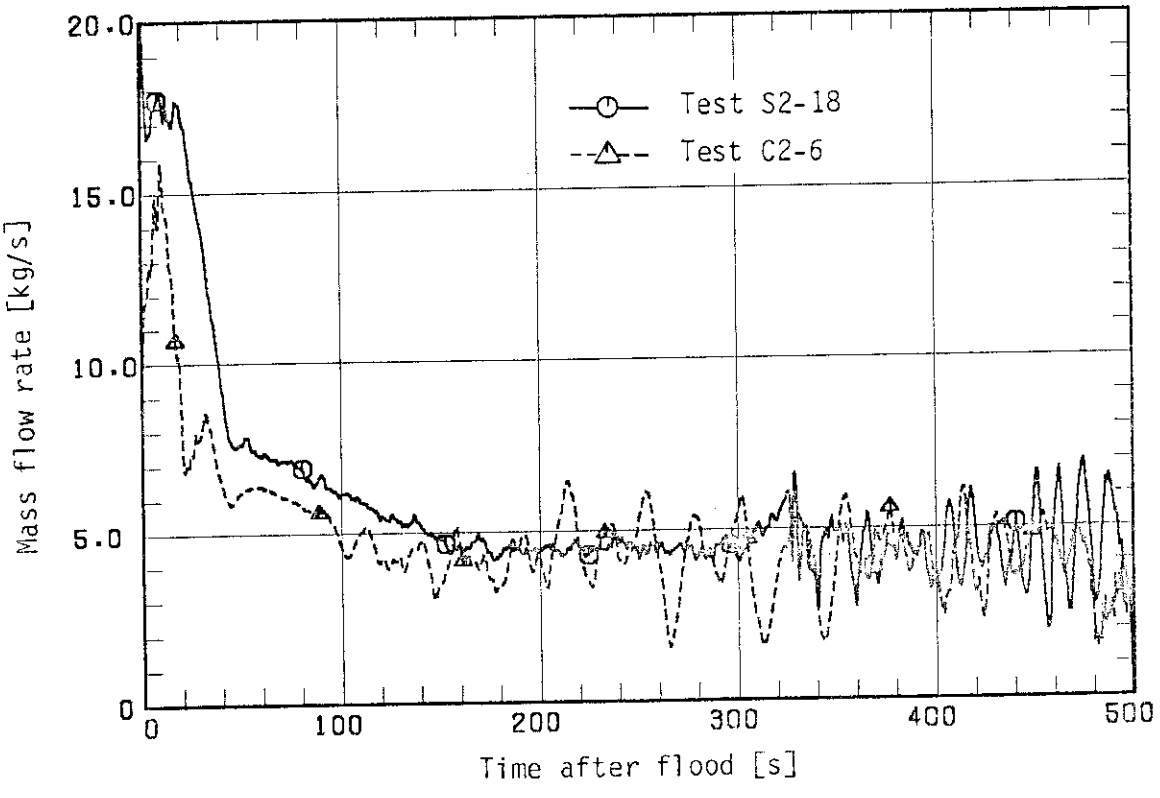

Fig. 3.18(a) Core flooding rate (evaluated value)

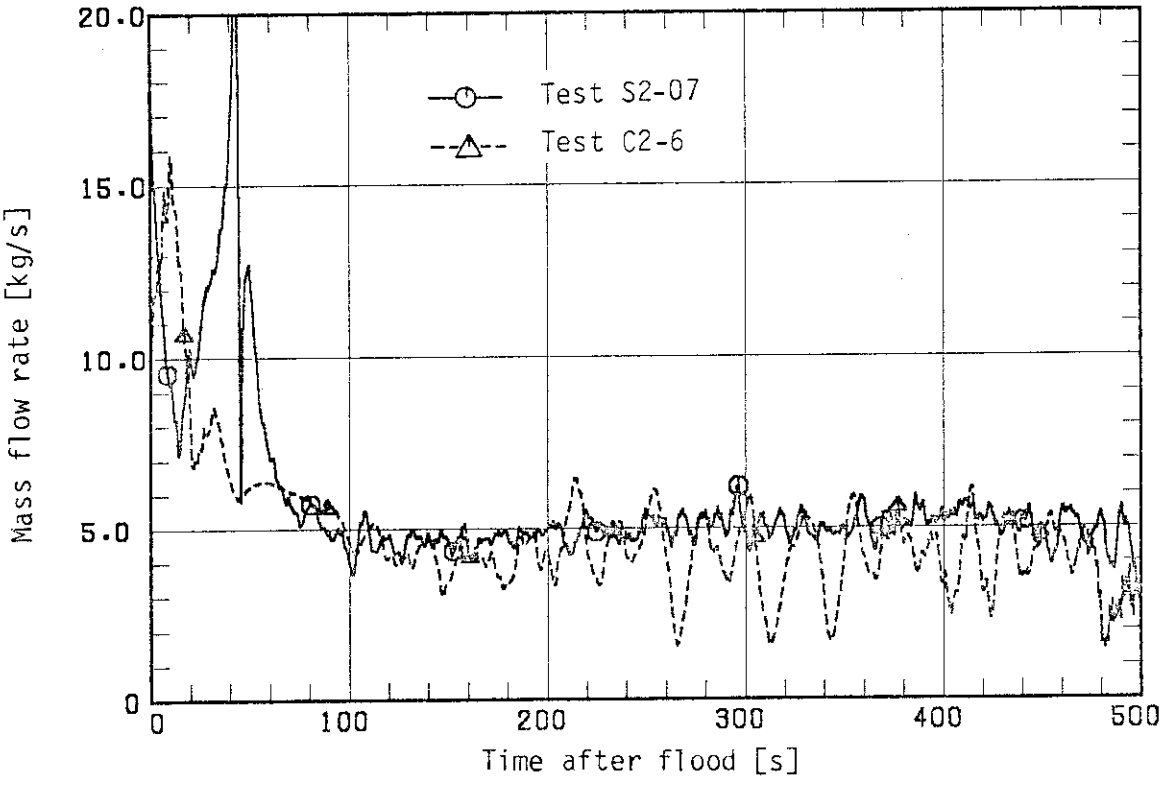

Fig. 3.18(b) Core flooding rate (Tests S2-07 and C2-6, evaluated value)

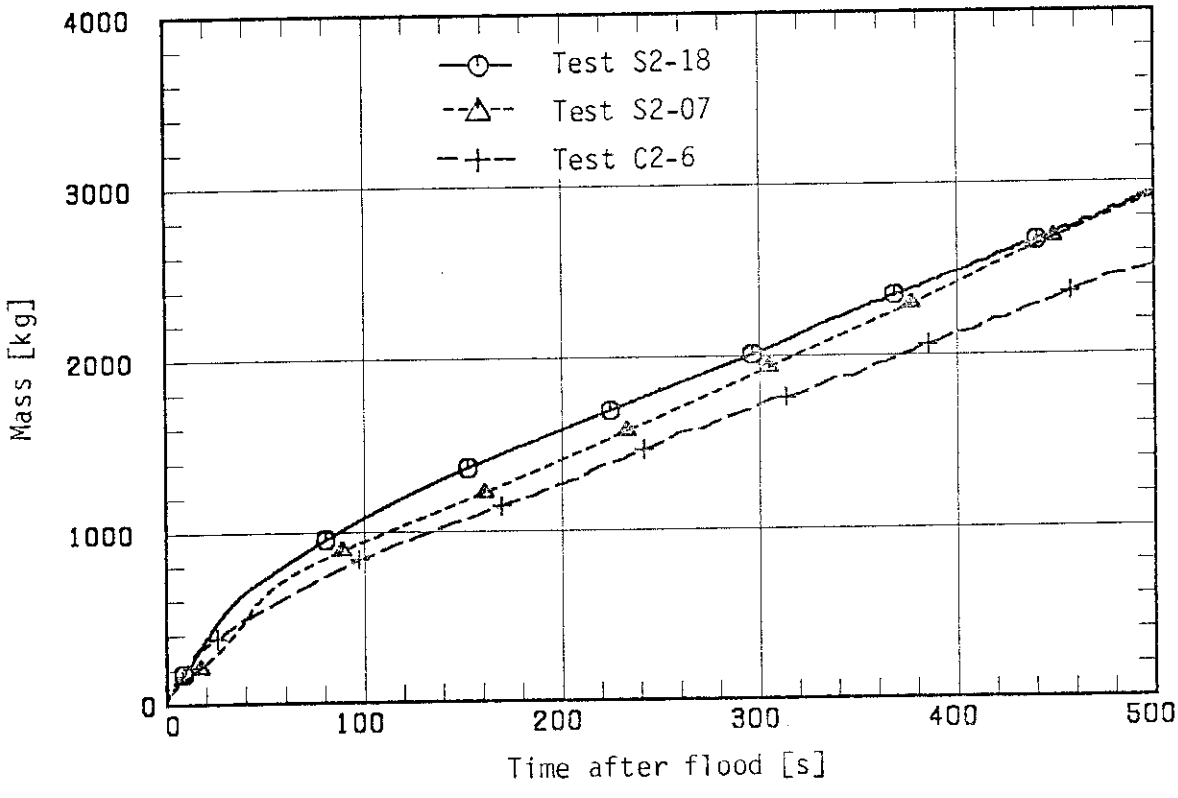

Fig. 3.18(c) Time-integration of core flooding rate

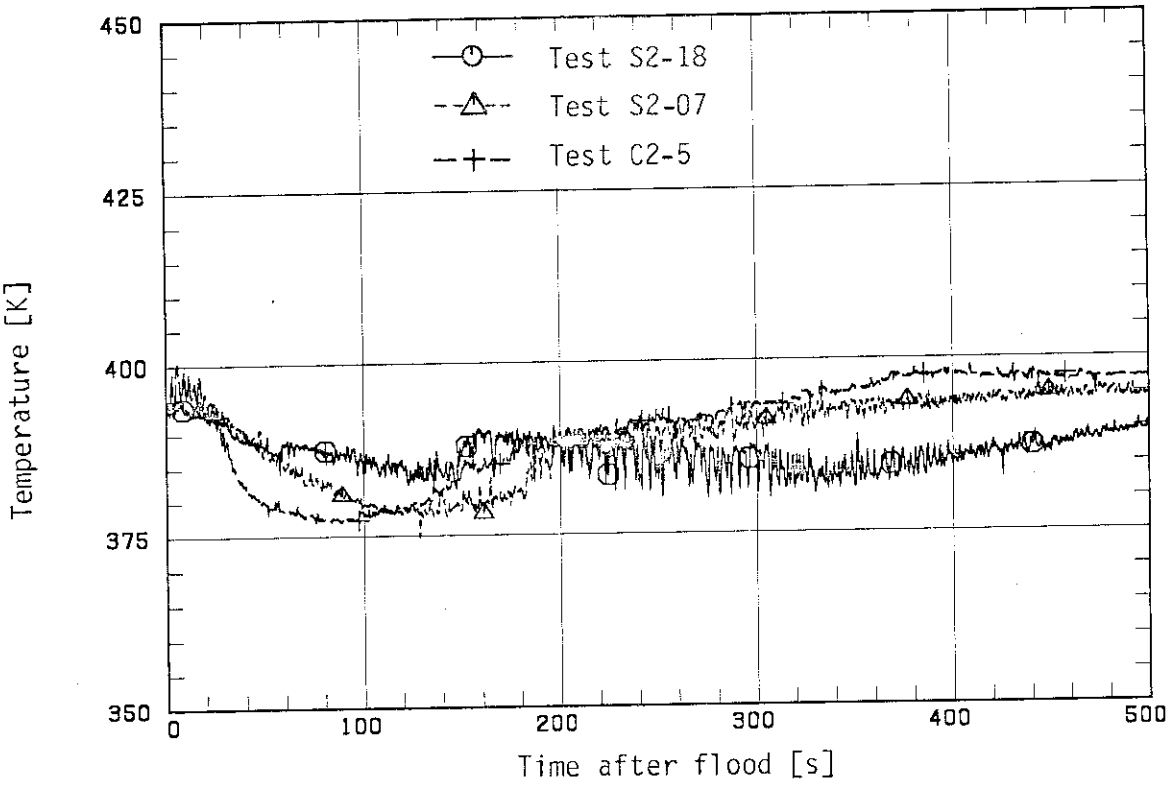

Fig. 3.19 Core inlet fluid temperature

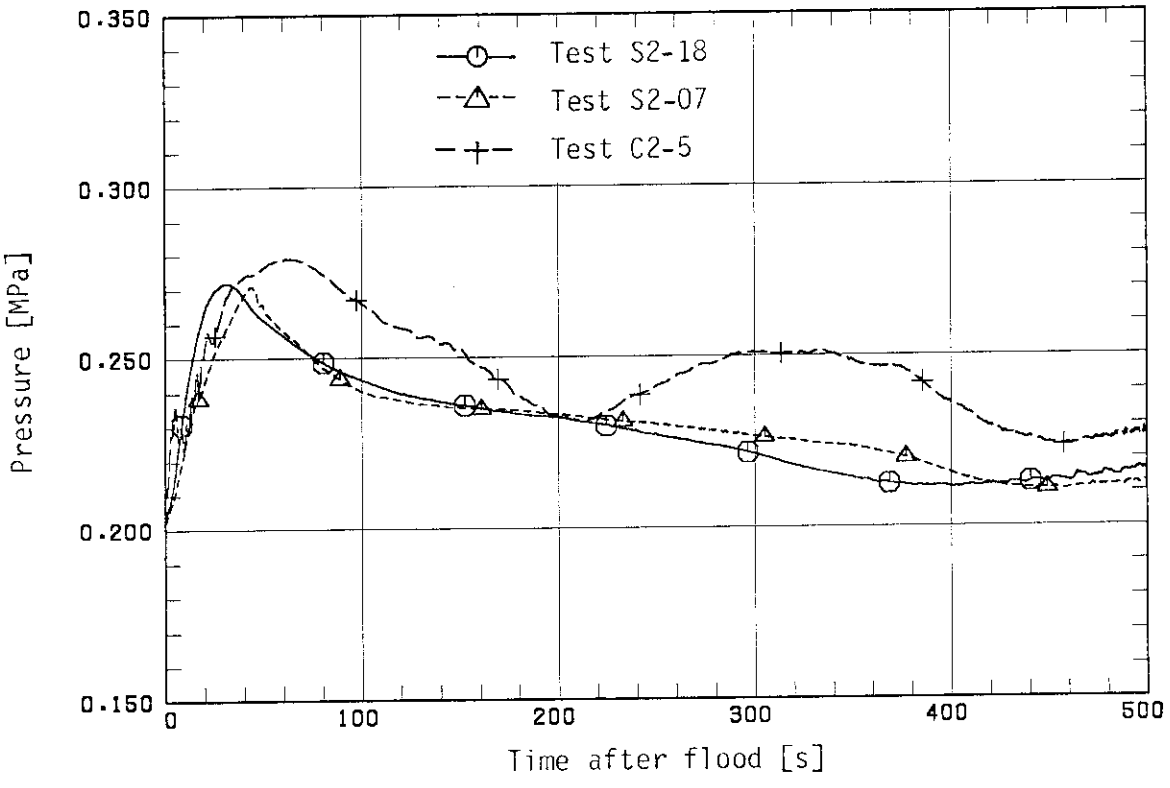

Fig. 3.20 Upper plenum pressure

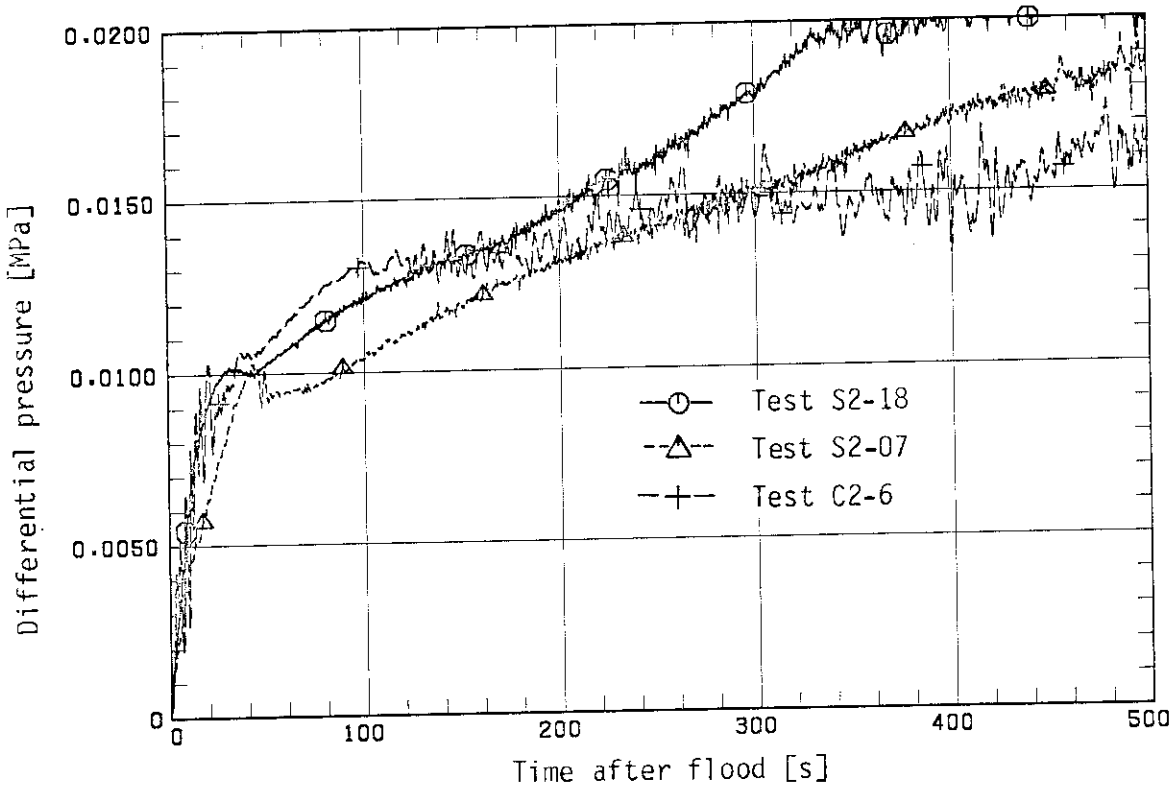

Fig. 3.21 Core differential pressure

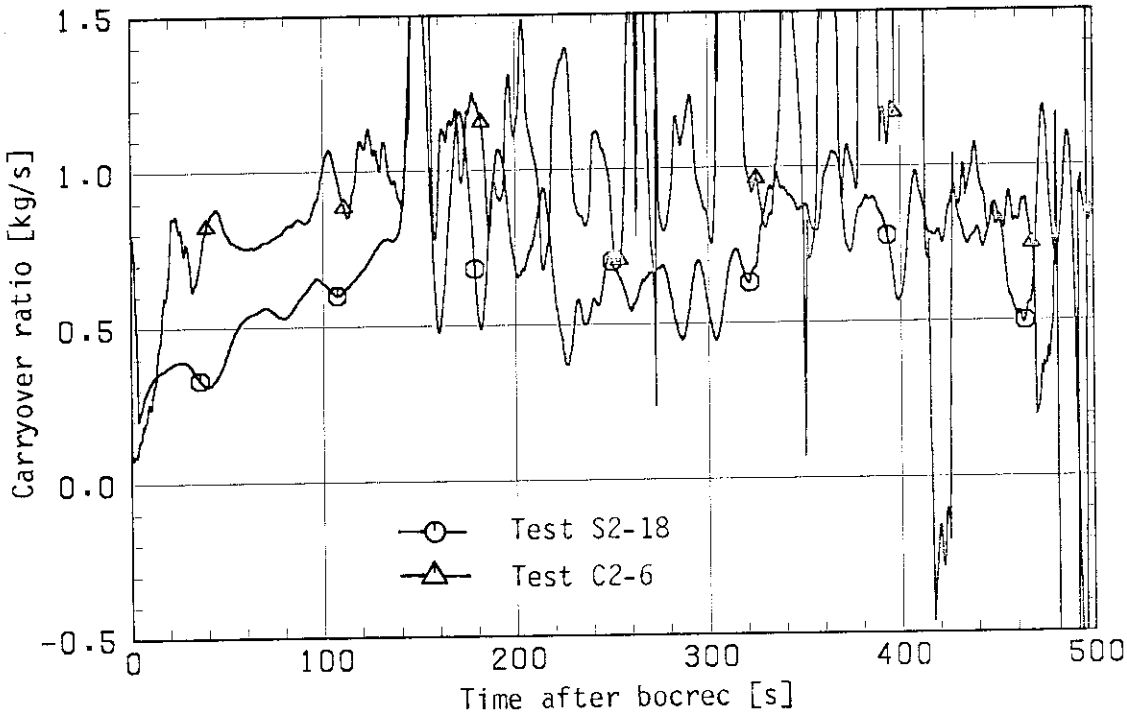

Fig. 3.22 Core carry over ratio

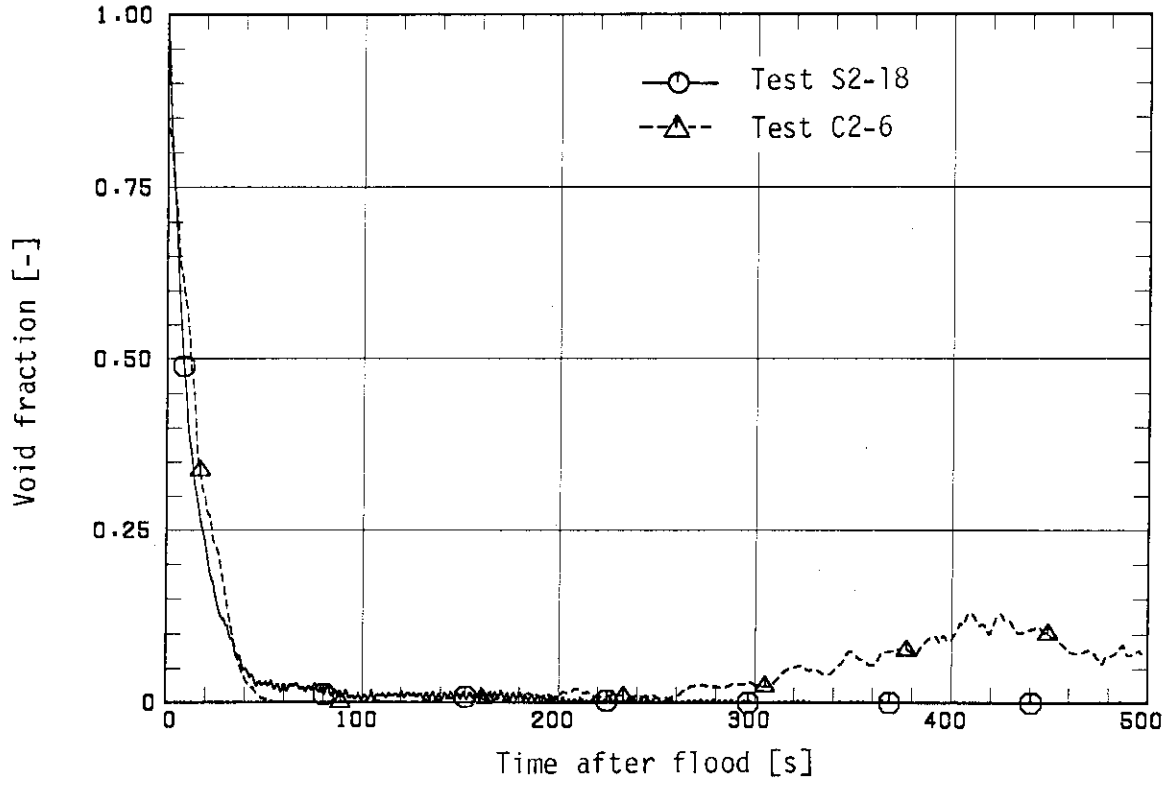

Fig. 3.23(a) Core void fraction (1)

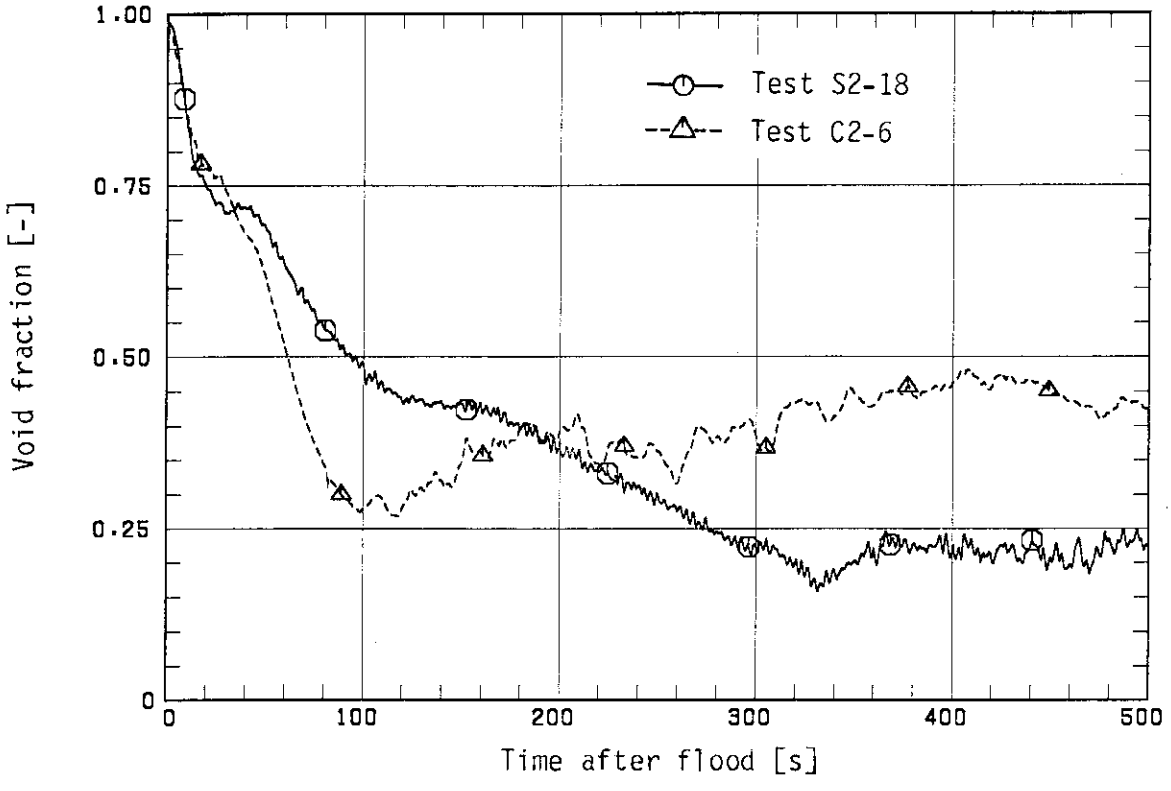

Fig. 3.23(b) Core void fraction (2)

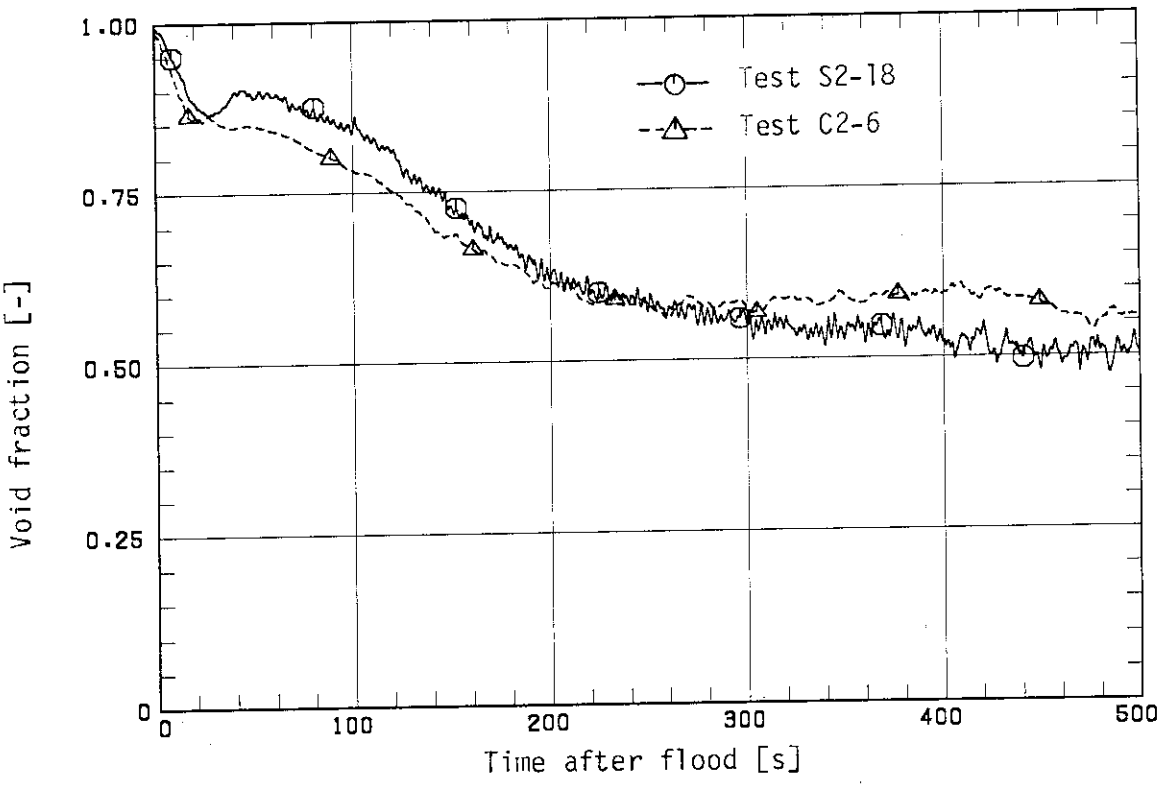

Fig. 3.23(c) Core void fraction (3)

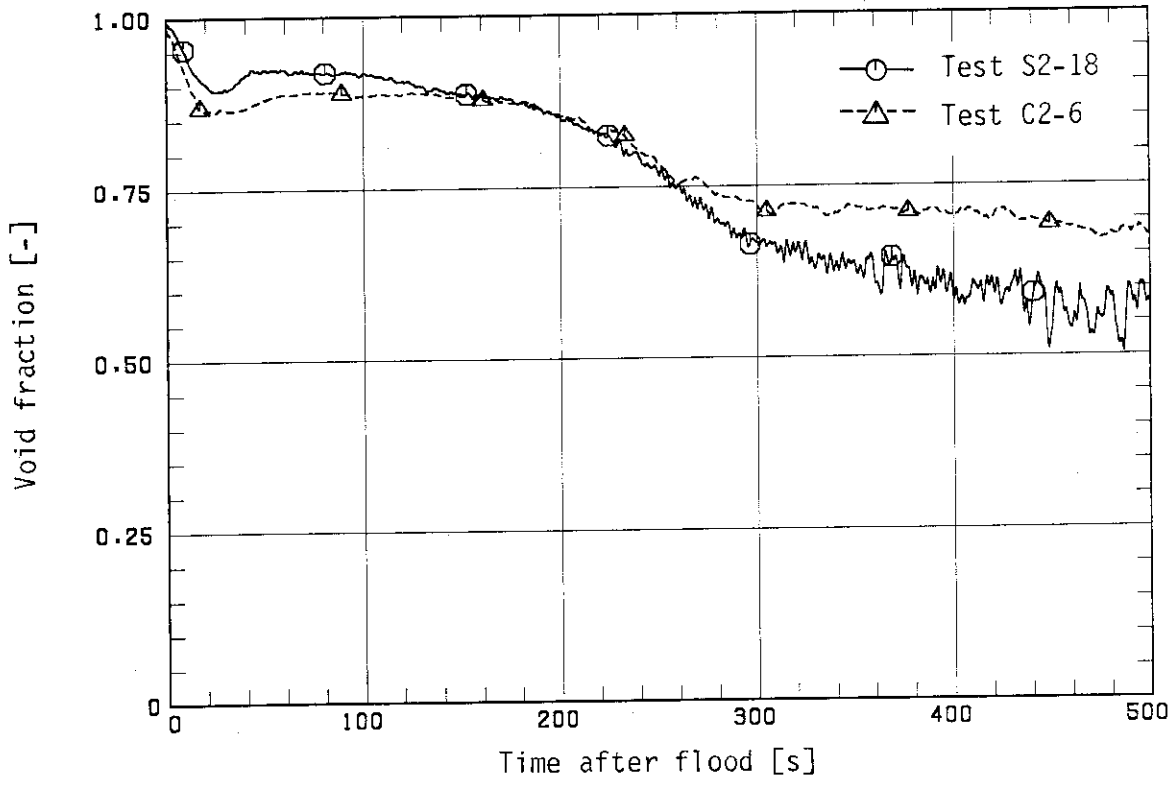

Fig. 3.23(d) Core void fraction (4)

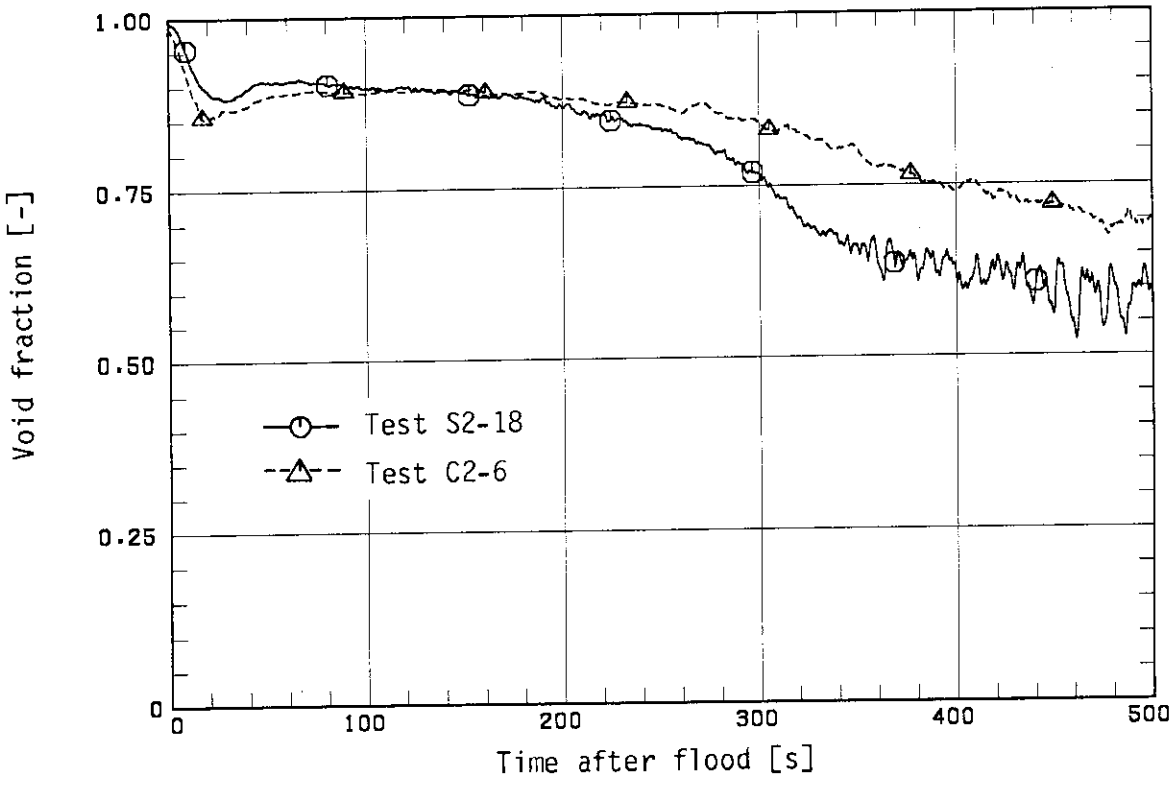

Fig. 3.23(e) Core void fraction (5)

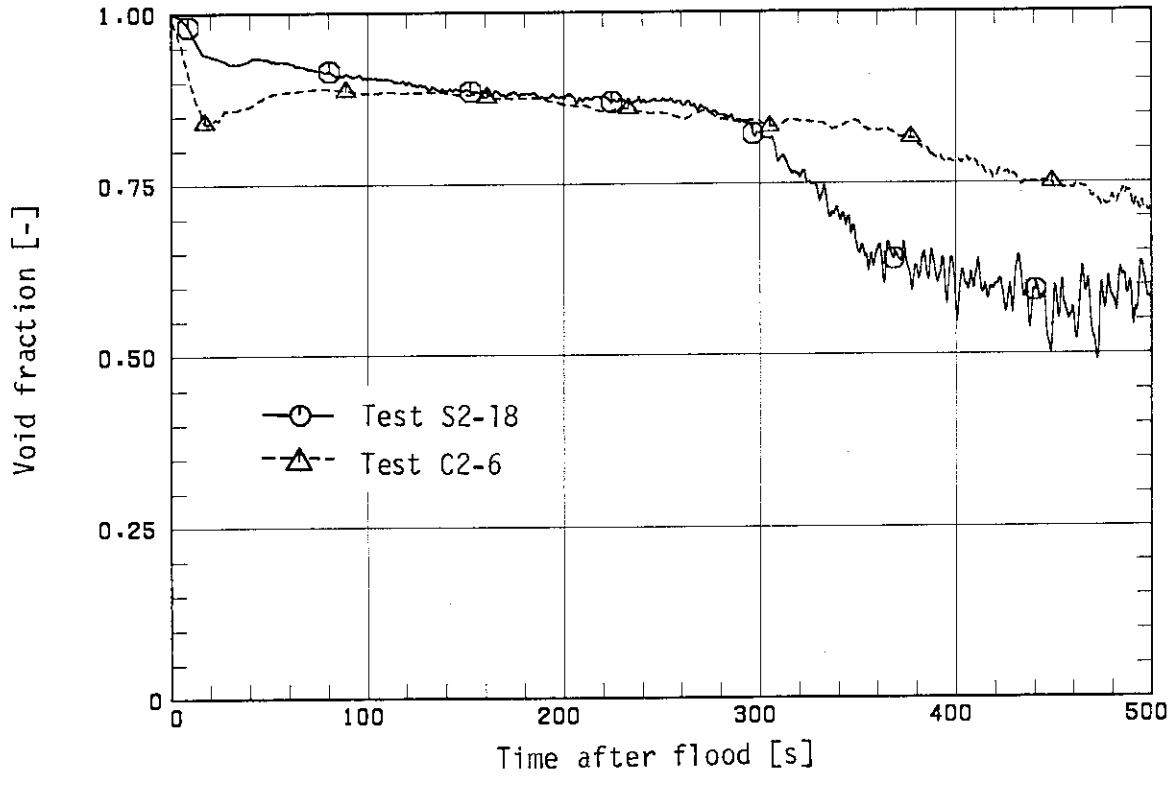

Fig. 3.23(f) Core void fraction (6)

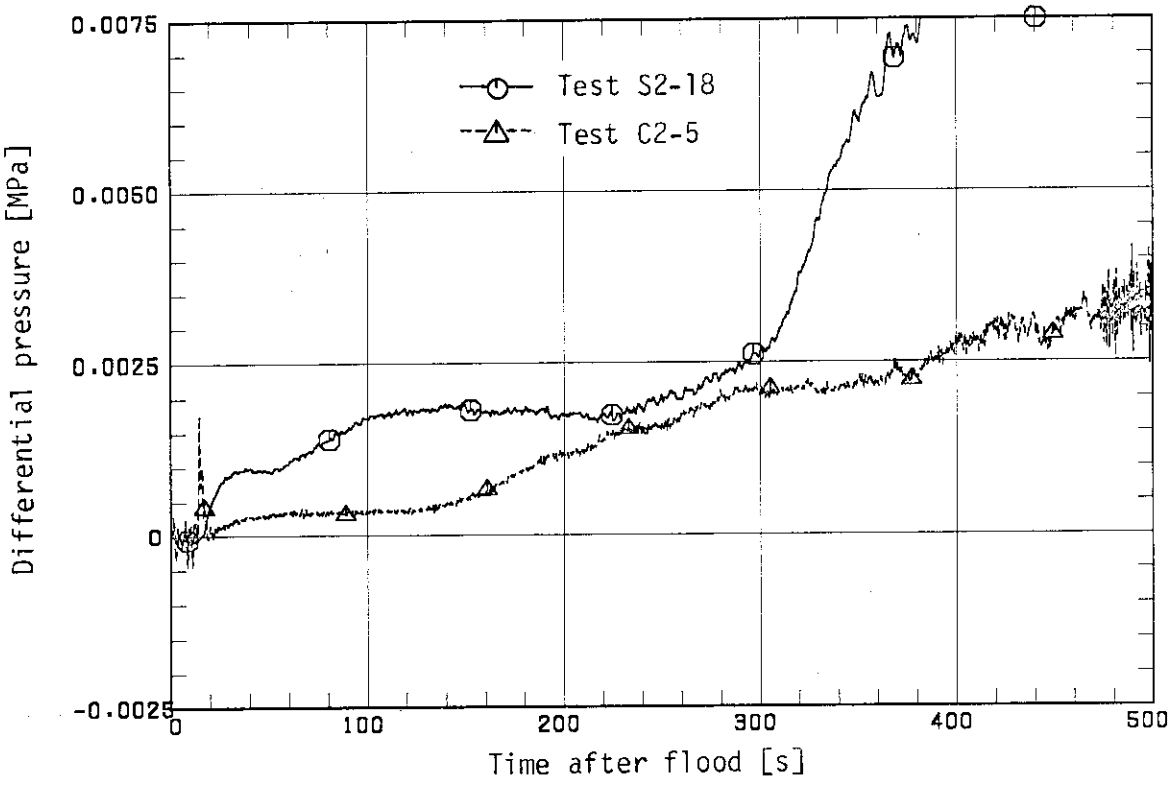

Fig. 3.24 Upper plenum differential pressure

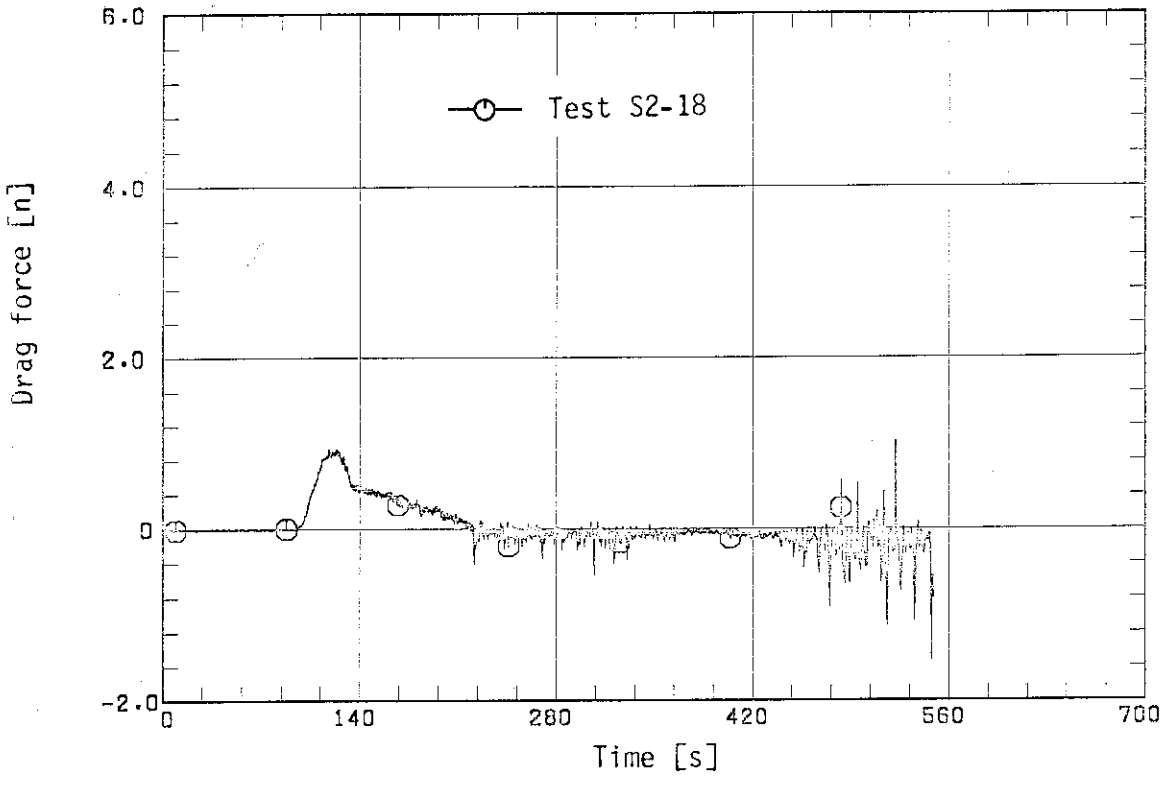

Fig. 3.25 Drag force in bottom region of hot leg

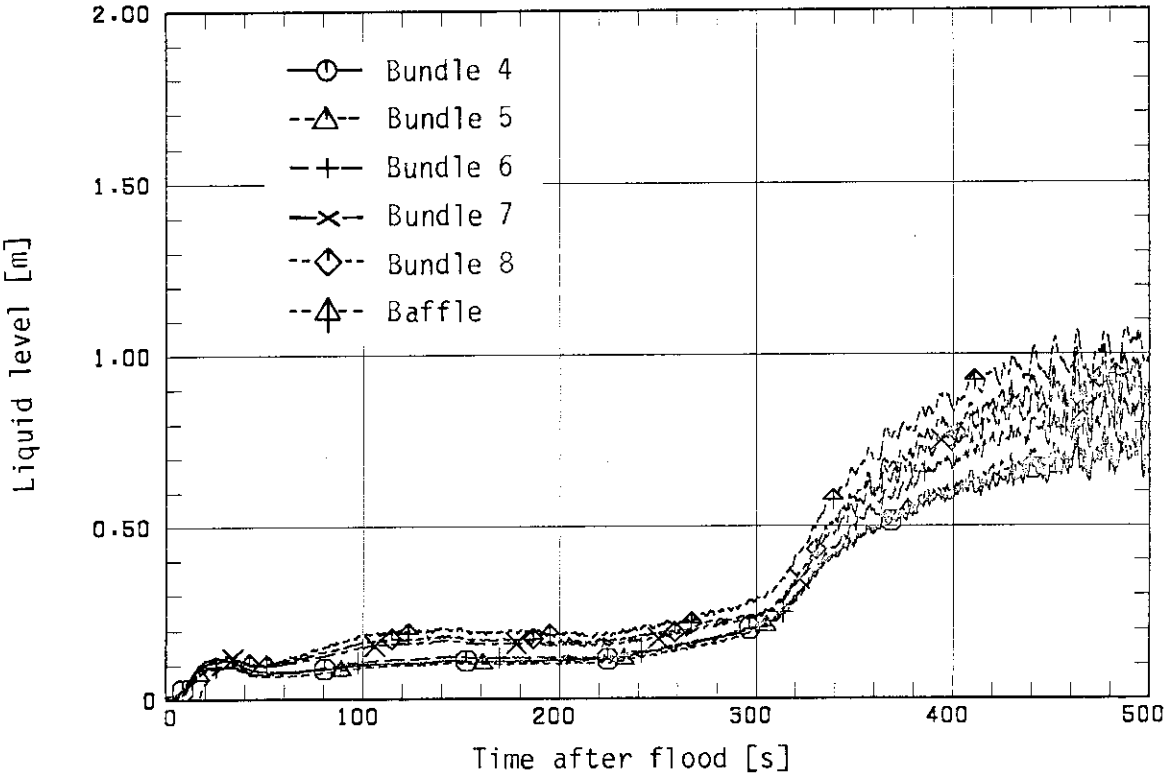

Fig. 3.26 Upper plenum water level above UCSP

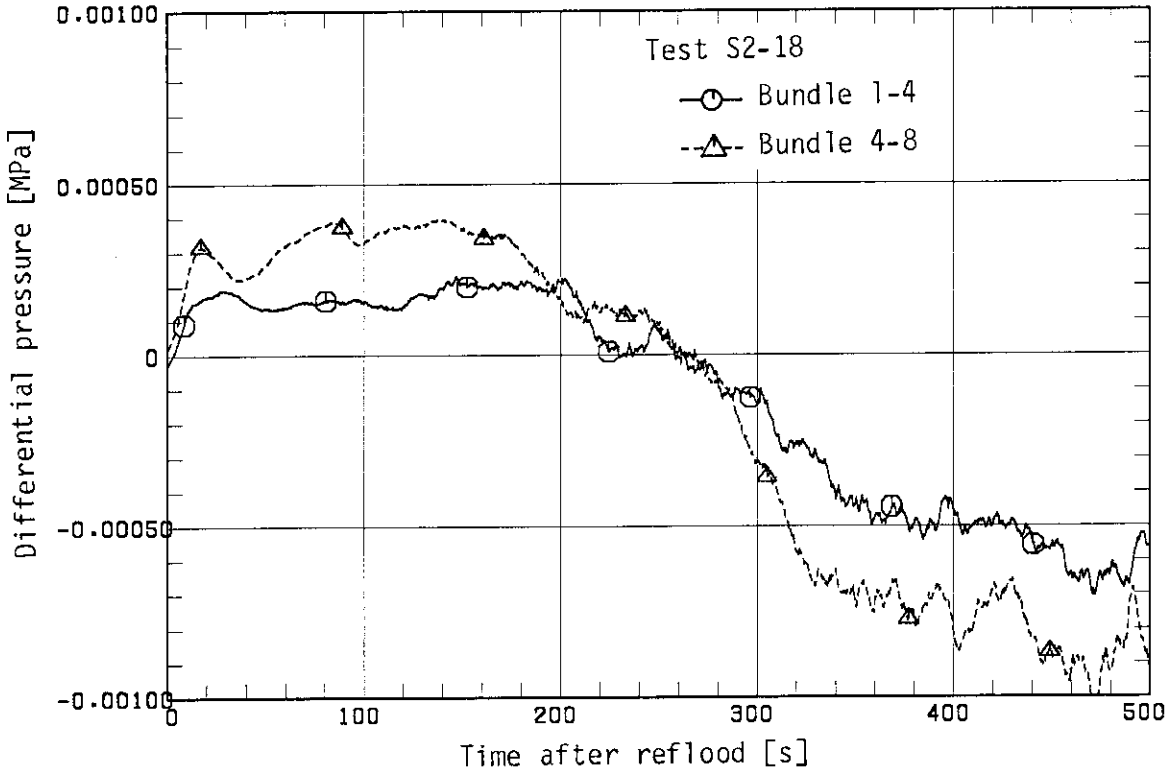

Fig. 3.27 Core horizontal differential pressure at 1.905 m elevation in Test S2-18

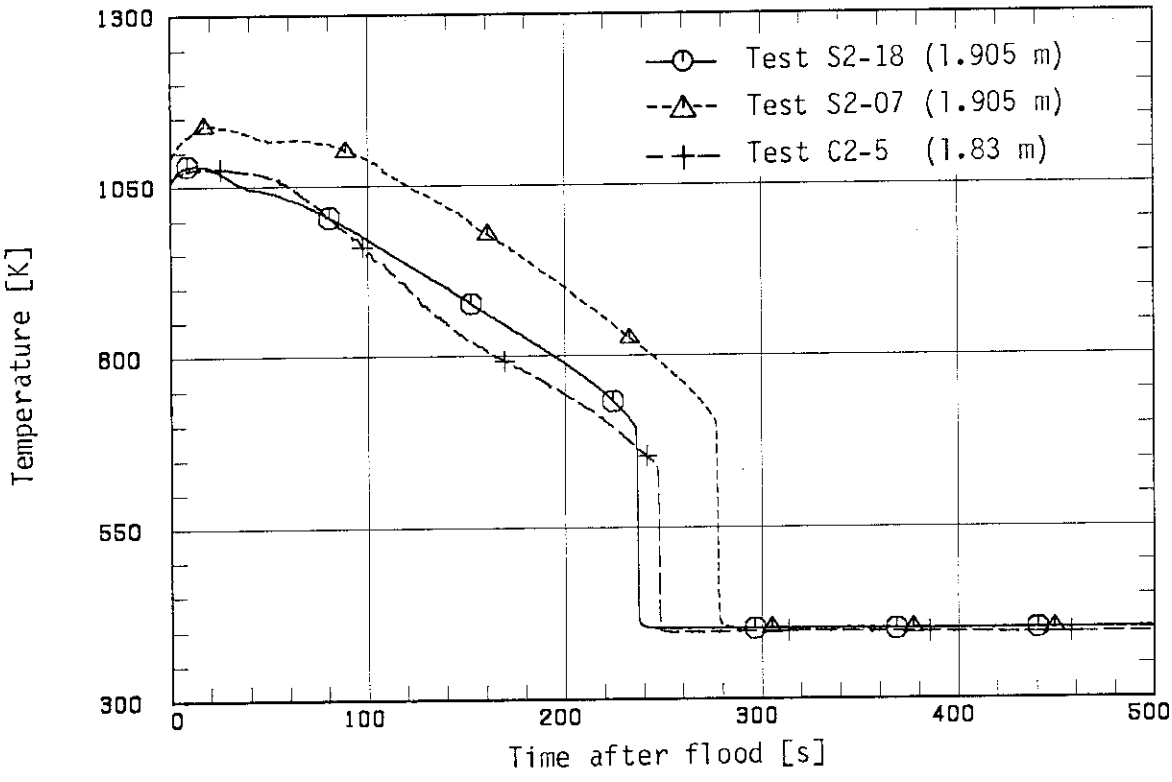

Fig. 3.28(a) Heater rod surface temperature history in high power region at midplane level

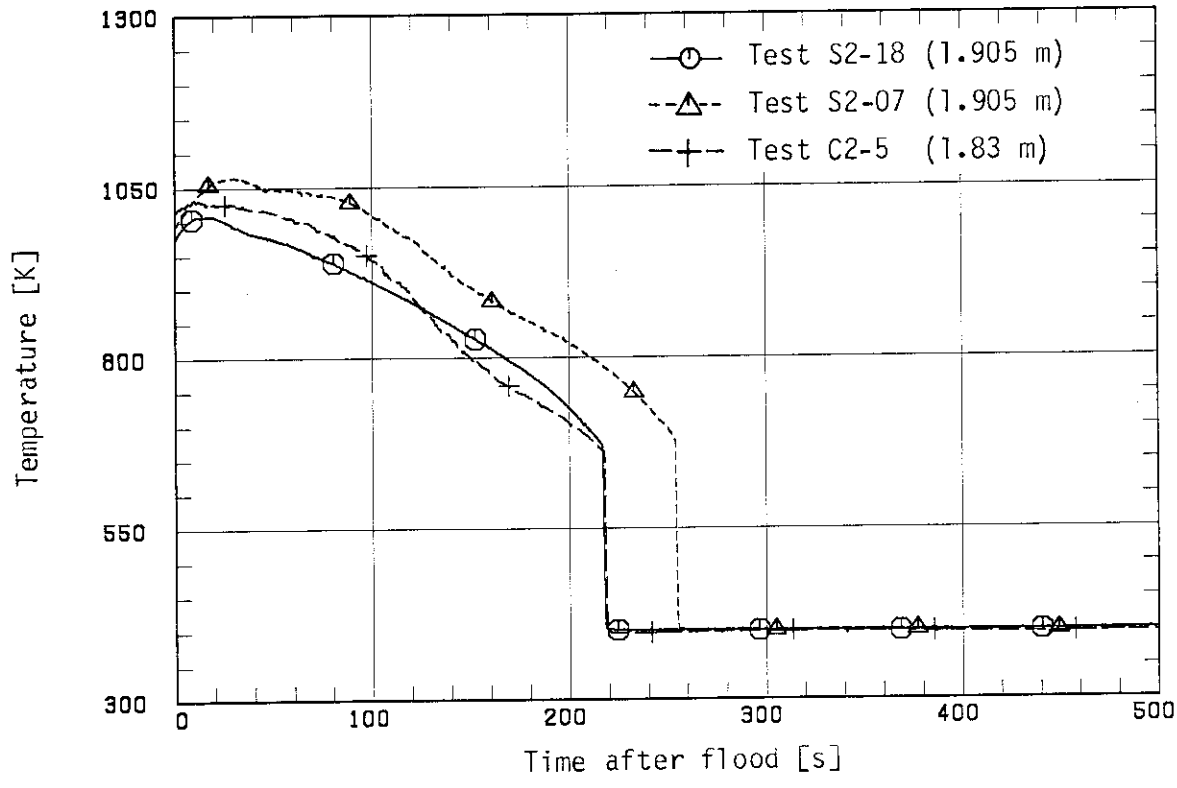

Fig. 3.28(b) Heater rod surface temperature history in medium power region at midplane level

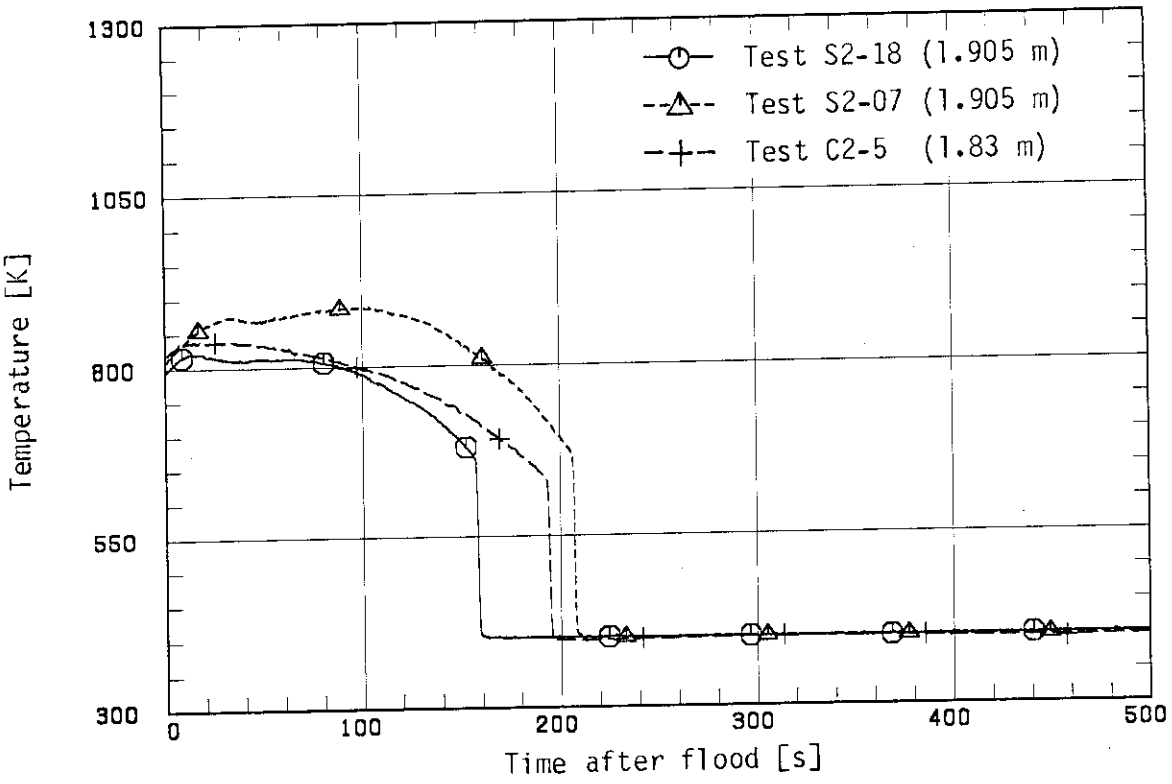

Fig. 3.28(c) Heater rod surface temperature history in low power region at midplane level

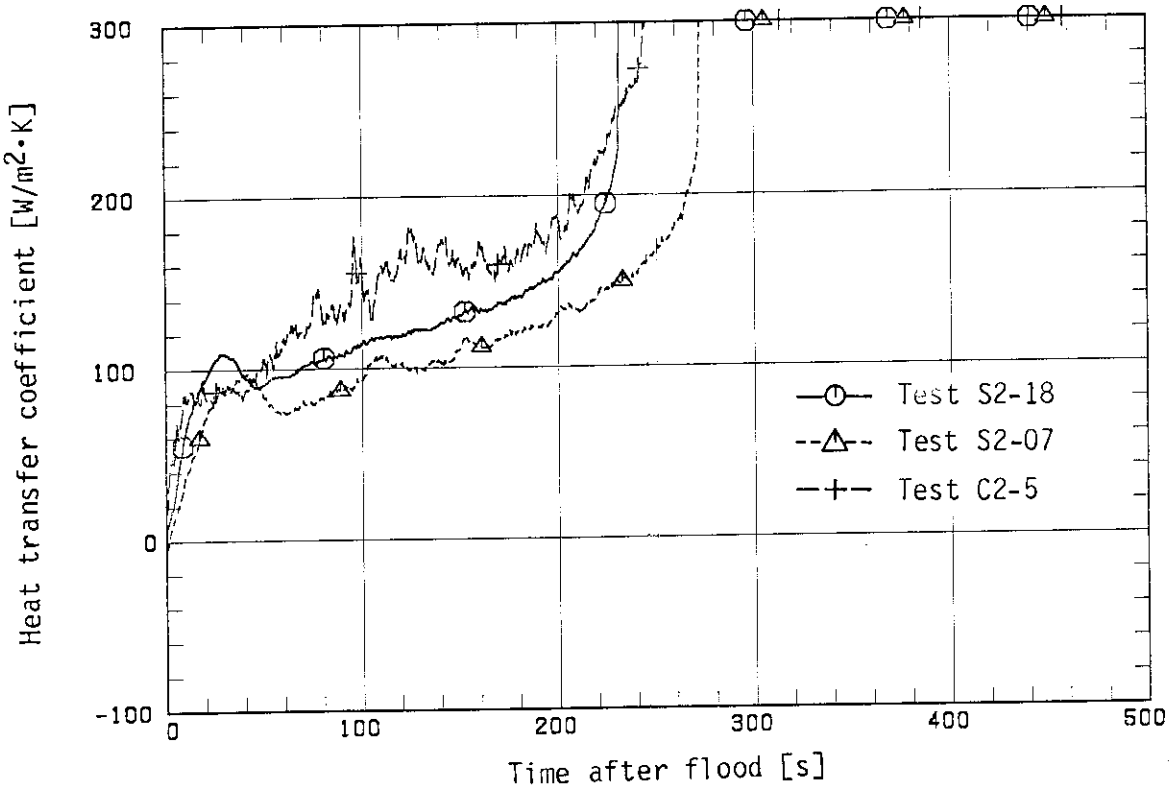

Fig. 3.29(a) Heat transfer coefficient history in high power region at midplane level

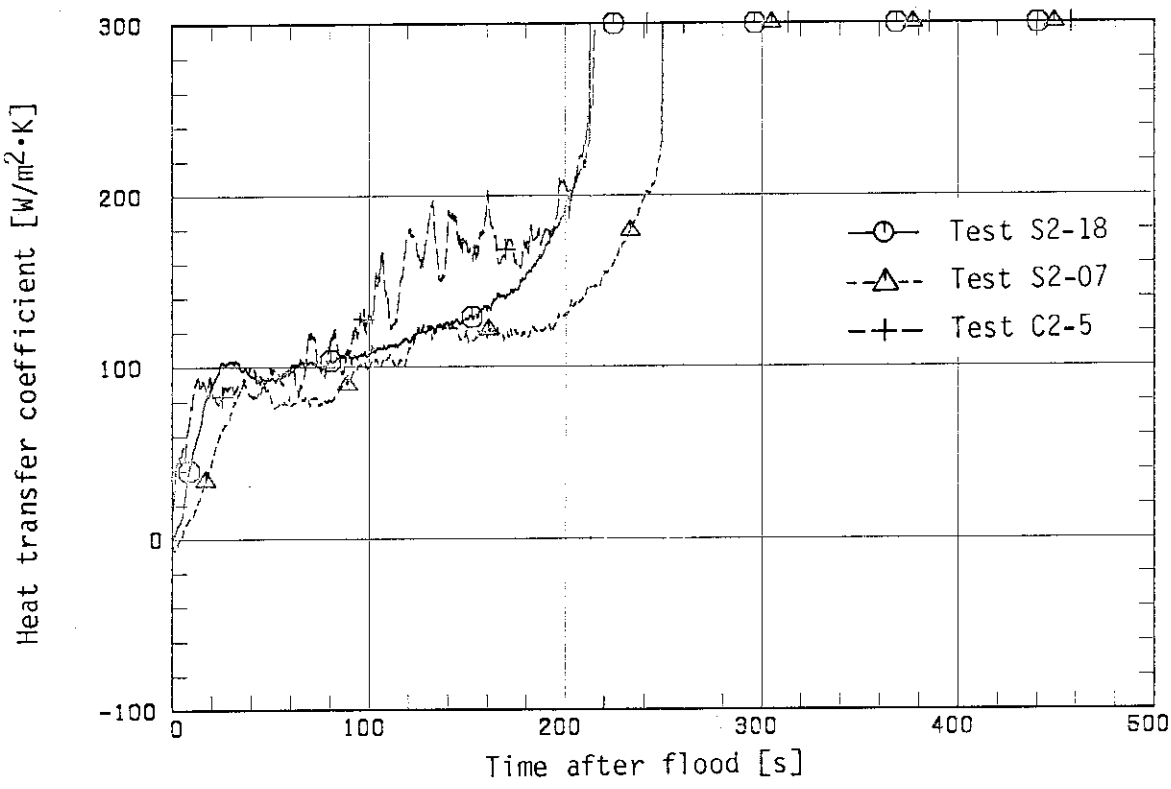

Fig. 3.29(b) Heat transfer coefficient history in medium power region at midplane level

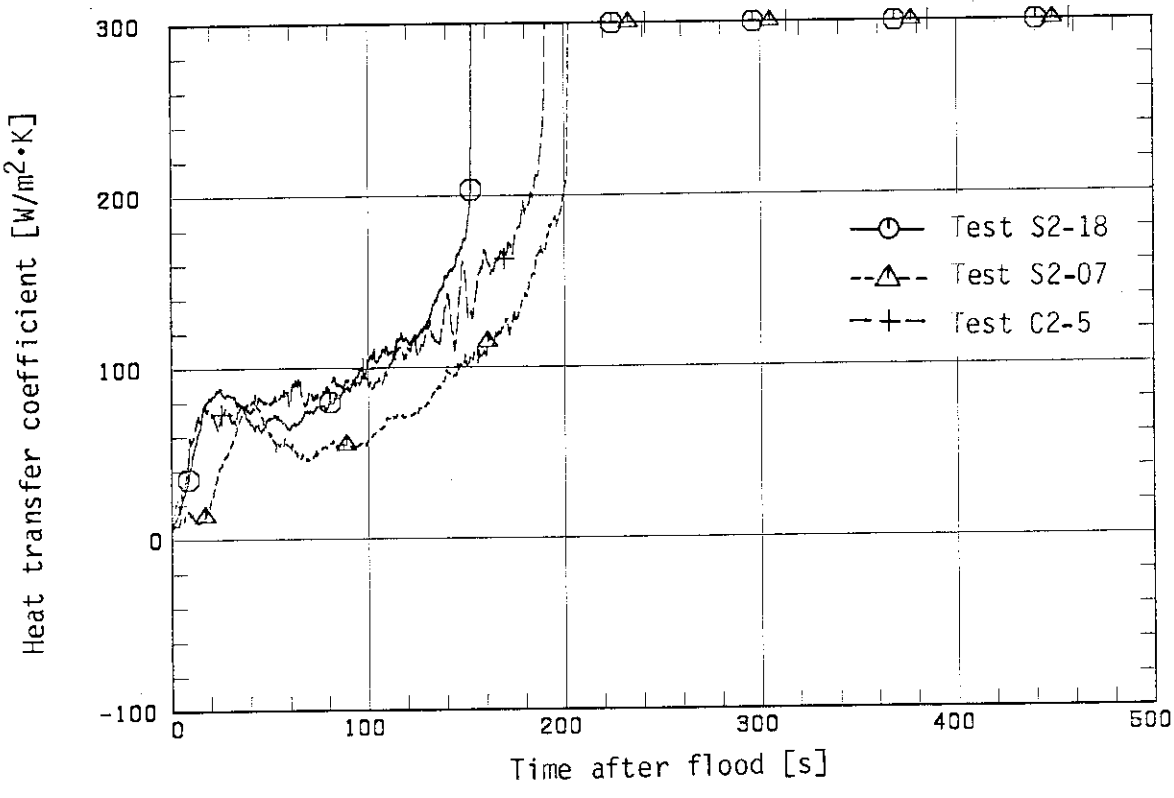

Fig. 3.29(c) Heat transfer coefficient history in low power region at midplane level

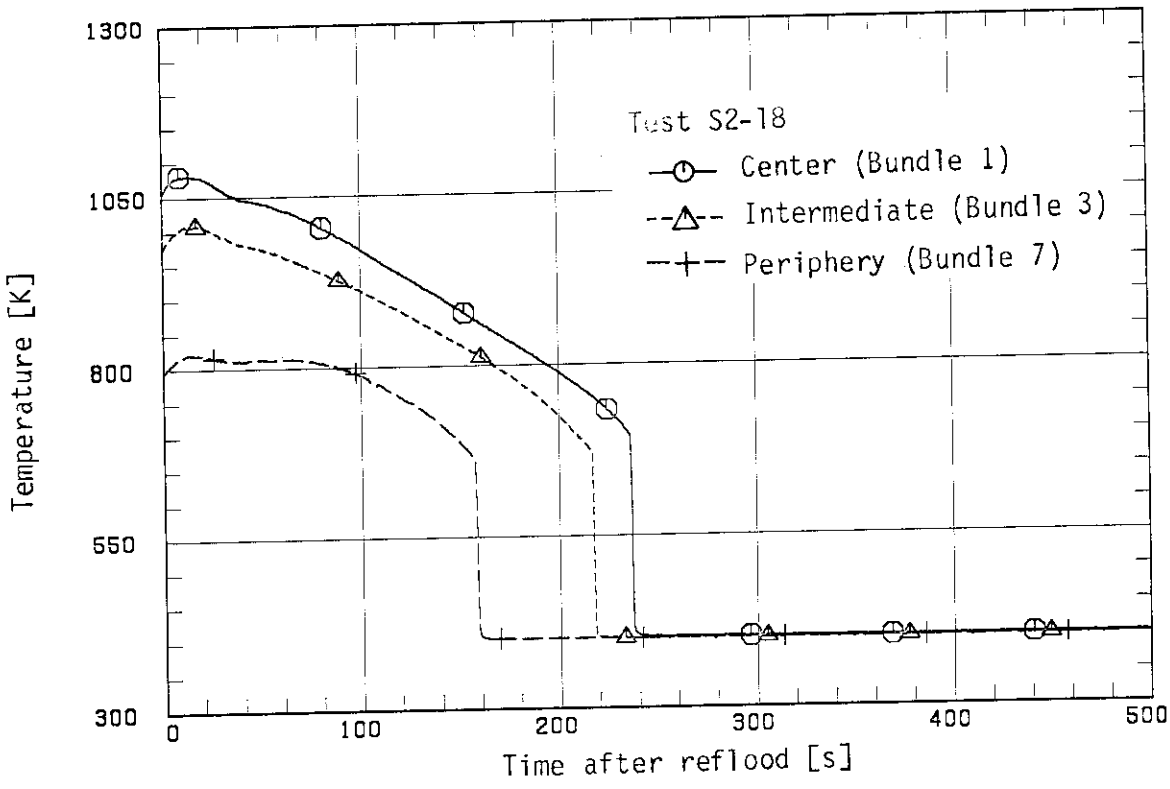

Fig. 3.30(a) Heater rod surface temperature history comparison in radial direction for Test S2-18 at 1.905 elevation

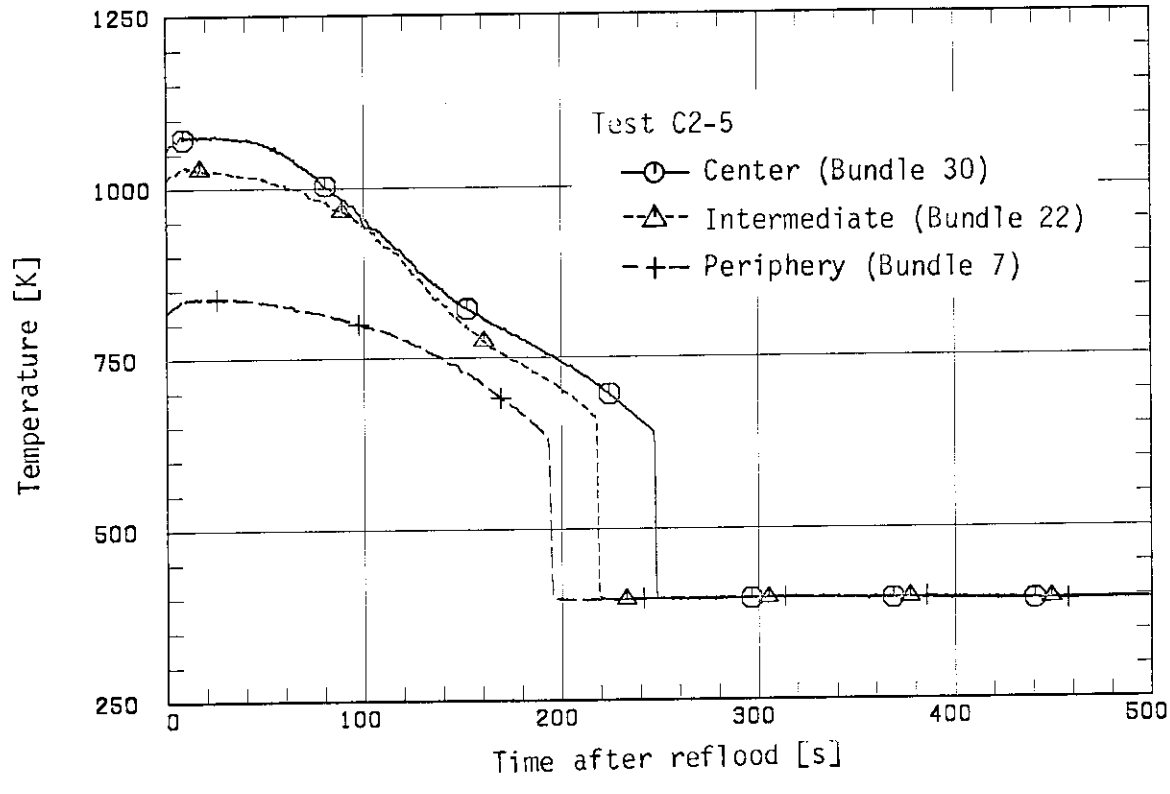

Fig. 3.30(b) Heater rod surface temperature history comparison in radial direction for Test C2-5 at 1.83 m elevation

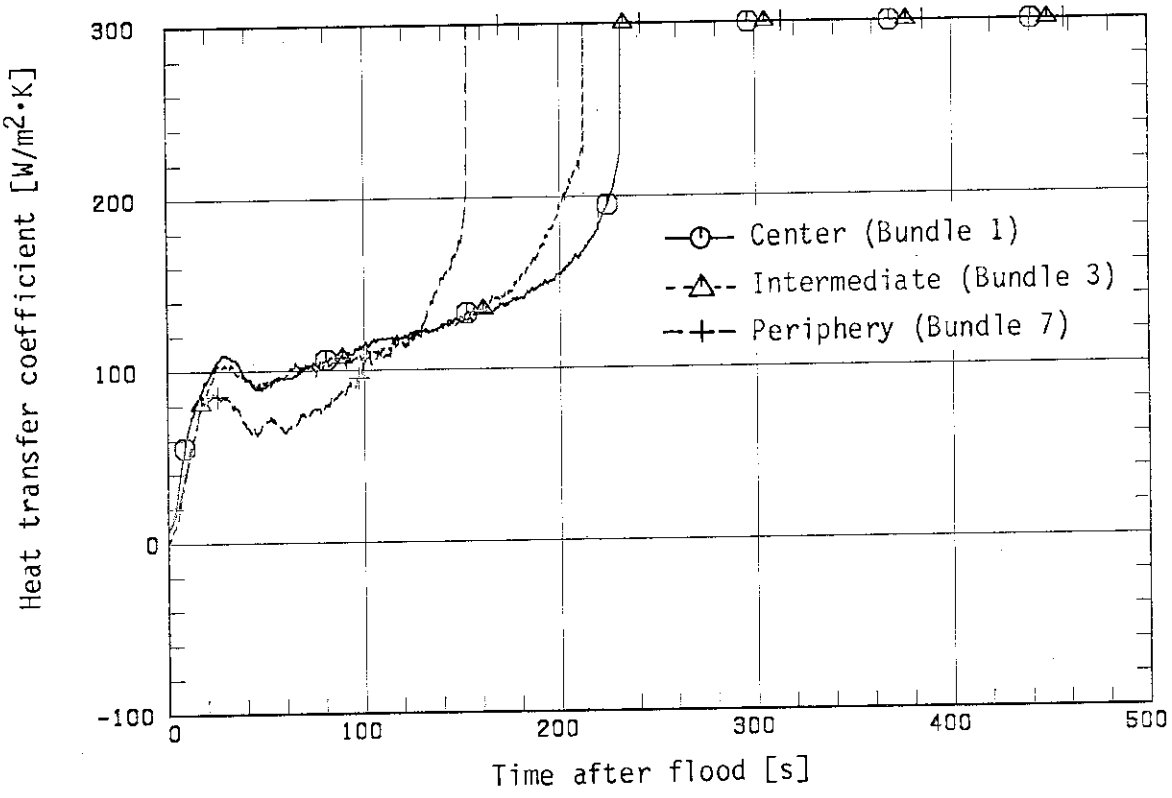

Fig. 3.31(a) Heat transfer coefficient history comparison in radial direction for Test S2-18 at 1.905 m elevation

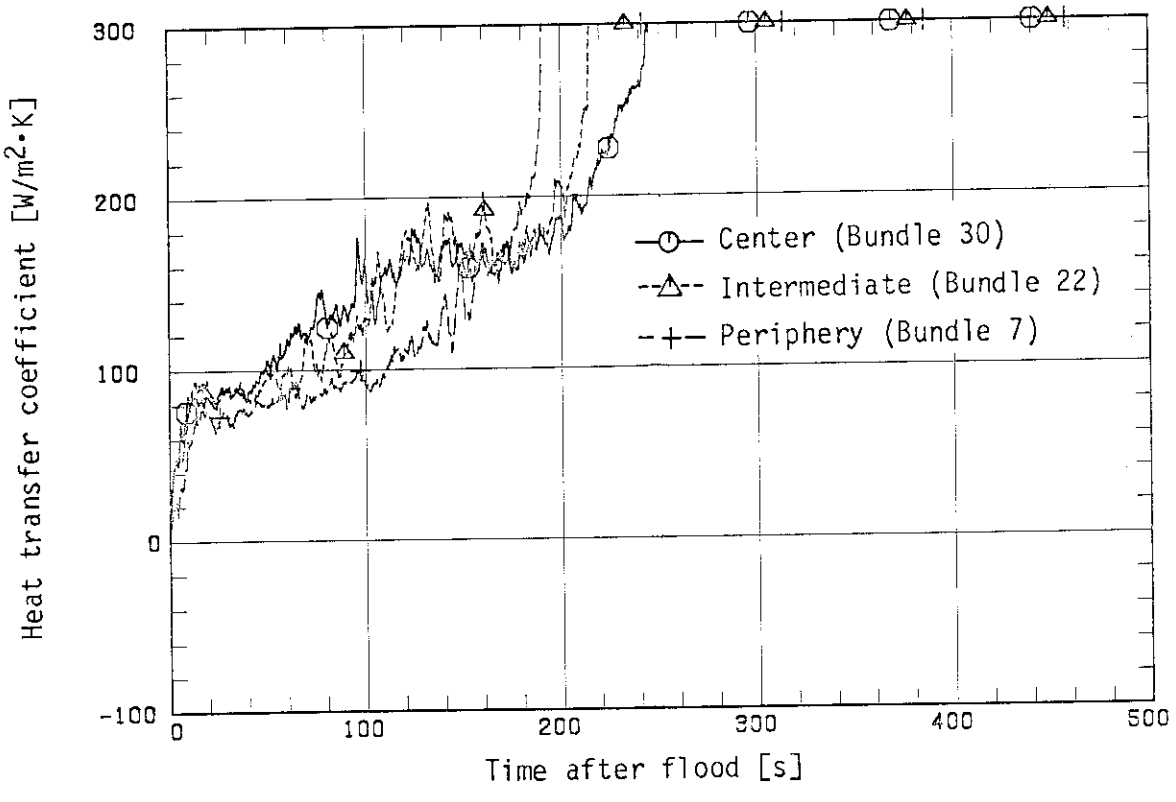

Fig. 3.31(b) Heat transfer coefficient history comparison in radial direction for Test C2-5 at 1.83 m elevation

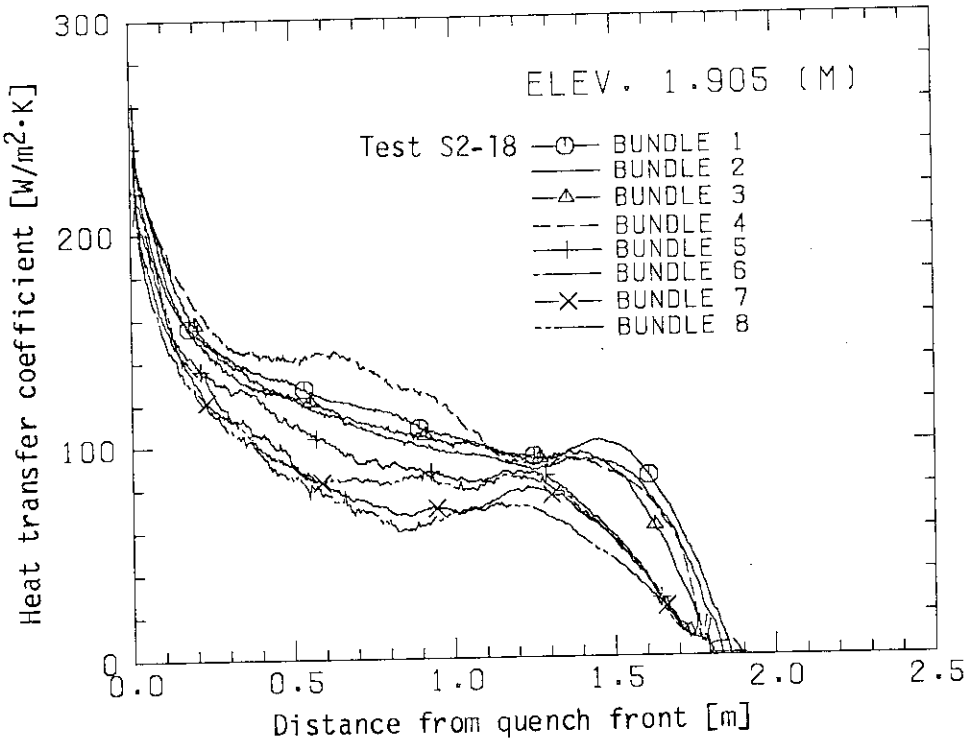

Fig. 3.32(a) Heat transfer coefficient history comparison in radial direction plotted against distance from quench front for Test S2-18 at 1.905 m elevation

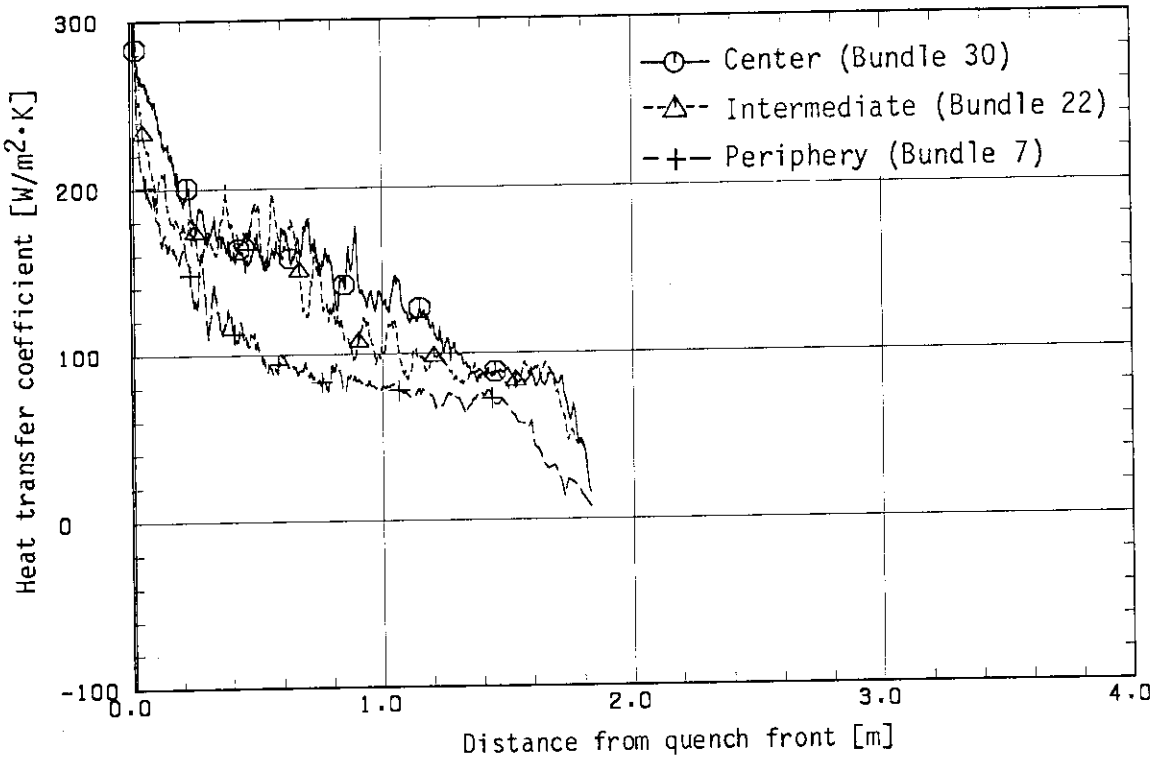

Fig. 3.32(b) Heat transfer coefficient history comparison in radial direction plotted against distance from quench front for Test C2-5 at 1.83 m elevation

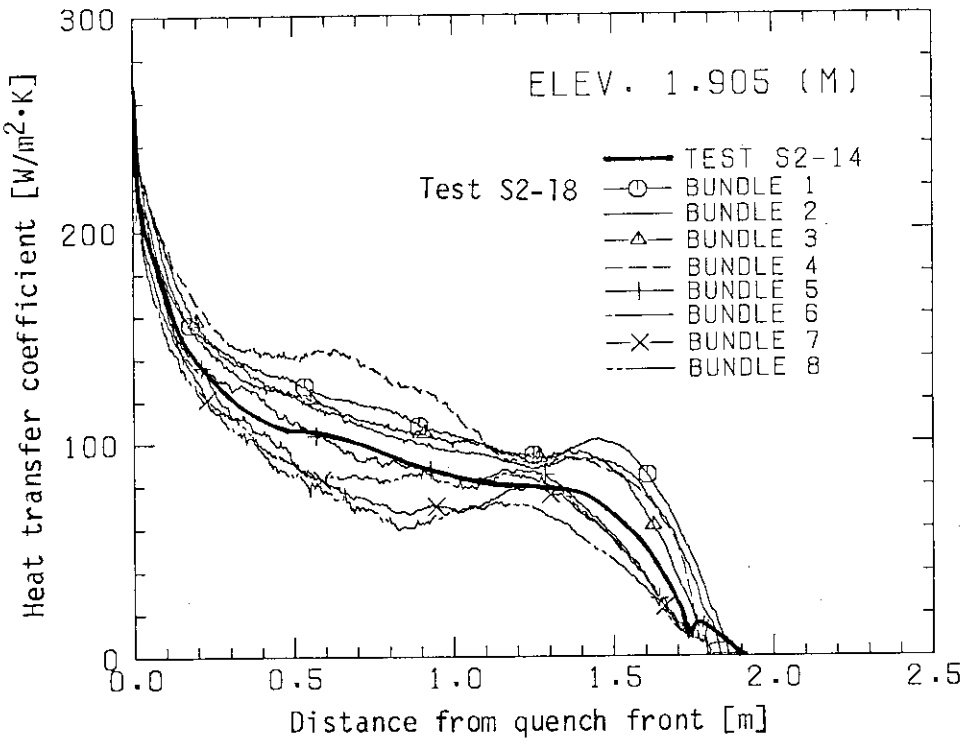

Fig. 3.32(c) Heat transfer coefficient history comparison between Tests S2-18 and S2-14 at 1.905 m elevation

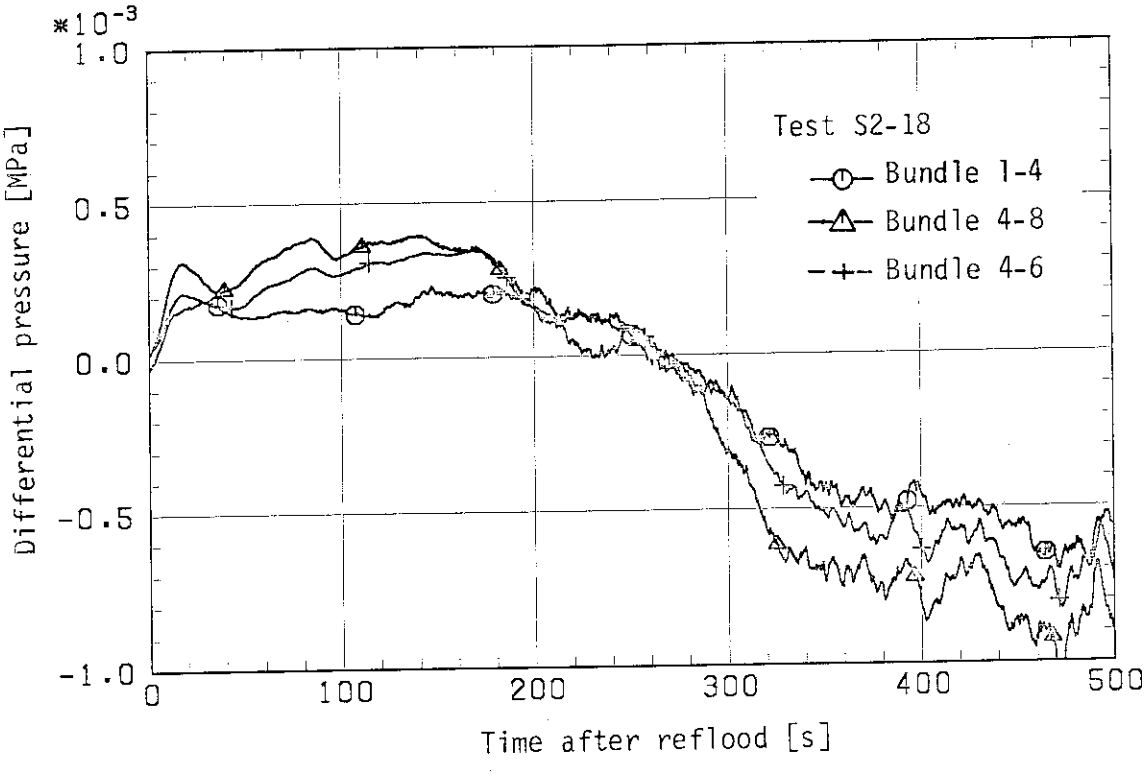

Fig. 3.33(a) Core horizontal differential pressure at 1.905 m elevation in Test S2-18

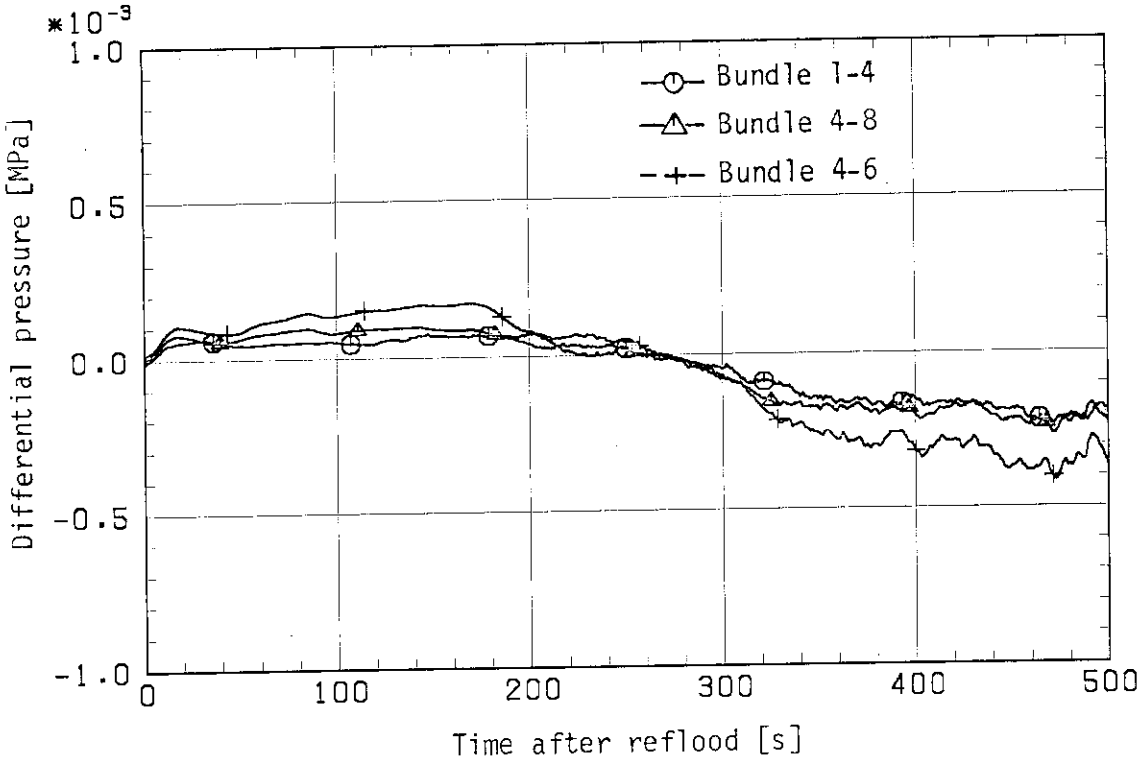

Fig. 3.33(b) Core horizontal differential pressure per bundle length at 1.905 m elevation in Test S2-18

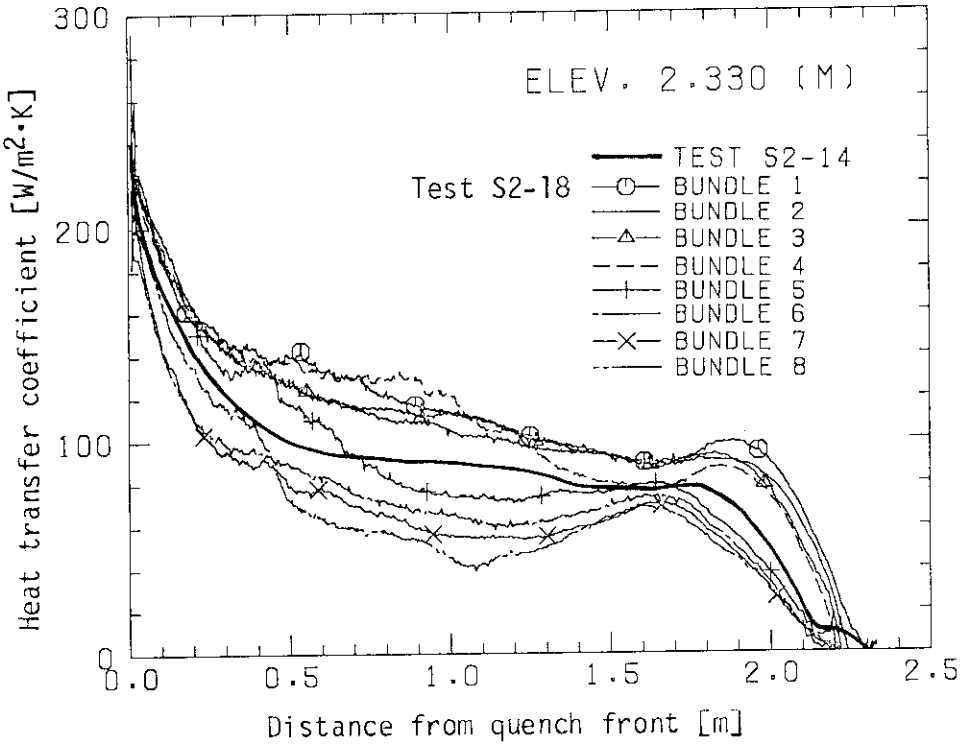

Fig. 3.34(a) Heat transfer coefficient history plotted against distance from quench front for SCTF tests at 2.33 m elevation

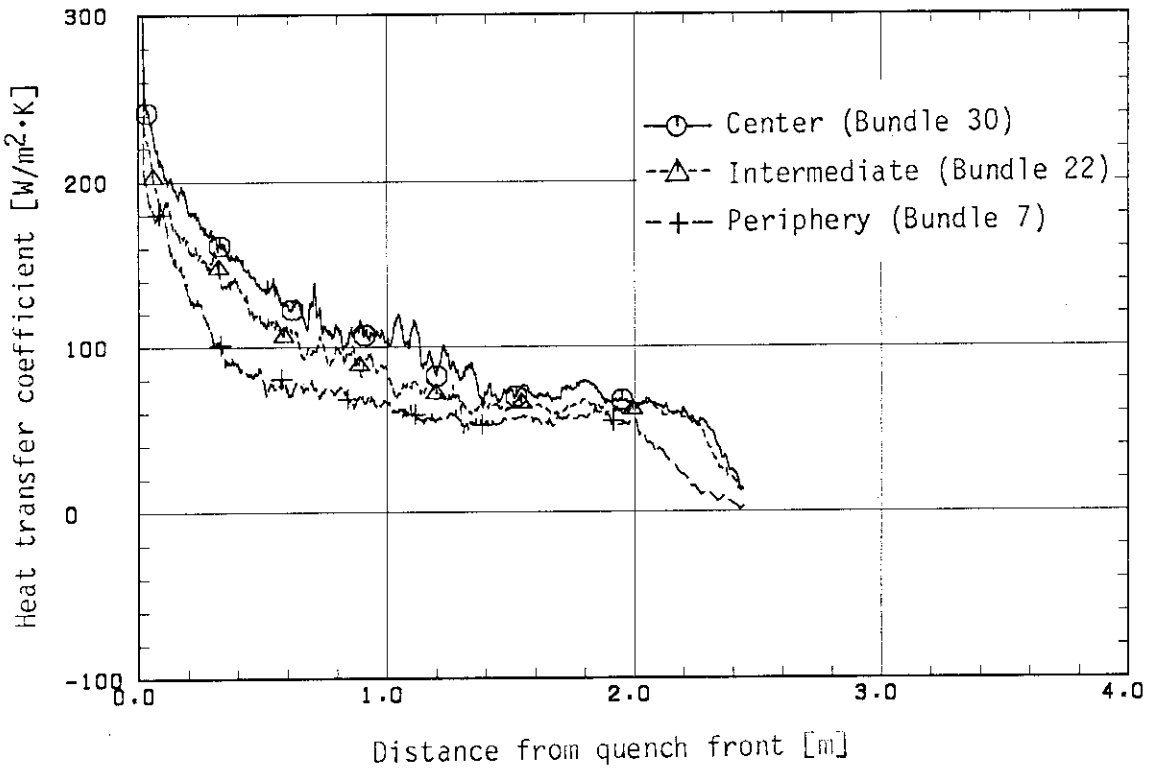

Fig. 3.34(b) Heat transfer coefficient history plotted against distance from quench front for CCTF Test C2-5 at 2.44 m elevation

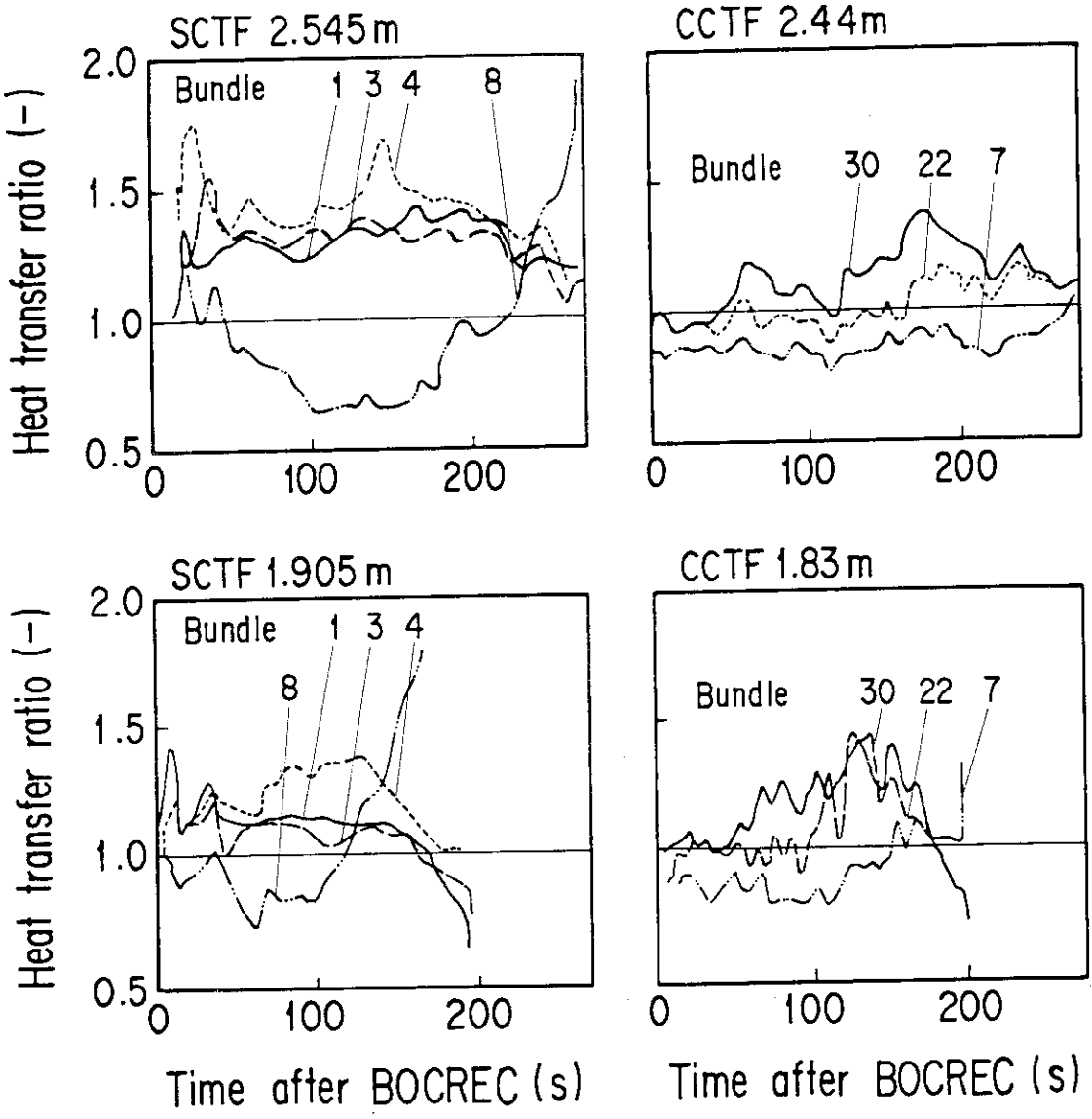

Fig. 3.34(c) Heat transfer ratios of slant radial core power profile test to flat radial core power profile test

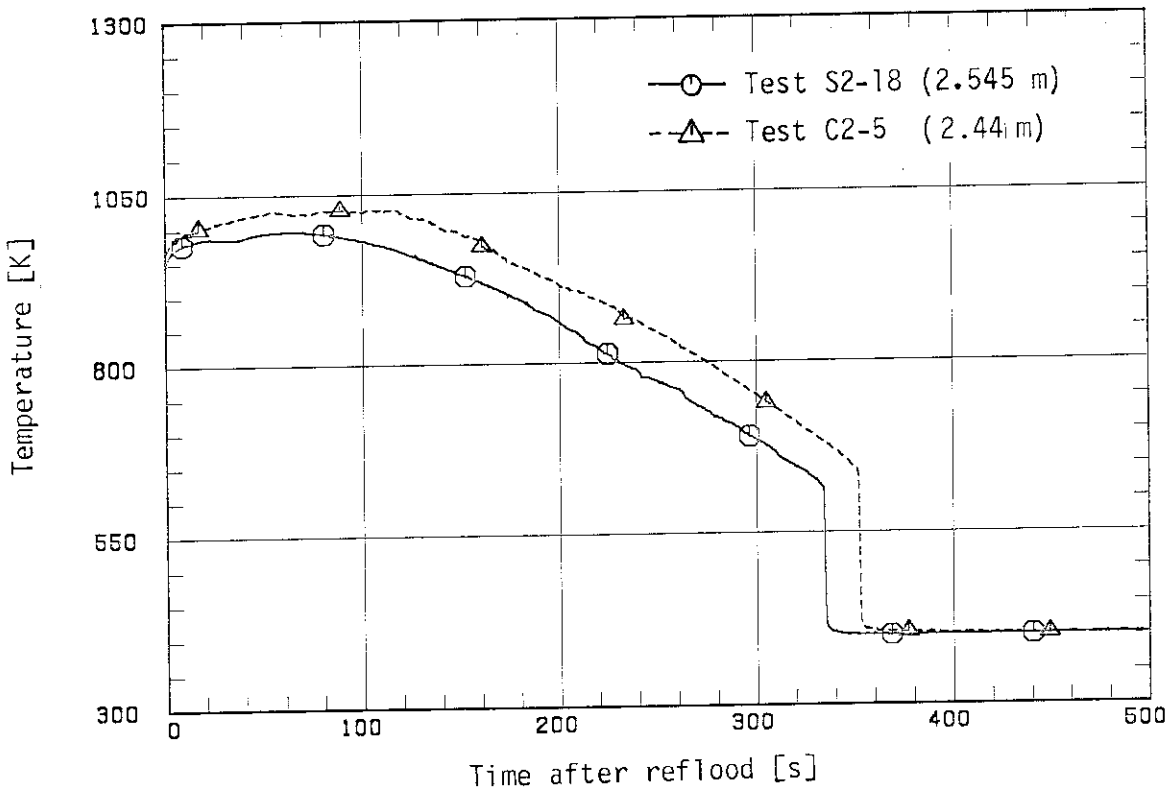

Fig. 3.34(d) Heater rod surface temperature history in core central side region at higher elevation than midplane level

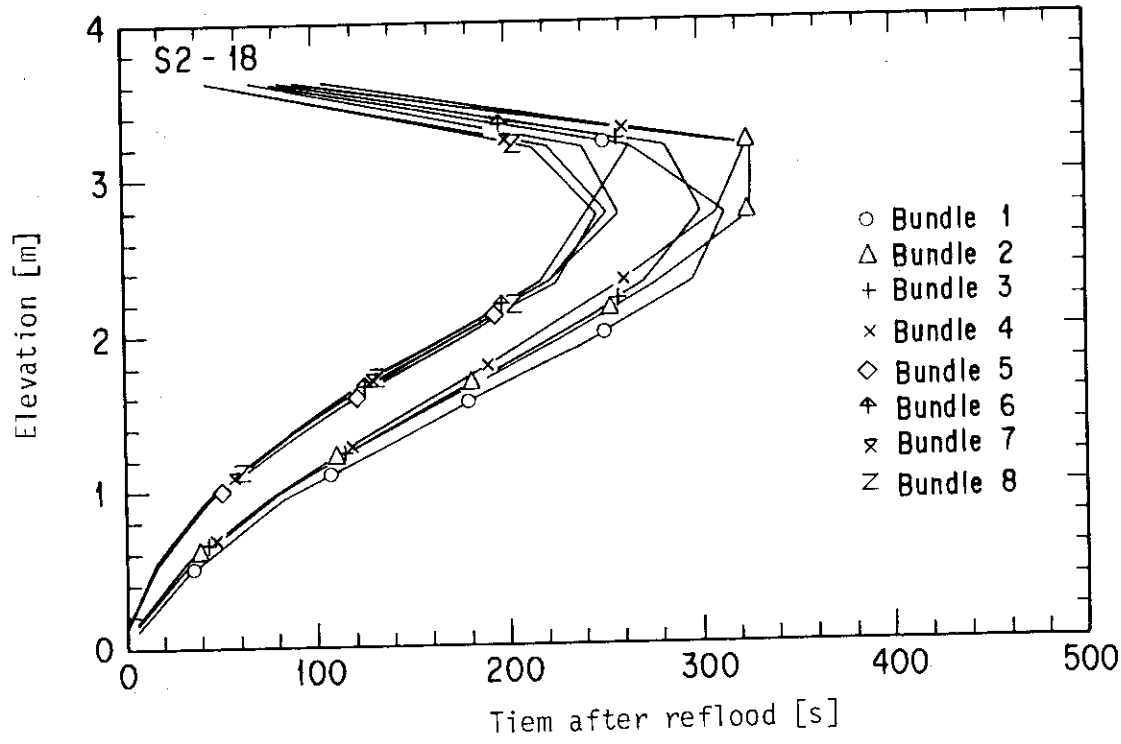

Fig. 3.35(a) Quench front envelope comparison in radial direction for Test S2-18

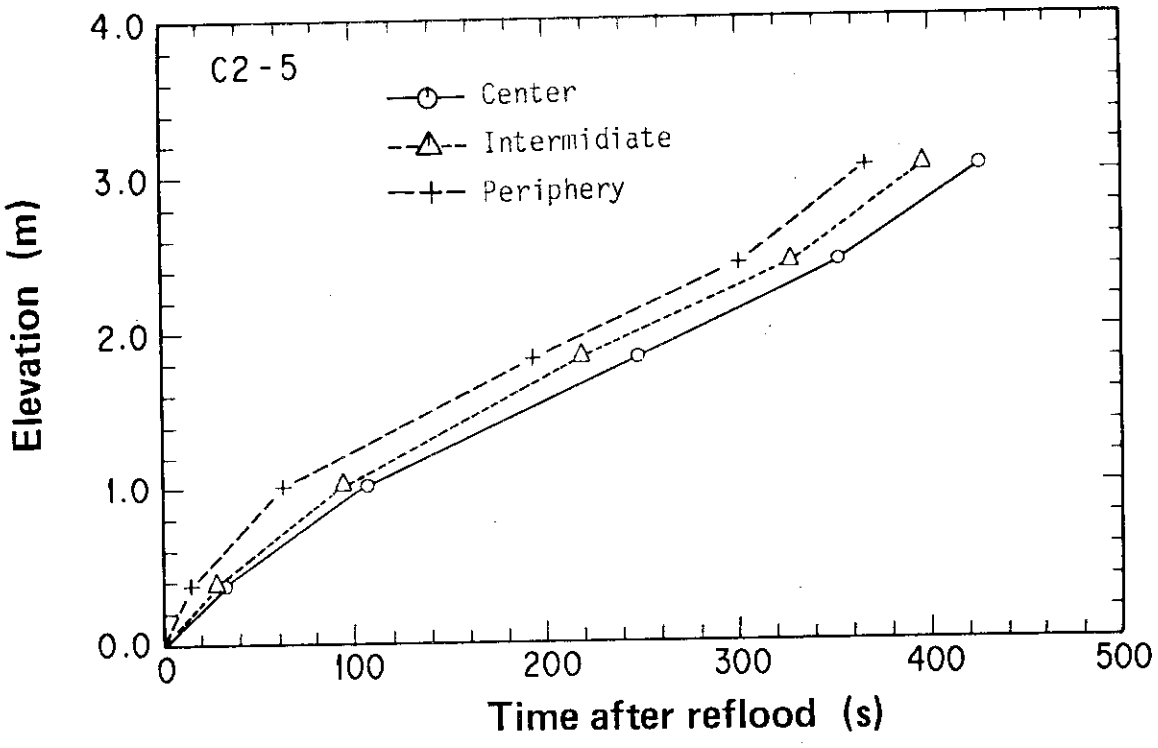

Fig. 3.35(b) Quench front envelope comparison in radial direction for Test C2-5

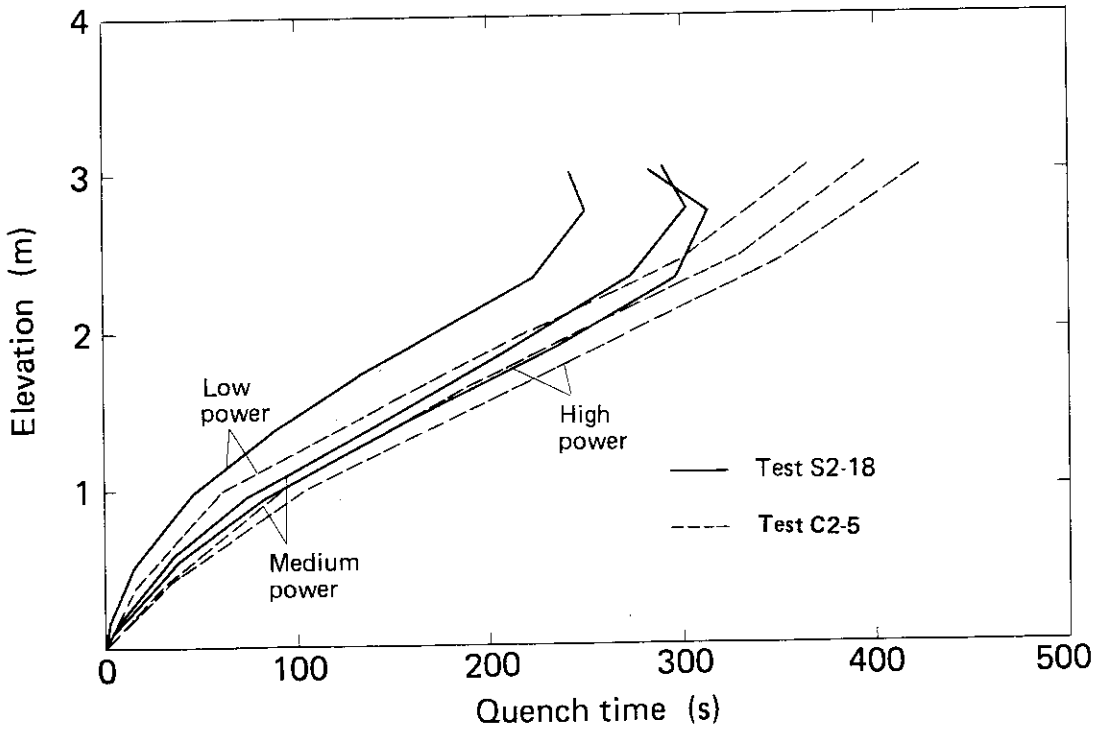

Fig. 3.35(c) Quench front envelope

4. Conclusions

Analyzing the data of the SCTF/CCTF counterpart tests and their corresponding CCTF tests, the following conclusions are obtained on the comparison of the reflooding behavior between the SCTF and the CCTF tests and on the effect of the core radial length on the two-dimensional core thermo-hydrodynamic behavior:

(1) Although there observed some differences between the SCTF and CCTF test results, the overall core reflooding behavior is considered to be similar taking account of the differences in test conditions and facility design. The main difference observed is core water accumulation characteristic. However, major part of this difference is quantitatively explained to be caused by the difference in the effective core flow area between the two facilities.

(2) The effect of the core radial length on the core two-dimensional thermo-hydrodynamic behavior has been observed to be significant and heat transfer enhancement or degradation in the radial direction is more significant for the longer radius core.

(3) In addition, where the core power varies significantly in the radial direction, a significant heat transfer enhancement has been observed in the higher power bundle during the LPCI period. On the other hand, in the peripheral region, the heat transfer degradation has been observed more significantly in the outer bundle even they have the same bundle power.

(4) Magnitude of the heat transfer enhancement or degradation was larger at the higher elevation than the midplane level in the SCTF test, whereas smaller in the CCTF test. This is considered to be caused by the difference in the upper plenum water accumulation distribution.

Acknowledgments

The authors wish to express their thanks to Mr. T. Iguchi and Dr. H. Akimoto for their helpful suggestions.

They are deeply indebted to Messrs. I. Arase, A. Kamoshida, T. Oyama, Y. Niitsuma, K. Nakajima, T. Chiba, H. Watanabe, K. Komori, H. Sonobe and A. Owada for their contribution to test conduction.

This work was performed under contract with the Atomic Energy Bureau of Science and Technology Agency of Japan.

4. Conclusions

Analyzing the data of the SCTF/CCTF counterpart tests and their corresponding CCTF tests, the following conclusions are obtained on the comparison of the reflooding behavior between the SCTF and the CCTF tests and on the effect of the core radial length on the two-dimensional core thermo-hydrodynamic behavior:

(1) Although there observed some differences between the SCTF and CCTF test results, the overall core reflooding behavior is considered to be similar taking account of the differences in test conditions and facility design. The main difference observed is core water accumulation characteristic. However, major part of this difference is quantitatively explained to be caused by the difference in the effective core flow area between the two facilities.

(2) The effect of the core radial length on the core two-dimensional thermo-hydrodynamic behavior has been observed to be significant and heat transfer enhancement or degradation in the radial direction is more significant for the longer radius core.

(3) In addition, where the core power varies significantly in the radial direction, a significant heat transfer enhancement has been observed in the higher power bundle during the LPCI period. On the other hand, in the peripheral region, the heat transfer degradation has been observed more significantly in the outer bundle even they have the same bundle power.

(4) Magnitude of the heat transfer enhancement or degradation was larger at the higher elevation than the midplane level in the SCTF test, whereas smaller in the CCTF test. This is considered to be caused by the difference in the upper plenum water accumulation distribution.

Acknowledgments

The authors wish to express their thanks to Mr. T. Iguchi and Dr. H. Akimoto for their helpful suggestions.

They are deeply indebted to Messrs. I. Arase, A. Kamoshida, T. Oyama, Y. Niitsuma, K. Nakajima, T. Chiba, H. Watanabe, K. Komori, H. Sonobe and A. Owada for their contribution to test conduction.

This work was performed under contract with the Atomic Energy Bureau of Science and Technology Agency of Japan.

References

[1] Hirano, K. and Murao, Y.: Large Scale Reflood Test, Nihon-Genshiryoku-Gakkai Shi (J. At. Energy Soc. Japan), 22[10], 681 (1980) [in Japanese].

[2] Sobajima, M. *et al.*: Design of Slab Core Test Facility (SCTF) in Large Scale Reflood Test Program, Part II: Core-II, to be published as a JAERI-M report.

[3] Iwamura, T. *et al.*: Two-dimensional Thermal-hydraulic Behavior in Core in SCTF Core-II Forced Feed Reflood Tests, JAERI-M 86-195 (1987).

[4] Iguchi, T. *et al.*: Evaluation Report on CCTF Core-II Reflood Test C2-5 (Run 63) -- Investigation of the Reflood Phenomena under Low Power Condition -- , to be published as a JAERI-M Report.

[5] Akimoto, H. *et al.*: Evaluation Report on CCTF Core-II Reflood Test C2-6 (Run 64) -- Effect of Radial Power Profile --, JAERI-M 85-027 (1985).

[6] Iguchi, T. and Murao, Y.: Predictability of REFLA Core Model for SCTF data, JAERI-M 87-163 (1987) [in Japanese].

[7] Murao, Y. *et al.*: REFLA-1D/MODE3: A Computer Code for Reflood Thermo-hydrodynamic Analysis during PWR-LOCA -- User's Manual --, JAERI-M 84-243 (1985).

[8] Iwamura, T. *et al.*: Effect of Radial Power Profile on Two-Dimensional Thermal-hydraulic Behavior in Core in SCTF Core-II Cold Leg Injection Tests, JAERI-M 85-106 (1985).

[9] For instance: Murao, Y. *et al.*: Analysis Report on CCTF Core-I Reflood Tests, to be published as a JAERI-M report.

[10] Iguchi, T. *et al.*: Visual Study of Flow Behavior in Upper Plenum during Simulated Reflood Phase of PWR-LOCA, J. Nucl. Sci. Technol., 20[8], 698 (1983).

Appendix A

Description of SCTF Core-Ⅱ

A.1 Test Facility

The Slab Core Test Facility is designed under the following design philosophy and design criteria:

a. Design Philosophy

(1) The facility should provide the capability to study the two-dimensional thermohydraulic behavior in a reactor pressure vessel especially due to the radial power distribution during the end of blowdown, refill and reflood pahses of a postulated LOCA in a PWR.

(2) To properly simulate the core heat transfer and hydrodynamics, a special emphasis is put on the proper simulation of the components in the pressure vessel. Provided as the components in the pressure vessel are the simulated core, downcomer, core baffle region, lower plenum, upper plenum and upper head. On the other hand, simplified primary coolant loops are also provided. Provided as the primary coolant loop components are a hot leg, an intact cold leg, broken cold legs and a steam/water separator which is to simulate single steam phase flow downstream of a steam generator and to measure the flow rate of carryover water coming from the upper plenum.

b. Design Criteria

(1) The reference reactor to be simulated in SCTF is the Trojan reactor in the United States which is a four-loop 3300 MWt PWR. The Ooi reactor etc. in Japan which are of the similar type to the Trojan reactor except the provision of UHI system are also referred.

(2) A full scale radial and axial section of core with single bundle width of the pressurized water reactor is provided as the simulated core of SCTF.

(3) The simulated core consists of 8 bundles arranged in a row. Each bundle has electrically heated rods simulating fuel rods and non-heated rods with 16×16 array, with the diameter and the pitch for Trojan which has 15×15 rod array.

(4) The flow area and fluid volume of components are scaled down based on the nominal core flow area scaling, 1/21.

(5) To properly simulate the flow behavior of carryover water or entrainment, the elevations of hot leg and cold legs are designed to be the same as the PWR as much as possible.

(6) A honeycomb structure is used for side walls with surface plates

which accomodates the slab core, the upper plenum and the upper part of lower plenum, so as to minimize the effect of walls on the core heat transfer and hydrodynamics.

(7) To investigate the effect of flow resistance in the primary loop are provided the orifices of which dimension is changeable.

(8) The maximum allowable temperature of the simulated fuel rods is 900°C (1173 K) and the maximum allowable pressure of the facility is 0.6 MPa.

(9) The facility is equipped with the hot leg equivalent to four hot legs connecting the upper plenum and the steam/water separator, the intact cold leg equivalent to three intact cold legs connecting the steam/water separator and the downcomer and the two broken cold legs, one is for the steam/water separator side and another for the pressure vessel side.

(10) The ECCS consists of an accumulator (Acc), a low pressure coolant injection (LPCI) system and a combined injection system.

(11) ECC water injection ports are at the cold leg, the hot leg, the upper plenum, the downcomer, the lower plenum and above the upper core support plate. These ports are to be chosen according to the objective of the test.

(12) For better simulation of lower plenum flow resistance, simulated fuel rods do not penetrate through the bottom plate of the lower plenum but terminate at below the bottom of the core.

(13) For measurements in the pressure vessel including core, the feature of the slab geometry of the pressure vessel is utilized as much as possible. Design and arrangement of the instruments are done so as to be able to carry out installation, calibration and removal of the instruments.

(14) View windows are provided where flow pattern recognition is important. Their locations are the interface between the core and the upper plenum, the hot leg, the pressure vessel side broken cold leg and the downcomer.

(15) Blocked bundle test is carried out in Core-I in order to investigate the effect of ballooned fuel rods on core cooling and unblocked normal bundle test follows in the Core-II and -III.

(16) Types of break simulated are cold leg break and hot leg break.

(17) The components and systems such as the containment tanks and ECC water supply system in CCTF are shared with SCTF to the maximum extent.

The overall schematic diagram of SCTF is shown in Fig. A-1. The principal dimensions of the facility is shown in Table A-1, and the comparison of dimensions between SCTF and the reference PWR is shown in Fig. A-2.

A.1.1 Pressure Vessel and Internals

The pressure vessel is of slab geometry as shown in Fig. A-3. The height of the components in the pressure vessel is almost the same as the reference reactor's, and the flow area and the fluid volume of each component are scaled down based on the nominal core flow area scaling, 1/21.

The core consists of 8 bundles arranged in a row and each bundle includes heater rods and non-heated rods with 16×16 array. The core is enveloped by the honeycomb thermal insulator which is attached on the back surface of core wall plate.

The downcomer is located at one end of the pressure vessel which corresponds to the periphery of the actual reactor pressure vessel. The core baffle region located between the core and the downcomer is basically isolated for Core-II to minimize uncertainty in actual core flow. However, some leak holes are still existing. For better understanding, the cross section of the pressure vessel at the elevation of midplance of the core is shown in Fig. A-4.

The design of upper plenum internals is based on that for the new Westinghouse 17×17 array fuel assemblies. The internals consist of control rod guide tubes, support columns and orifice plates which are attached to the upper core support plate (UCSP). The UCSP has some open holes without internals. Those arrangement is shown in Fig. A-5. The radius of each internal is scaled down based on the factor of 8/15 of an actual reactor. Baffle plates are inserted in the guide tubes. The elevation and the configuration of baffle plates are shown in Fig. A-6.

The heights of the hot leg and cold legs are designed as close to the reference PWR as possible. However, in order to avoid the interference of the nozzles in the downcomer, the heights of nozzles for the broken cold leg and the intact cold leg are shifted down compared to that of the hot leg as shown in Fig. A-3.

A.1.2 Simulated Core

The simulated core for the SCTF Core-II consists of 8 heater rod bundles arranged in a row. Each bundle has 234 electrically heated rods and 22 non-heated rods. The dimensions of the heater rods are based on 15×15 fuel rods bundle for a PWR and the heated length and the outer diameter of each heater rod are 3.66 m and 10.7 mm, respectively. A heater rod consists of a nichrome heater element, boron nitride (BN) or magnesium oxide (MgO) depending on elevation in the heated zone and Nichrofer 7216 (equivalent to Inconel 600) sheath. The sheath thickness is about 1.0 mm and is thicker than the actual fuel cladding because of the requirements for thermocouple installation. The heater element is a helical coil and has a 17 step chopped cosine axial power profile as shown in Fig. A-7. The peaking factor is 1.4.

Non-heated rods are either pipes or solid rods of stainless steel with 13.8 mm O.D. The heater rods and non-heated rods are fixed at the top of the core allowing downward expansion. In Fig. A-11, relative elevation of rods and spacers is shown.

For better simulation of flow resistance in the lower plenum the simulated fuel rods end in the lower plenum and do not penetrate through the bottom plate of the lower plenum as shown in Fig. A-3.

A.1.3 Primary Loops and ECCS

Primary loops consist of a hot leg equivalent to four hot legs in area, a steam/water separator for simulating single steam phase flow downstream of the steam generator and for measuring flow rate of carry over water, an intact cold leg equivalent to three intact loops, a broken cold leg on the pressure vessel side and a broken cold leg on the steam/water separator side. These two broken cold legs are connected to two containment tanks through break valves, respectively. The arrangement of the primary loops is shown in Fig. A-9. The flow area of each loop is scaled down based on the core flow area scaling, 1/21. It should be emphasized that the cross section of the hot leg is an elongated circle with an actual height to realize proper flow pattern in the hot leg. The steam/water separator has a steam generator inlet plenum simulator to correctly simulate the flow characteristics of carryover water into the U-tubes. The cross section of the hot leg and the configuration of the steam genrator inlet plenum simulator are

shown in Fig. A-8.

A pump simulator and a loop seal part are provided for the intact cold leg. The arrangement of the intact cold leg is shown in Fig. A-9. The pump simulator consists of the casing and duct simulators and an orifice plate as shown in Fig. A-10. The loop resistance is adjusted with the orifice plates attached to the intact cold leg, the steam/water separator side and pressure vessel side broken cold legs and the pump simulator.

ECCS consists of the Acc and an LPCI systems. Injection ports are located as already described in the design criteria section. Besides, the UCSP water extraction system and the UCSP water injection system are provided for combined injection tests.

A.1.4 Containment Tanks and Auxiliary System

Two containment tanks are provided to SCTF. The containment tank-I is connected with the downcomer through the pressure vessel side broken cold leg and the containment tank-II is connected with the steam/water separator through the steam/water separator side broken cold leg. Especially in the containment tank-I, carryover water from the downcomer is measured by the differentiation of the liquid level. These containment tanks and auxiliary system such as a pressurizer for injecting water from the Acc tanks, etc. are shared with CCTF.

A.2 Instrumentation

A.2.1 Measurement Items

The instrumentation in SCTF has been provided both by JAERI and USNRC. The JAERI-provided instrumentation includes the measurement of temperatures, pressures, differential pressures, liquid levels, flow velocities, and heating powers. USNRC has provided film probes, impedance probes, string probes, liquid level detectors (LLDs), fluid distribution grids (FDGs), turbine meters, drag disks, densitometers, spool pieces and video optical probes.

A.2.2 Identification of Instruments

The description of the identification number of the instruments is given in Tables A-2, A-3 and A-4.

A.2.3 Measurement Location

A.2.3.1 Pressure Vessel

The relative elevations of in-core and downcomer instruments except those for pressure and differential pressure measurements are shown in Fig. A-11. The horizontal arrangement of heater rods and non-heated rods with instruments are shown in Fig. A-12. Figure A-13 through A-17 shows the relative elevations of the instruments in the core and the upper plenum.

(1) Temperature measurement in the core

The location of thermocouples on the heater rods and non-heated rods are shown in Figs. A-13, A-14, A-15 and A-16. These thermocouples measure the temperatures of the heater rod surface (Fig. A-13), the non-heated rod surface (Fig. A-14), the fluid (Fig. A-15) and the steam (Fig. A-16) in the core.

(2) Temperature measurement in the pressure vessel except the core

The vertical location of thermcouples in the presssure vessel except the core are shown in Fig. A-17. Figure A-18 and Fig. A-19 show the horizontal location of thermocouples in the upper plenum and the other portion in the pressure vessel except the core, respectively. The configuration of thermocouple tip location has variety and that for the core wall is shown in Fig. A-20.

The fluid temperatures at the core inlet are measured with thermocouples attached on the non-heated rods as shown in Fig. A-21. Figure A-22 shows in detail the location of fluid temperature measurements just above and below the end box tie plate. The configuration of the thermocouples for the temperature measurements at the center and periphery of the UCSP holes is shown in detail in Fig. A-23,

The horizontal and vertical locations of the fluid temperature measurements above the UCSP is shown in Figs. A-24.

(3) Absolute pressure

In the pressure vessel, absolute pressures are measured in the upper plenum, the core, the lower plenum and the downcomer as shown in Fig. A-25.

(4) Differential pressure

The locations of the vertical and horizontal differential pressure measurements are shown in Figs. A-26 and A-27, respectively. Figure A-27 also shows the location of the differential pressure measurement between the end box and the inlet of hot leg.

The locations of the differential pressure measurements across the end box tie plate are shown in Fig. A-28. The location of the differential pressure measurement between the top of upper plenum and the bottom of lower plenum is shown in Fig. A-25. The figure also shows the location of the horizontal differential pressure measurement in the downcomer.

(5) Collapsed liquid level (D/P cells)

The locations of the liquid level measurement in the downcomer and the lower plenum are shown in Fig. A-25. The liquid levels on the UCSP and the end box tie plate are measured at the locations shown in Fig. A-28. The liquid level measurement in the core baffle region is also made.

The USNRC-provided turbine flow meters are installed at the inlet of the core, above the UCSP holes and in the upper pelnum to measure the fluid velocity as shown in Figs. A-29 and A-30.

The fluid velocities in the top and bottom of the downcomer are measured with the USNRC-provided drag disks shown in Figs. A-29 and A-30.

(6) Fluid density (γ-densitometer)

The vertical and horizontal locations of the γ-densitometer are shown in Figs. A-29 and A-30, respectively.

(7) Film thickness, film velocity, void fraction, and droplet velocity.

The locations of the film and impedance probes for measuring film thickness film velocity, void fraction, and droplet velocity are shown in Figs. A-29 and A-30.

(8) Liuid level (LLD and FDG)

The LLDs for measuring liquid level in the core and the FDGs for measuring liquid level distribution in the upper plenum and downcomer are also provided.

A.2.3.2 Primary Coolant Loops and Auxiliary Systems

The locations of temperature, pressure, differential pressure, liquid level and mass flow rate measurements in the primary coolant loops and auxiliary systems are shown in Figs. A-31 through A-38.

In these figures there are the lists of pressure tap location corresponding to the tag number. In these lists 'L' shows the lower pressure side of D/P cell and 'H' the higher pressure side.

The elevations relative to the bottom of the pressure vessel are shown in the parenthesis. In SCTF, three USNRC-provided spool pieces are installed. They are the hot leg spool piece, the pressure vessel side broken cold leg spool piece and the vent line spool piece.

A.2.4 Data Reduction

The flow chart of the data reduction procedure is shown in Fig. A-39.

The data from the JAERI-provided instruments (1,346 ch) are recorded on the magnetic disk in a mini-computer (FACOM U-400) and partly on a magnetic tape and then converted to physical values with the computer. After plotting preliminary graphs by using a X-Y plotter, these data are investigated and transfered to a magnetic tape (MTJD). With the use of the JAERI-data processing programs for the large computer (FACOM M-380), final engineering data graphs, processed data graphs and some tables are obtained.

The data from the ORNL instruments (201 ch) and the INEL instruments (74 ch) except LLDs and FDGs are recorded on the analog tape of a PCM recorder and transfered to six digital magnetic tapes, five for ORNL data (MT01 ~ 5) and one for INEL data (MT11). These raw data are converted to physical values by using a data processing software which

includes ORNL and INEL subroutines.

The raw data from the LLDs and FDGs are recorded on a floppy disk or an analog tape of FM recorder and impedance data plots for every sensor are obtained by using a mini-computer (LSI-11). Threshold values between wet and dry are determined from these plots and the raw data are converted to wet and dry plot. The results are displayed also on a CRT color display.

Table A-1 Principal Dimensions of Test Facility

1.	Core Dimension	
(1)	Quantity of Bundle	8 Bundles
(2)	Bundle Array	1×8
(3)	Bundle Pitch	230 mm
(4)	Rod Array in a Bundle	16×16
(5)	Rod Pitch in a Bundle	14.3 mm
(6)	Quantity of Heater Rod in a Bundle	234 rods
(7)	Quantity of Non-Heated Rod in a Bundle	22 rods
(8)	Total Quantity of Heater Rods	234×8=1872 rods
(9)	Total Quantity of Non-Heated Rods	22×8-176 rods
(10)	Effective Heated Length of Heater Rod	3660 mm
(11)	Diameter of Heater Rod	10.7 mm
(12)	Diameter of Non-Heated Rod	13.8 mm
2.	Flow Area & Fluid Volume	
(1)	Core Flow Area (Nominal)	0.227 m^2
(2)	Core Fluid Volume	0.92 m^3
(3)	Baffle Region Flow Area	0.10 m^2
(4)	Baffle Region Fluid Volume (Nominal)	0.36 m^3
(5)	Effective Core Flow Area Based on the Measured Level-Volume Relationship Including Gap between Core Barrel and Pressure Vessel Wall and Various Penetration Holes	0.35 m^2
(6)	Downcomomer Flow Area	0.121 m^2
(7)	Upper Annulus Flow Area	0.158 m^2
(8)	Upper Plenum Horizontal Flow Area	0.525 m^2
(9)	Upper Plenum Fluid Volume	1.16 m^3
(10)	Upper Head Fluid Volume	0.86 m^3
(11)	Lower Plenum Fluid Volume	1.38 m^3
(12)	Steam Generator Inlet Plenum Simulator Flow Area	0.626 m^2
(13)	Steam Generator Inlet Plenum Simulator Fluid Volume	0.931 m^3
(14)	Steam Water Separator Fluid Volume	5.3 m^3
(15)	Flow Area at the Top Plate of Steam Generator Inlet Plenum Simulator	0.195 m^2
(16)	Hot Leg Flow Area	0.0826m^2
(17)	Intact Cold Leg Flow Area (Diameter = 297.9 mm)	0.9697m^2
(18)	Broken Cold Leg Flow Area (Diameter = 151.0 mm)	0.0179m^2

Table A-1 (Continued)

(19)	Containment Tank-I Fluid Volume	30	m^3
(20)	Containment Tank-II Fluid Volume	50	m^3
(21)	Flow Area of Exhausted Steam Line from Containment Tank-II to the Atmospherc	see Ref. (1)	

3. Elevation & Height

(1)	Top Surface of Upper Core Support Plate (UCSP)	0	mm
(2)	Bottom Surface of UCSP	- 76	mm
(3)	Top of the Effective Heated Length of Heater Rod	- 393	mm
(4)	Bottom of the Skirt in the Lower Plenum	-5270	mm
(5)	Bottom of Intact Cold Leg	+ 724	mm
(6)	Bottom of Hot Leg	+1050	mm
(7)	Top of Upper Plenum	+2200	mm
(8)	Bottom of Steam Generator Inlet Plenum Simulator	+1933	mm
(9)	Centerline of Loop Seal Bottom	-2281	mm
(10)	Bottom Surface of End Box	- 185.1	mm
(11)	Top of the Upper Annulus of Downcomer	+2234	mm
(12)	Height of Steam Generator Inlet Plenum Simulator	1595	mm
(13)	Height of Loop Seal	3140	mm
(14)	Inner Height of Hot Leg Pipe	737	mm
(15)	Bottom of Lower Plenum	-5770	mm
(16)	Top of Upper Head	+2887	mm

Table A-2 Description of Tag-ID Number (In-Core)

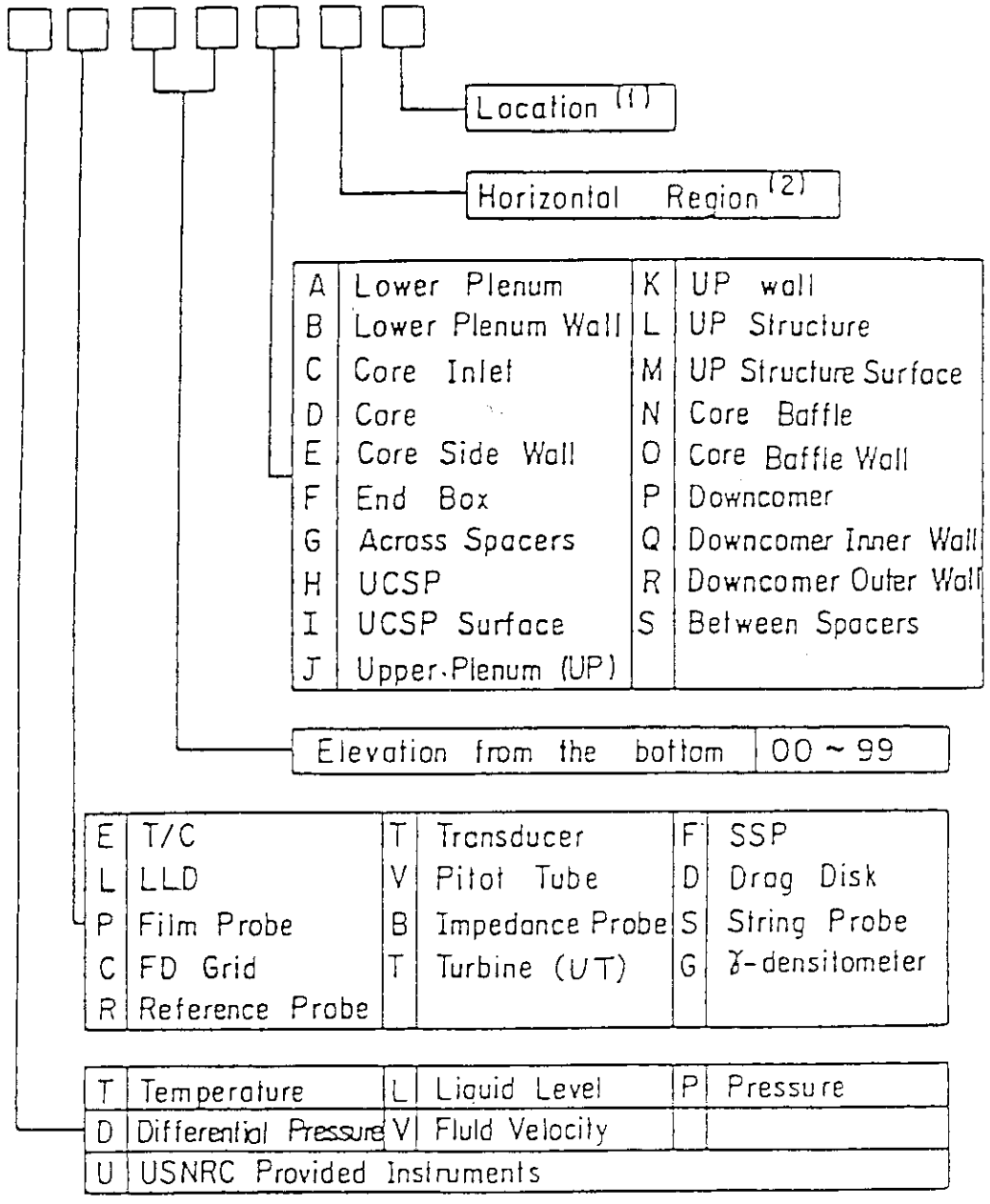

Note :

(1)

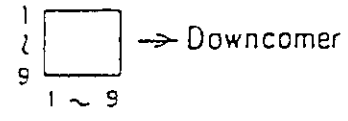

(2)

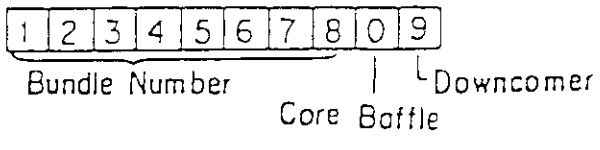

Table A-3 Description of Tag-ID Number (Pressure Vessel Except Core)

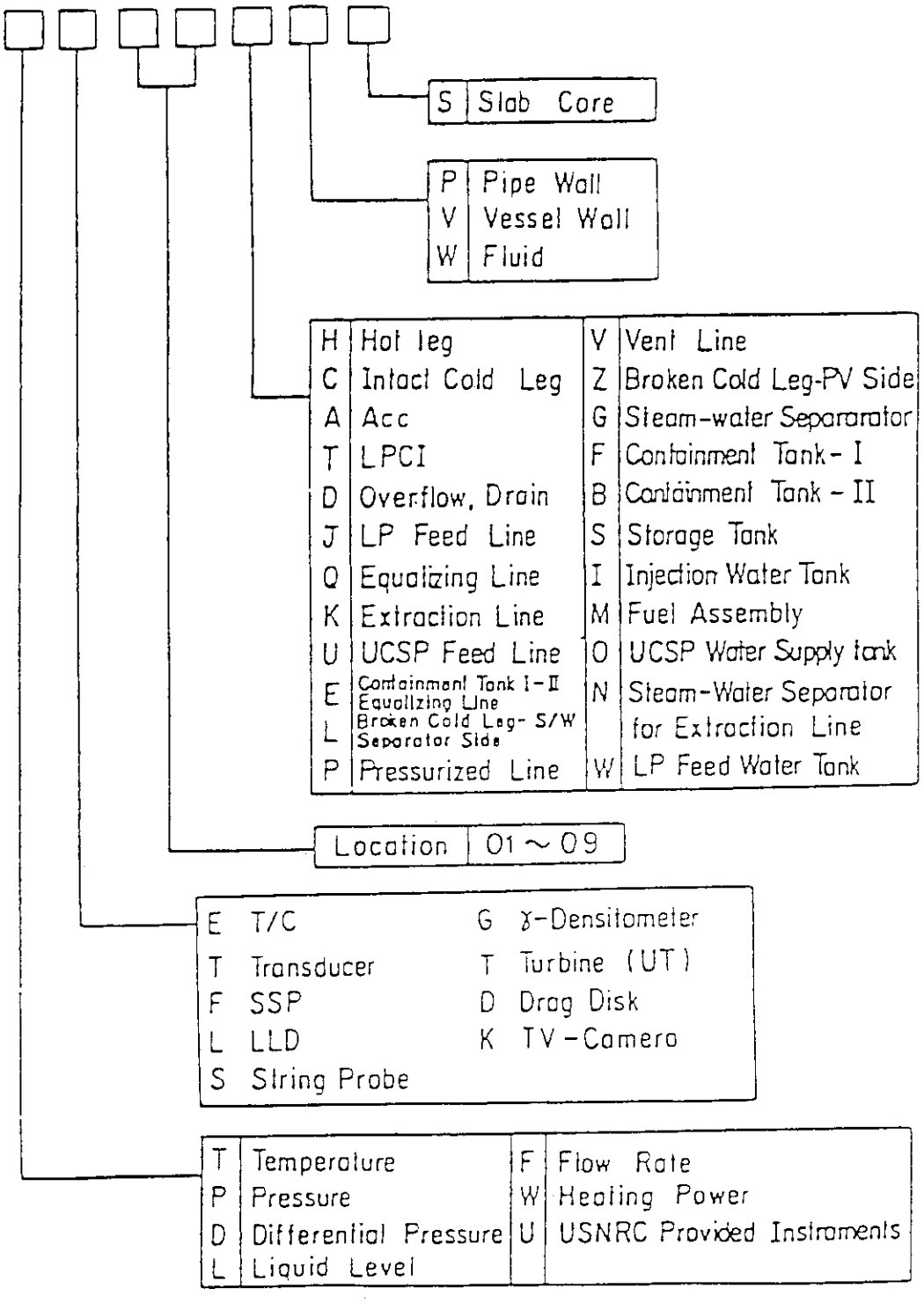

Table A-4 Description of Tag-ID Number (Except Pressure Vessel)

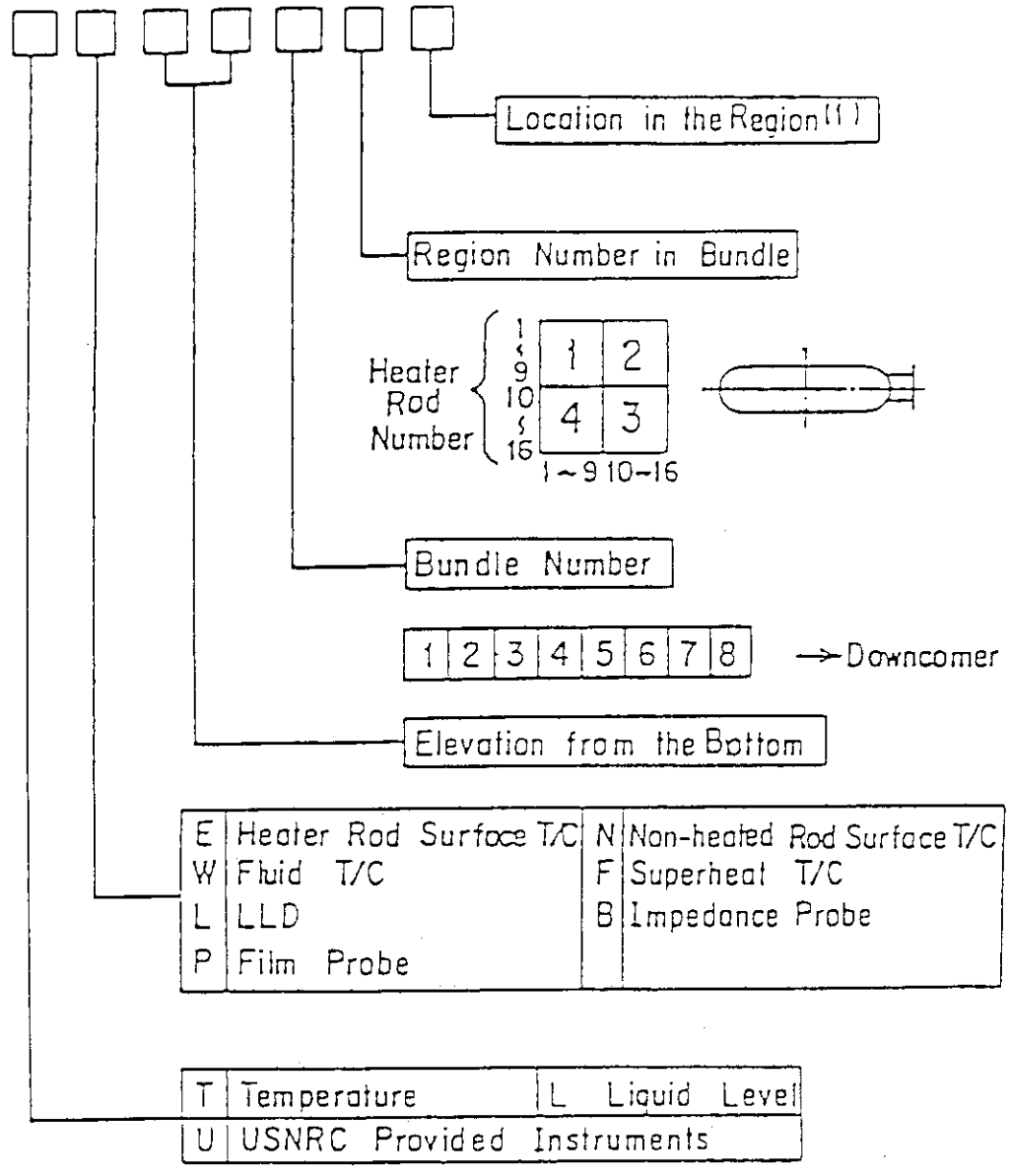

Note : (1) for Heater Rod T/C

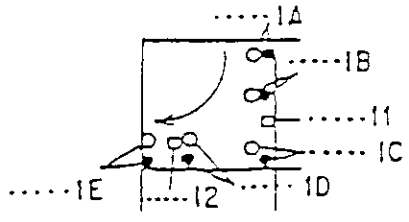

○ Upper half } Clockwise
● Lower half } A~E
□ Center } 1~2

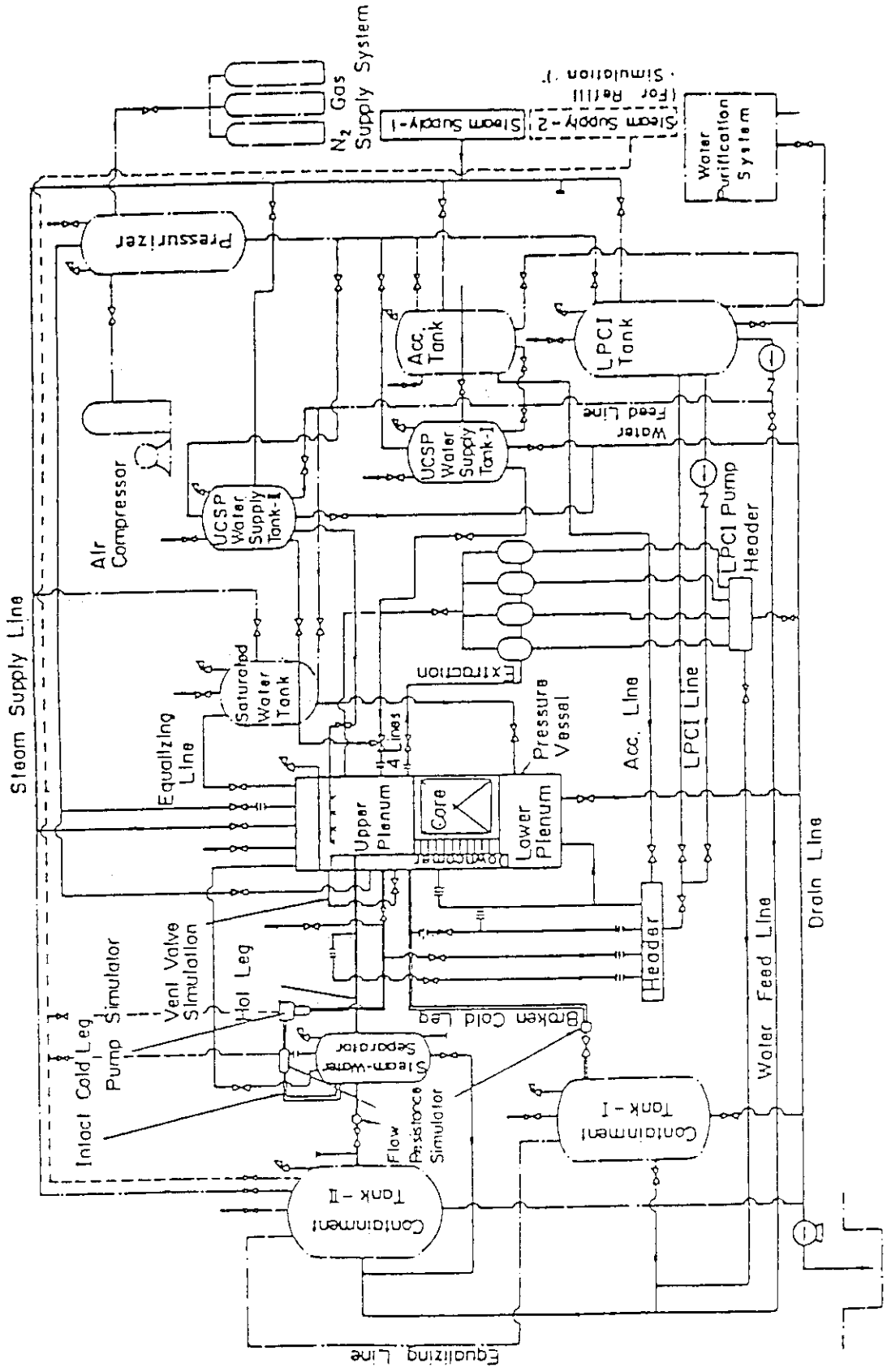

Fig. A - 1 Schematic Diagram of Slab Core Test Facility

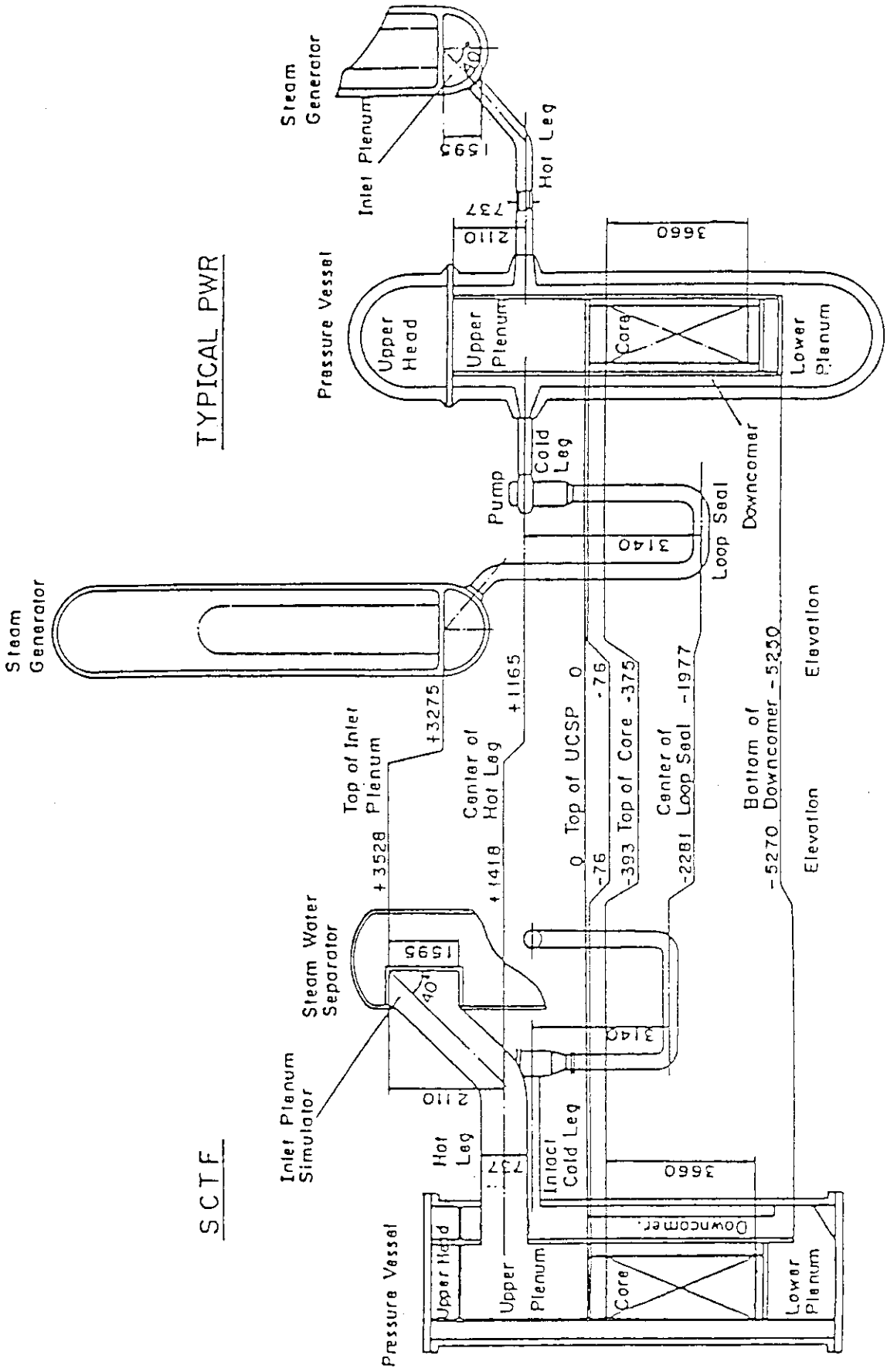

Fig. A - 2 Comparison of Dimensions between SCTF and a Reference PWR

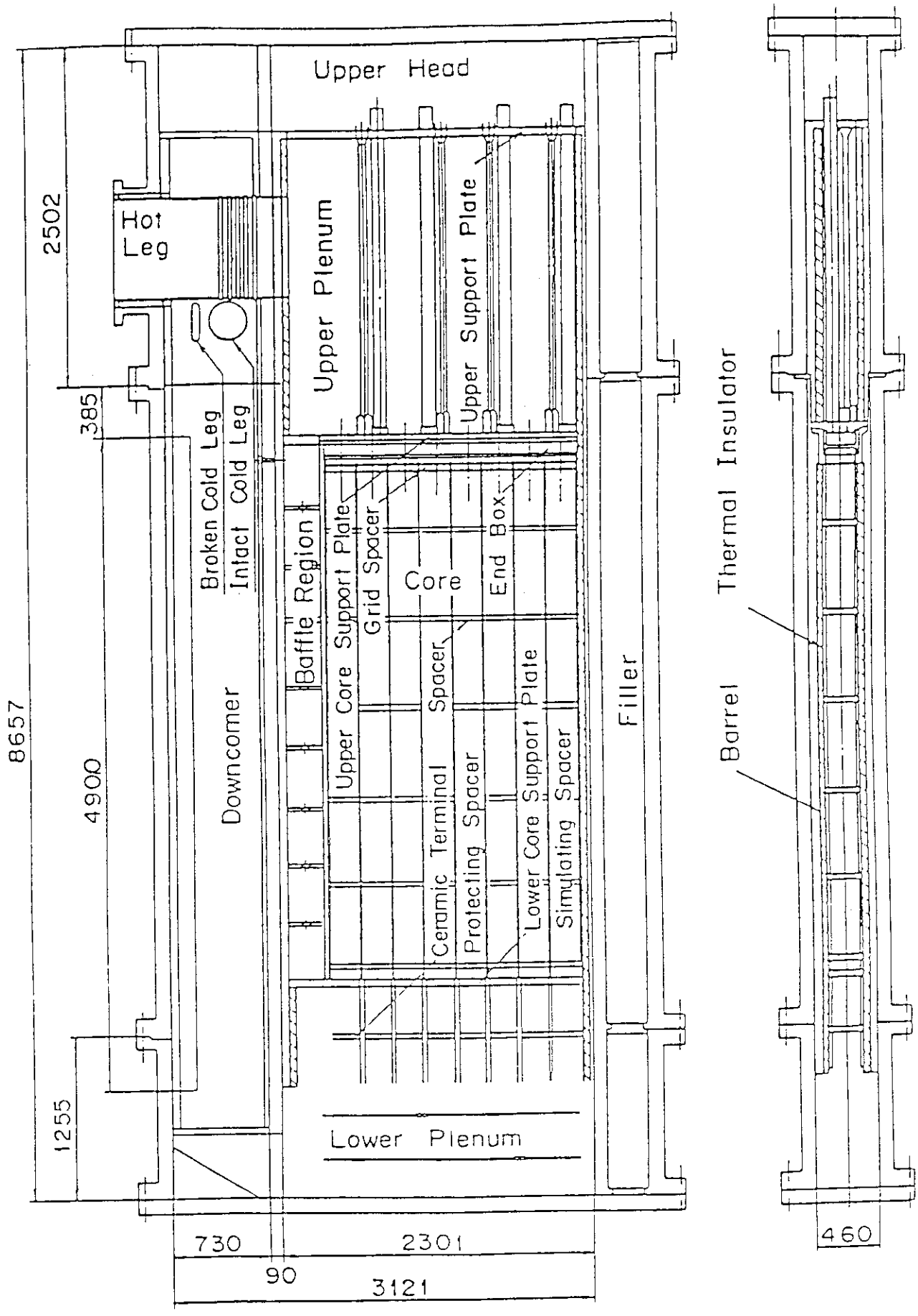

Fig. A－3 Vertical Cross Section of the Pressure Vessel

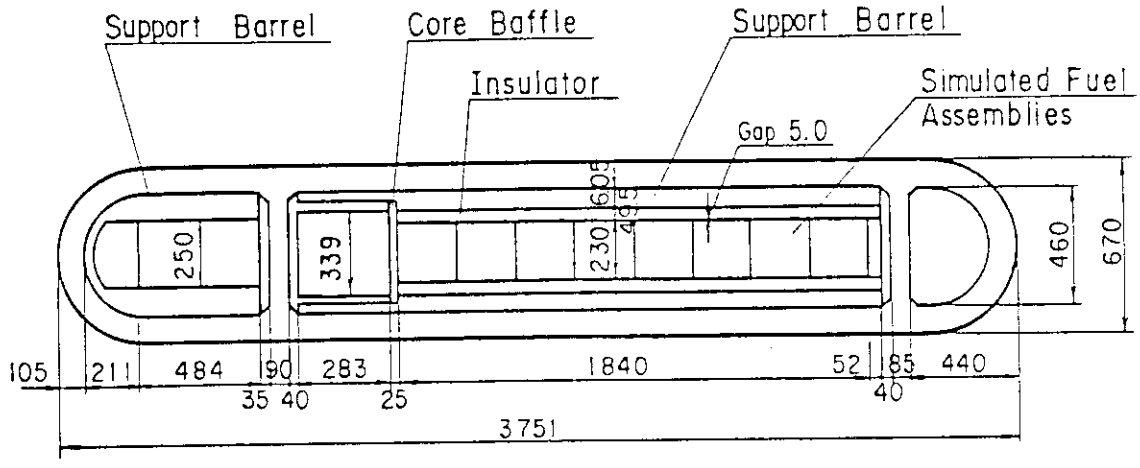

Fig. A－4 Horizontal Cross Section of the Pressure Vessel (1)

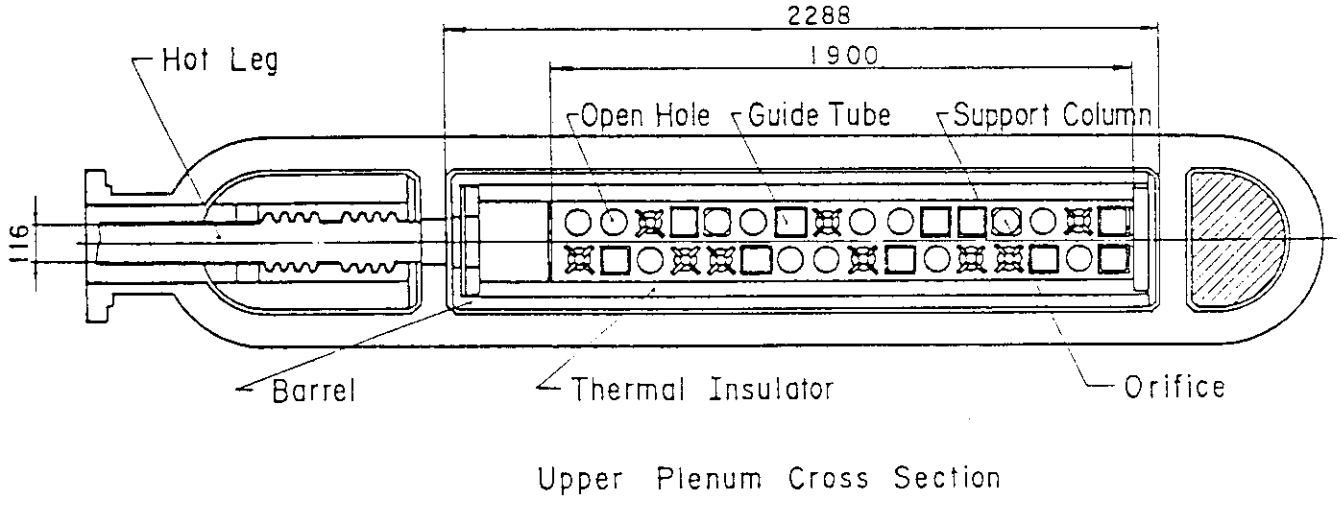

Fig. A－5 Horizontal Cross Section of the Pressure Vessel (2)

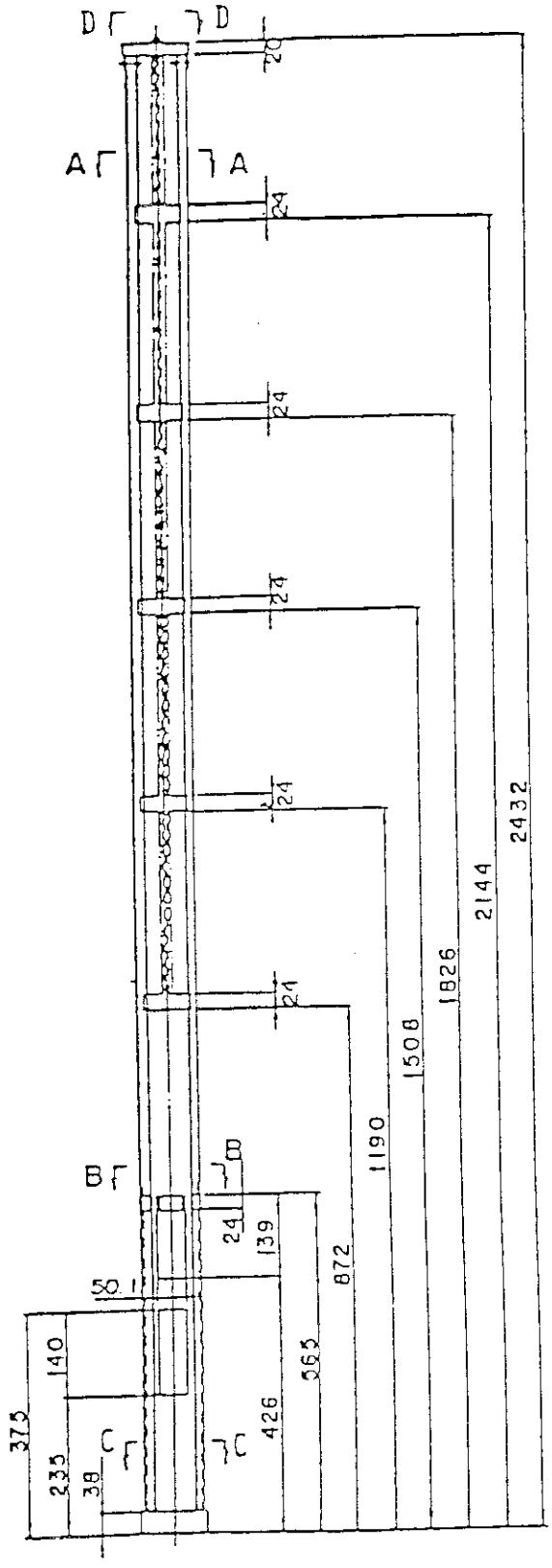

Fig. A－6　Dimension of Guide Tube (1)

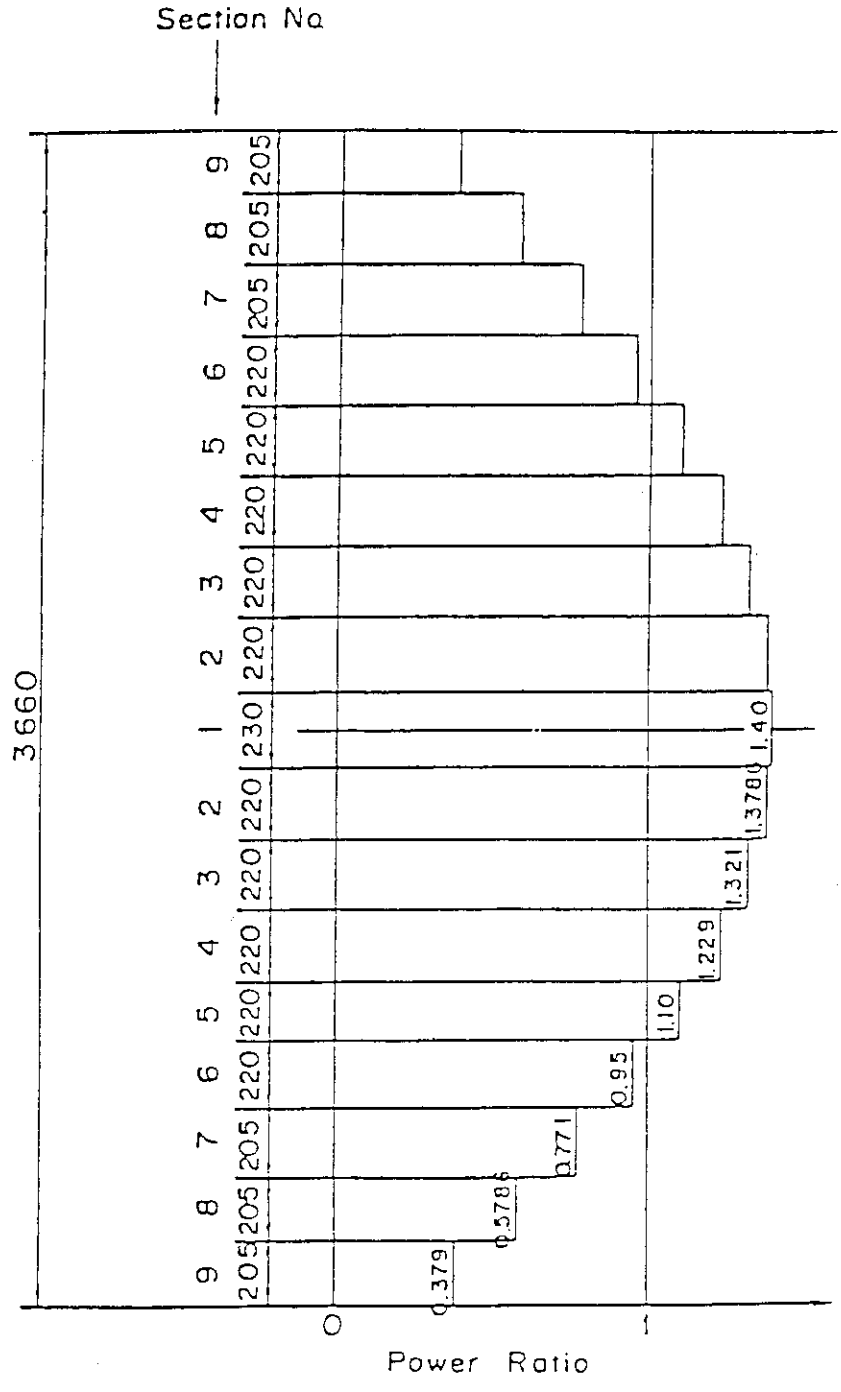

Fig. A－7　Axial Power Distribution of Heater Rod

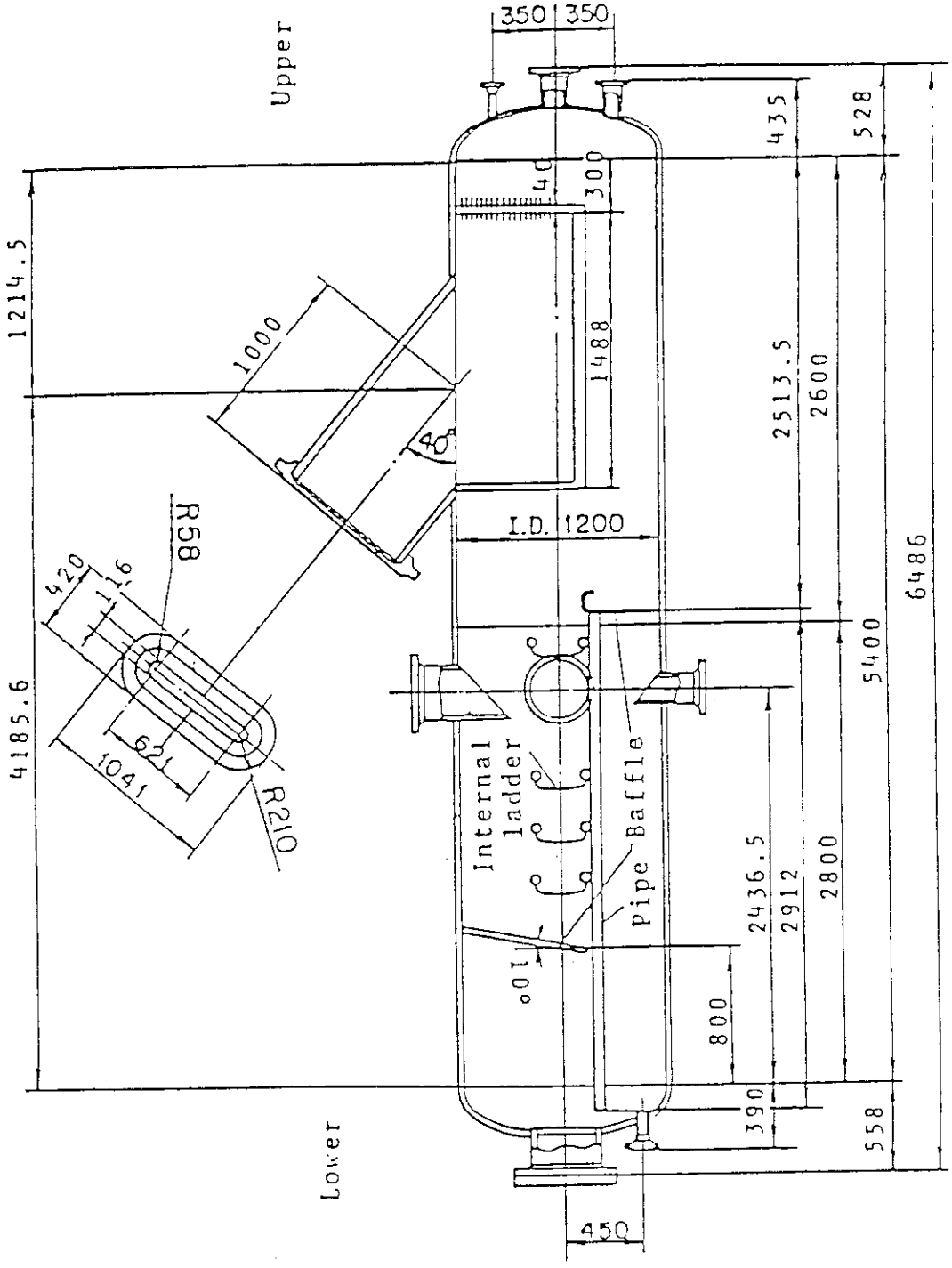

Fig. A－8 Steam/Water Separator

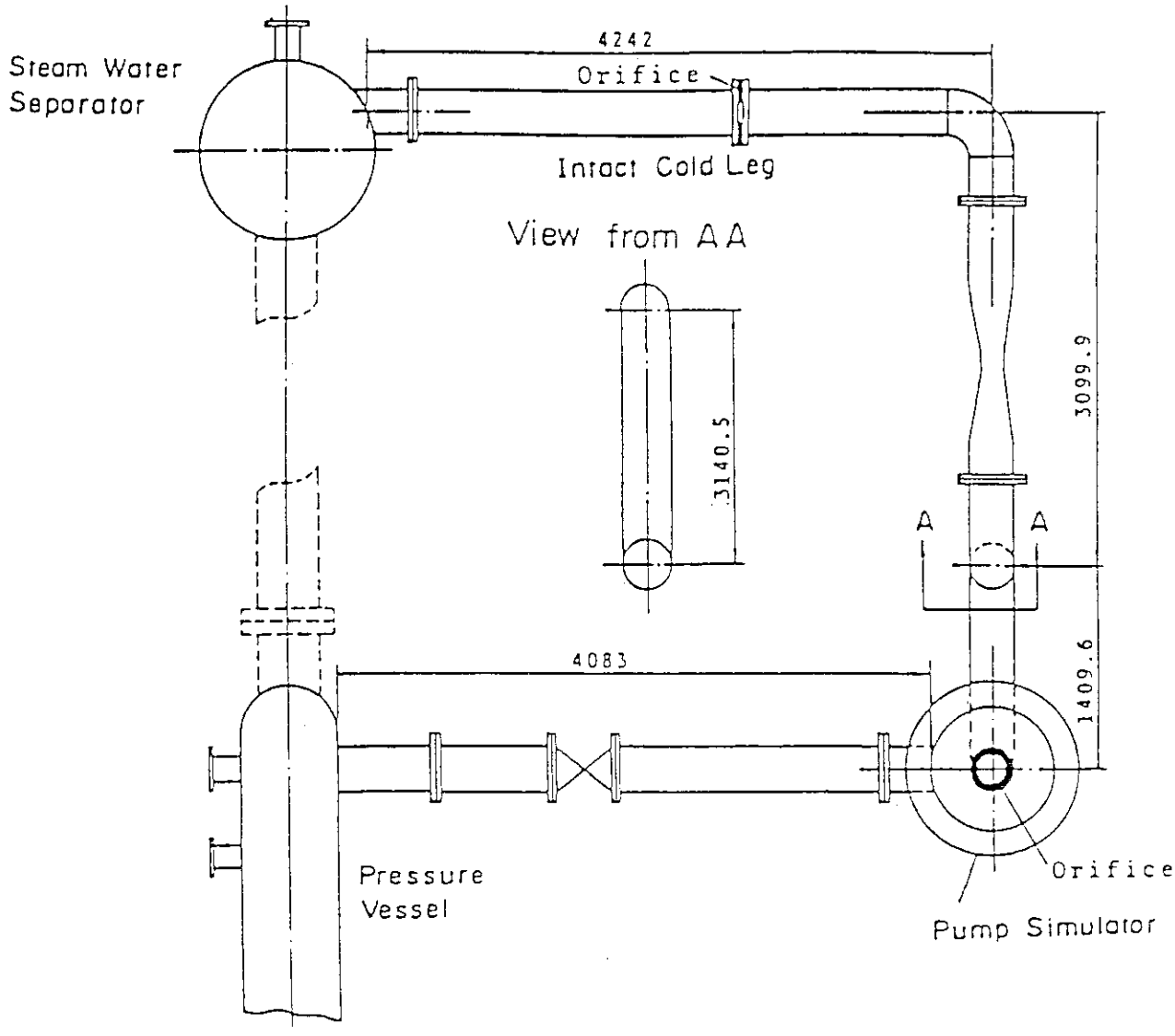

Fig. A－9 Arrangement of Intact Cold Leg

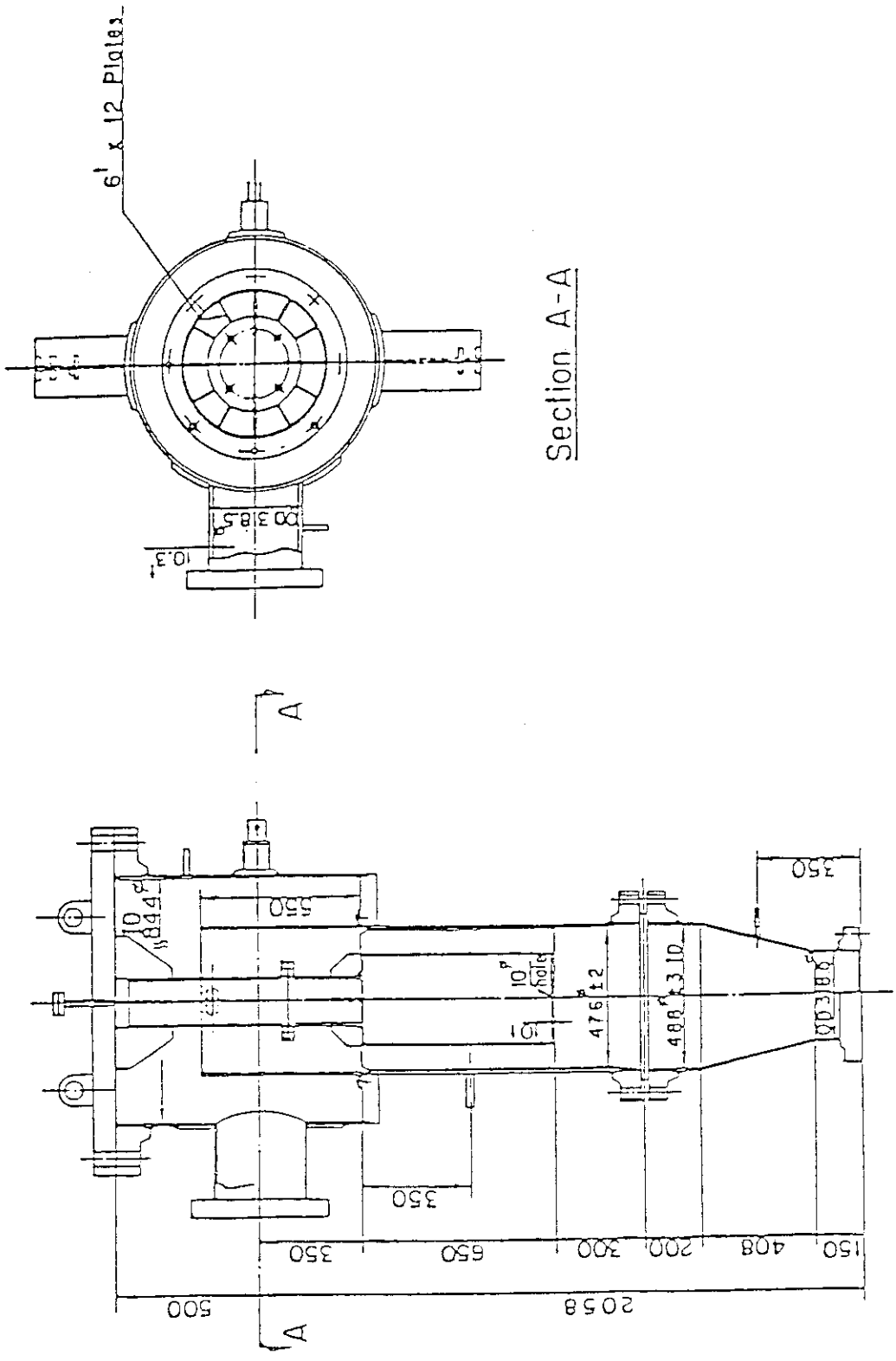

Fig. A-10 Configuration and Dimension of Pump Simulator

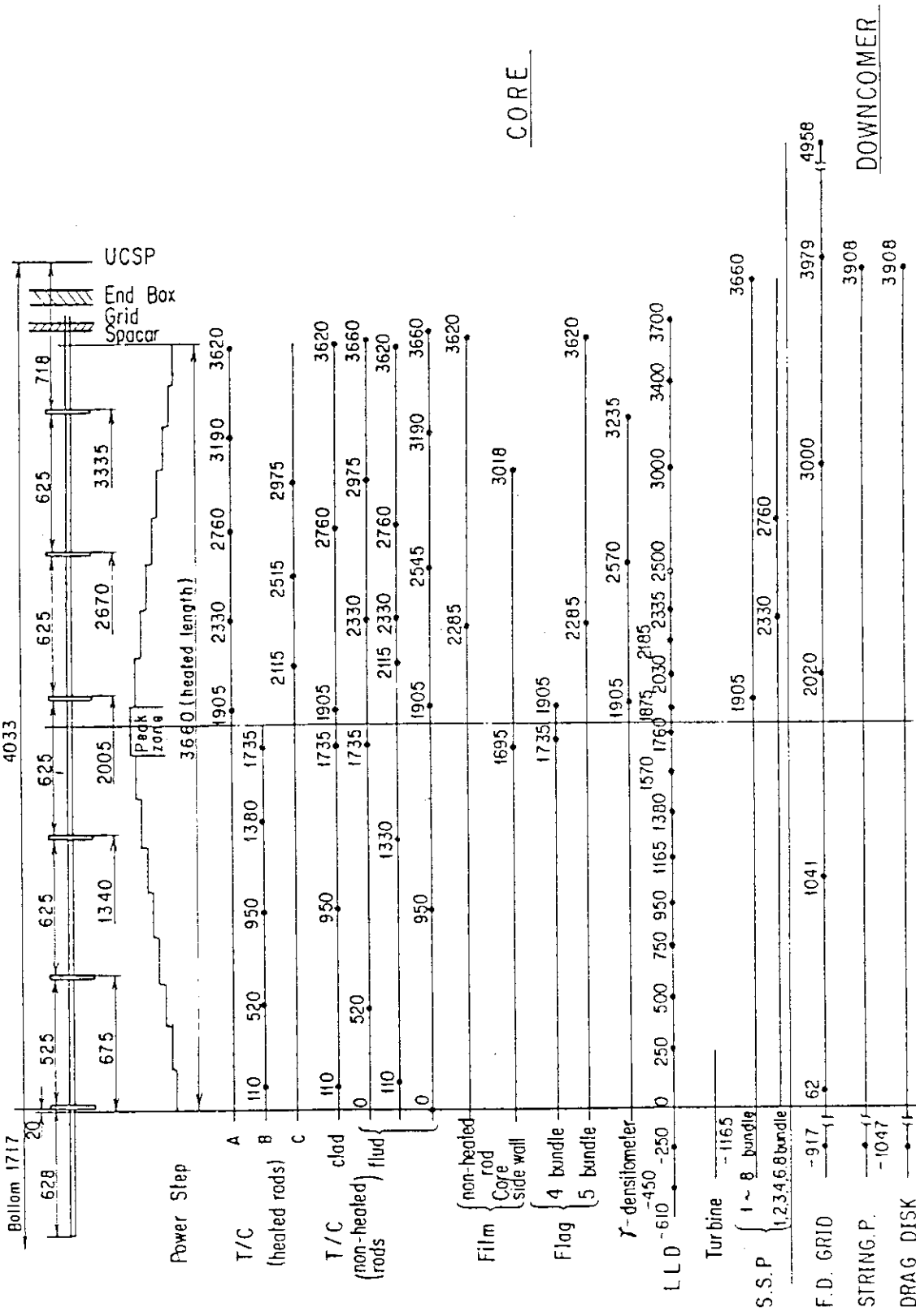

Fig A - 11 Relative Elevation of In-Core and Downcomer Instrumentation

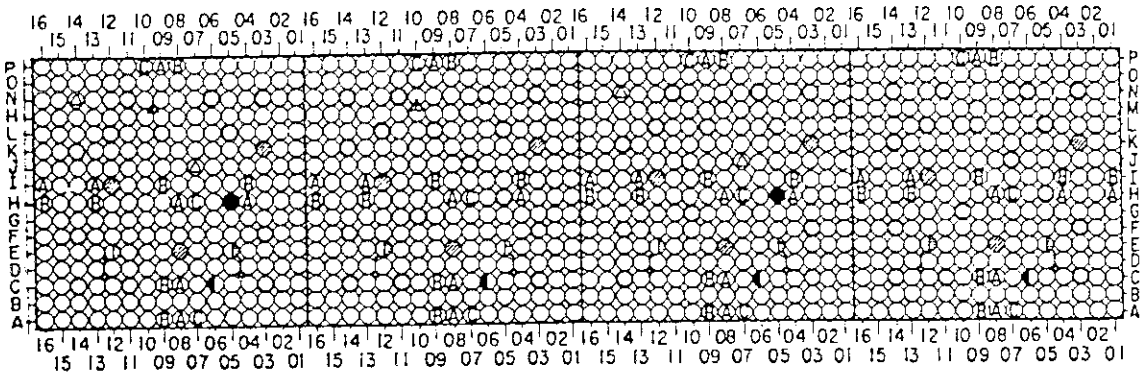

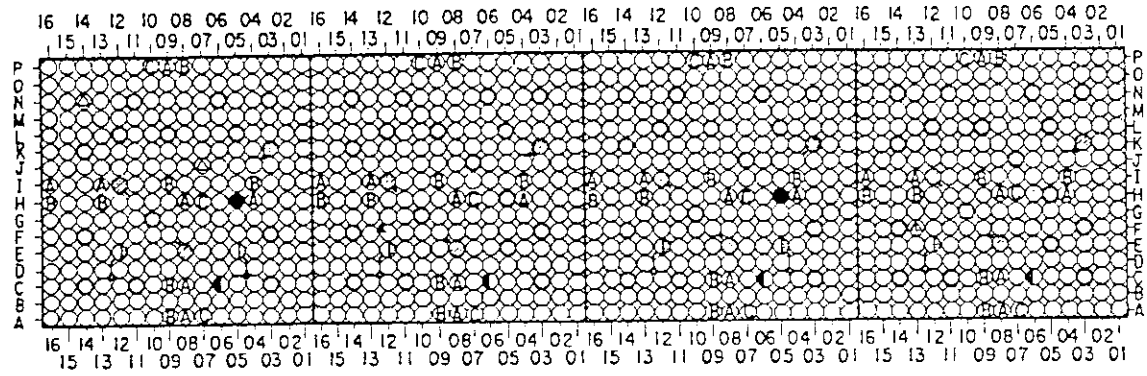

Bundle No.		1	2	3	4	5	6	7	8	Total		Symbol
Heated Rods	Without T/C	215	217	217	217	217	217	217	217	1734	1872	○
	With T/C	19	17	17	17	17	17	17	17	138		ⒶⒷⒸ
Non-heated Rods	Surface Temp.	1	1	△1	△1	1	1	1	1	△8		◐
	Fluid Temp.	3	3	3	3	3	3	3	3	24		▨
	Steam Temp.	2	2	2	2	△1	2	△1	2	△14		◑
	FP / EP	—	2	—	2	—	—	—	2	6		◬
	FLAG PROBE	—	—	—	1	1	—	—	—	2		▢
	LLD	—	1	—	1	—	1	—	1	4		●
	Tie Rod	16	13	△16	△12	△16	15	△17	13	118		○
Total		256	256	256	256	256	256	256	256	2048		

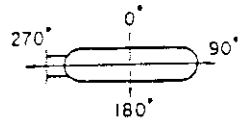

Ⓐ Upper half
Ⓑ Lower half
Ⓒ Upper middle

Fig. A – 12 Horizontal Arrangement of Instrumented Rods

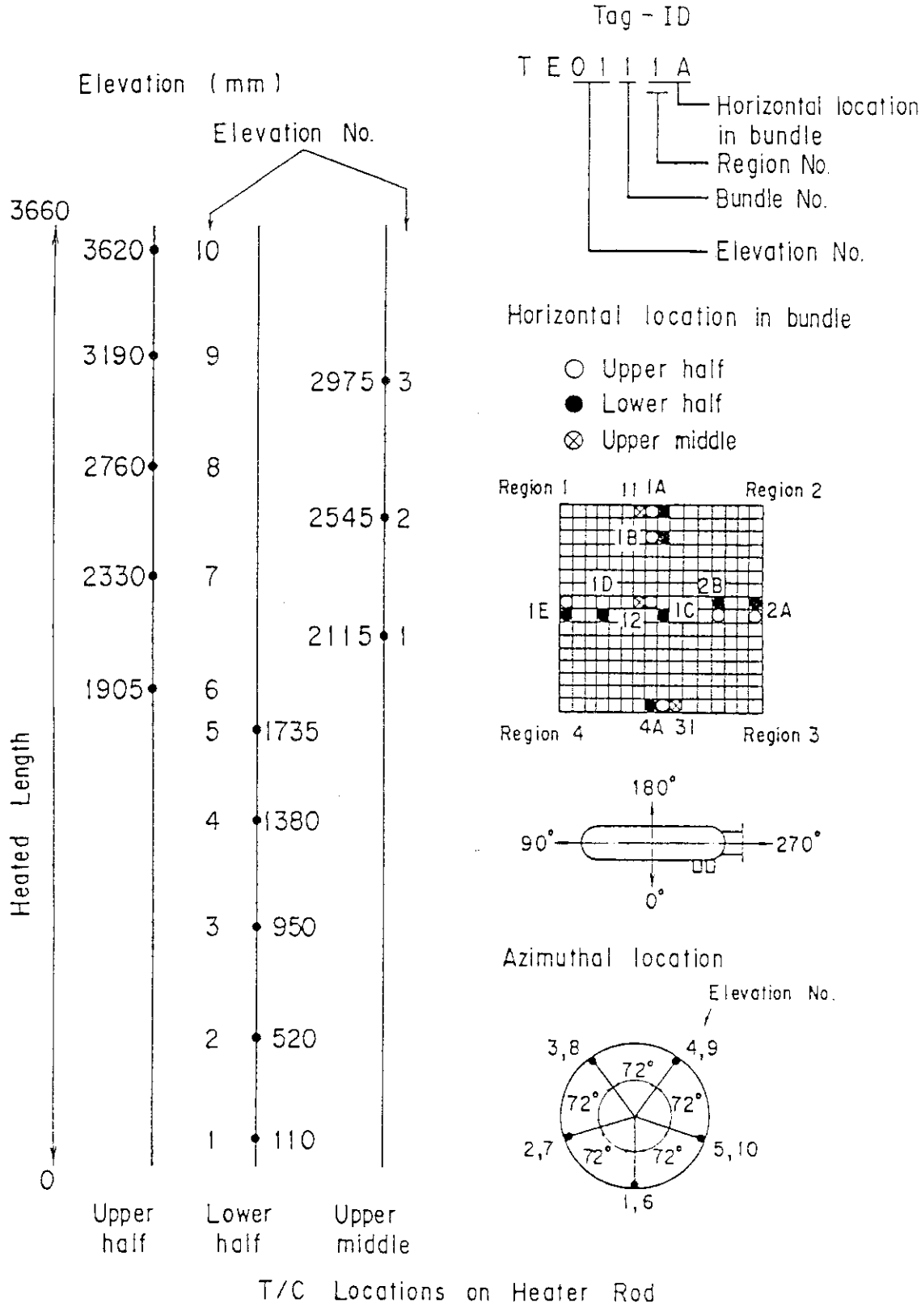

Fig. A-13 Thermocouple Locations of Heater Rod Surface Temperature Measurements

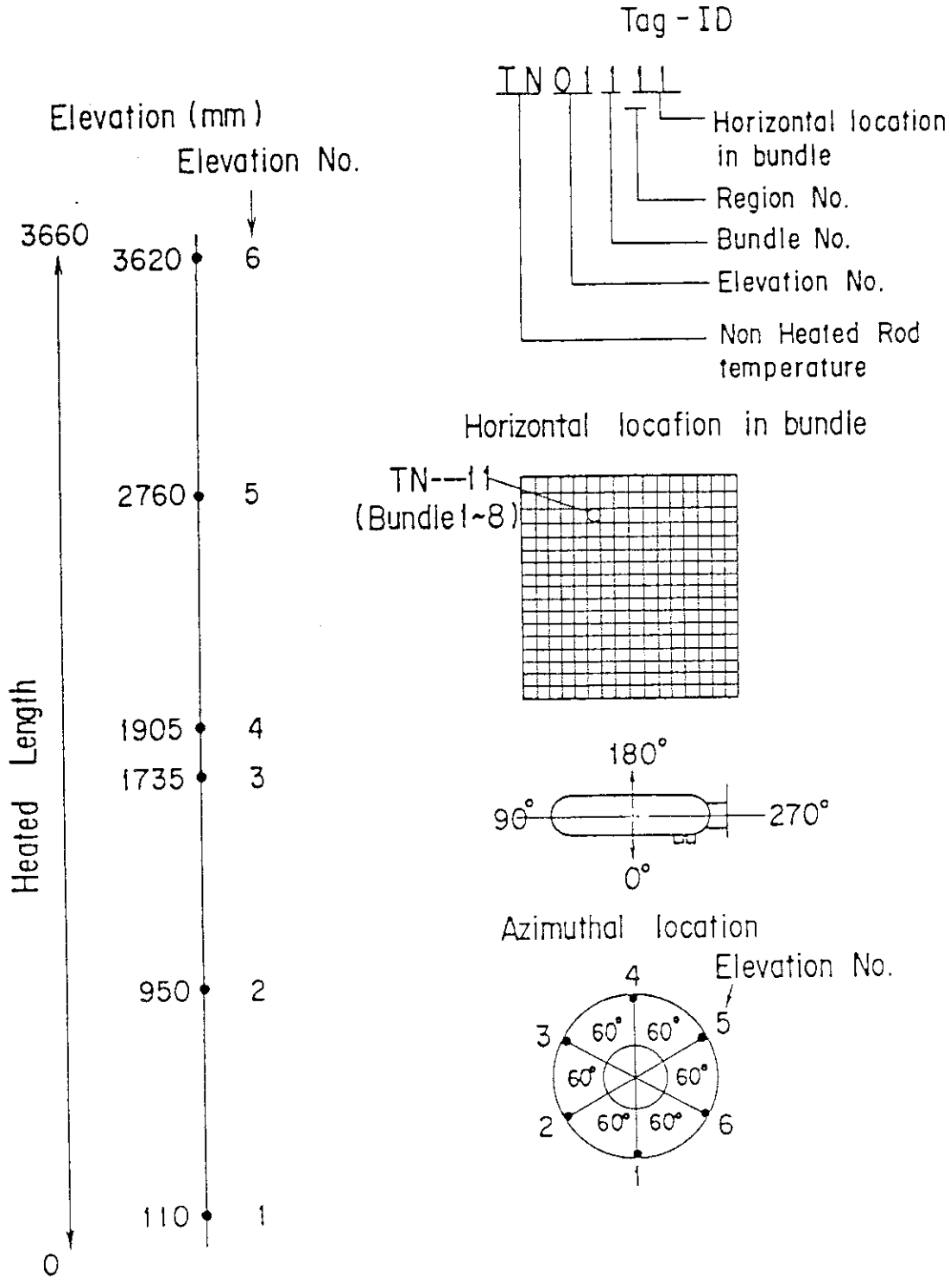

Fig. A - 14 Thermocouple Location of Non-Heated Rod Surface Temperature Measurements

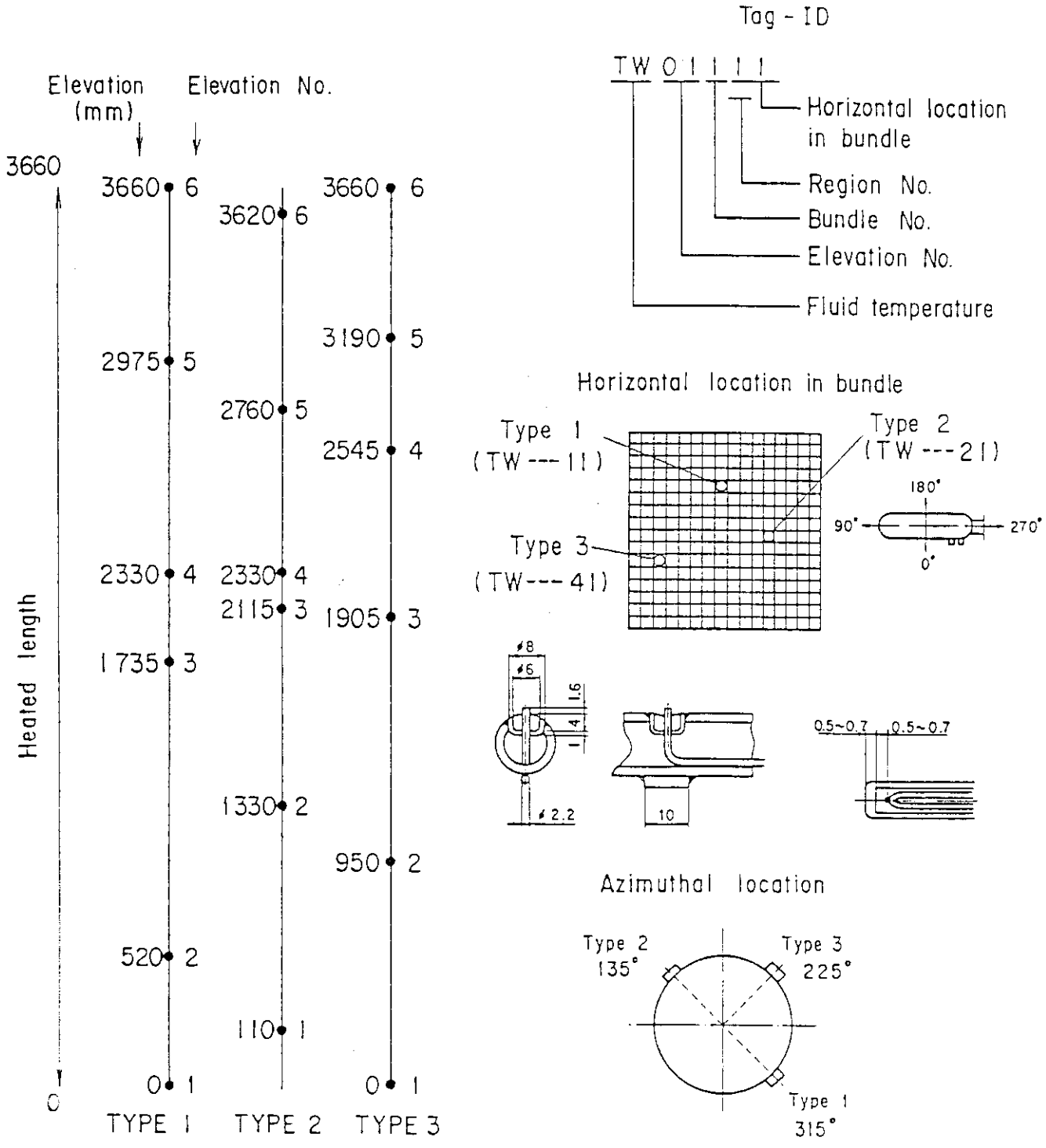

Fig. A－15 Thermocouple Location of Fluid Temperature (Sputtering) Measurements in Core

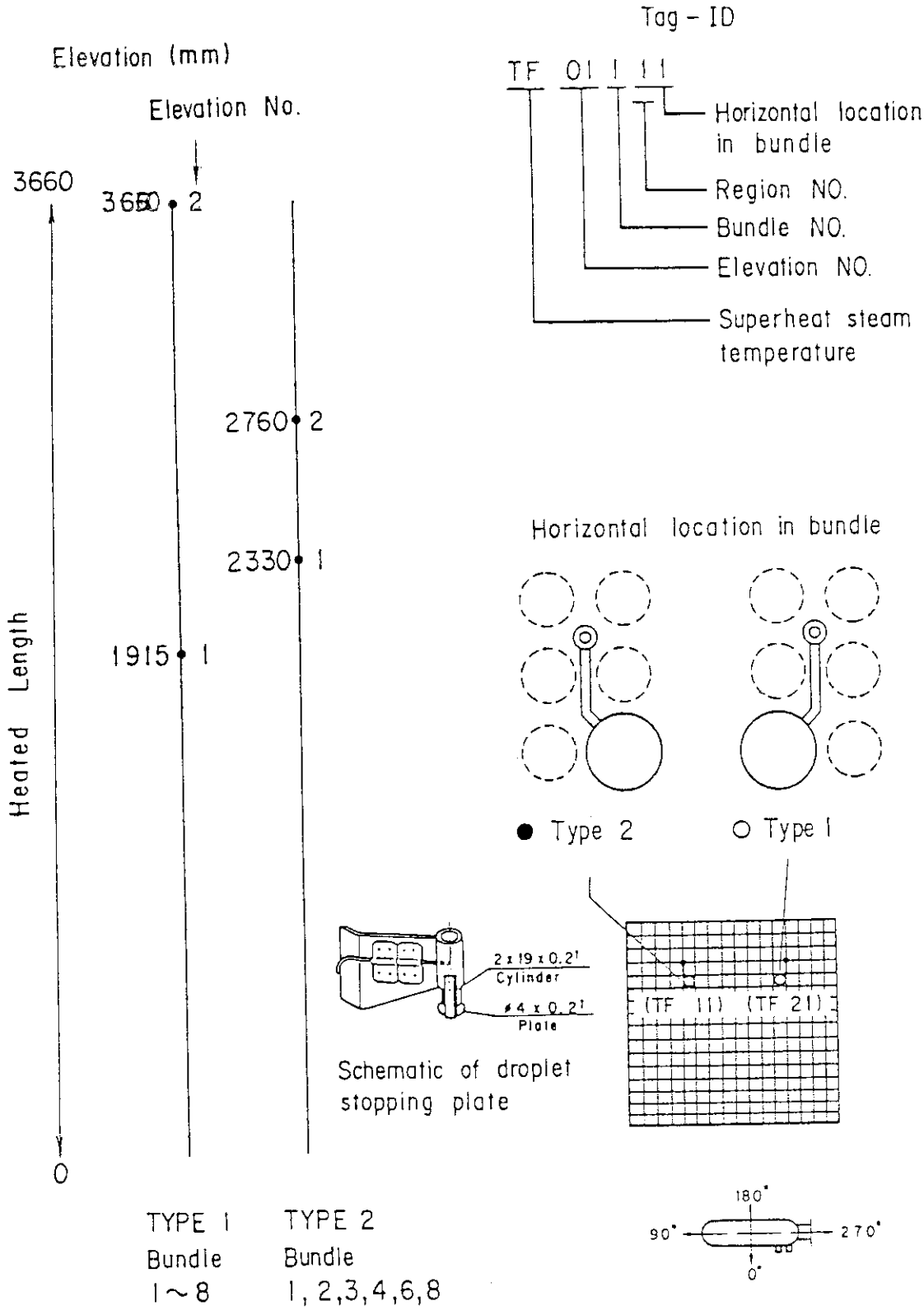

Fig. A – 16 Thermocouple Locations of Steam Temperature Measurements in Core

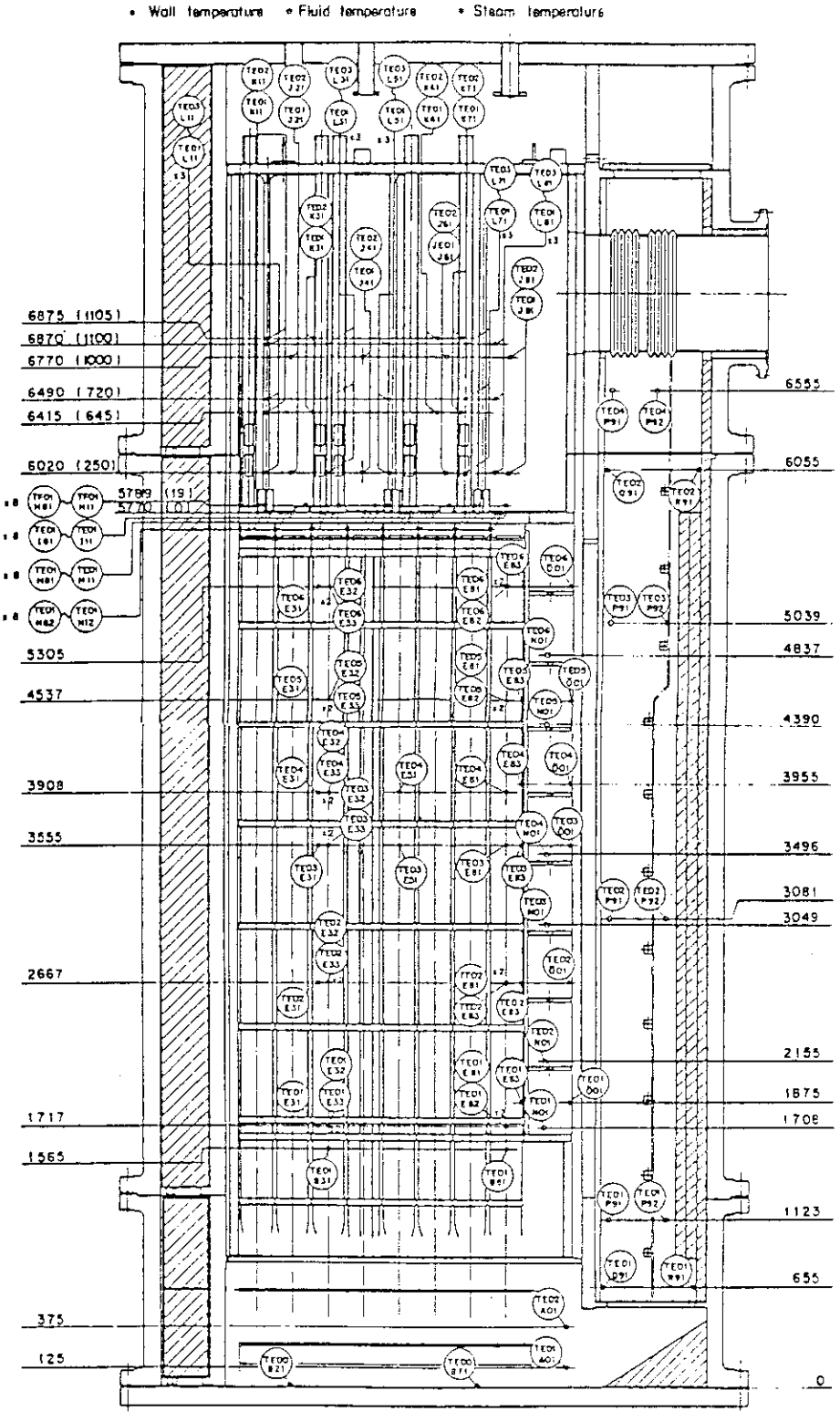

Fig. A - 17 Thermocouple Locations of Temperature Measurements in Pressure Vessel except Core Region (Vertical View)

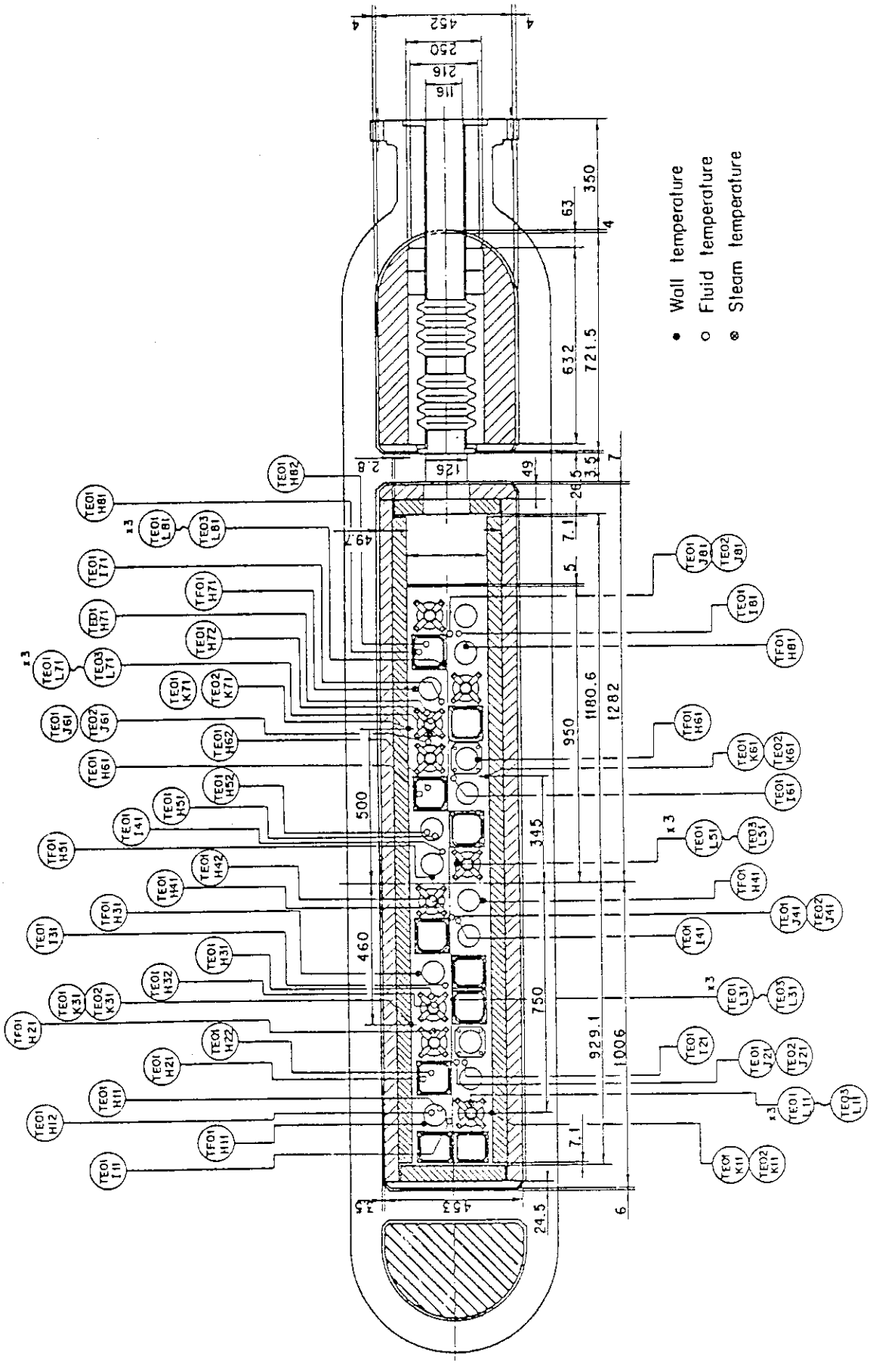

Fig. A - 18 Thermocouple Locations of Temperature Measurements in Upper Plenum (Horizontal View)

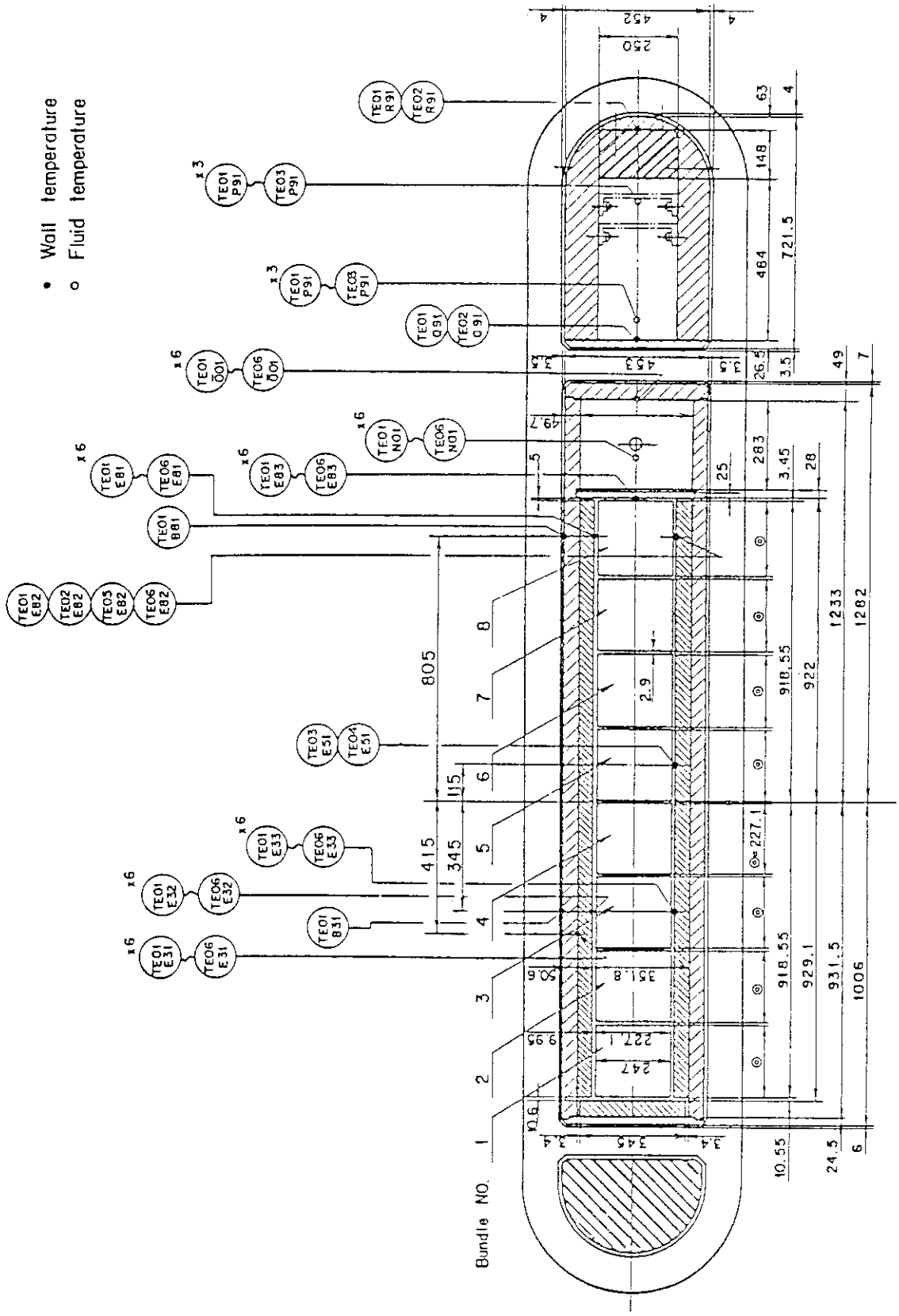

Fig. A - 19 Thermocouple Locations of Temperature Measurements in Pressure Vessel except Upper Plenum (Horizontal View)

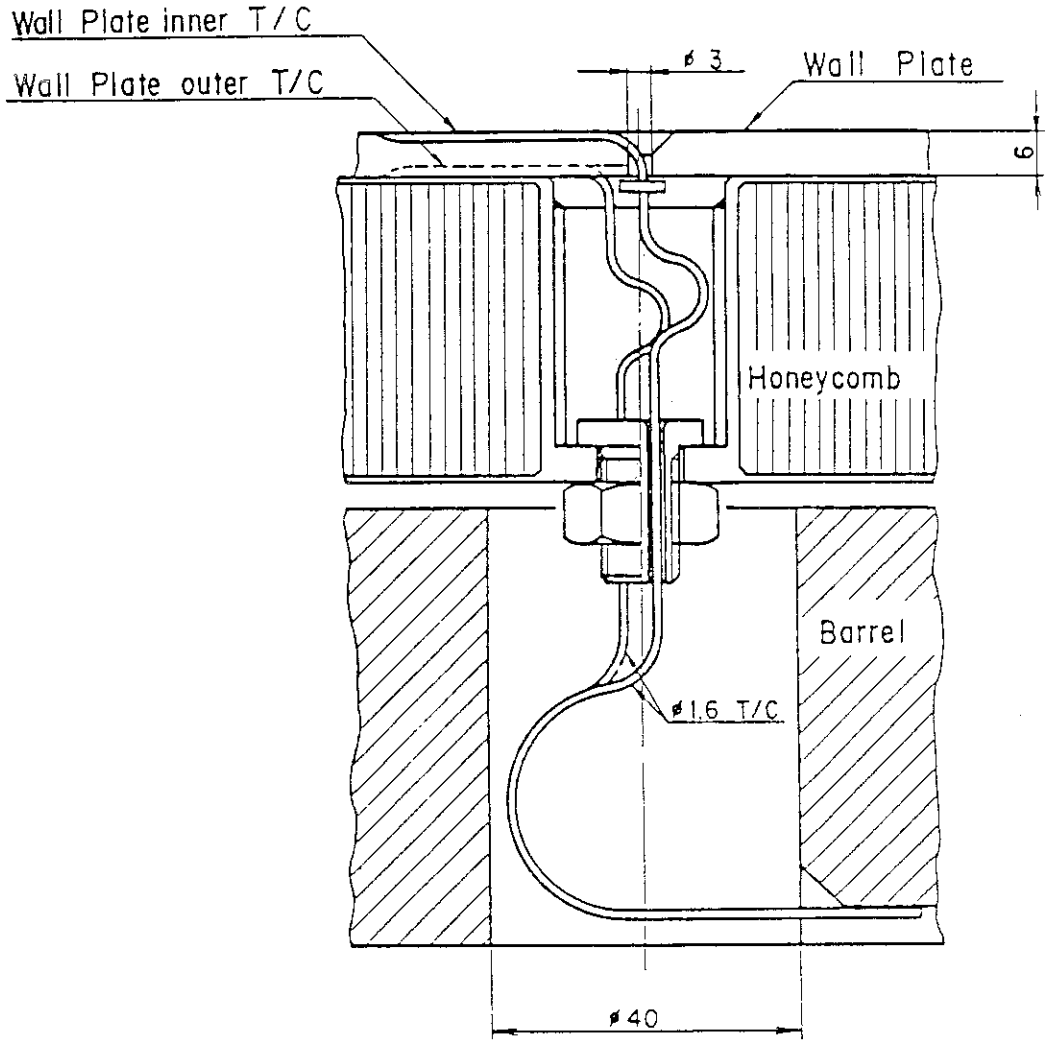

Fig. A - 20 Attachement method of thermocouple on the core wall

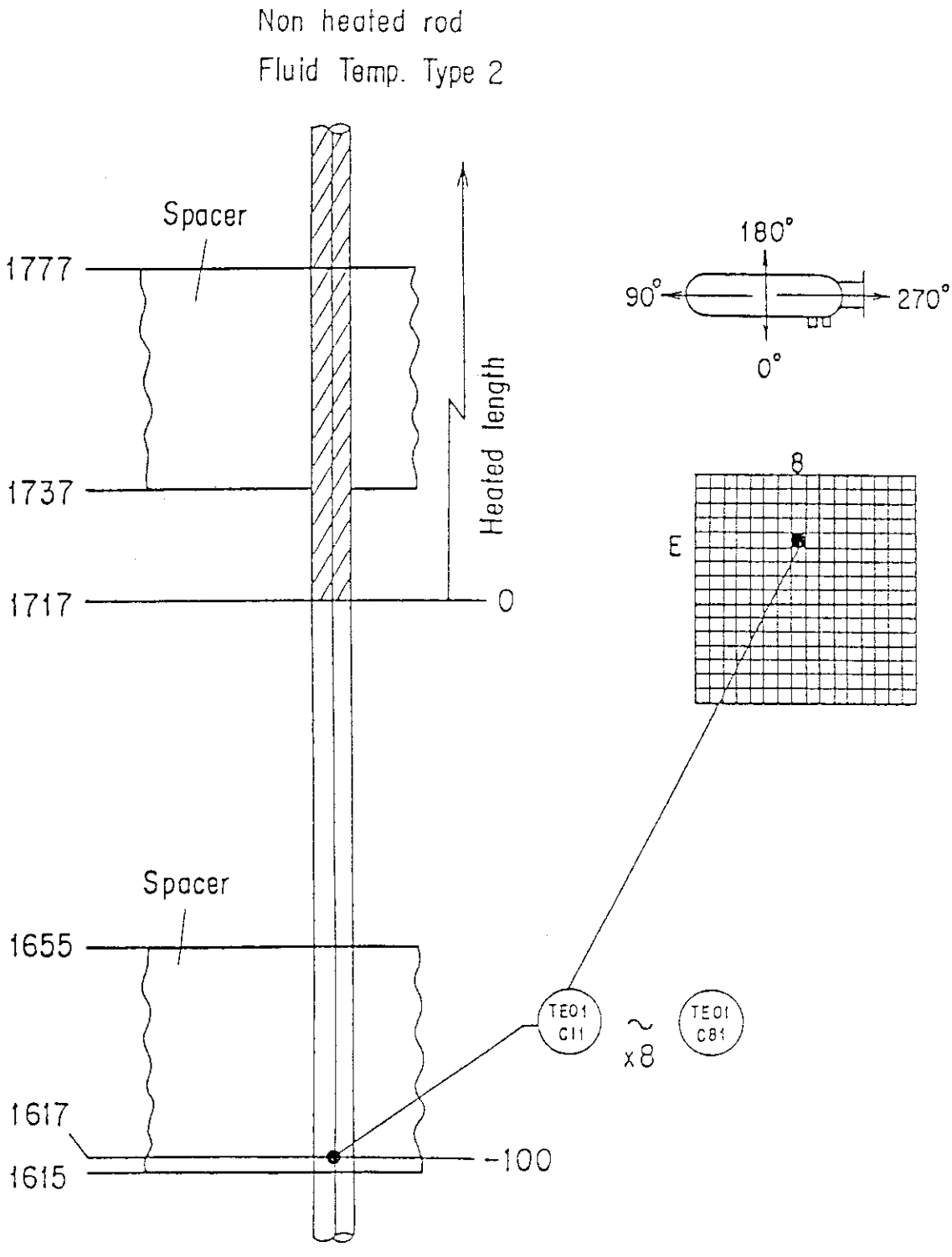

Fig. A – 21 Thermocouple Locations of Fluid Temperature Measurements at Core Inlet

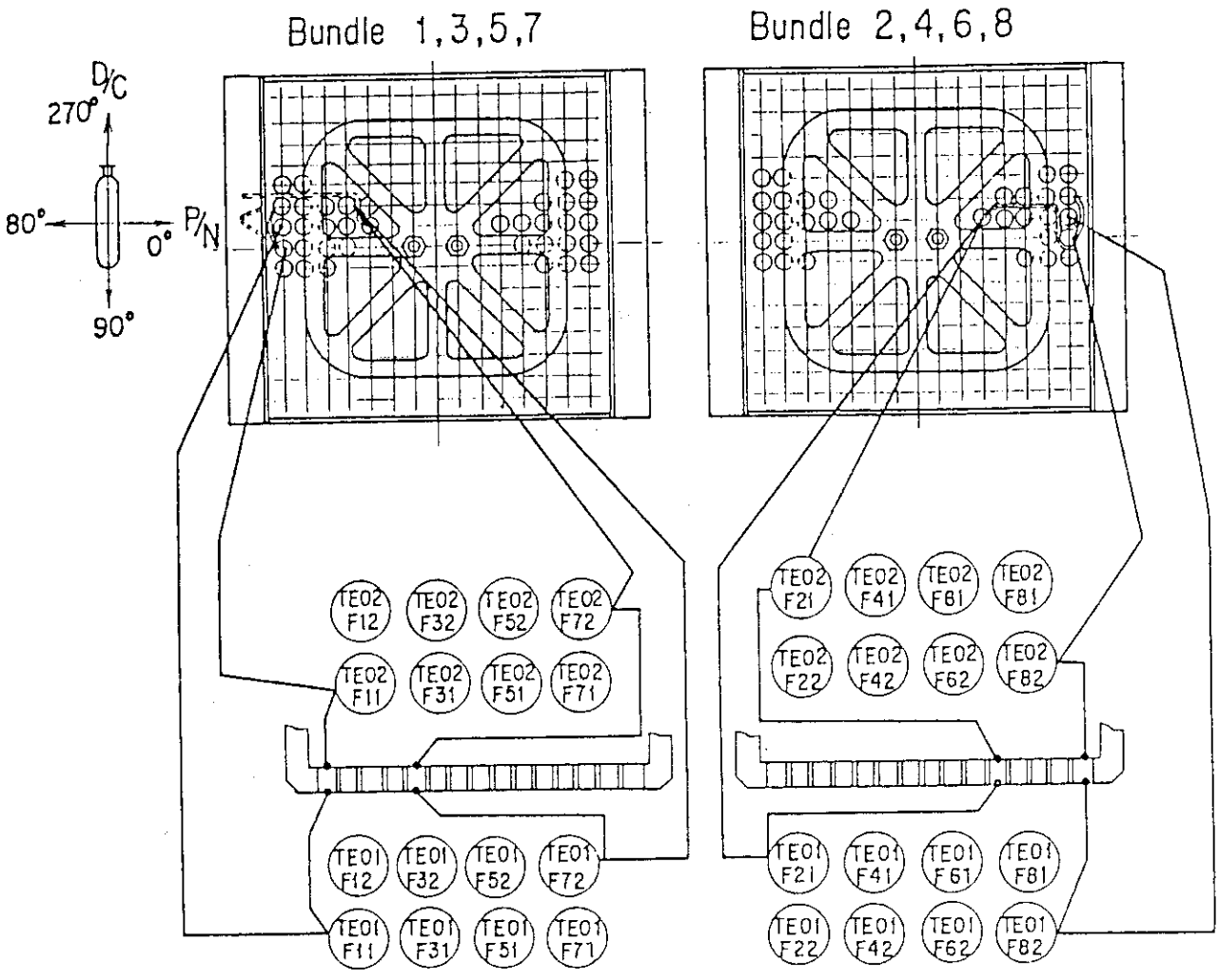

Fig. A – 22 Thermocouple Locations of Fluid Temperature Measurements Just above and below End Box Tie Plate

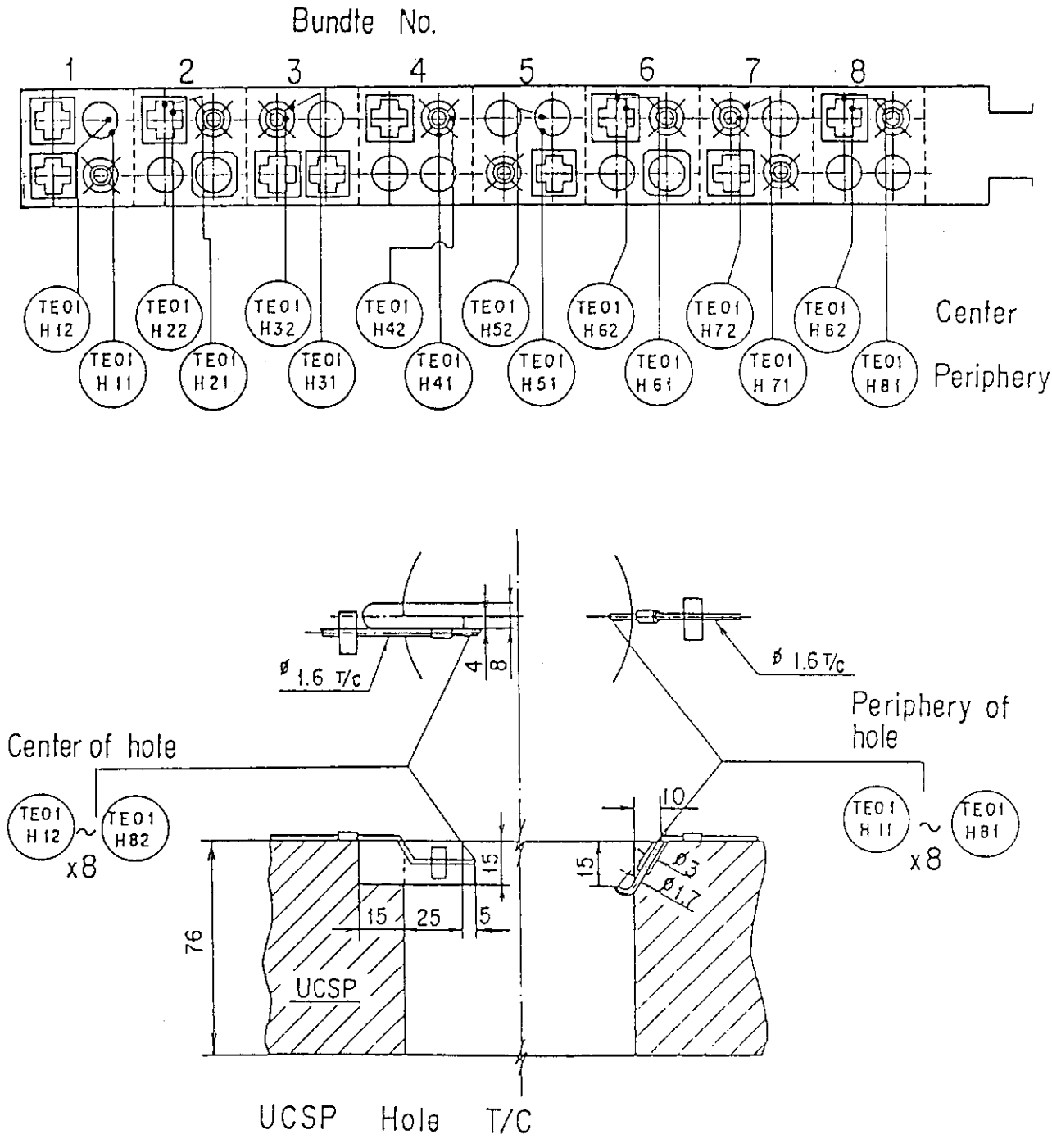

Fig. A – 23 Thermocouple Locations of Fluid Temperature Measurements at Center and Periphery of UCSP Holes

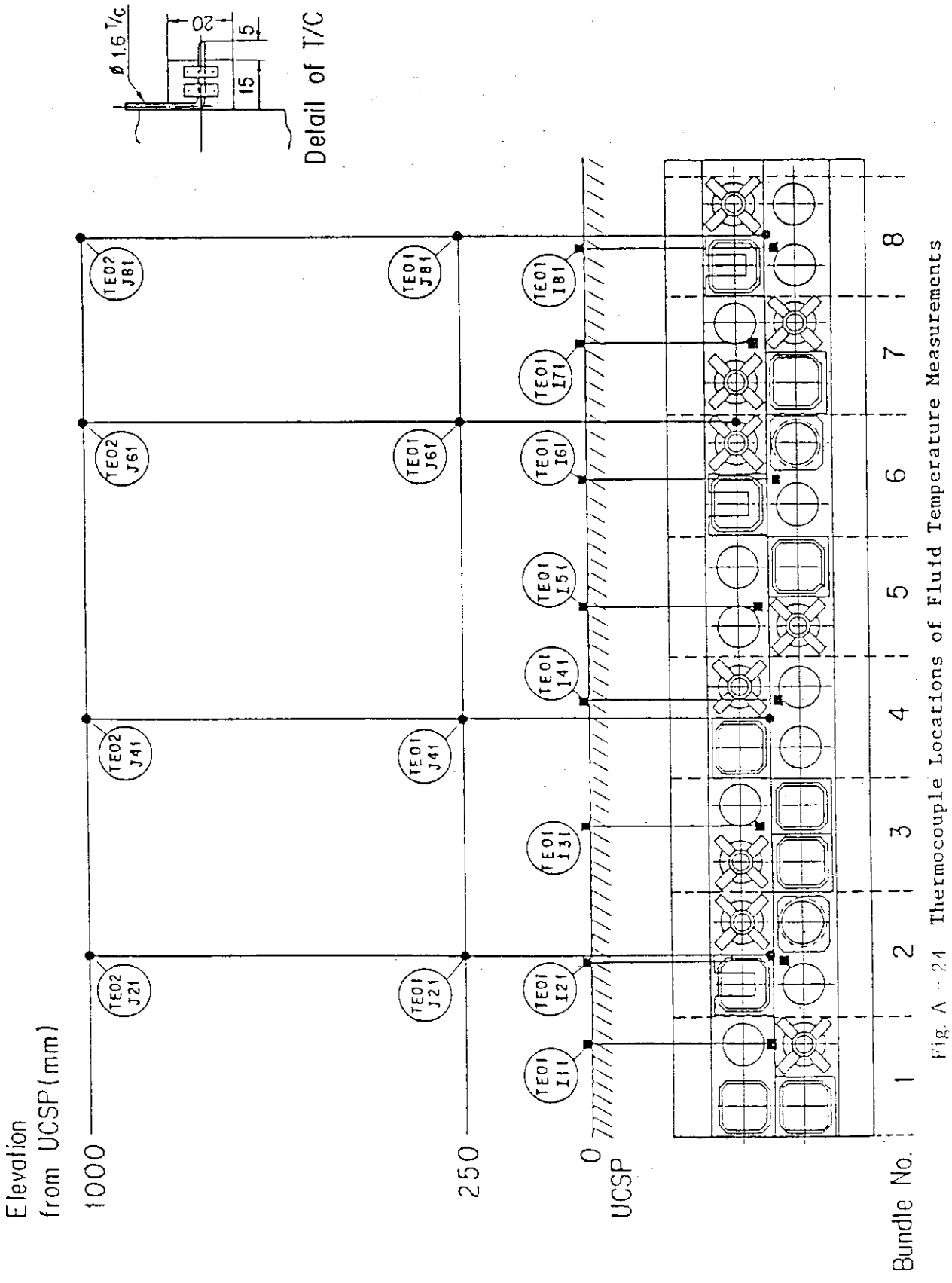

Fig. A.24 Thermocouple Locations of Fluid Temperature Measurements on and above UCSP

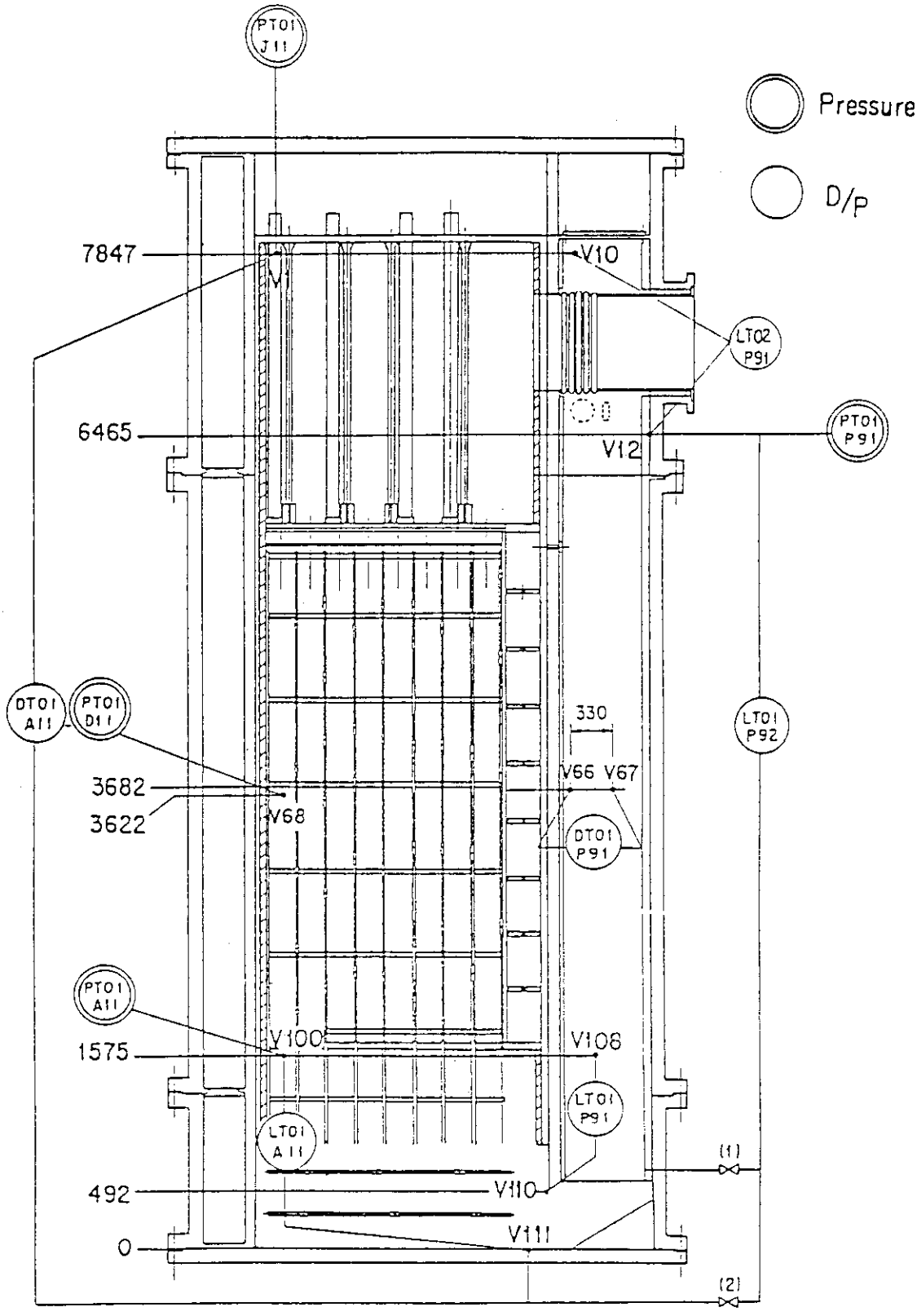

Fig. A – 25 Location of Pressure Measurements in Pressure Vessel, Differential Pressure Measurements between Upper and Lower Plenum and Liquid Level Measurements in Downcomer and Lower Plenum

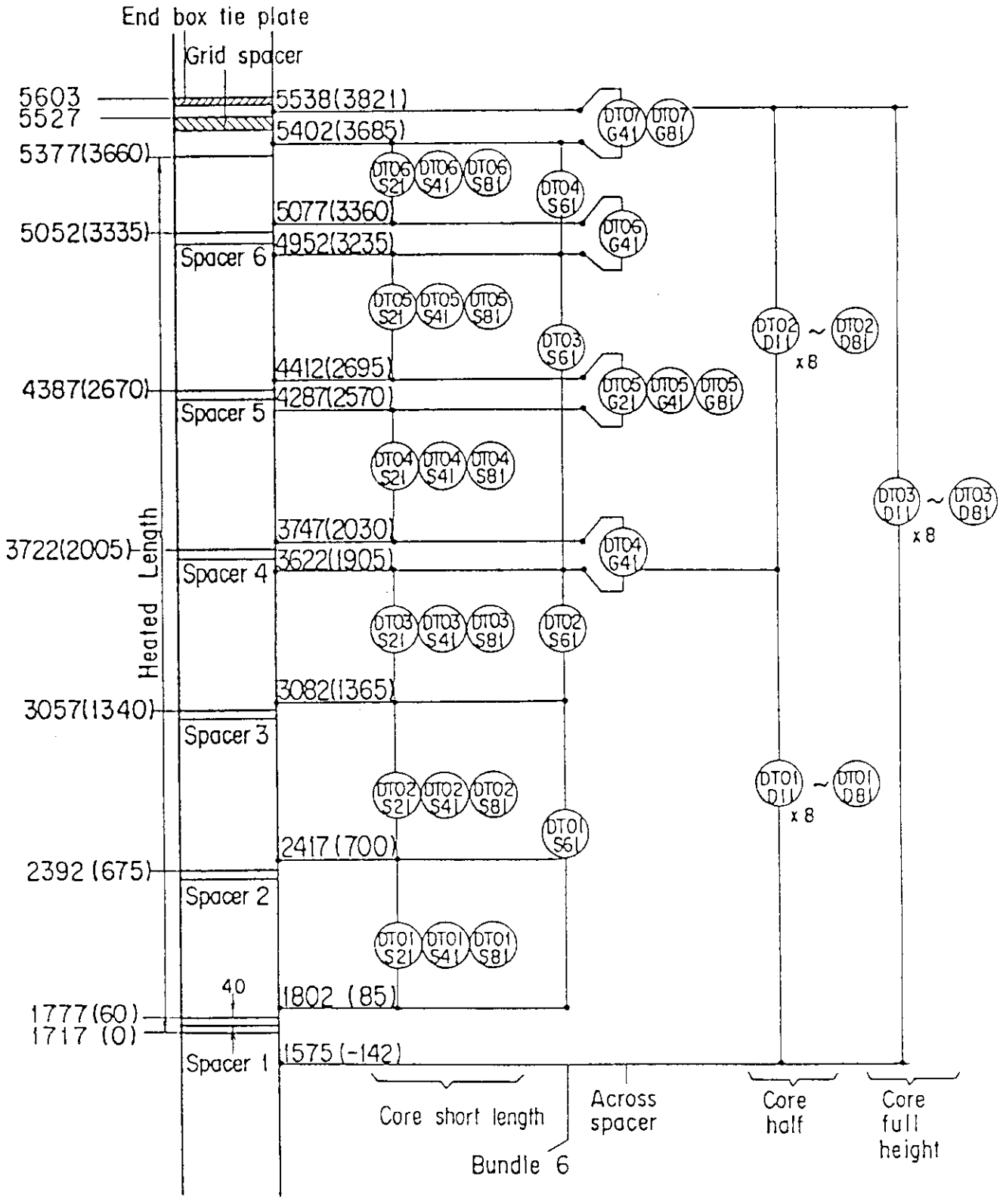

Fig. A – 26 Locations of Vertical Differential Pressure Measurements in Core

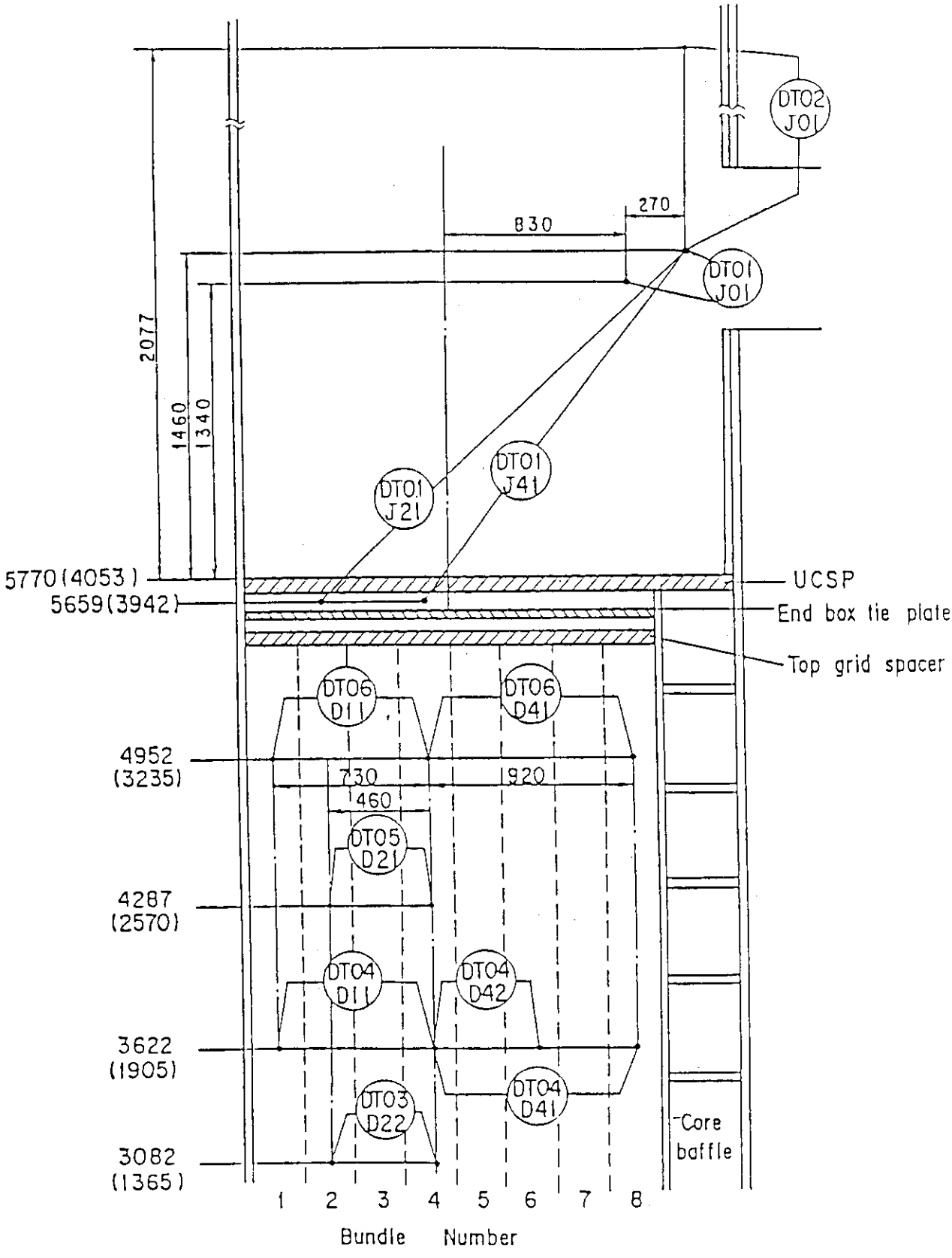

Fig. A－27 Locations of Horizontal Differential Pressure Measurements in Core and Differential Pressure Measurements between End Box and Inlet of Hot Leg

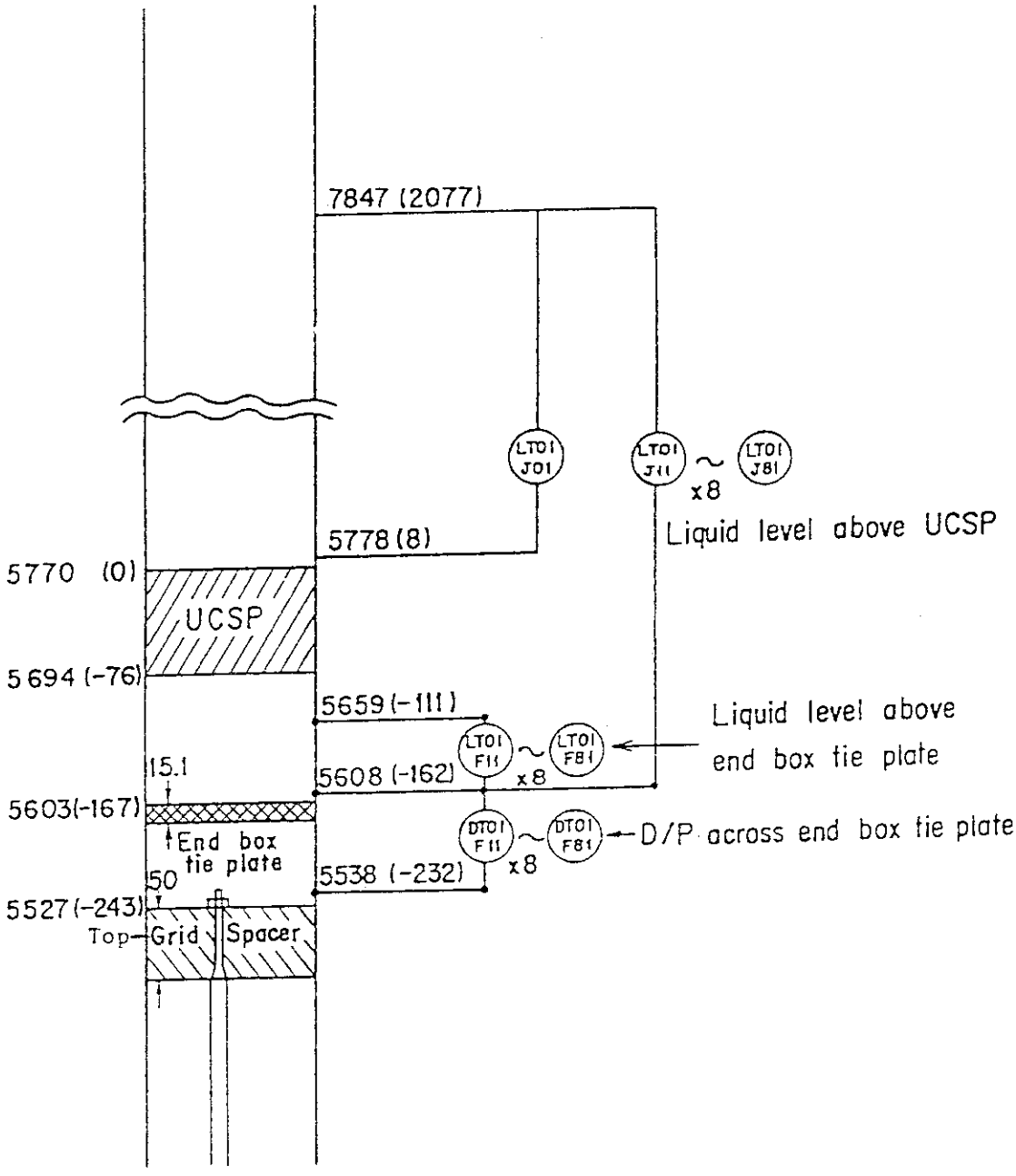

Fig. A – 28 Locations of Differential Pressure Measurements across End Box Tie Plate and Liquid Level Measurements above UCSP and End Box Tie Plate

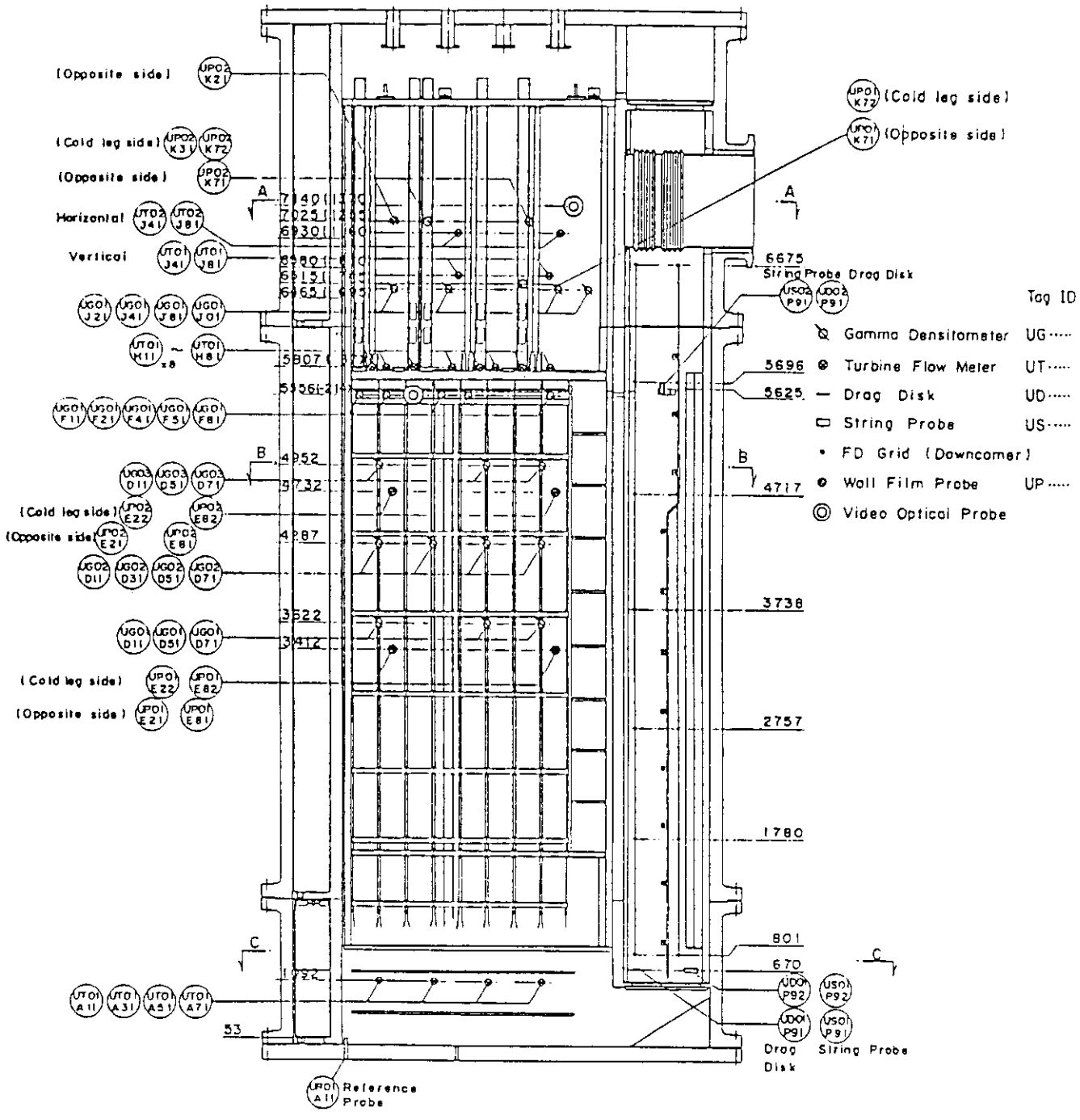

Fig. A - 29. Vertical Locations of USNRC-Provided Instruments in Pressure Vessel

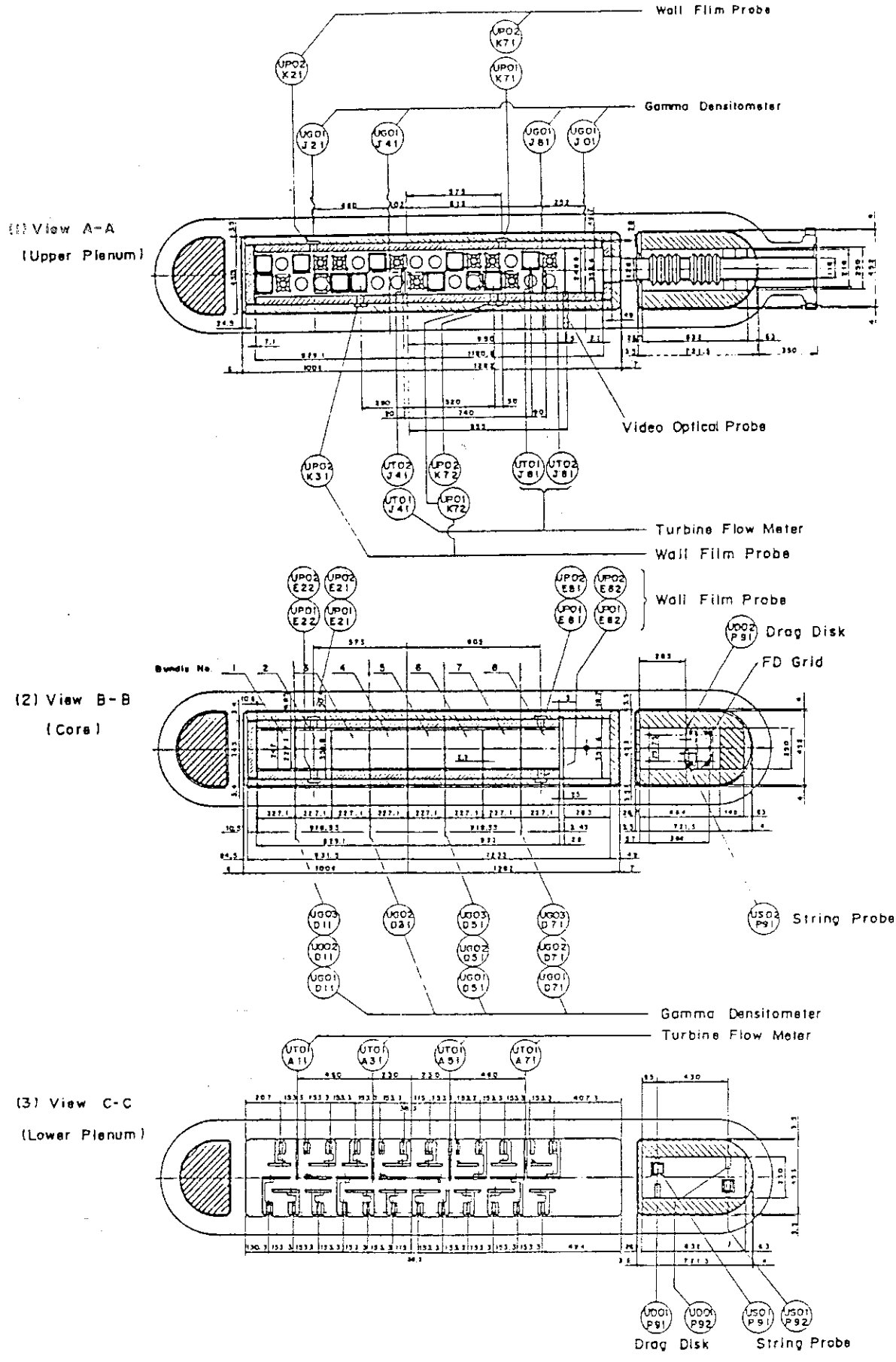

Fig. A - 30 Horizontal Locations of USNRC-Provided Instruments in Pressure Vessel

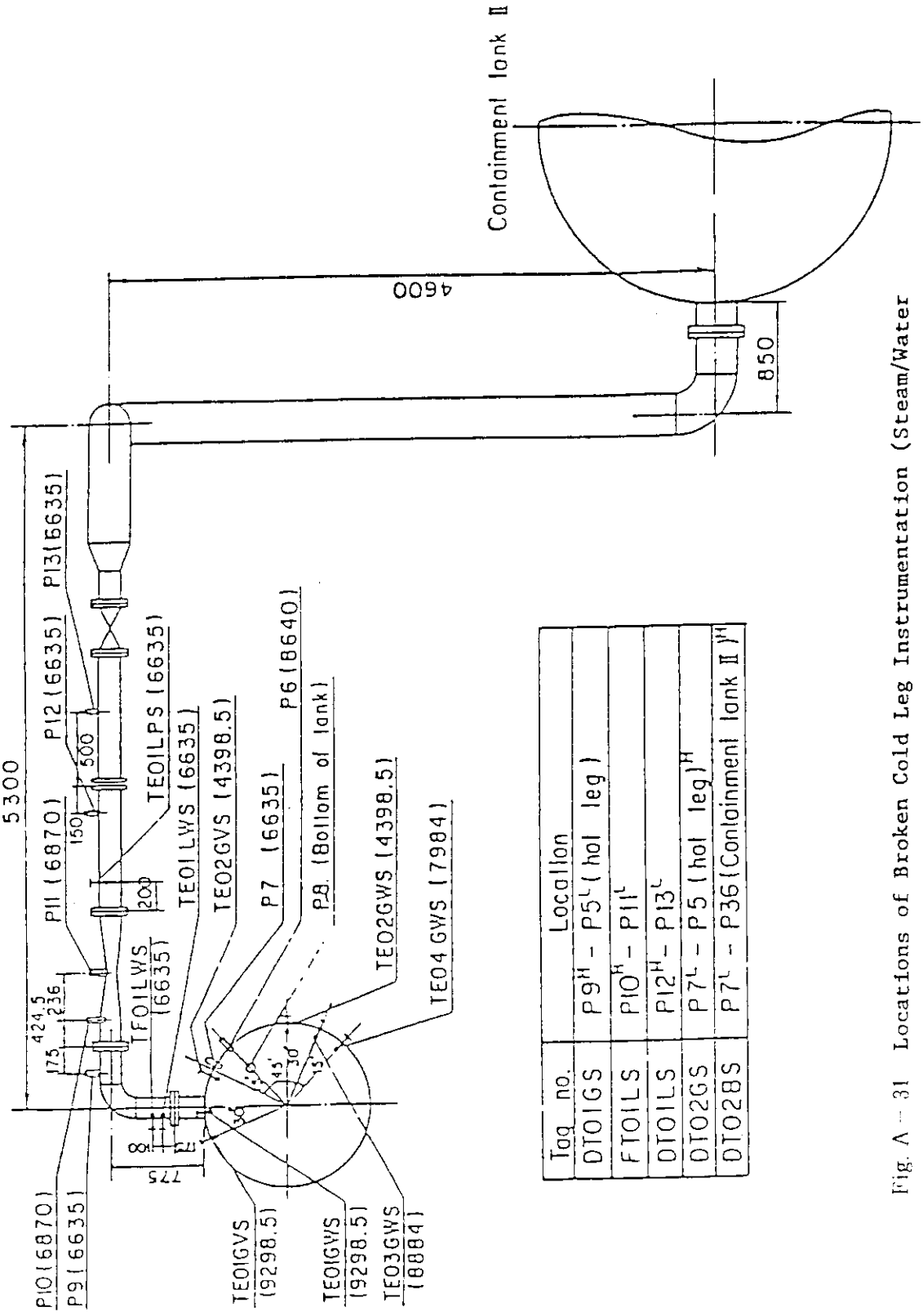

Fig. A - 31 Locations of Broken Cold Leg Instrumentation (Steam/Water Separator Side)

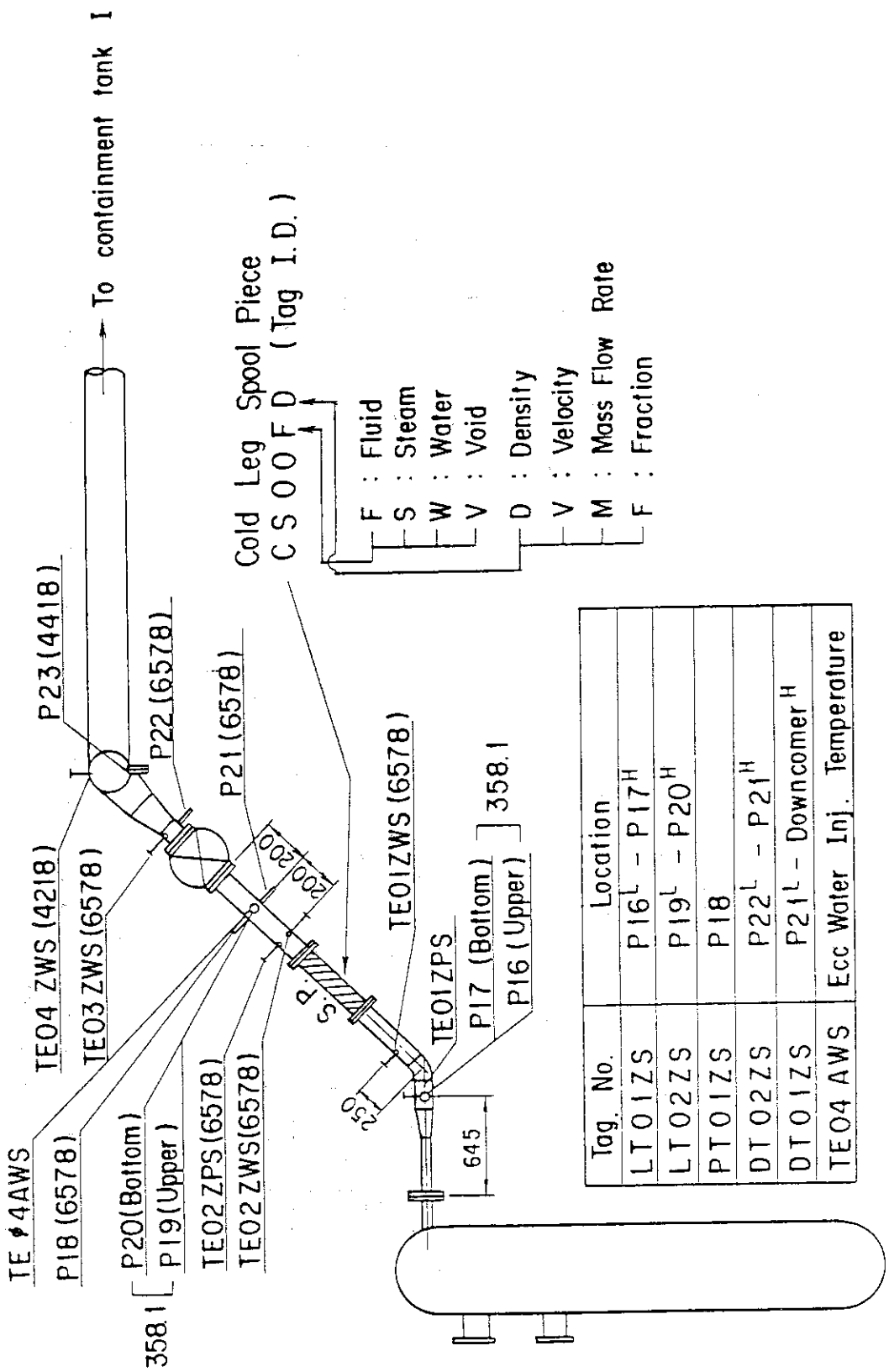

Fig. A 32 Location of Broken Cold Leg Instrumentation
(Pressure Vessel Side)

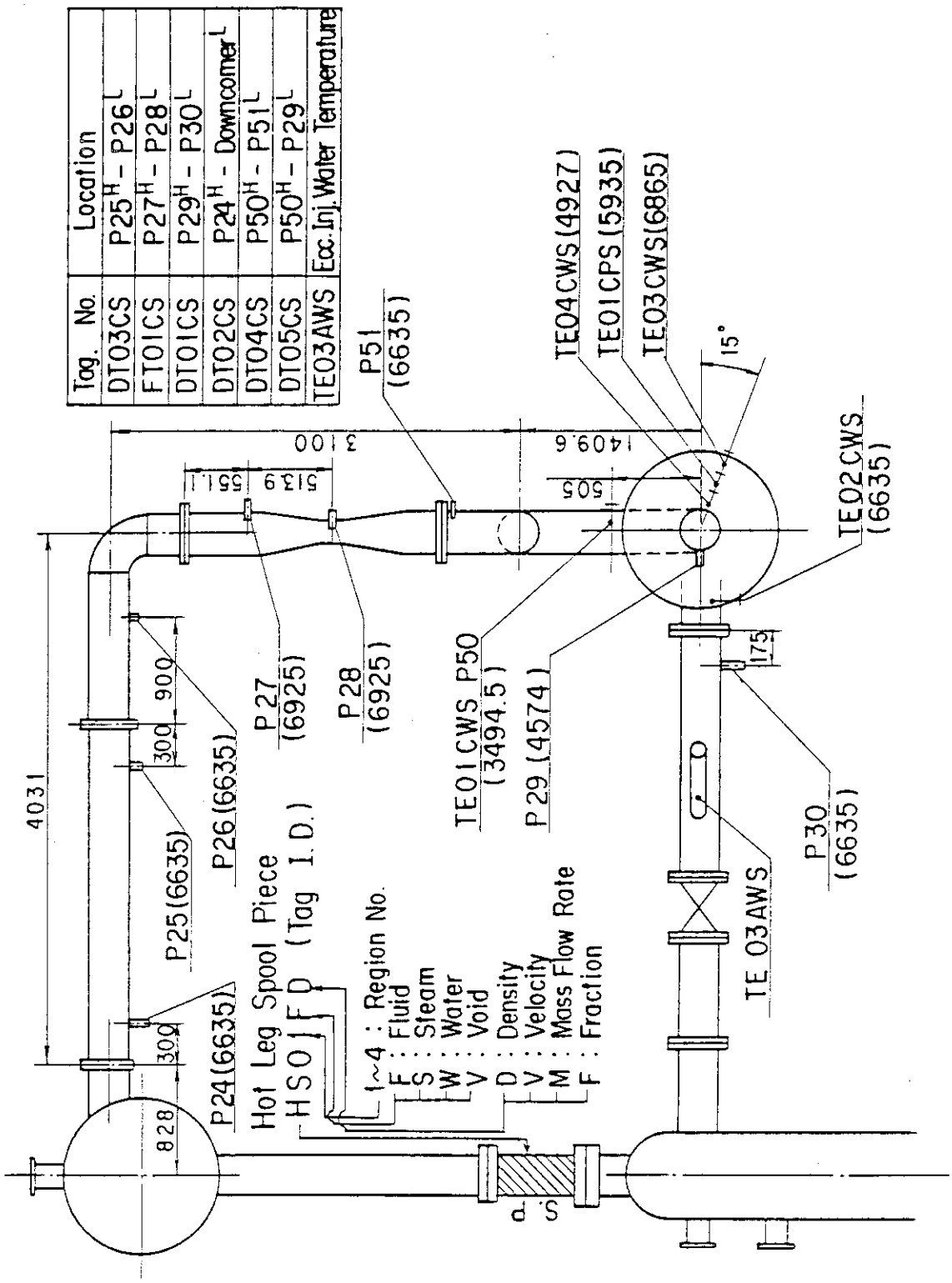

Fig. A - 33 Location of Hot Leg and Intact Cold Leg Instrumetation

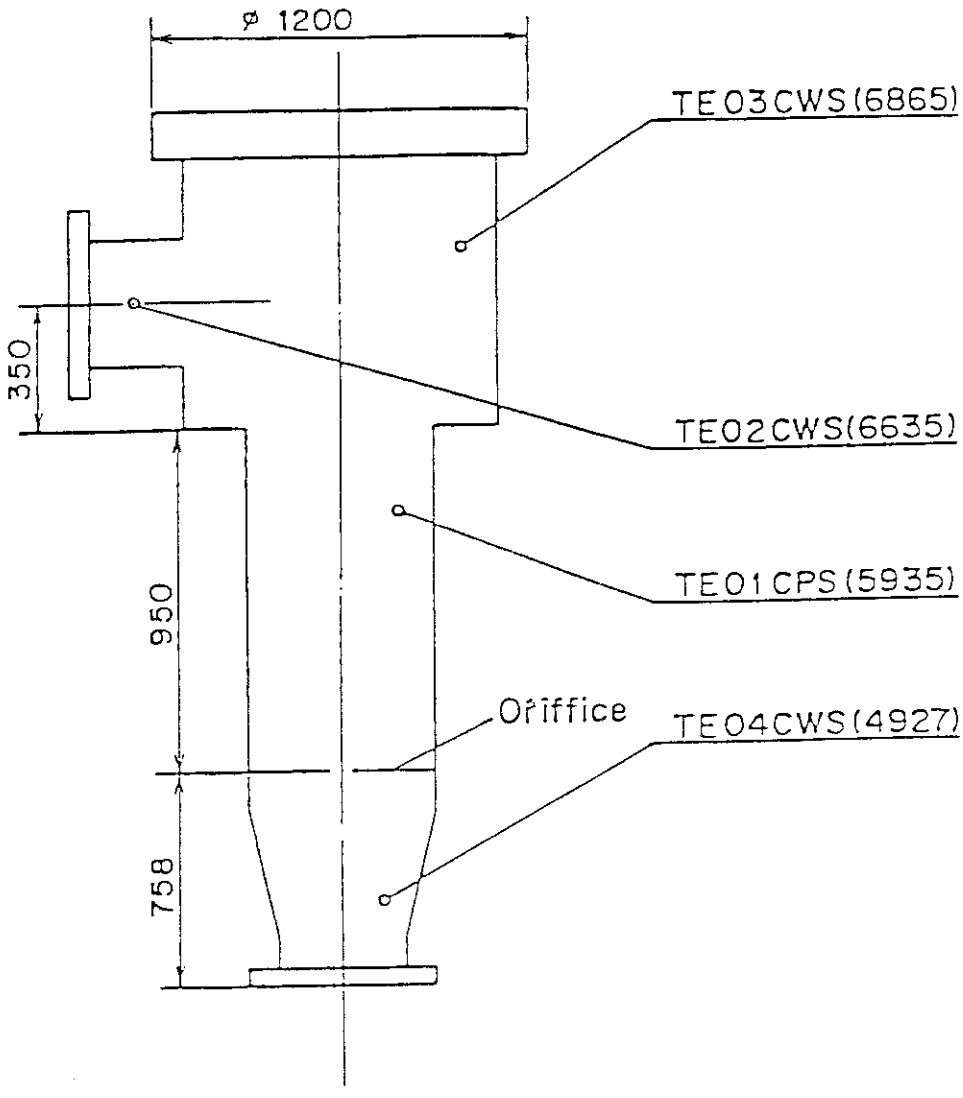

Fig. A – 34 Locations of Pump Simulator Instrumentation

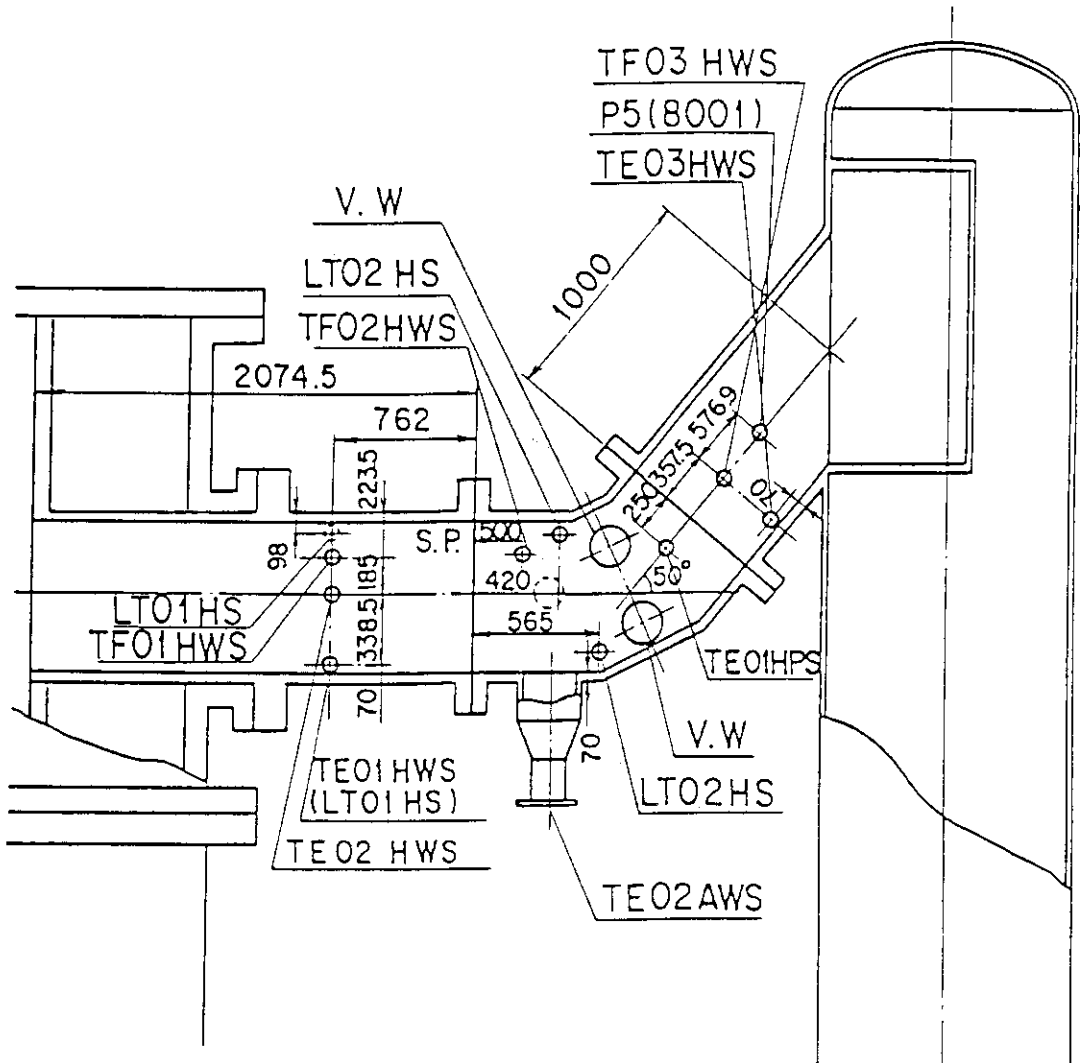

Tag. No.	Location
DT01 HS	$P5^{L}$ - Inlet of hot leg^{H}
DT01 GS	$P5^{L}$ - Broken cold leg (S-W separator $side)^{H}$
DT02GS	$P5^{H}$ - S-W separator $tank^{L}$
TE02 AWS	ECC injection water temperature

Fig. A－35 Locations of Hot Leg Instrumentation

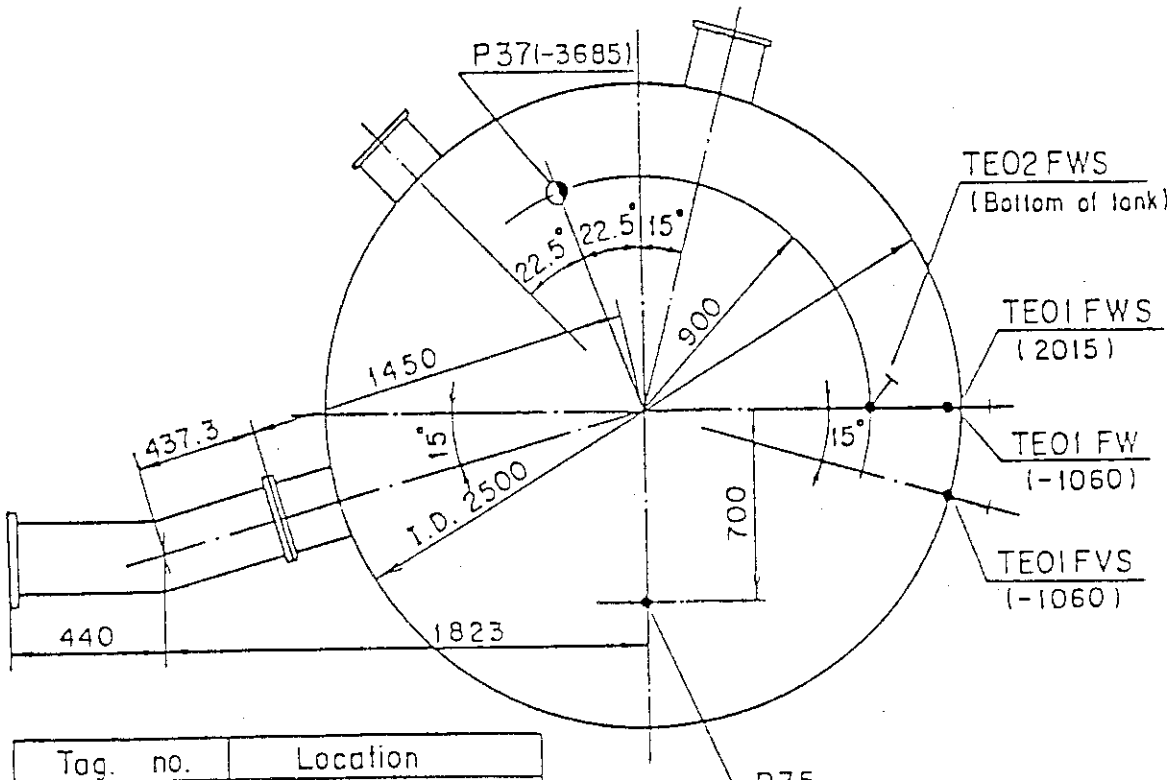

Tag. no.	Location
LT01 FS	$P35^{L}$ – $P37^{H}$
DT01 FS	$P35^{H}$ – $Downcomer^{L}$
DT01 E	$P35^{H}$ – P36 (C.T. II)^{H}
PT01 F	P35

Fig. A – 36 Locations of Containment Tank-I Instrumentation

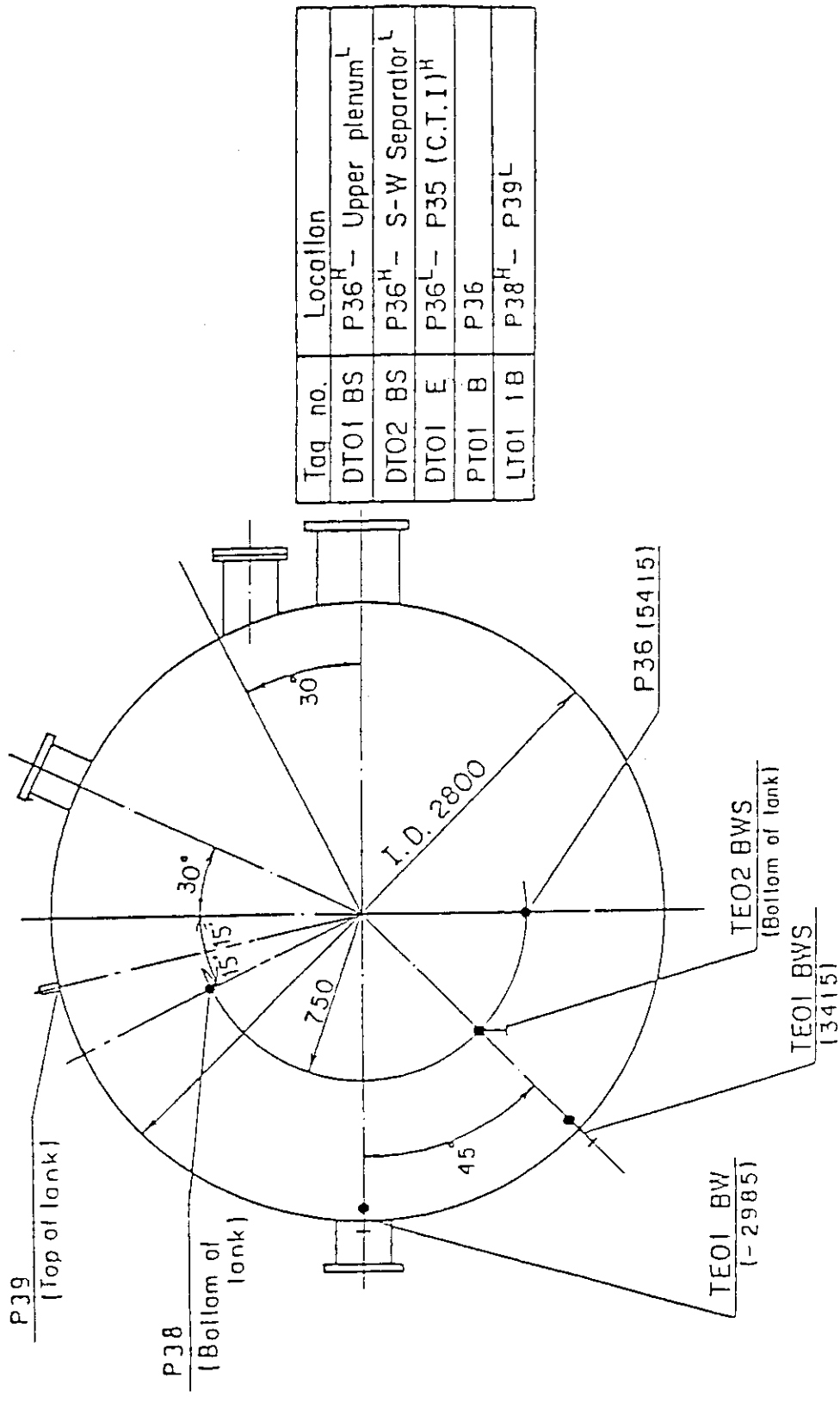

Fig. A - 37 Locations of Containment Tank-II Instrumentation

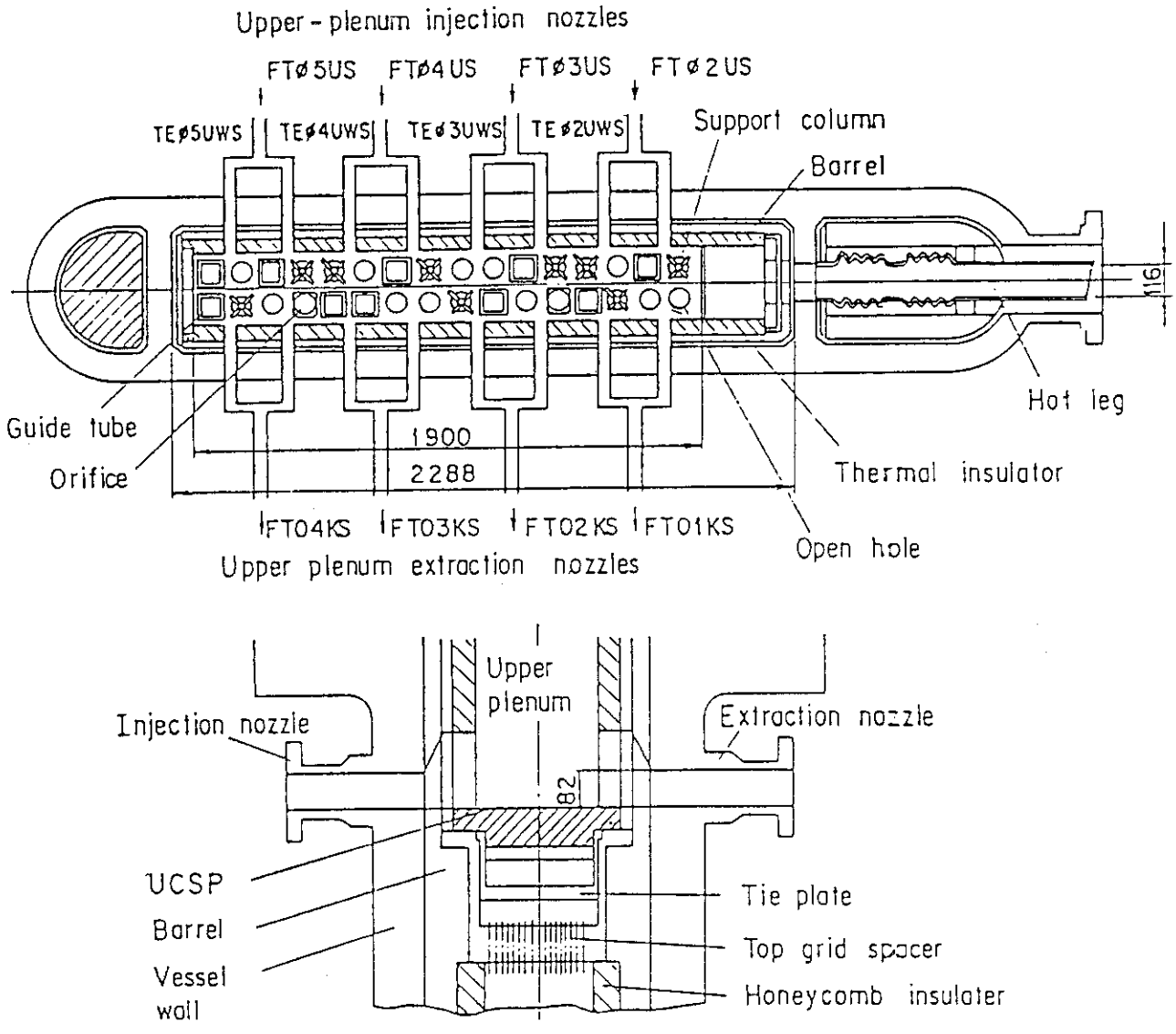

Fig. A - 38 Locations of UCSP Water Injection System Instrumentation

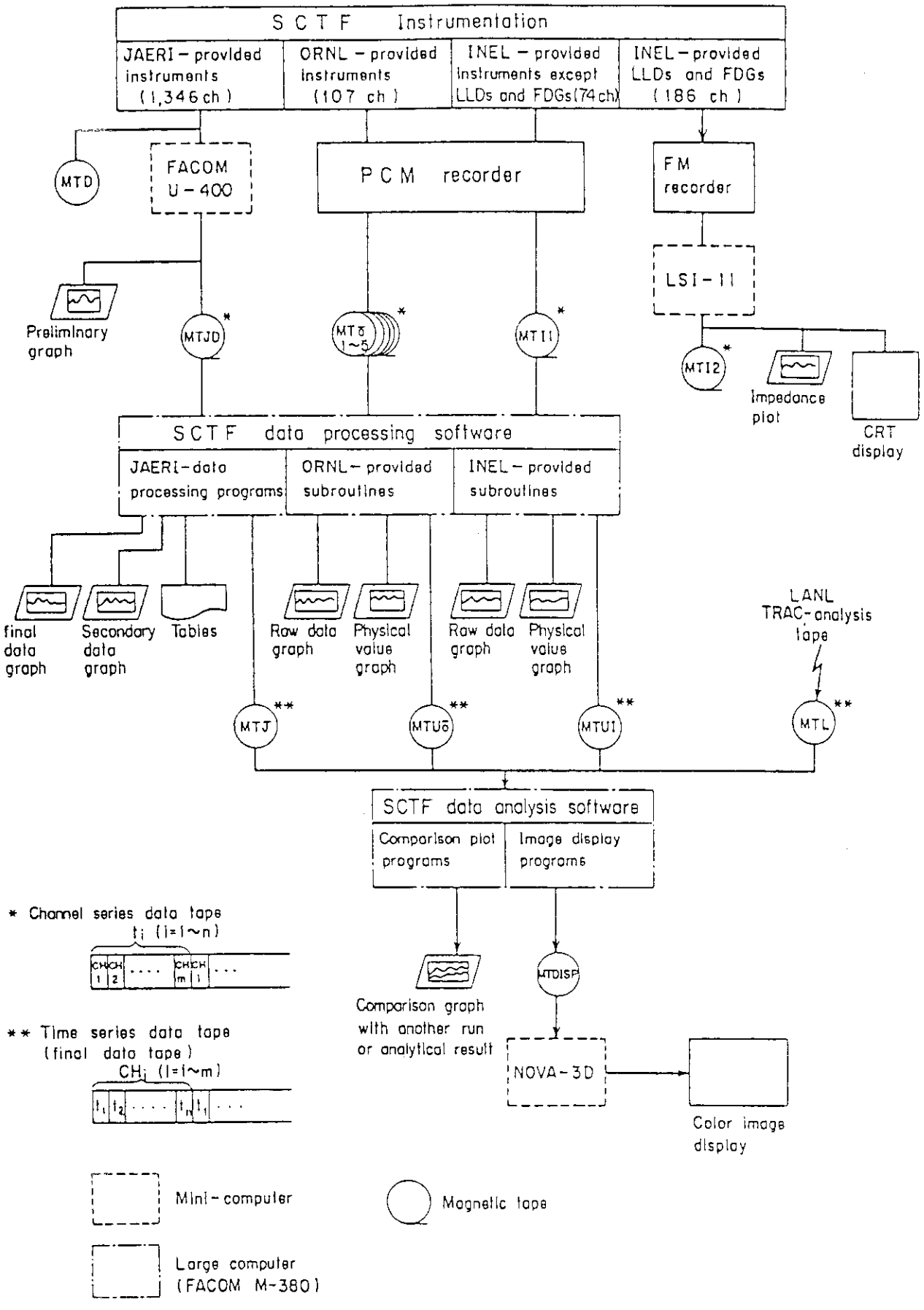

Fig. A - 39 Flow Chart of Data Reduction

Appendix B

Selected Data from Test S2-07

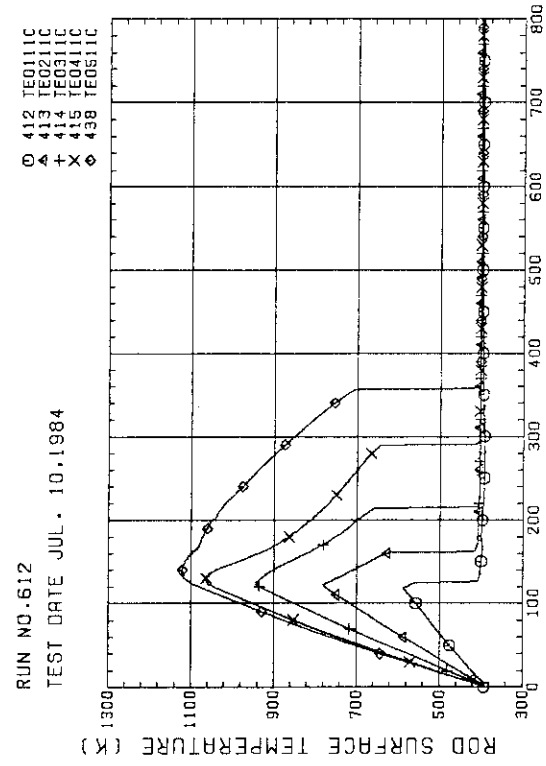

Fig. B-1 HEATER ROD TEMPERATURE (BUNDLE 1-1A, LOWER HALF)

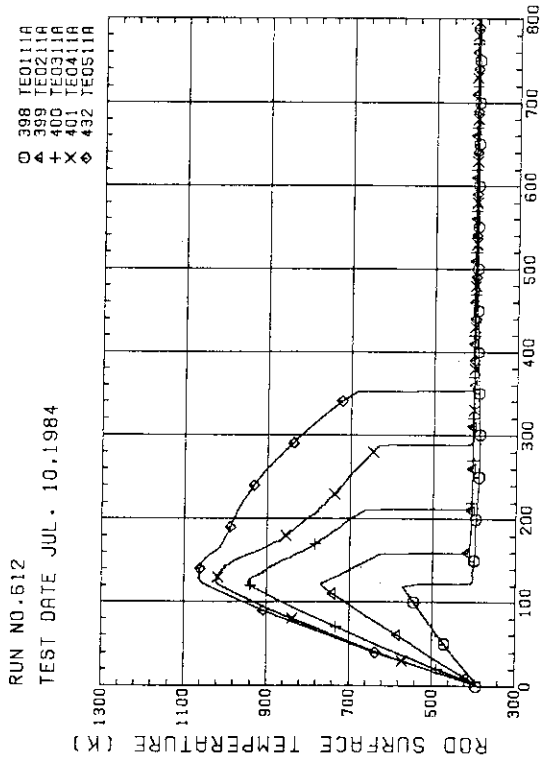

Fig. B-2 HEATER ROD TEMPERATURE (BUNDLE 1-1A, UPPER HALF)

Fig. B-3 HEATER ROD TEMPERATURE (BUNDLE 1-1C, LOWER HALF)

Fig. B-4 HEATER ROD TEMPERATURE (BUNDLE 1-1C, UPPER HALF)

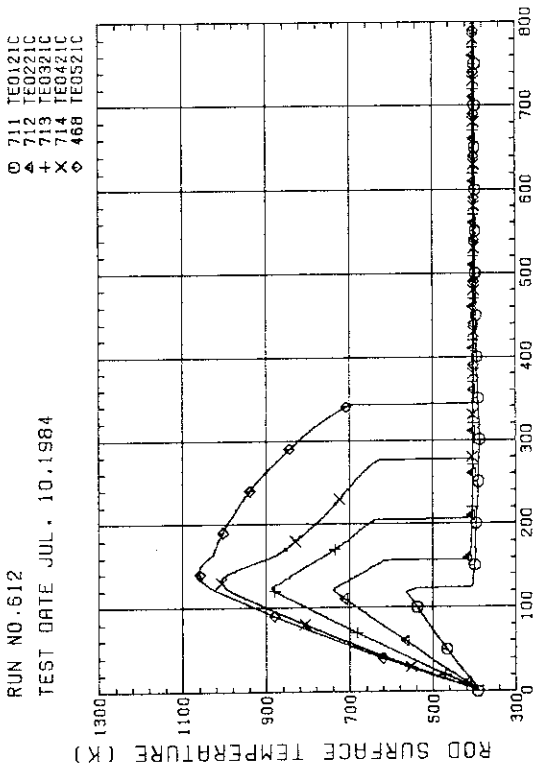

Fig. B-7 HEATER ROD TEMPERATURE (BUNDLE 2-1C, LOWER HALF)

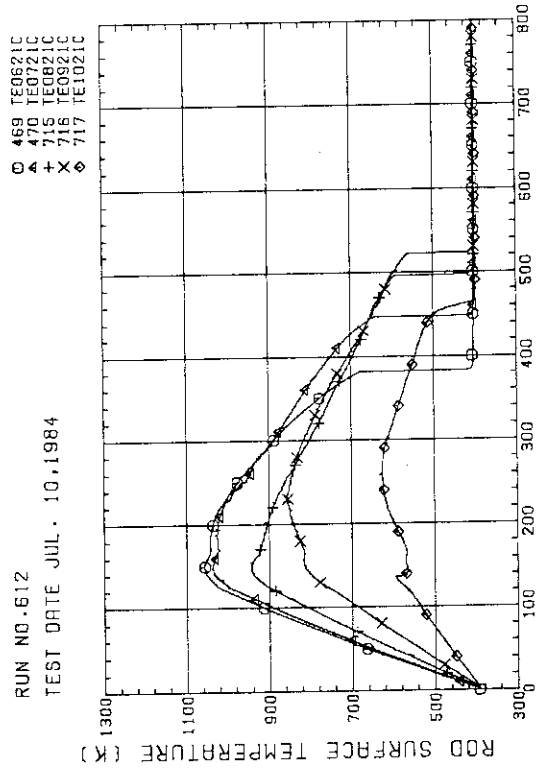

Fig. B-8 HEATER ROD TEMPERATURE (BUNDLE 2-1C, UPPER HALF)

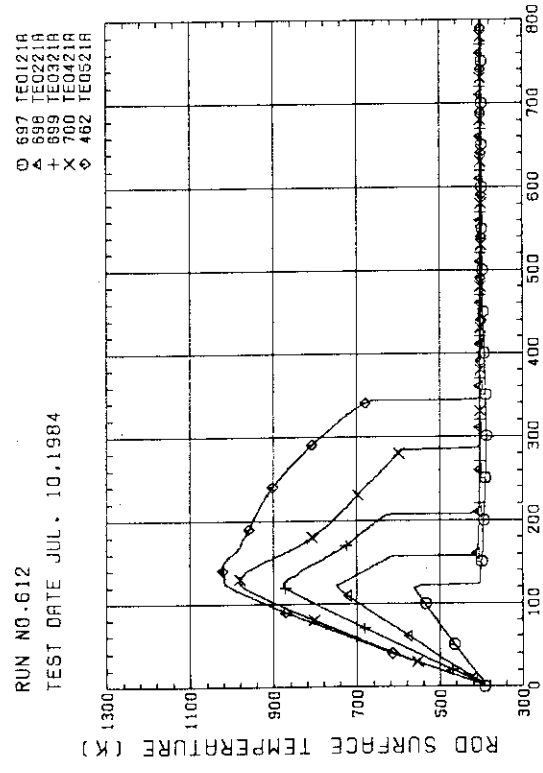

Fig. B-5 HEATER ROD TEMPERATURE (BUNDLE 2-1A, LOWER HALF)

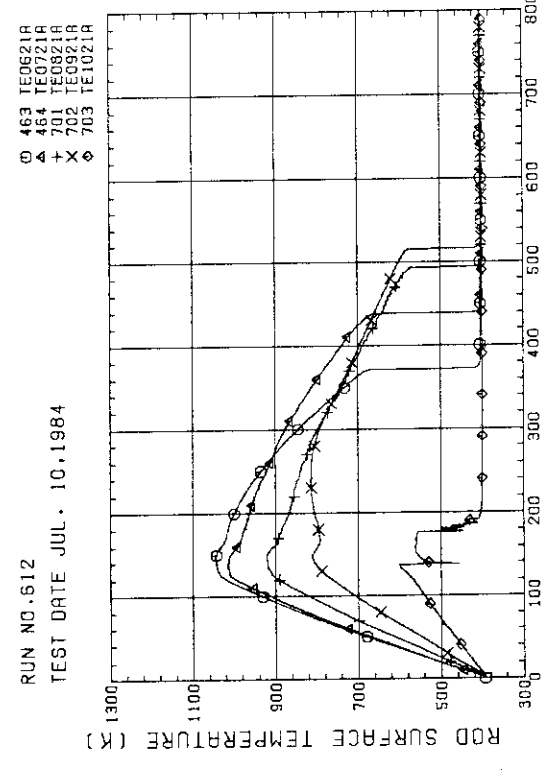

Fig. B-6 HEATER ROD TEMPERATURE (BUNDLE 2-1A, UPPER HALF)

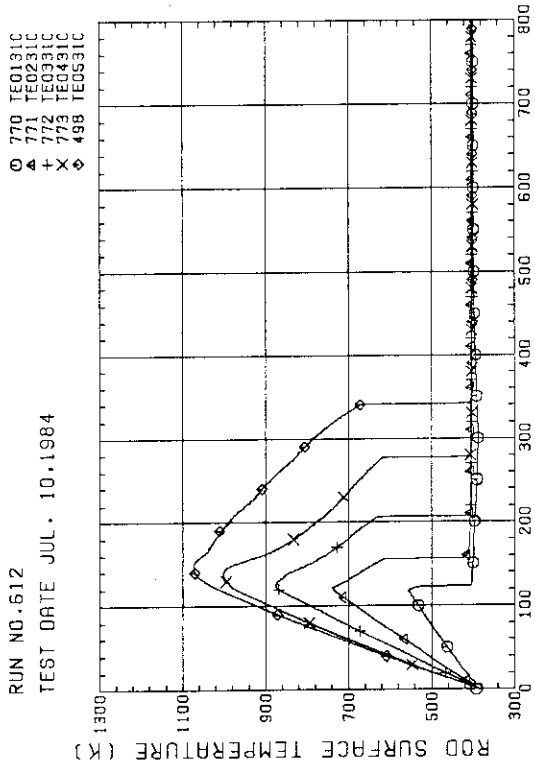

Fig. B-9 HEATER ROD TEMPERATURE (BUNDLE 3-1A, LOWER HALF)

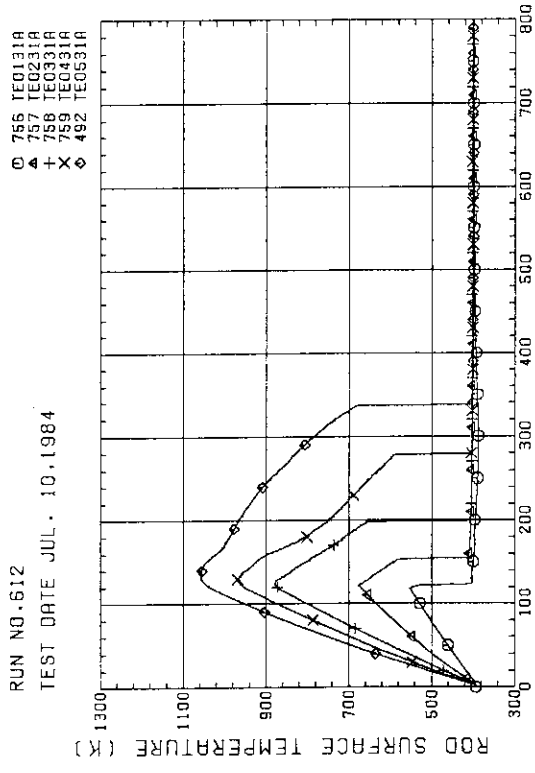

Fig. B-10 HEATER ROD TEMPERATURE (BUNDLE 3-1A, UPPER HALF)

Fig. B-11 HEATER ROD TEMPERATURE (BUNDLE 3-1C, LOWER HALF)

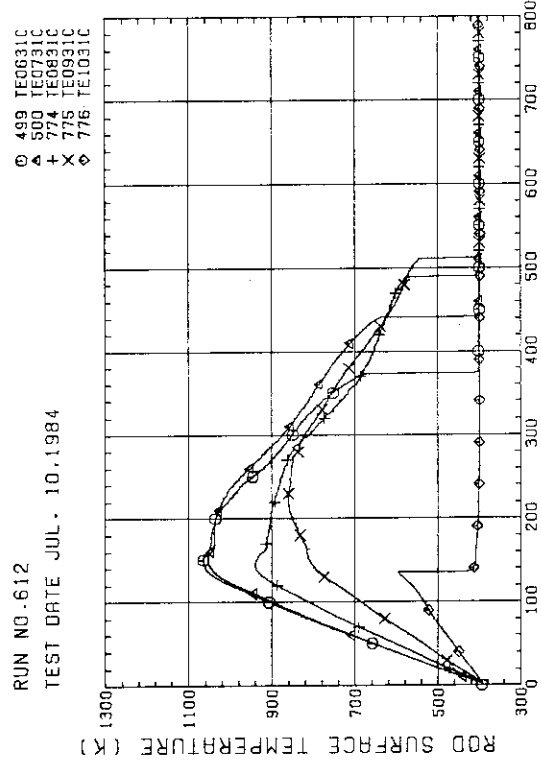

Fig. B-12 HEATER ROD TEMPERATURE (BUNDLE 3-1C, UPPER HALF)

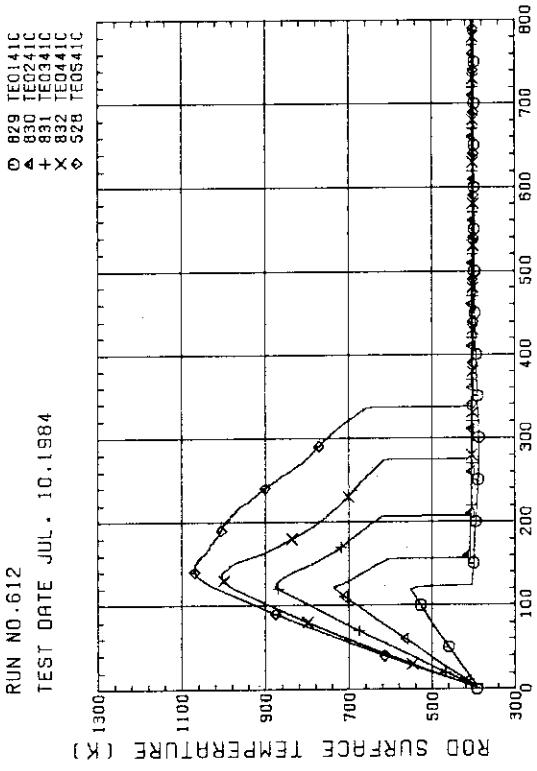

Fig. B-15 HEATER ROD TEMPERATURE (BUNDLE 4-1C, LOWER HALF)

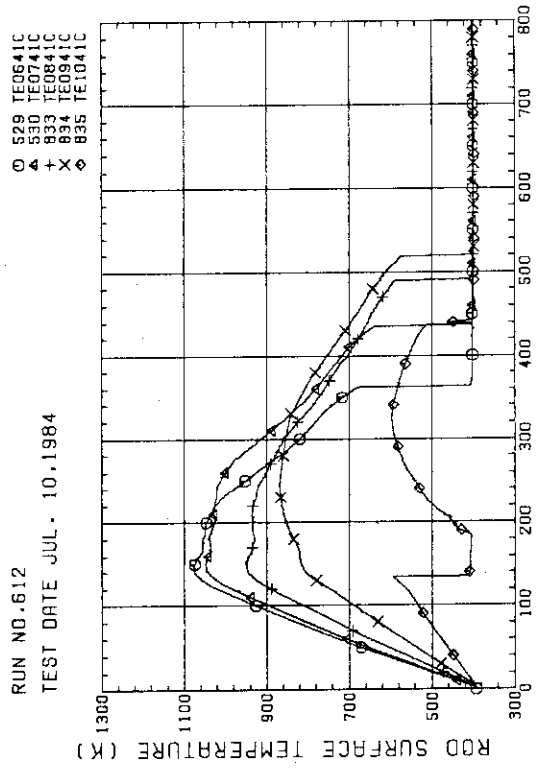

Fig. B-16 HEATER ROD TEMPERATURE (BUNDLE 4-1C, UPPER HALF)

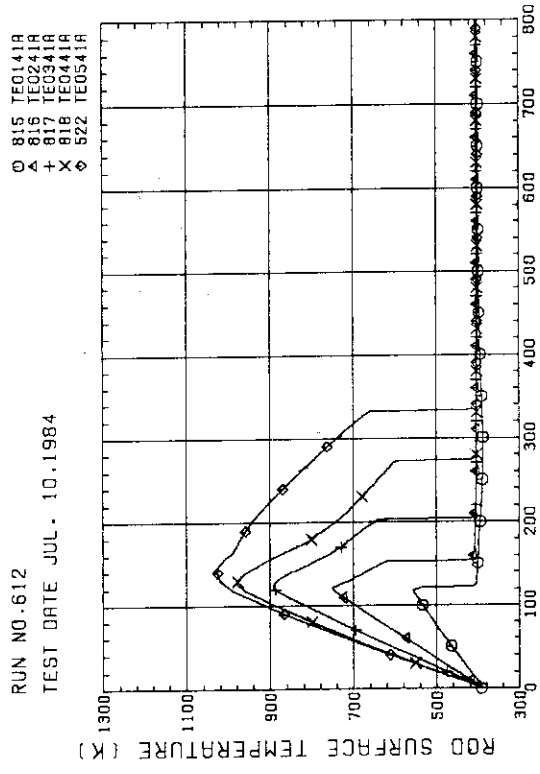

Fig. B-13 HEATER ROD TEMPERATURE (BUNDLE 4-1A, LOWER HALF)

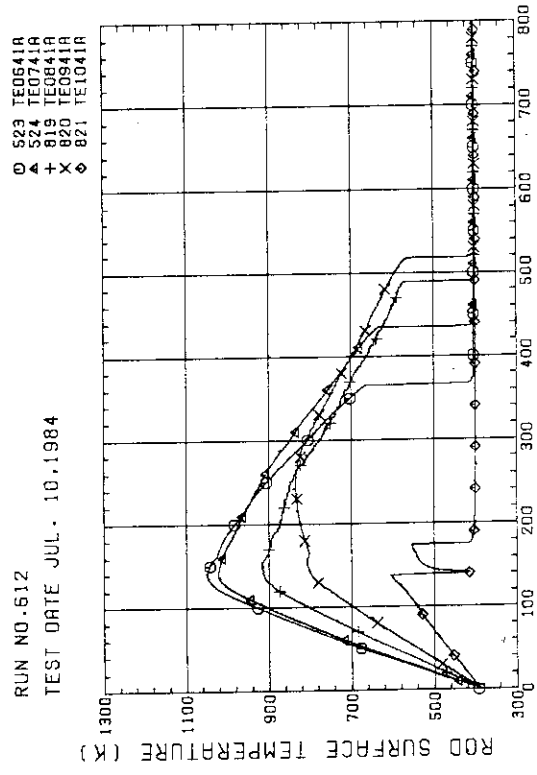

Fig. B-14 HEATER ROD TEMPERATURE (BUNDLE 4-1A, UPPER HALF)

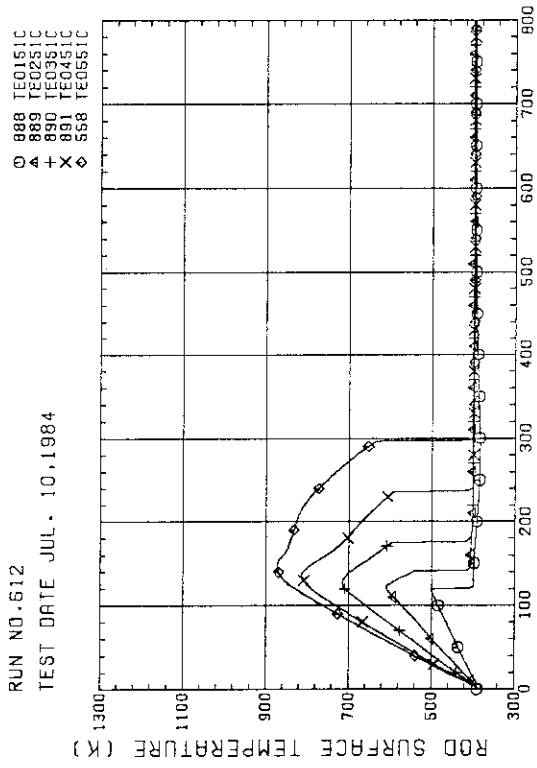

Fig. B-19 HEATER ROD TEMPERATURE (BUNDLE 5-1C, LOWER HALF)

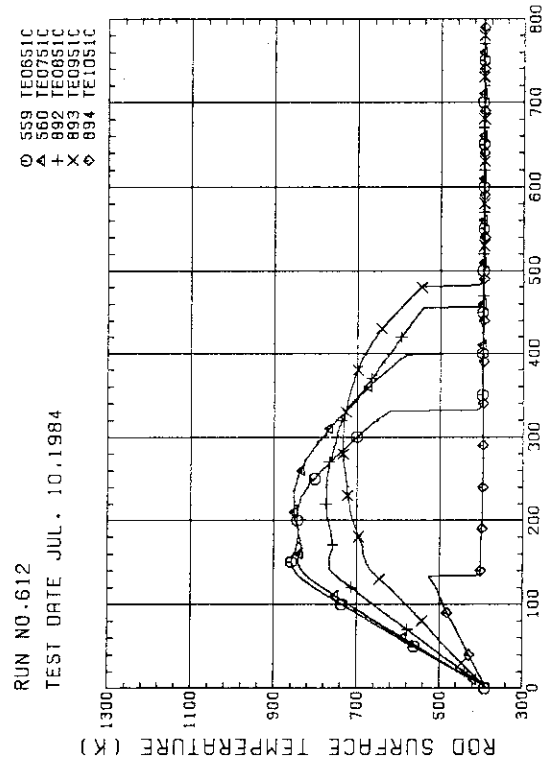

Fig. B-20 HEATER ROD TEMPERATURE (BUNDLE 5-1C, UPPER HALF)

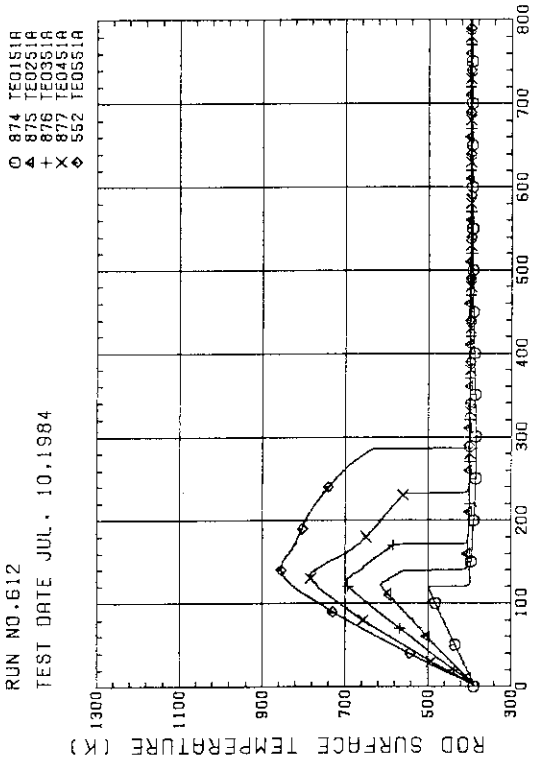

Fig. B-17 HEATER ROD TEMPERATURE (BUNDLE 5-1A, LOWER HALF)

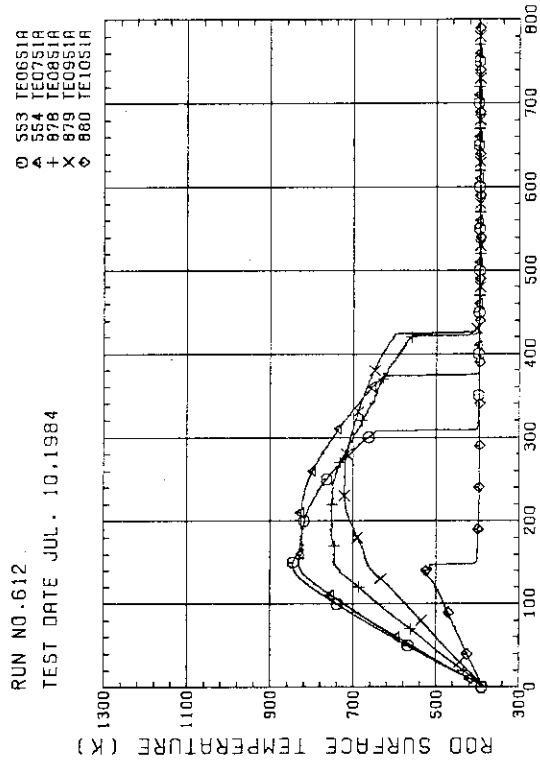

Fig. B-18 HEATER ROD TEMPERATURE (BUNDLE 5-1A, UPPER HALF)

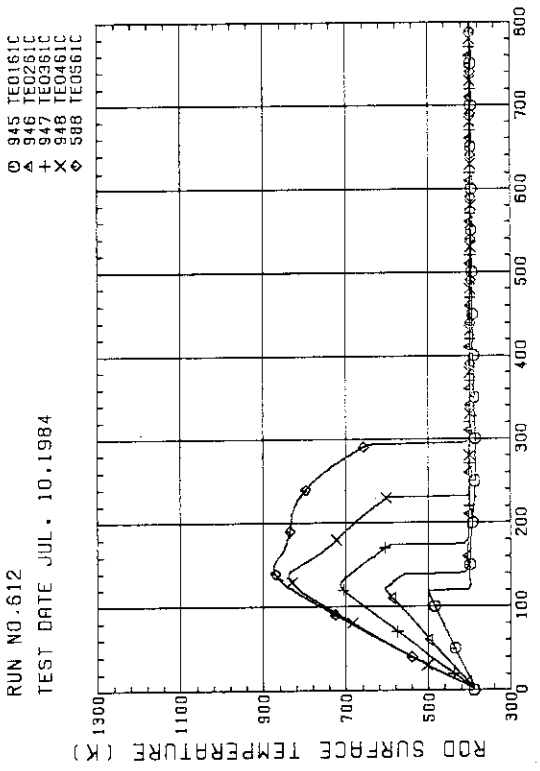

Fig. B-23 HEATER ROD TEMPERATURE (BUNDLE 6-1C, LOWER HALF)

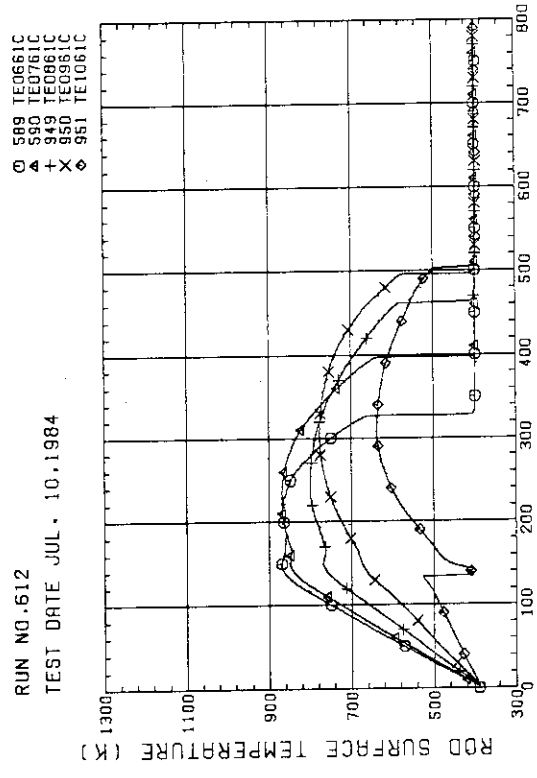

Fig. B-24 HEATER ROD TEMPERATURE (BUNDLE 6-1C, UPPER HALF)

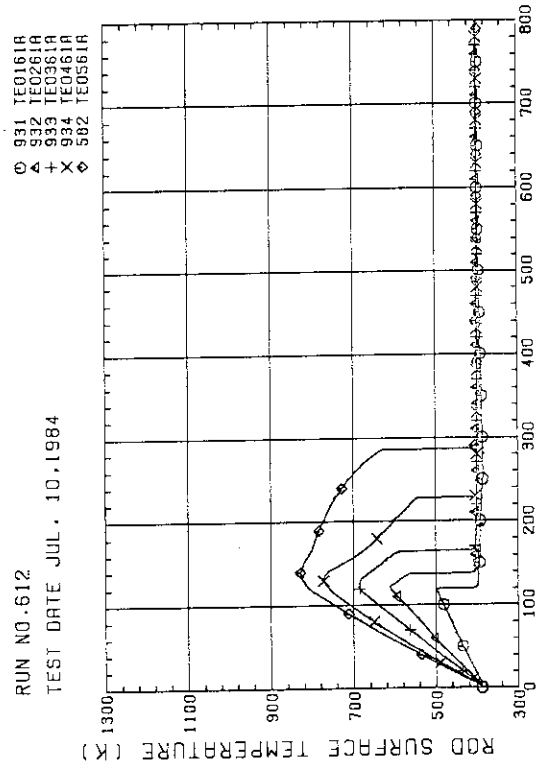

Fig. B-21 HEATER ROD TEMPERATURE (BUNDLE 6-1A, LOWER HALF)

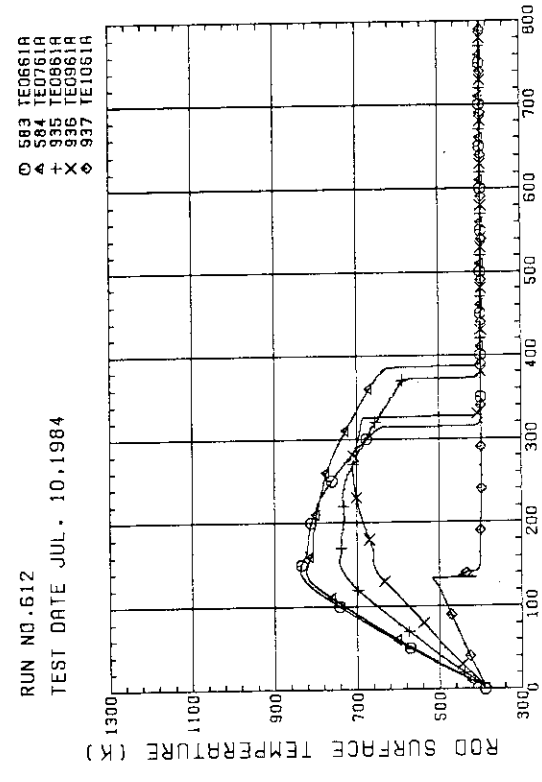

Fig. B-22 HEATER ROD TEMPERATURE (BUNDLE 6-1A, UPPER HALF)

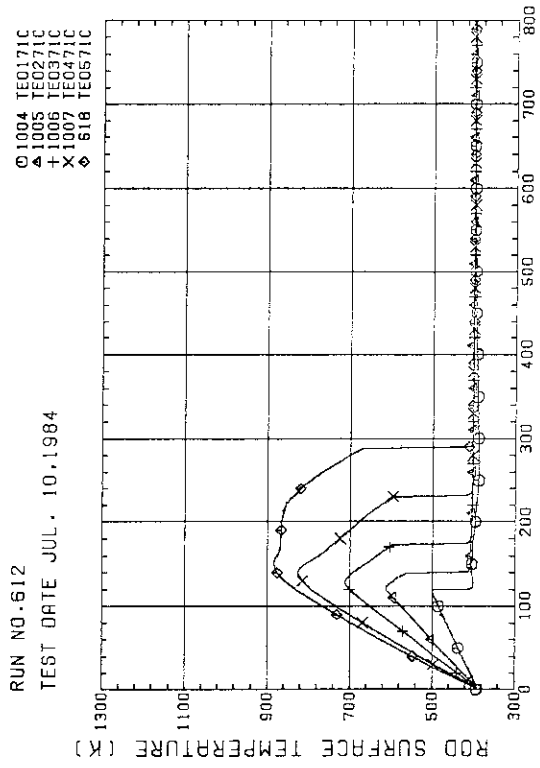

Fig. B-25 HEATER ROD TEMPERATURE (BUNDLE 7-1A, LOWER HALF)

Fig. B-27 HEATER ROD TEMPERATURE (BUNDLE 7-1C, LOWER HALF)

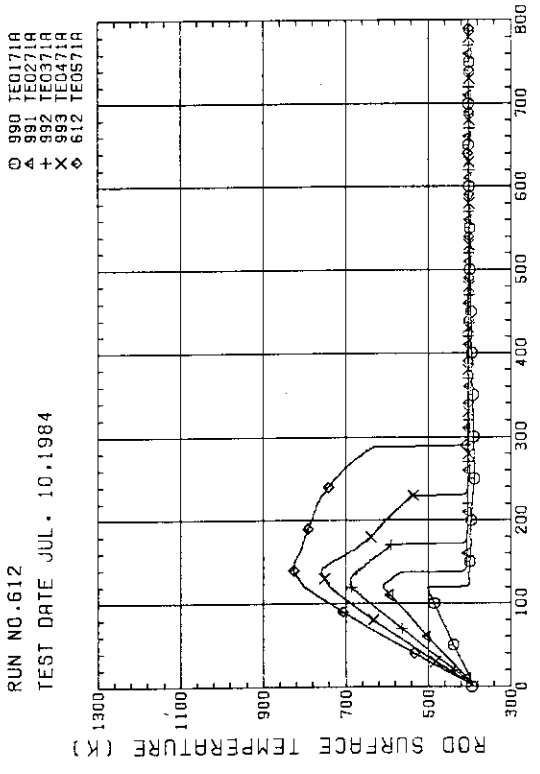

Fig. B-26 HEATER ROD TEMPERATURE (BUNDLE 7-1A, UPPER HALF)

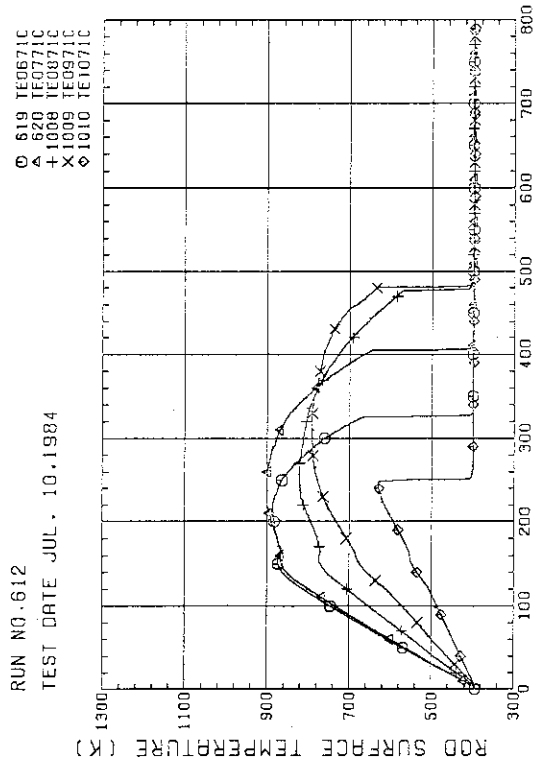

Fig. B-28 HEATER ROD TEMPERATURE (BUNDLE 7-1C, UPPER HALF)

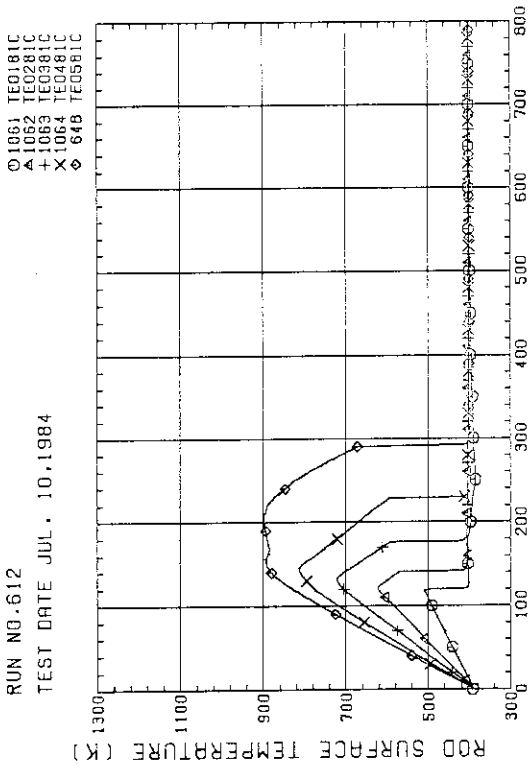

Fig. B-31 HEATER ROD TEMPERATURE (BUNDLE 8-1C, LOWER HALF)

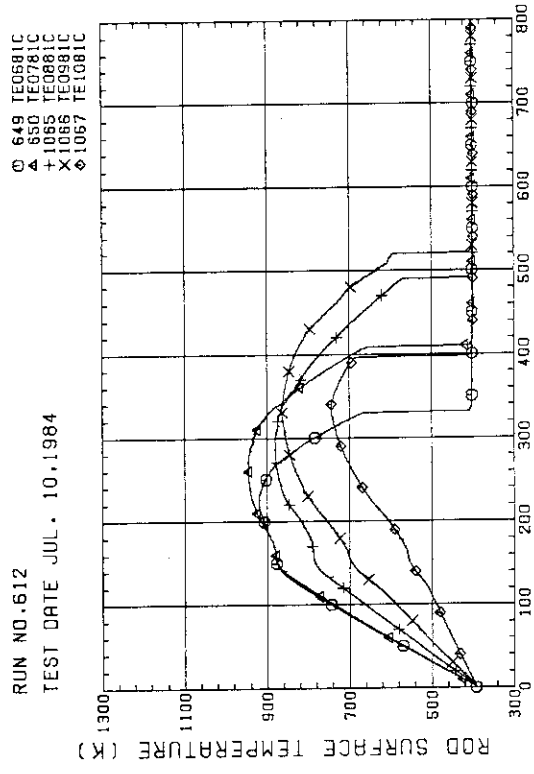

Fig. B-32 HEATER ROD TEMPERATURE (BUNDLE 8-1C, UPPER HALF)

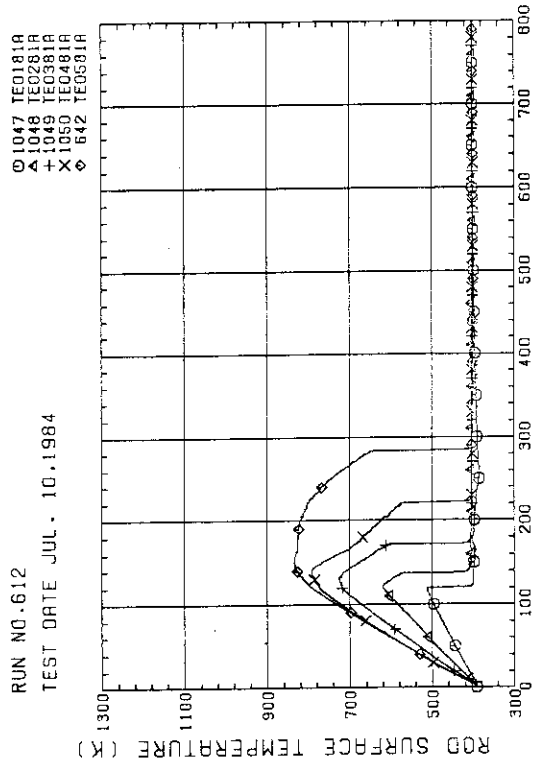

Fig. B-29 HEATER ROD TEMPERATURE (BUNDLE 8-1A, LOWER HALF)

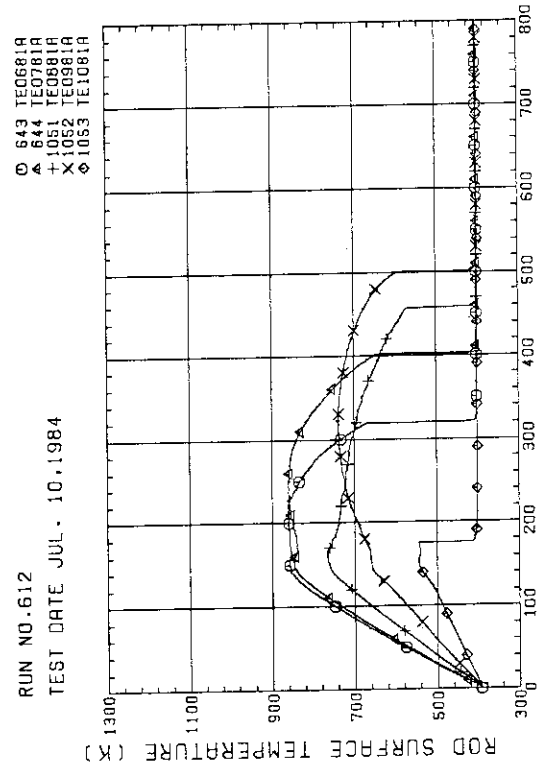

Fig. B-30 HEATER ROD TEMPERATURE (BUNDLE 8-1A, UPPER HALF)

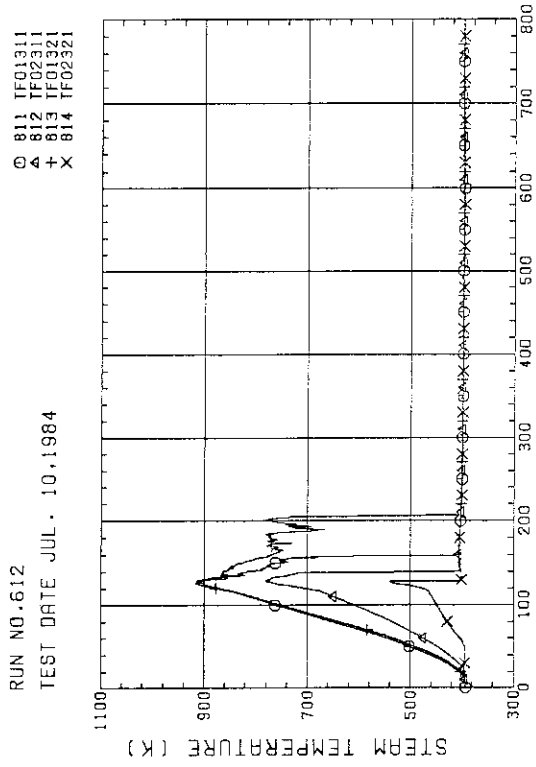

Fig. B-35 STEAM TEMPERATURE IN CORE, BUNDLE 3

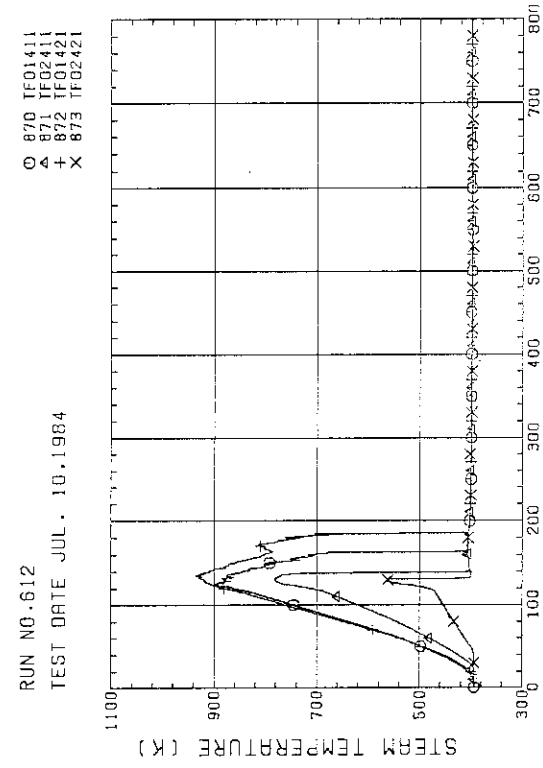

Fig. B-36 STEAM TEMPERATURE IN CORE, BUNDLE 4
(01411-1.735M, 02411-1.875M, 01421-1.38M, 02421-1.915M)

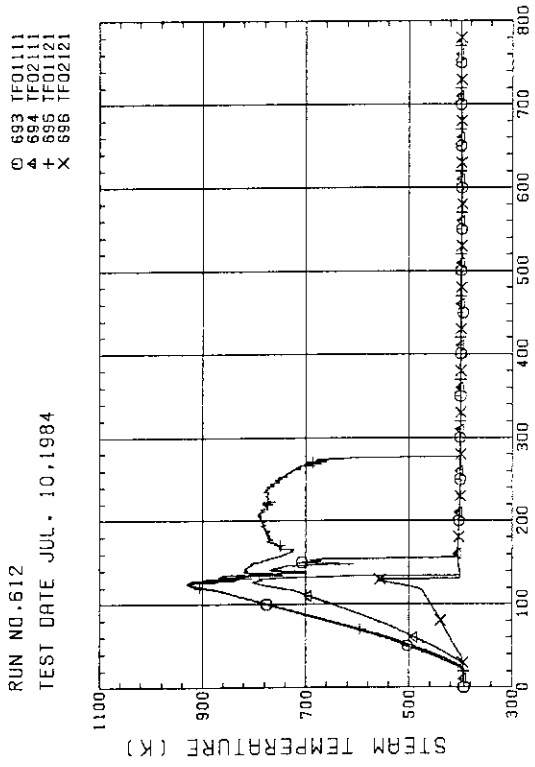

Fig. B-33 STEAM TEMPERATURE IN CORE, BUNDLE 1

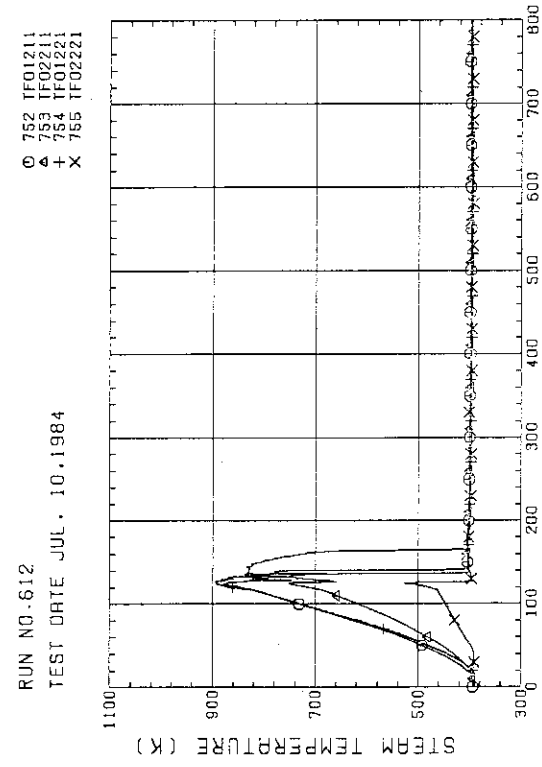

Fig. B-34 STEAM TEMPERATURE IN CORE, BUNDLE 2
(01211-1.735M, 02211-1.875M, 01221-1.38M, 02221-1.915M)

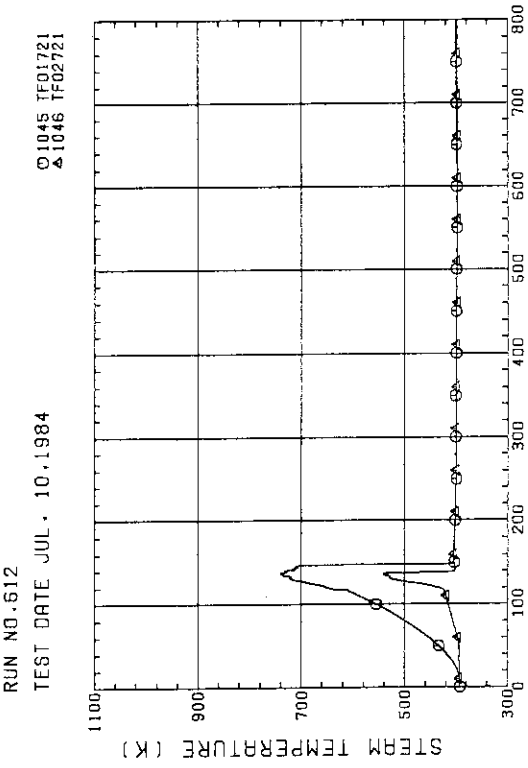

Fig. B-37 STEAM TEMPERATURE IN CORE, BUNDLE 5

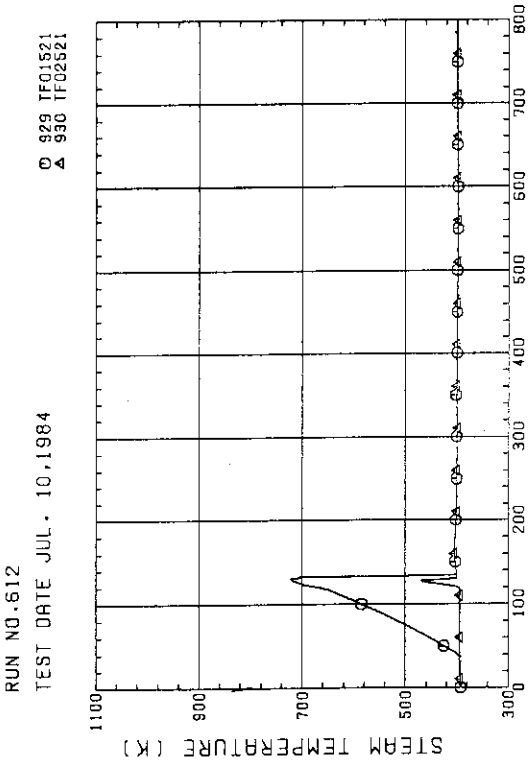

Fig. B-38 STEAM TEMPERATURE IN CORE, BUNDLE 6

Fig. B-39 STEAM TEMPERATURE IN CORE, BUNDLE 7

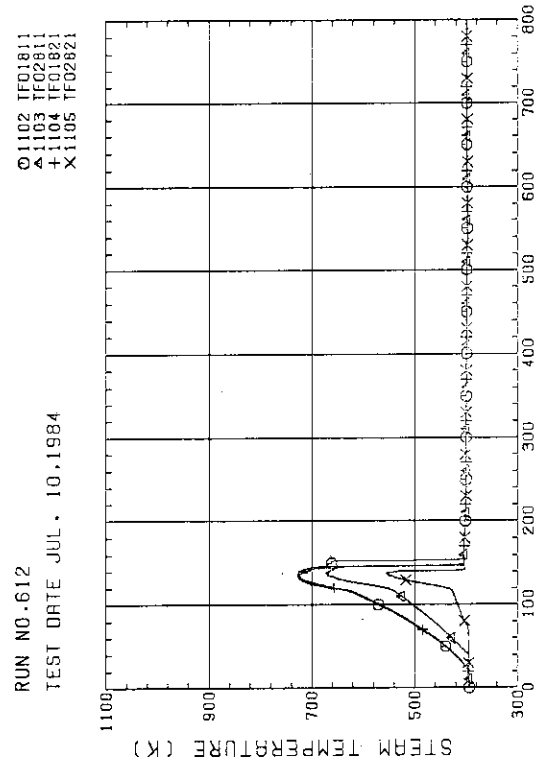

Fig. B-40 STEAM TEMPERATURE IN CORE, BUNDLE 8

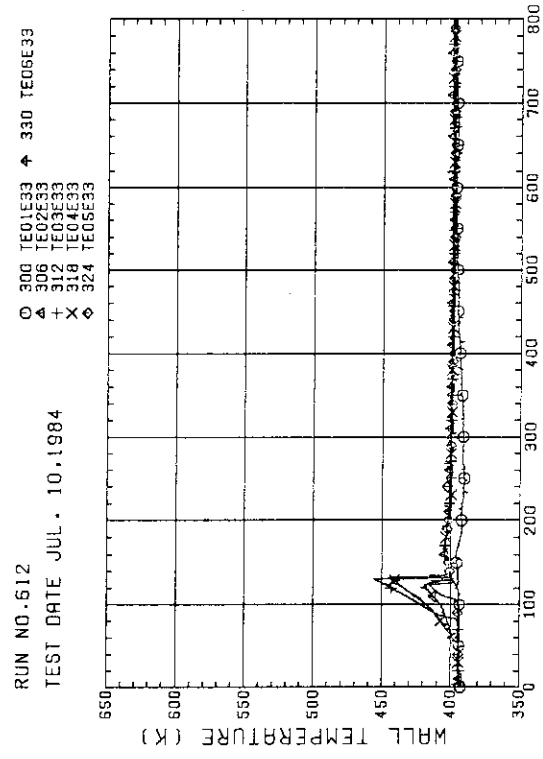

Fig. B-41 TEMPERATURE BETWEEN BAFFLE AND HONEYCOMB (BUNDLE 3, OPPOSITE SIDE OF COLD LEG)

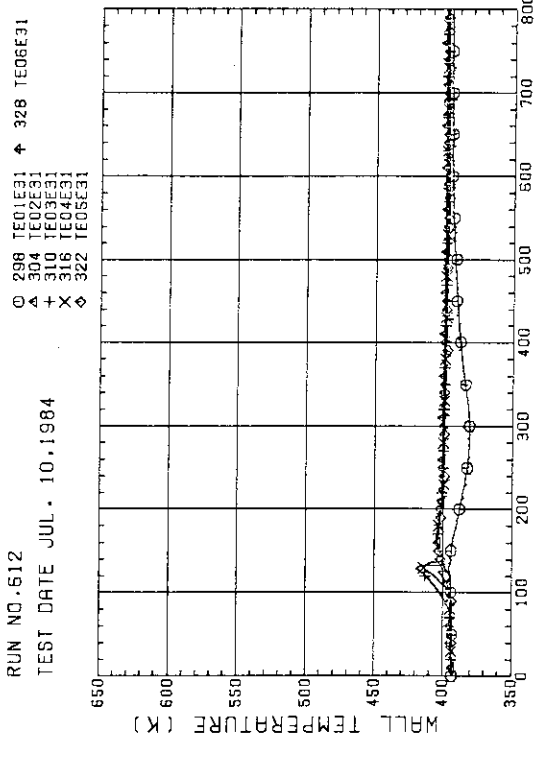

Fig. B-42 SURFACE TEMPERATURE OF CORE SIDE WALL (BUNDLE 3, OPPOSITE SIDE OF COLD LEG, INNER SURFACE

Fig. B-43 SURFACE TEMPERATURE OF CORE SIDE WALL (BUNDLE 3, COLD LEG SIDE, INNER SURFACE)

Fig. B-44 SURFACE TEMPERATURE OF CORE SIDE WALL (BUNDLE 8, COLD LEG SIDE, INNER SURFACE)

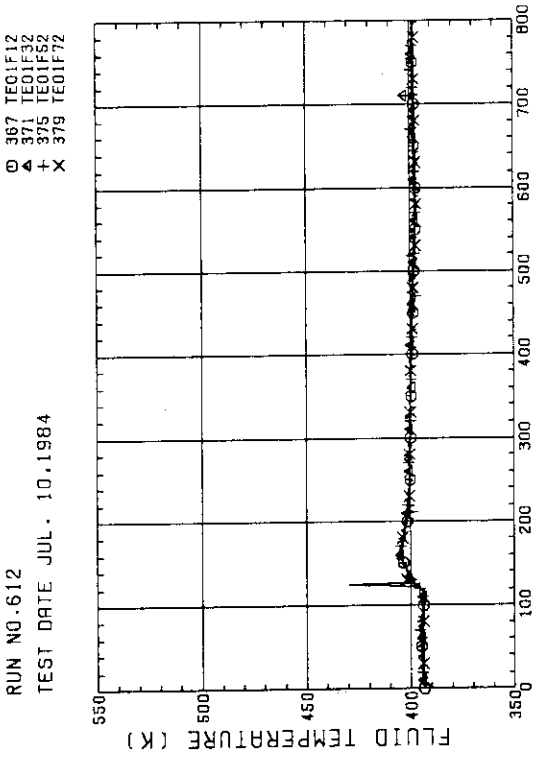

Fig. B-45 FLUID TEMPERATURE JUST BELOW END BOX TIE PLATE (BUNDLE 1,3,5,7, OPPOSITE SIDE OF COLD LEG, OUTER)

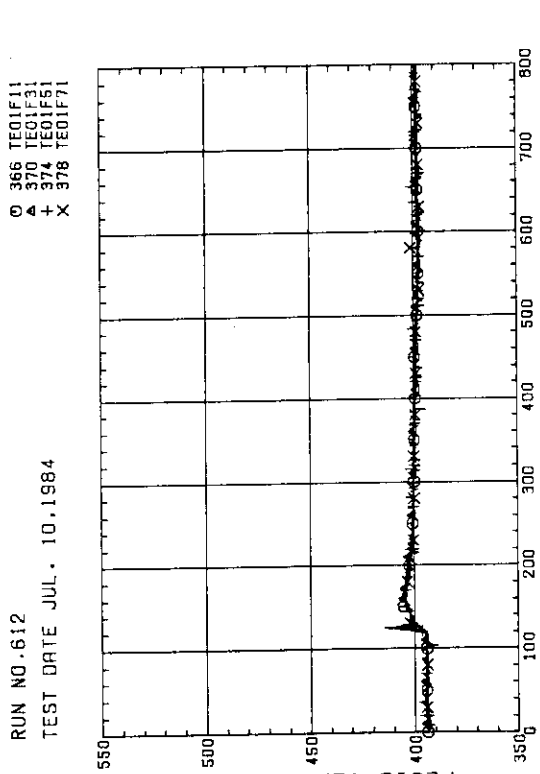

Fig. B-47 FLUID TEMPERATURE JUST BELOW END BOX TIE PLATE (BUNDLE 1,3,5,7, OPPSITE SIDE OF COLD LEG, INNER)

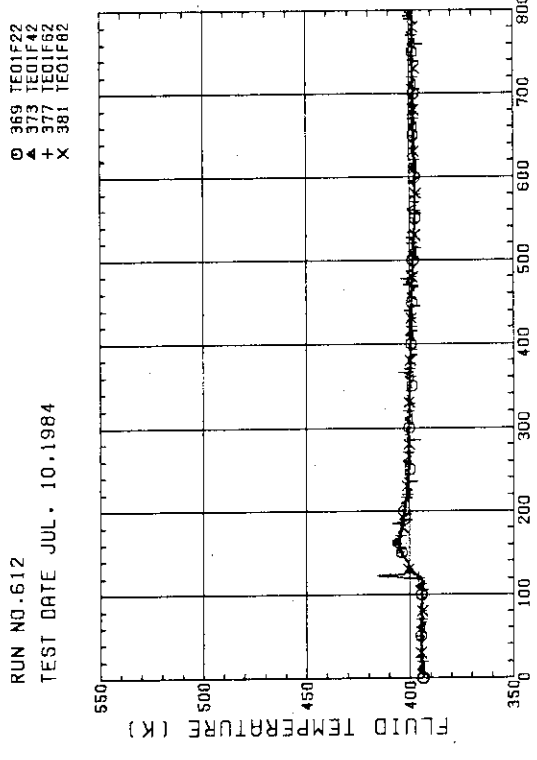

Fig. B-46 FLUID TEMPERATURE JUST BELOW END BOX TIE PLATE (BUNDLE 2,4,6,8, COLD LEG SIDE, INNER)

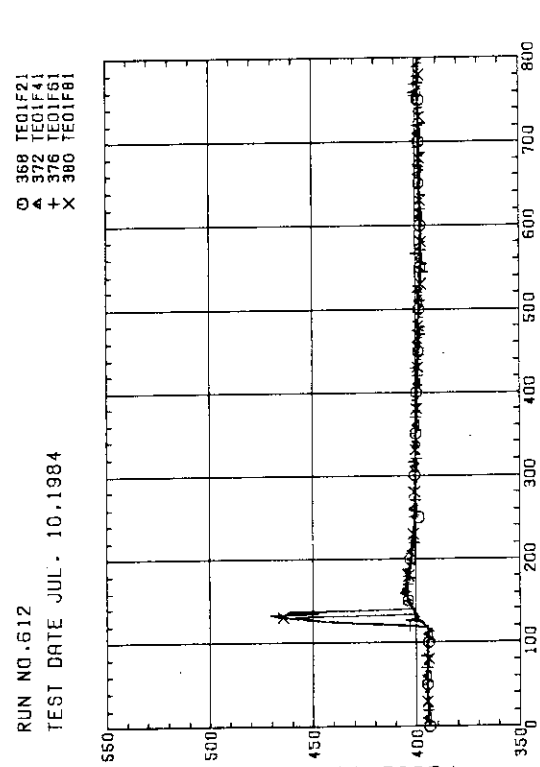

Fig. B-48 FLUID TEMPERATURE JUST BELOW END BOX TIE PLATE (BUNDLE 2,4,6,8, COLD LEG SIDE, OUTER)

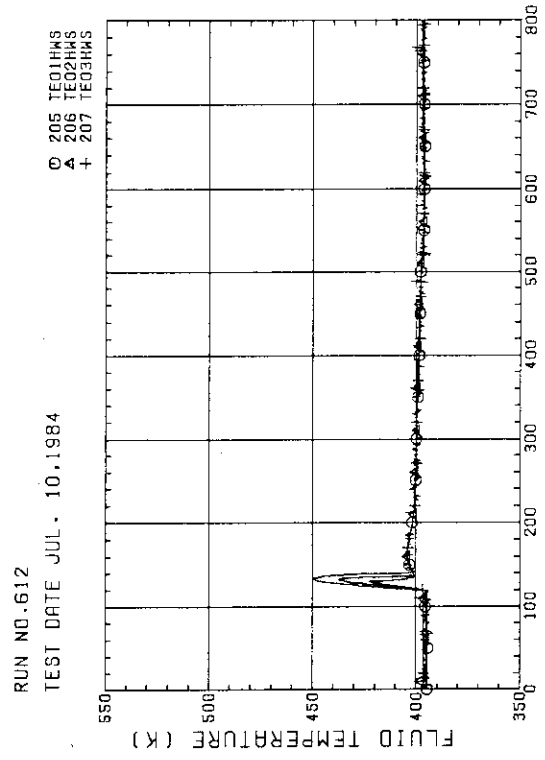

Fig. B-51 FLUID TEMPERATURE IN HOT LEG
(01,02,03 - FROM PV TO STEAM/WATER SEPARATOR)

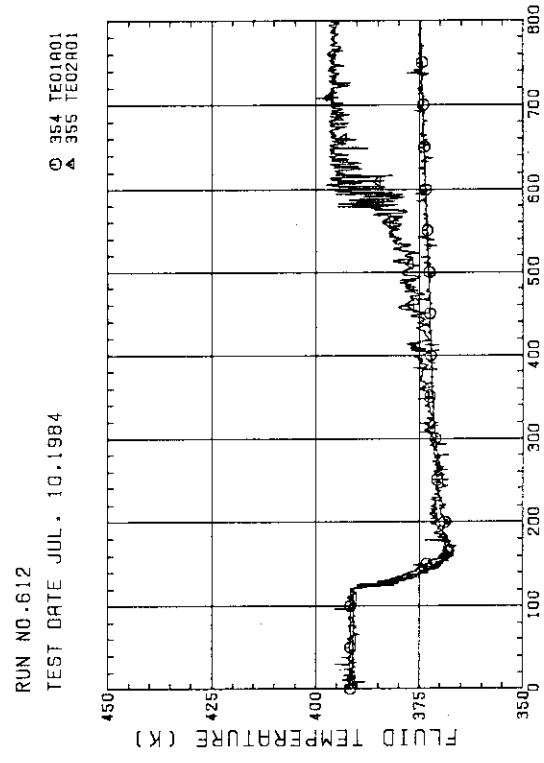

Fig. B-52 FLUID TEMPERATURE AT LOWER PLENUM INLET

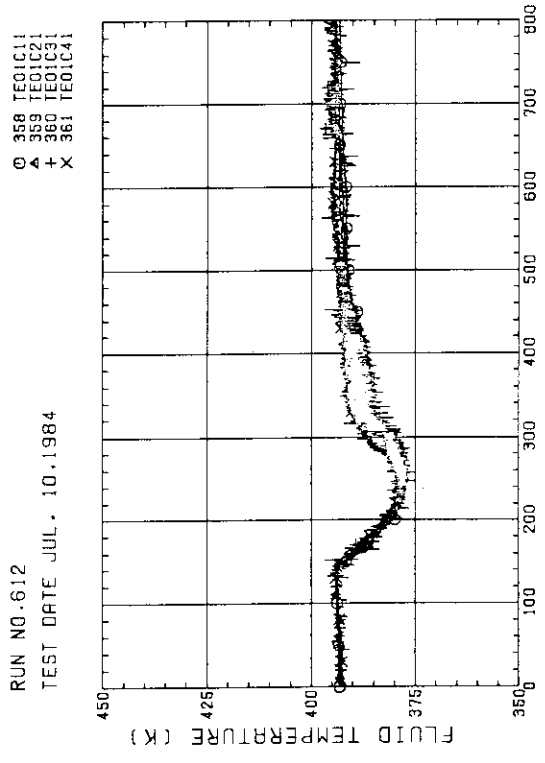

Fig. B-49 FLUID TEMPERATURE AT CORE INLET
(BUNDLE 1,2,3,4, 100MM BELOW HEATED PART)

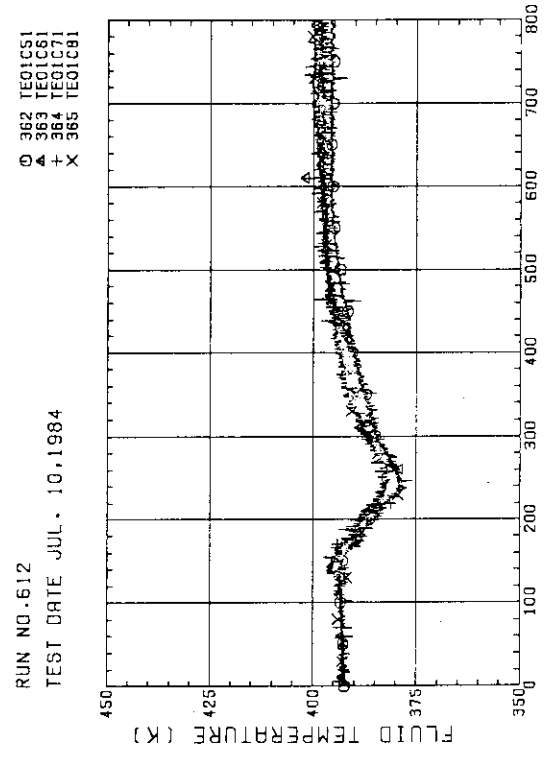

Fig. B-50 FLUID TEMPERATURE AT CORE INLET
(BUNDLE 5,6,7,8, 100MM BELOW HEATED PART)

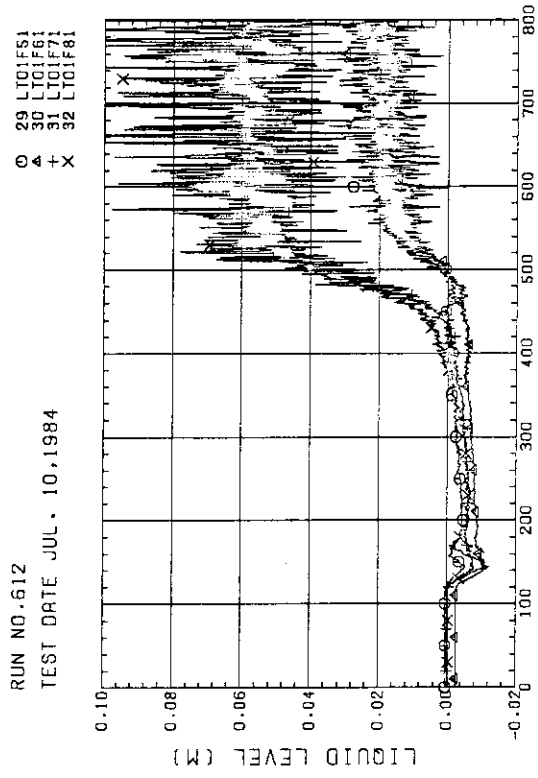

Fig. B-55 LIQUID LEVEL ABOVE END BOX TIE PLATE (BUNDLE 5,6,7,8)

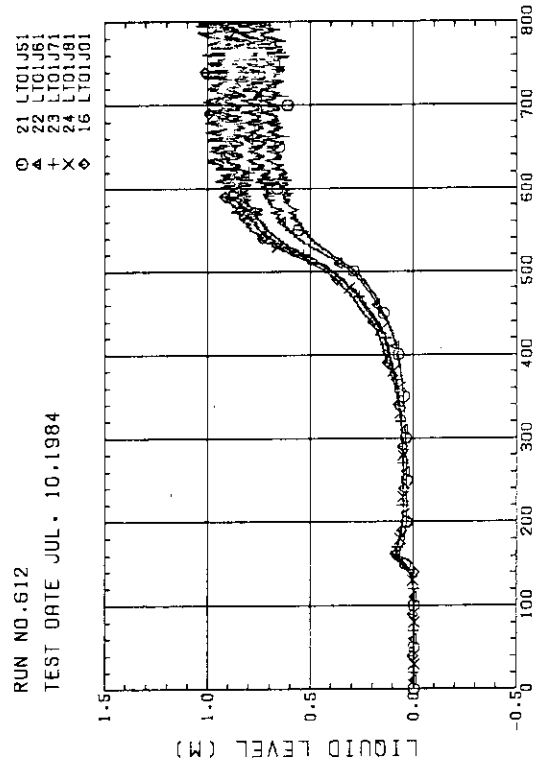

Fig. B-56 LIQUID LEVEL ABOVE UCSP (BUNDLE 5,6,7,8 AND CORE BAFFLE)

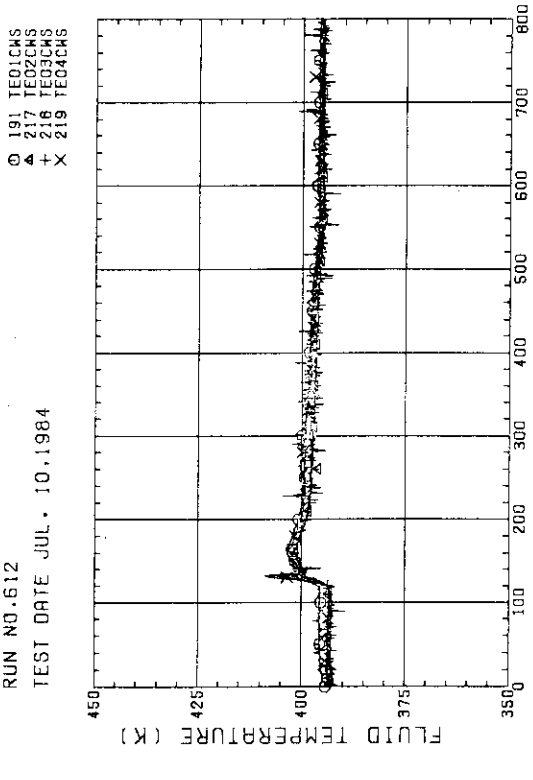

Fig. B-53 FLUID TEMPERATURE IN INTACT COLD LEG (BETWEEN PUMP SIMULATOR AND S/W SEPARATOR)

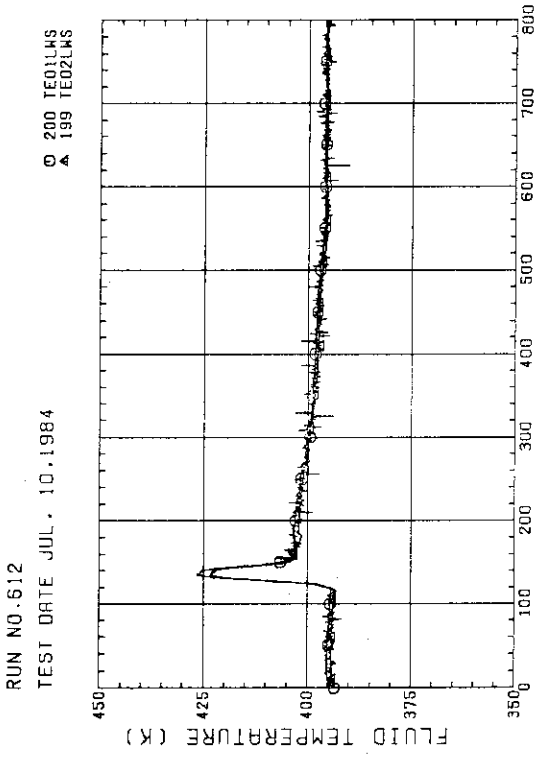

Fig. B-54 FLUID TEMPERATURE IN BROKEN COLD LEG

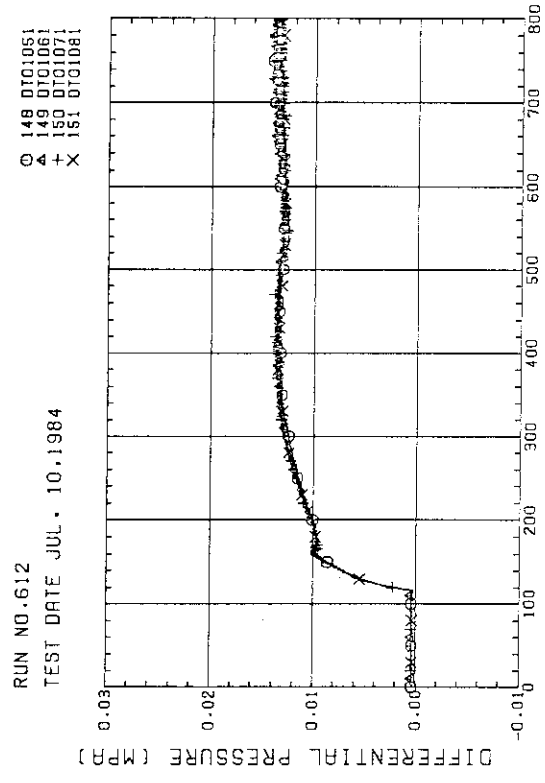

Fig. B-59 DIFFERENTIAL PRESSURE OF CORE LOWER HALF (BUNDLE 5,6,7,8)

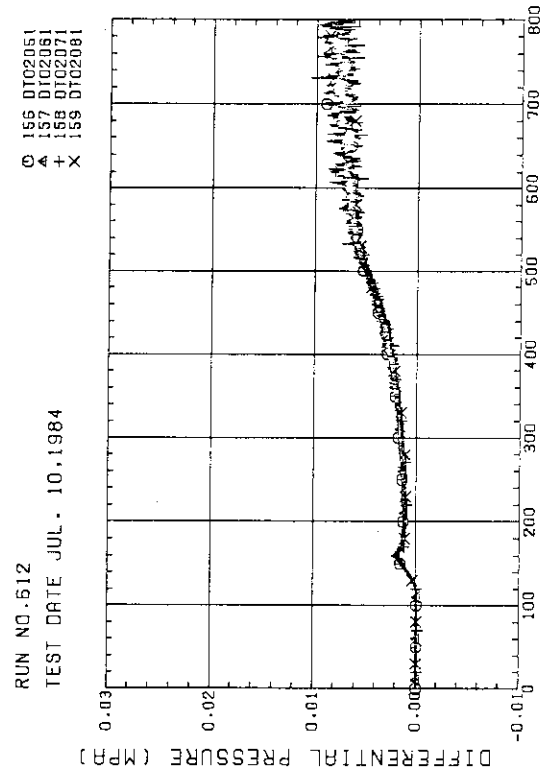

Fig. B-60 DIFFERENTIAL PRESSURE OF CORE UPPER HALF (BUNDLE 5,6,7,8)

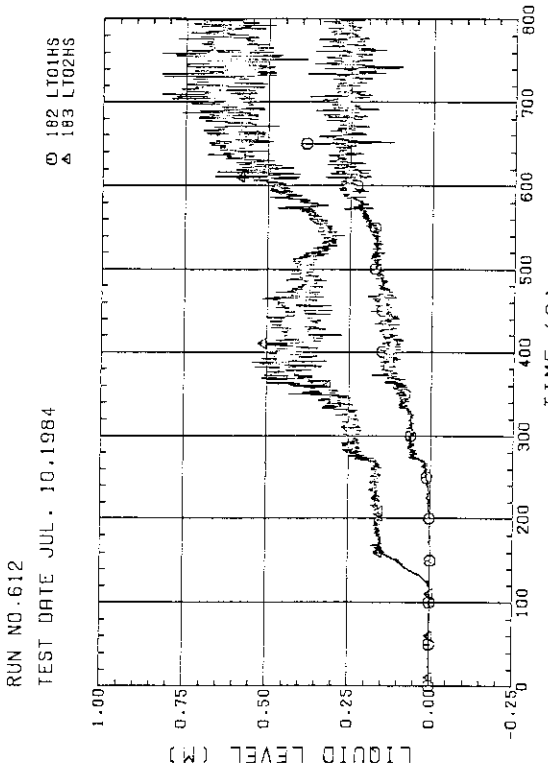

Fig. B-57 LIQUID LEVEL IN HOT LEG (O1HS - PV SIDE, O2HS - STEAM/WATER SEPARATOR SIDE)

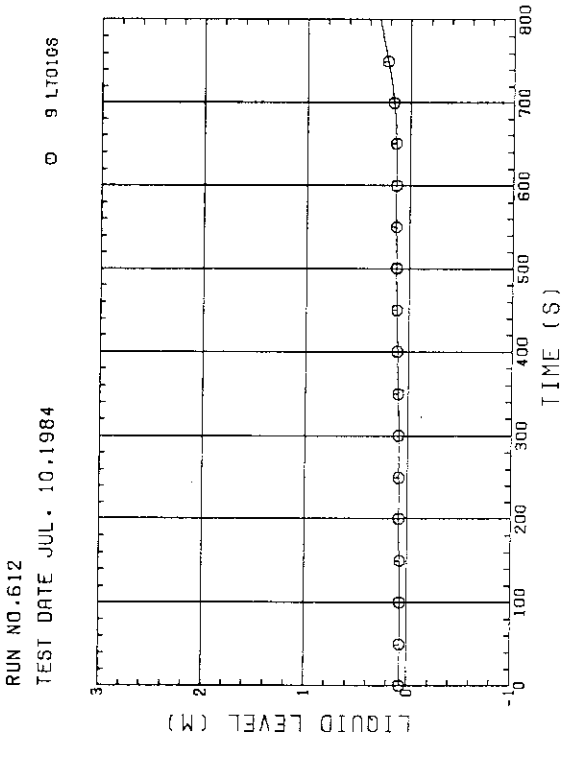

Fig. B-58 LIQUID LEVEL IN STEAM/WATER SEPARATOR

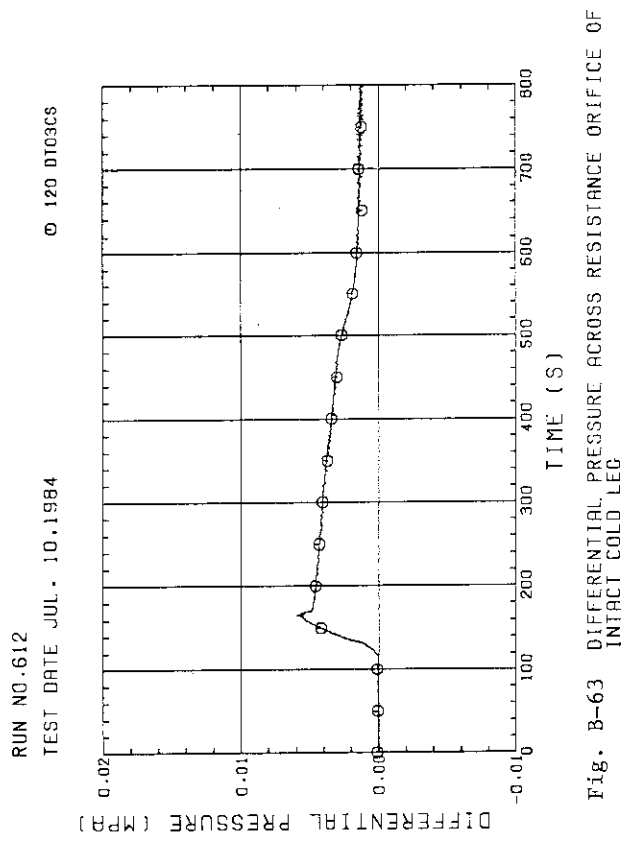

Fig. B-63 DIFFERENTIAL PRESSURE ACROSS RESISTANCE ORIFICE OF INTACT COLD LEG

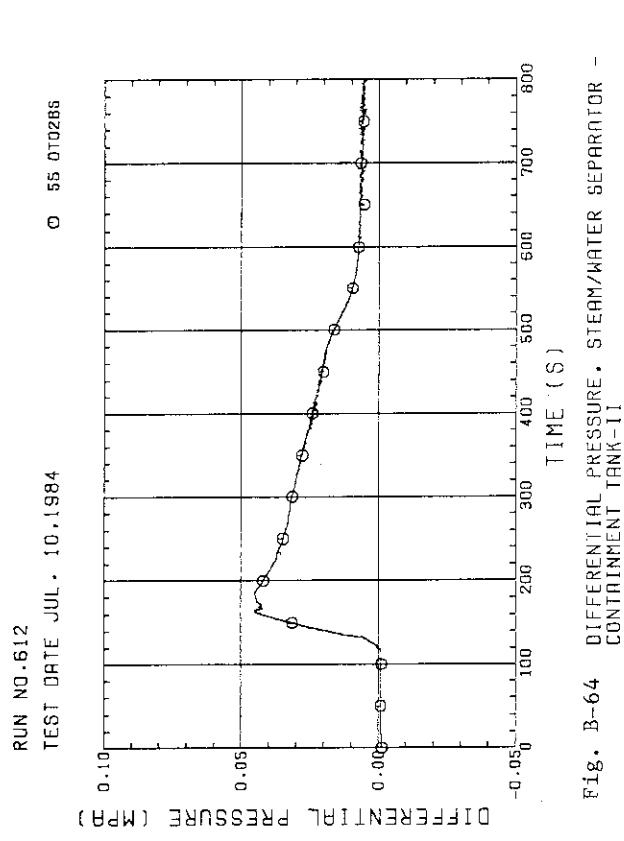

Fig. B-64 DIFFERENTIAL PRESSURE, STEAM/WATER SEPARATOR - CONTAINMENT TANK-II

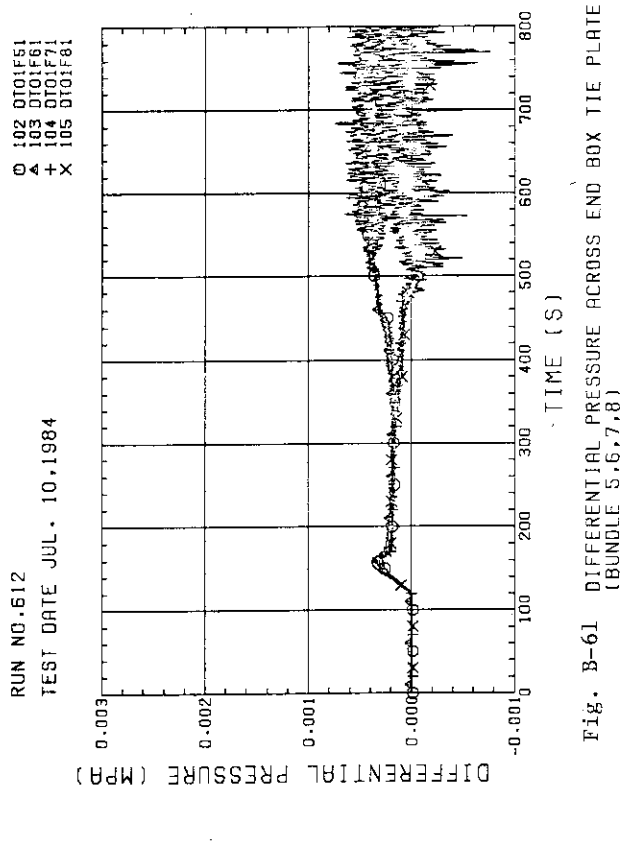

Fig. B-61 DIFFERENTIAL PRESSURE ACROSS END BOX TIE PLATE (BUNDLE 5,6,7,8)

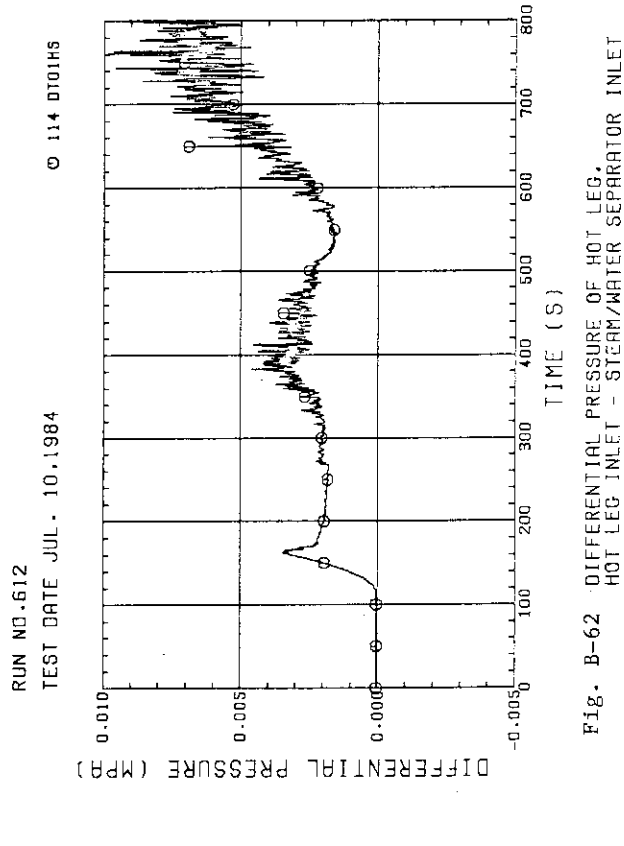

Fig. B-62 DIFFERENTIAL PRESSURE OF HOT LEG, HOT LEG INLET - STEAM/WATER SEPARATOR INLET

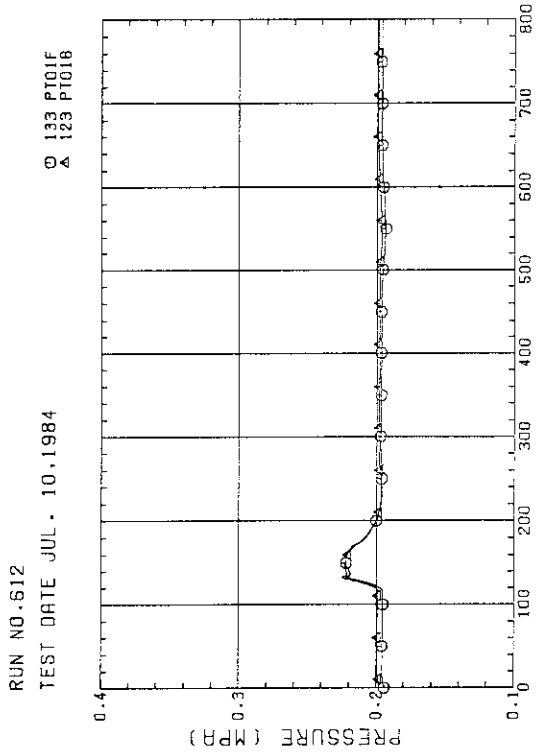

Fig. B-67 PRESSURE AT TOP OF CONTAINMENT TANK-I AND CONTAINMENT TANK-II (F-CONTAINMENT TANK-I, B-CONTAINMENT TANK-II)

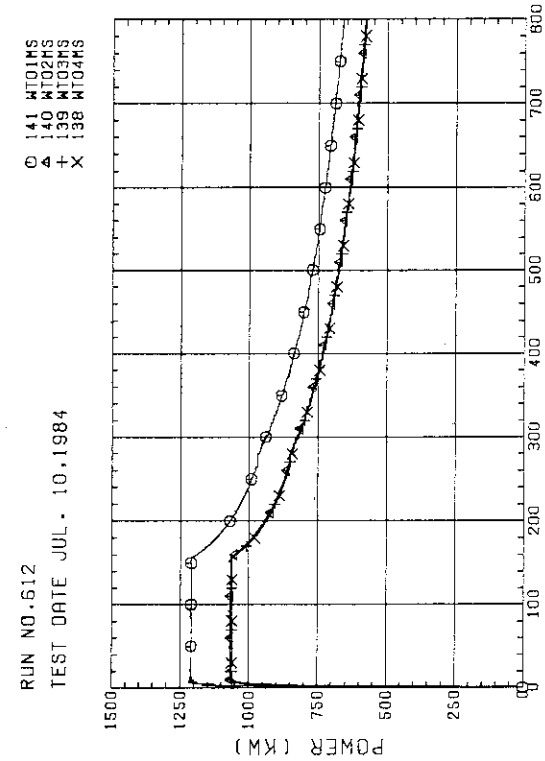

Fig. B-68 BUNDLE POWER (BUNDLE 1,2,3,4)

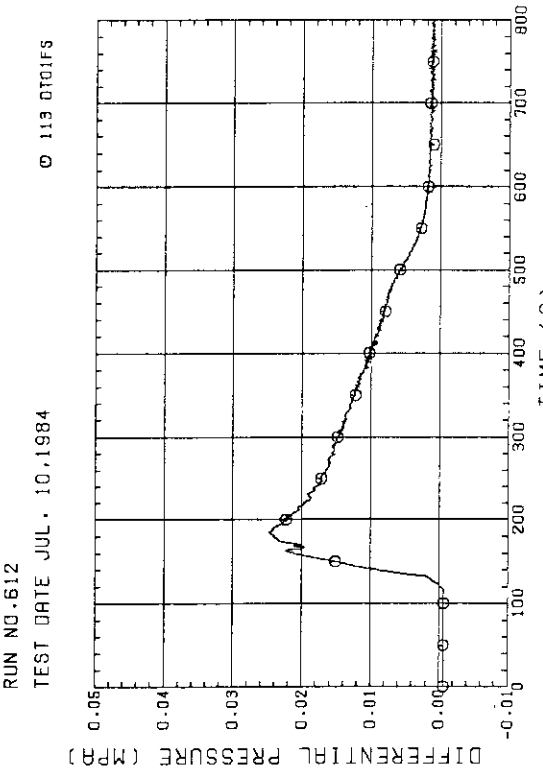

Fig. B-65 DIFFERENTIAL PRESSURE OF BROKEN COLD LEG - PV SIDE. DOWNCOMER - CONTAINMENT TANK-I

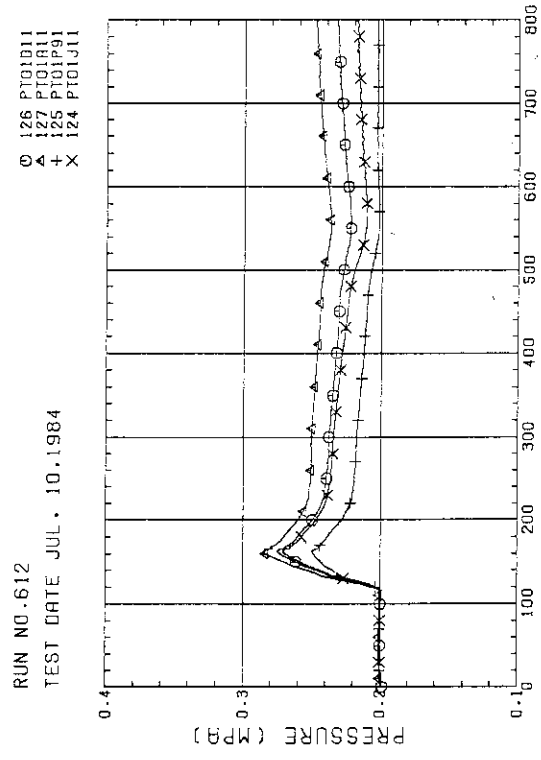

Fig. B-66 PRESSURE IN PV (J - TOP OF PV, D - CORE CENTER, A - CORE INLET, P - BELOW COLD LEG NOZZLE IN DOWNCOMER)

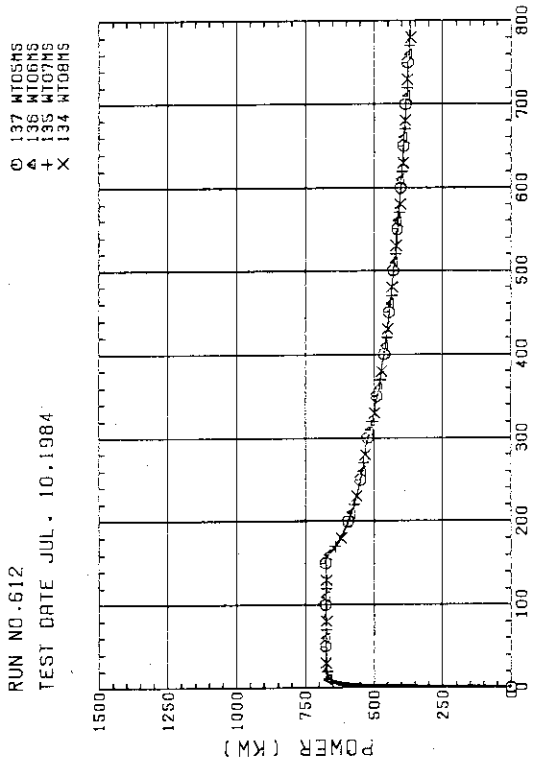

Fig. B-69 BUNDLE POWER
(BUNDLE 5,6,7,8)

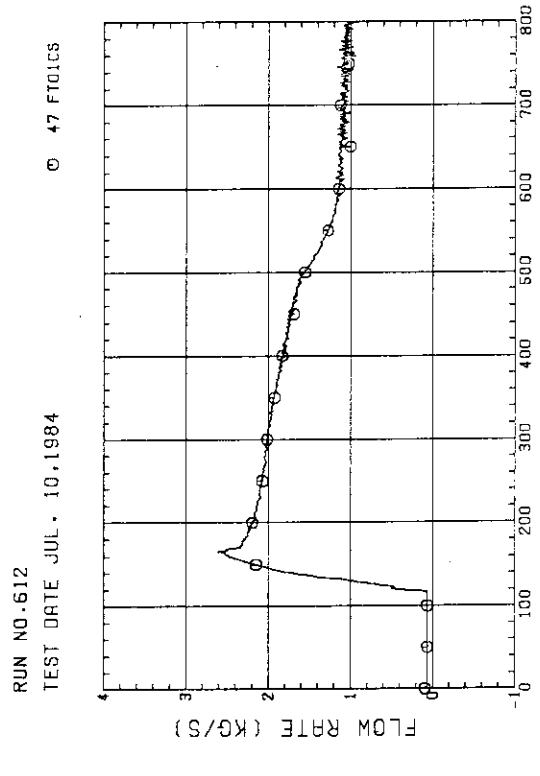

Fig. B-70 MASS FLOW RATE OF INTACT COLD LEG

Appendix C

Selected Data from Test S2-18

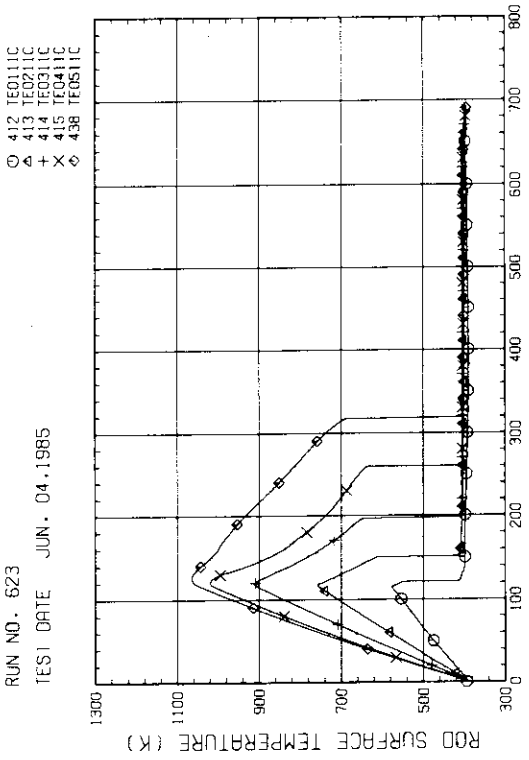

Fig. C-1 HEATER ROD TEMPERATURE (BUNDLE 1-1A, LOWER HALF)

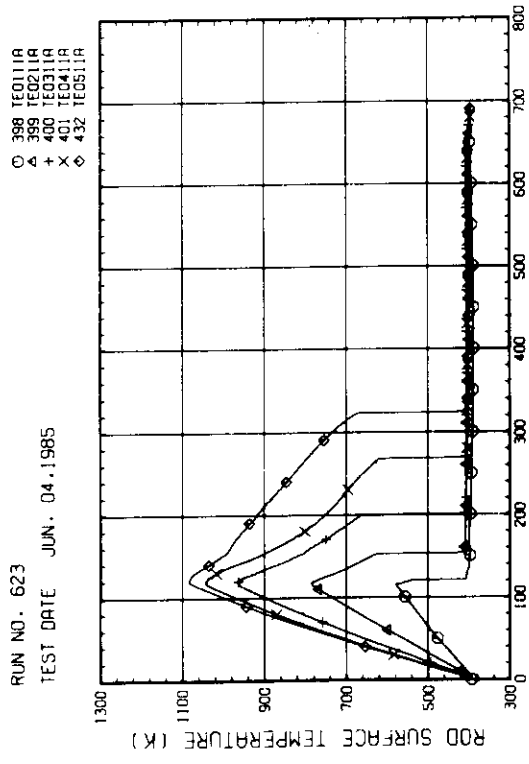

Fig. C-3 HEATER ROD TEMPERATURE (BUNDLE 1-1C, LOWER HALF)

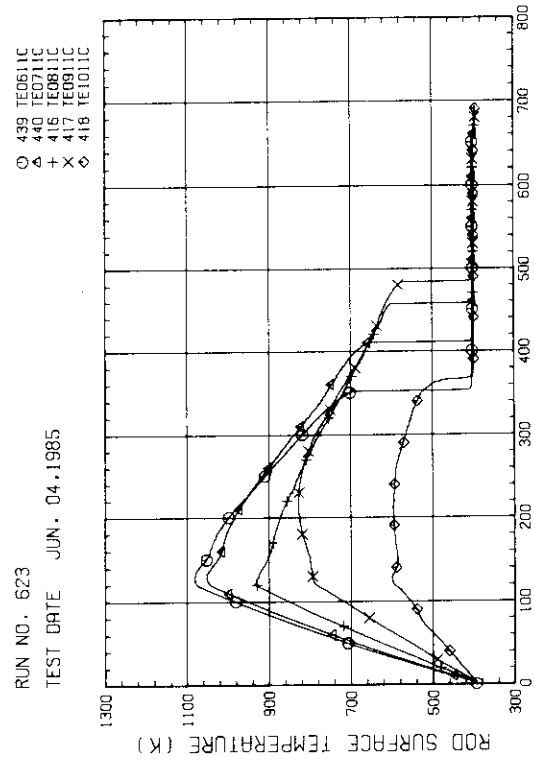

Fig. C-2 HEATER ROD TEMPERATURE (BUNDLE 1-1A, UPPER HALF)

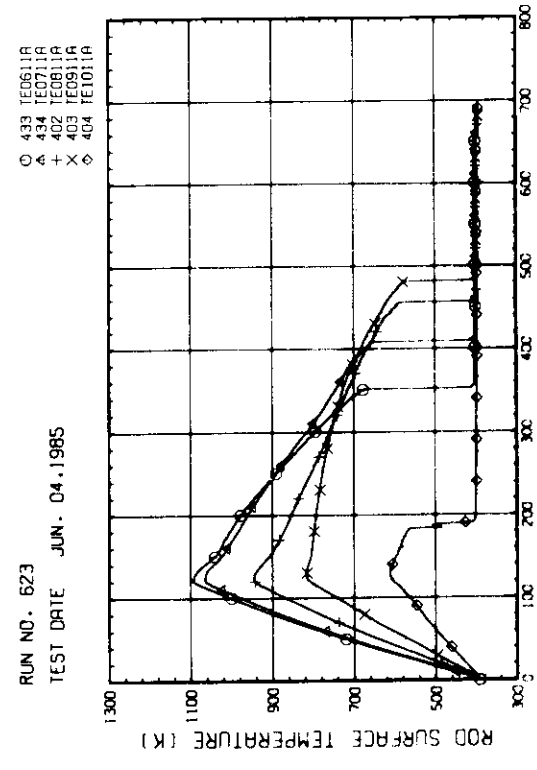

Fig. C-4 HEATER ROD TEMPERATURE (BUNDLE 1-1C, UPPER HALF)

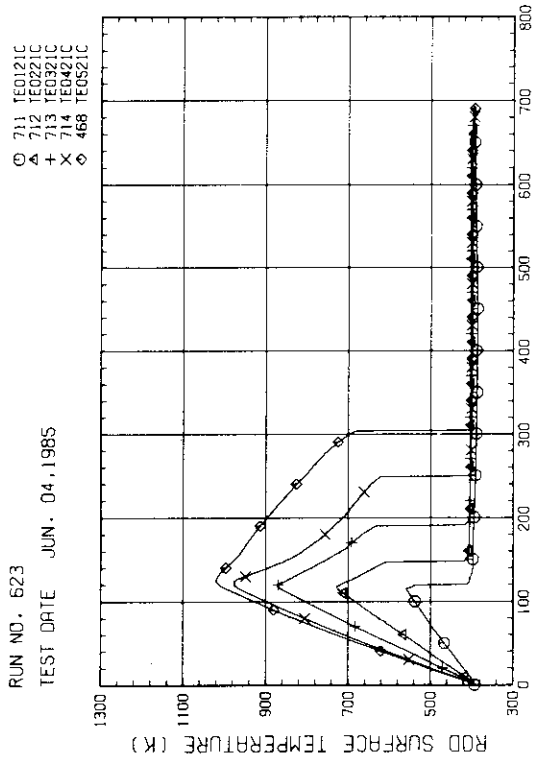

Fig. C-5 HEATER ROD TEMPERATURE (BUNDLE 2-1A, UPPER HALF)

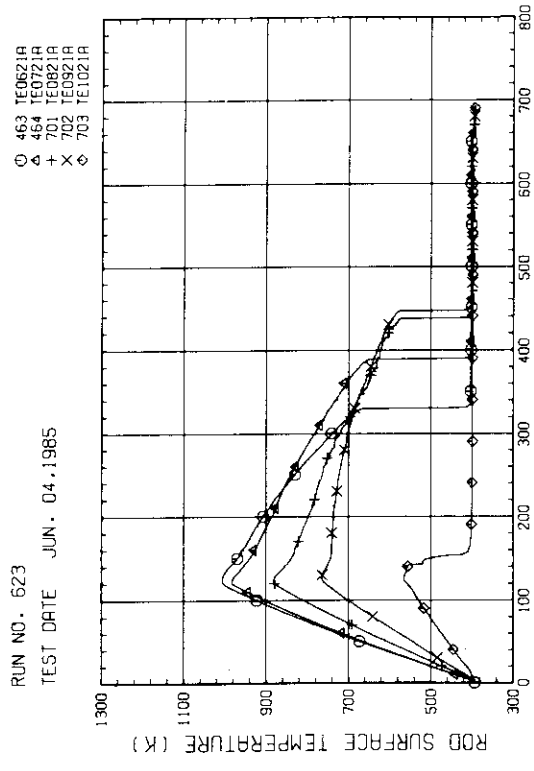

Fig. C-6 HEATER ROD TEMPERATURE (BUNDLE 2-1B, LOWER HALF)

Fig. C-7 HEATER ROD TEMPERATURE (BUNDLE 2-1C, LOWER HALF)

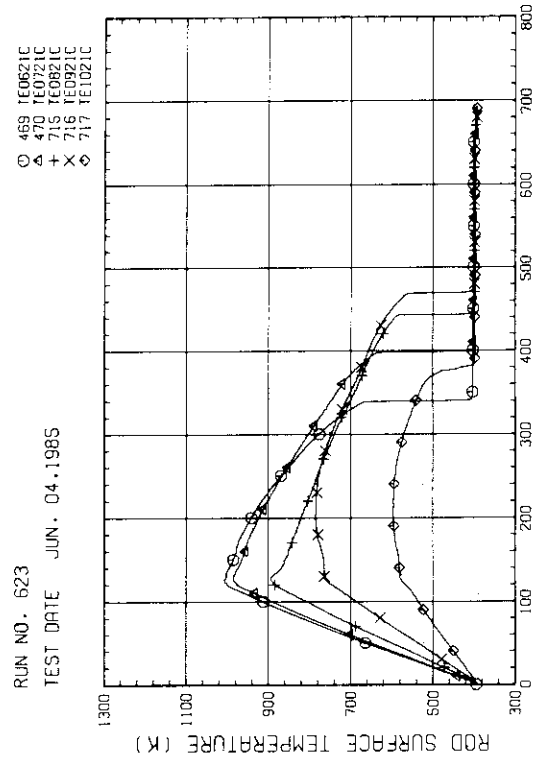

Fig. C-8 HEATER ROD TEMPERATURE (BUNDLE 2-1C, UPPER HALF)

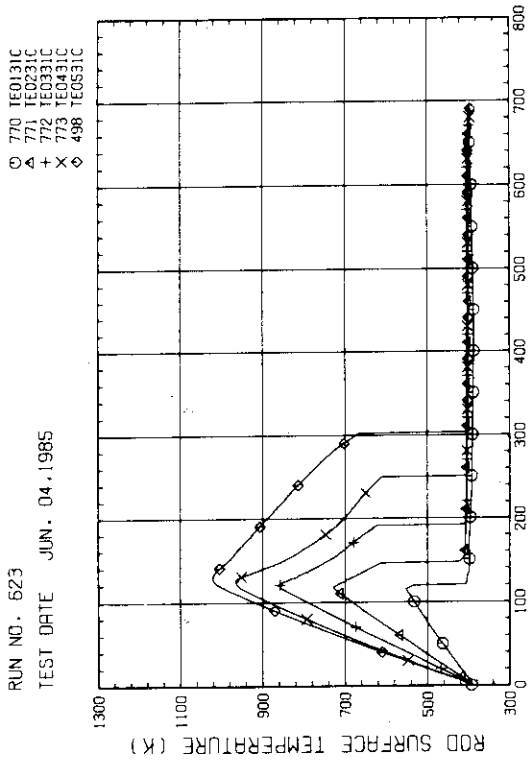

Fig. C-11 HEATER ROD TEMPERATURE (BUNDLE 3-1C, LOWER HALF)

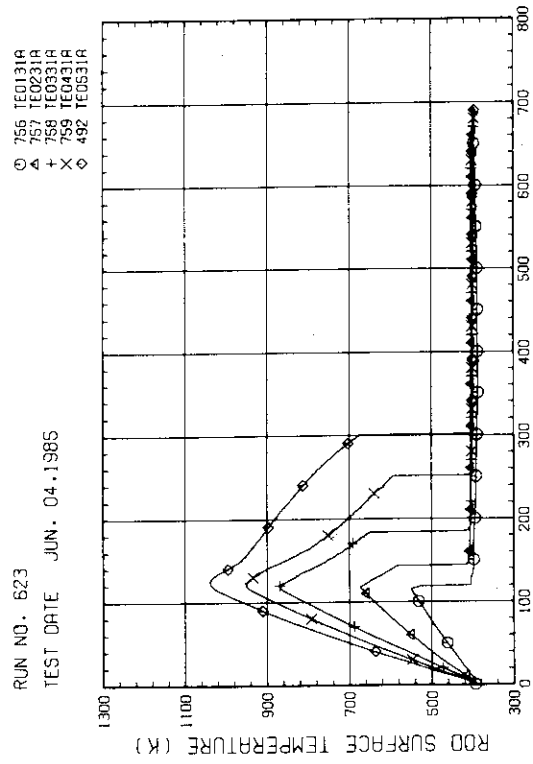

Fig. C-9 HEATER ROD TEMPERATURE (BUNDLE 3-1A, LOWER HALF)

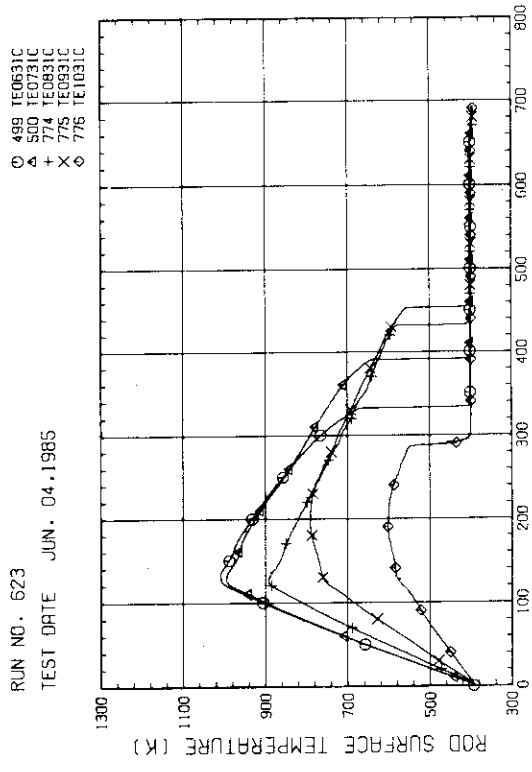

Fig. C-12 HEATER ROD TEMPERATURE (BUNDLE 3-1C, UPPER HALF)

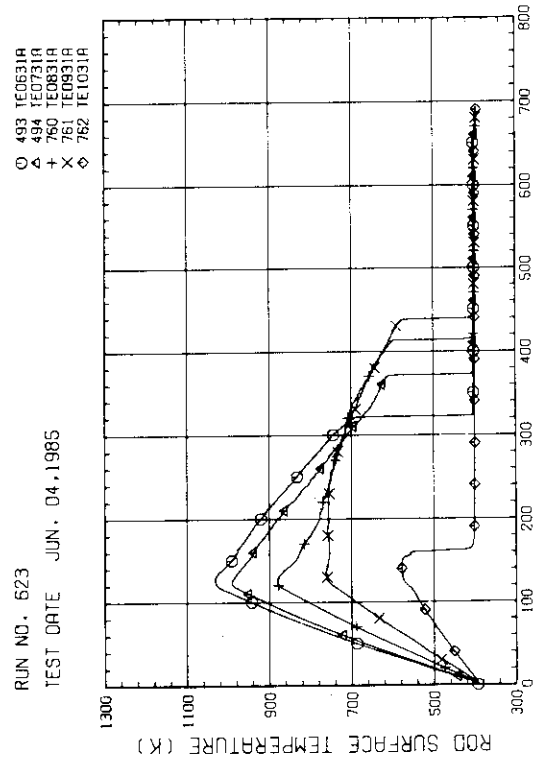

Fig. C-10 HEATER ROD TEMPERATURE (BUNDLE 3-1A, UPPER HALF)

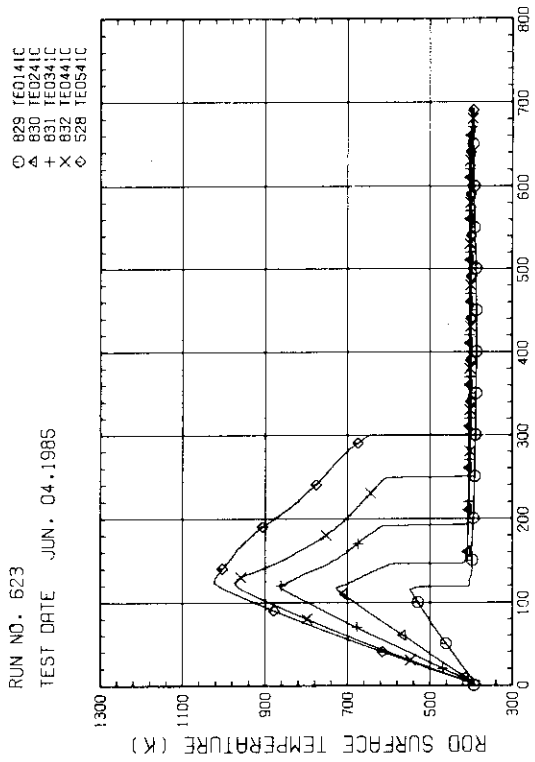

Fig. C-15 HEATER ROD TEMPERATURE (BUNDLE 4-1C, LOWER HALF)

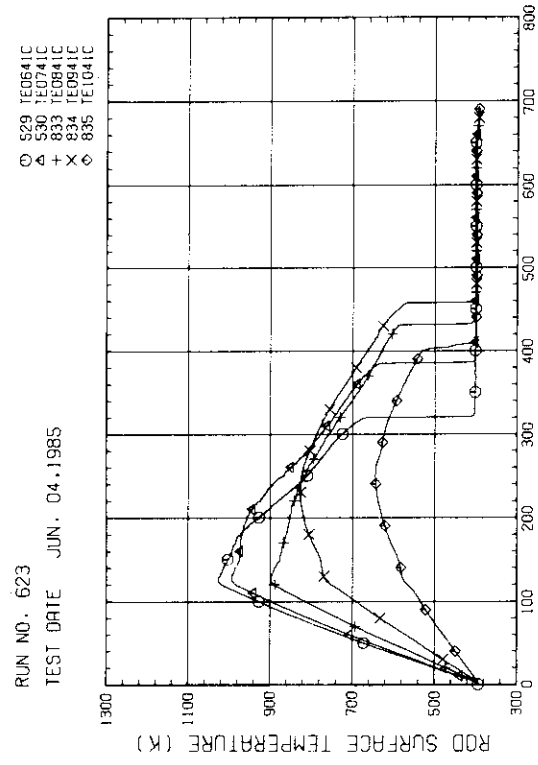

Fig. C-16 HEATER ROD TEMPERATURE (BUNDLE 4-1C, UPPER HALF)

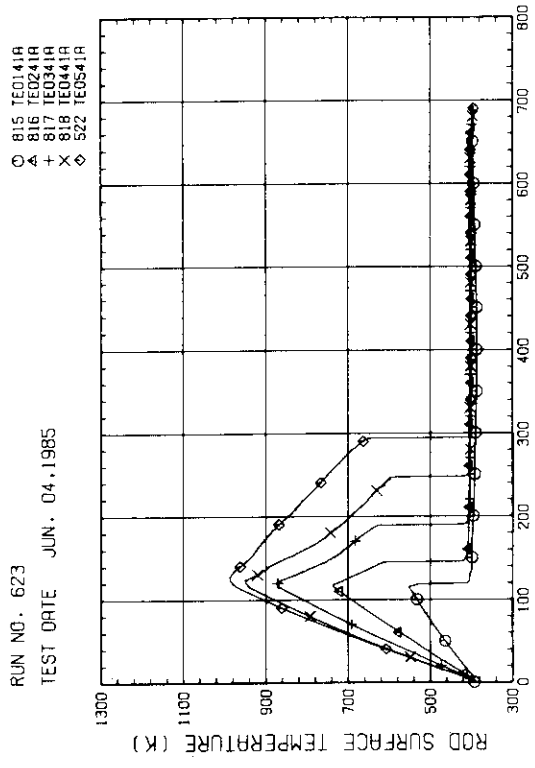

Fig. C-13 HEATER ROD TEMPERATURE (BUNDLE 4-1A, LOWER HALF)

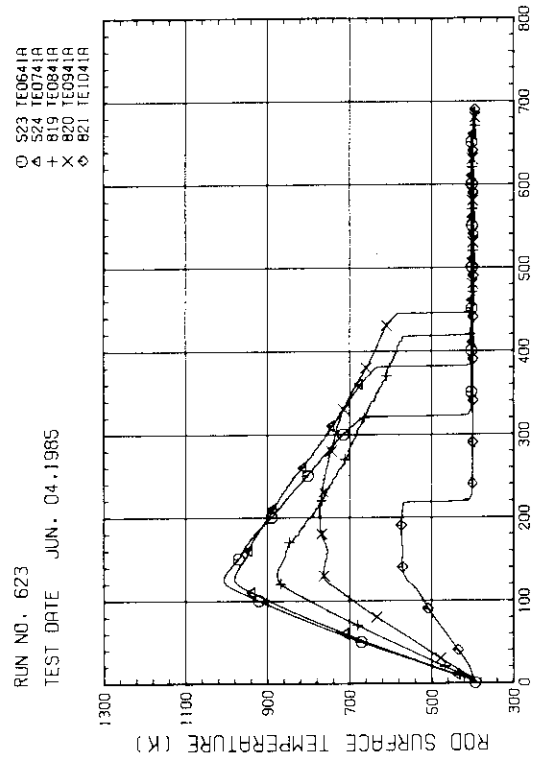

Fig. C-14 HEATER ROD TEMPERATURE (BUNDLE 4-1A, UPPER HALF)

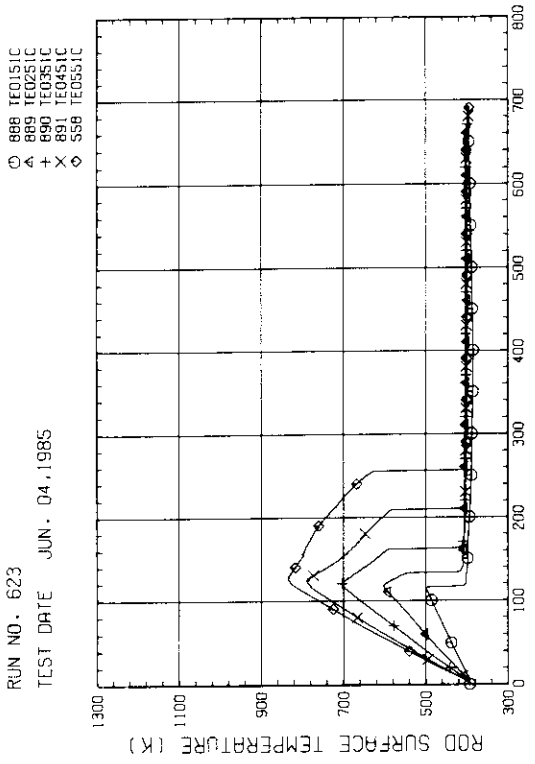

Fig. C-19 HEATER ROD TEMPERATURE (BUNDLE 5-1C, LOWER HALF)

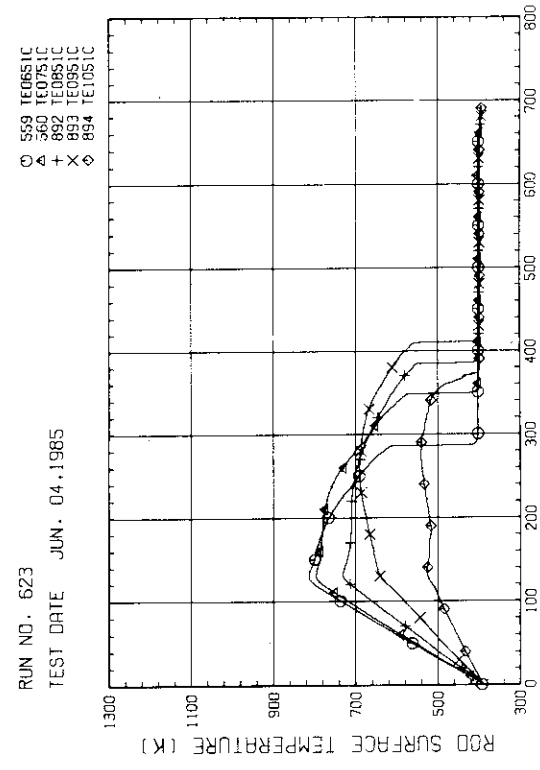

Fig. C-20 HEATER ROD TEMPERATURE (BUNDLE 5-1C, UPPER HALF)

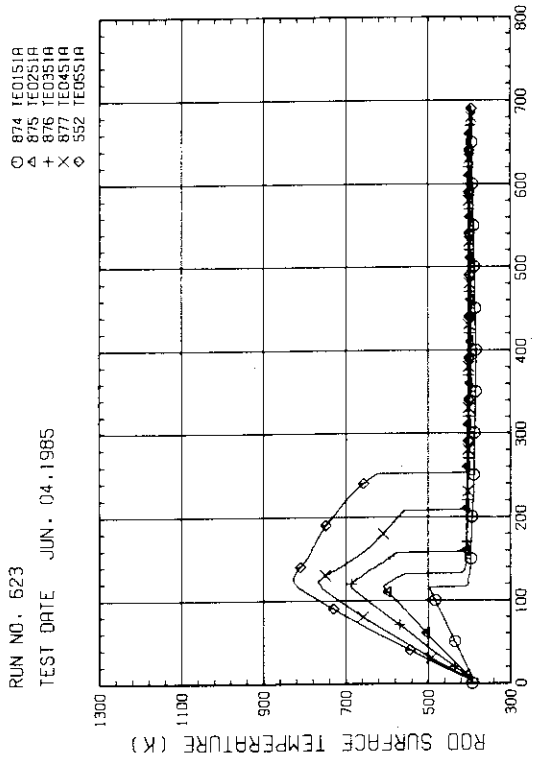

Fig. C-17 HEATER ROD TEMPERATURE (BUNDLE 5-1A, LOWER HALF)

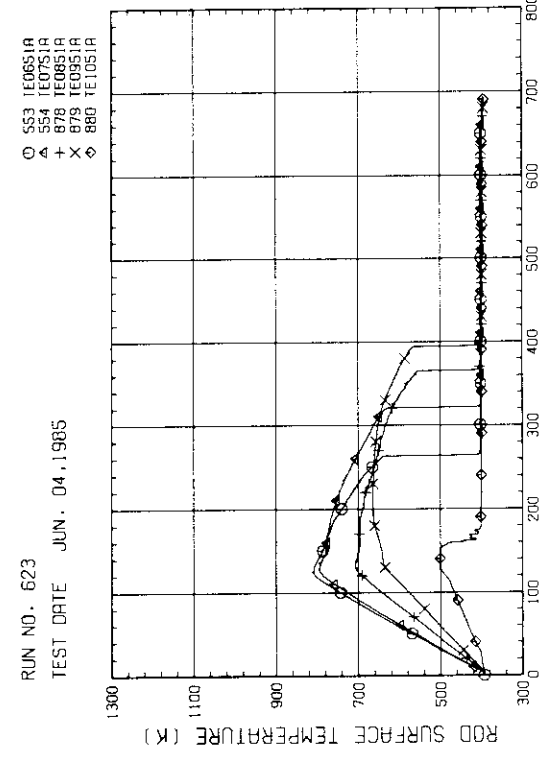

Fig. C-18 HEATER ROD TEMPERATURE (BUNDLE 5-1A, UPPER HALF)

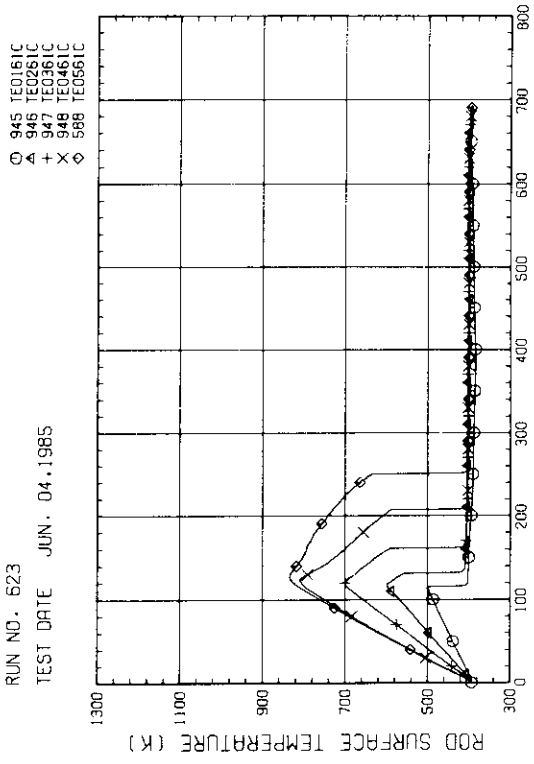

Fig. C-21 HEATER ROD TEMPERATURE (BUNDLE 6-1A, LOWER HALF)

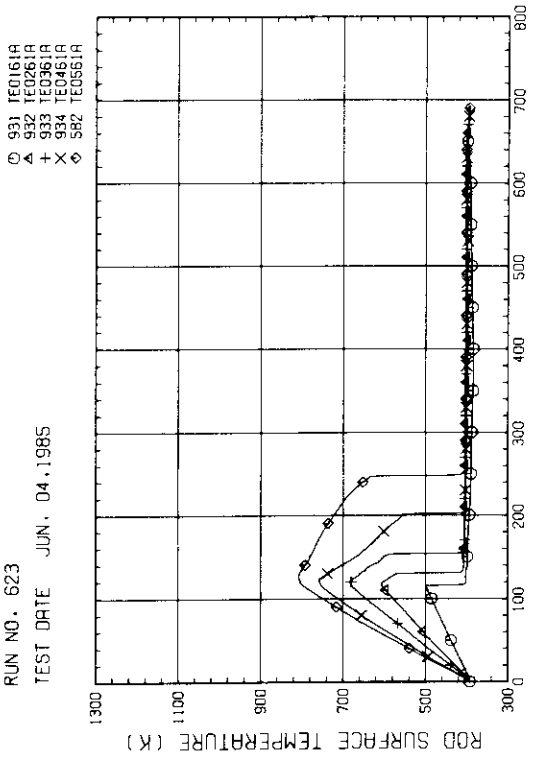

Fig. C-23 HEATER ROD TEMPERATURE (BUNDLE 6-1C, LOWER HALF)

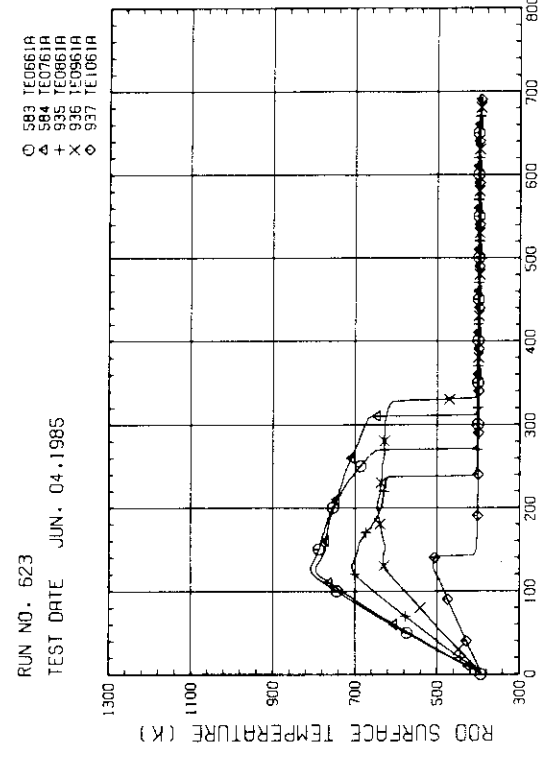

Fig. C-24 HEATER ROD TEMPERATURE (BUNDLE 6-1C, UPPER HALF)

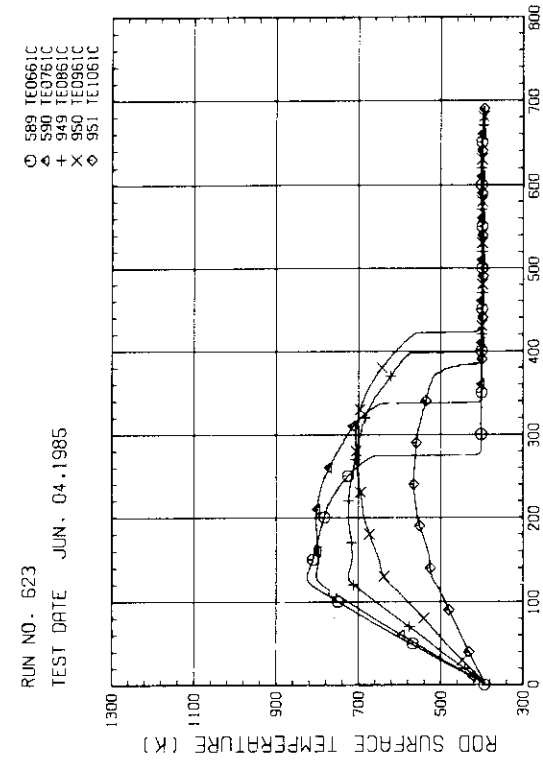

Fig. C-22 HEATER ROD TEMPERATURE (BUNDLE 6-1A, UPPER HALF)

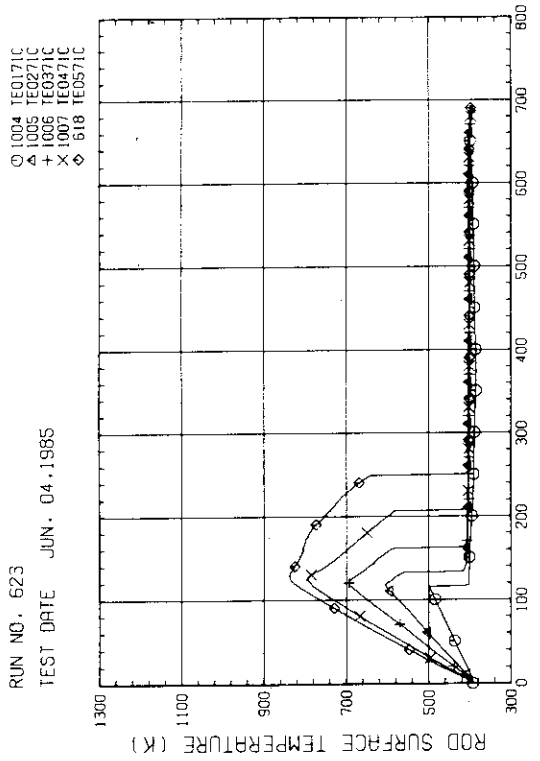

Fig. C-27 HEATER ROD TEMPERATURE (BUNDLE 7-1C, LOWER HALF)

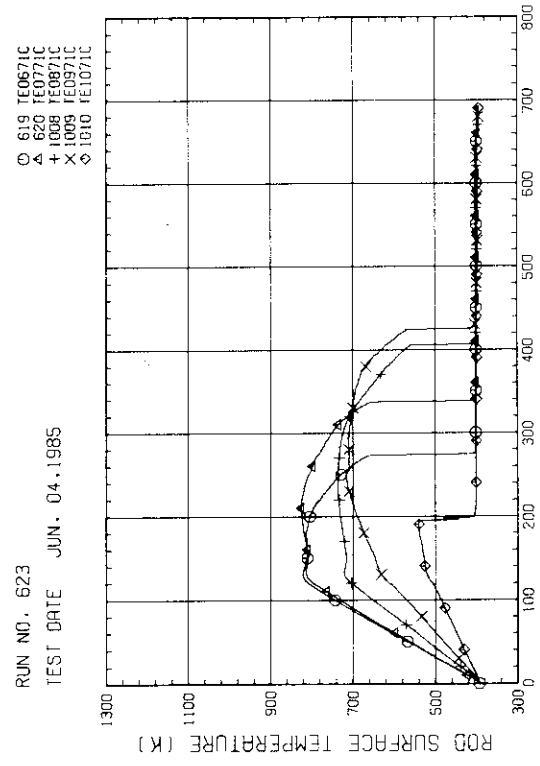

Fig. C-28 HEATER ROD TEMPERATURE (BUNDLE 7-1C, UPPER HALF)

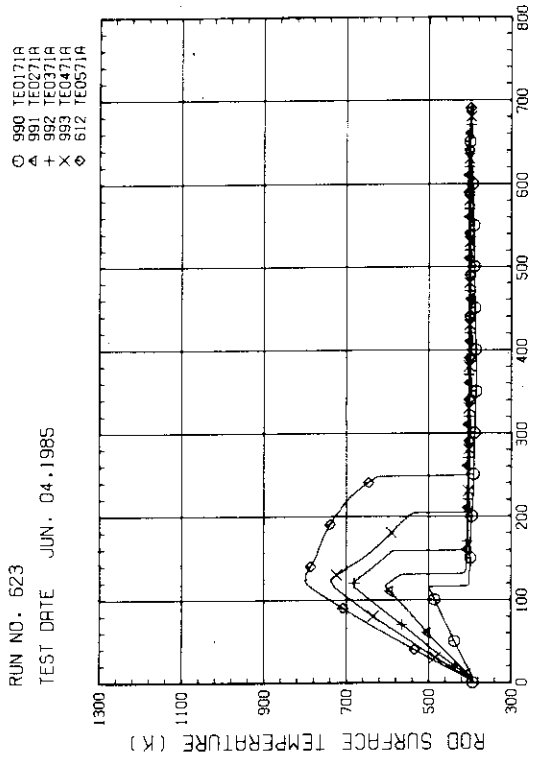

Fig. C-25 HEATER ROD TEMPERATURE (BUNDLE 7-1A, LOWER HALF)

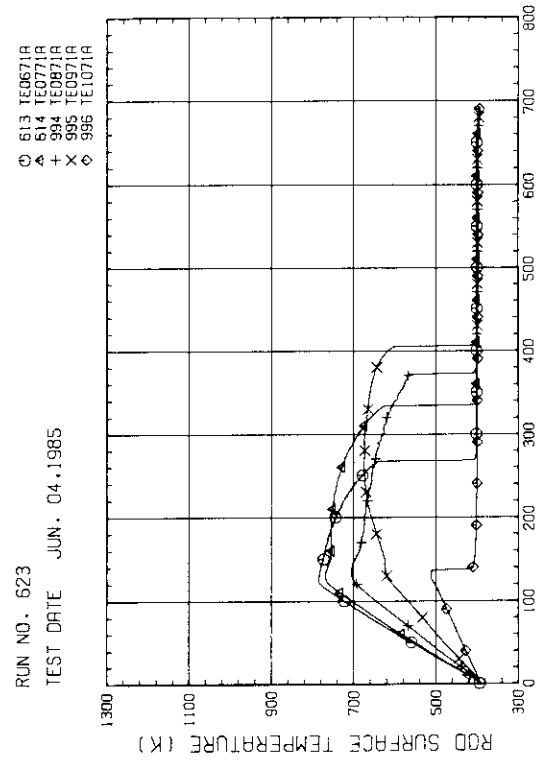

Fig. C-26 HEATER ROD TEMPERATURE (BUNDLE 7-1A, UPPER HALF)

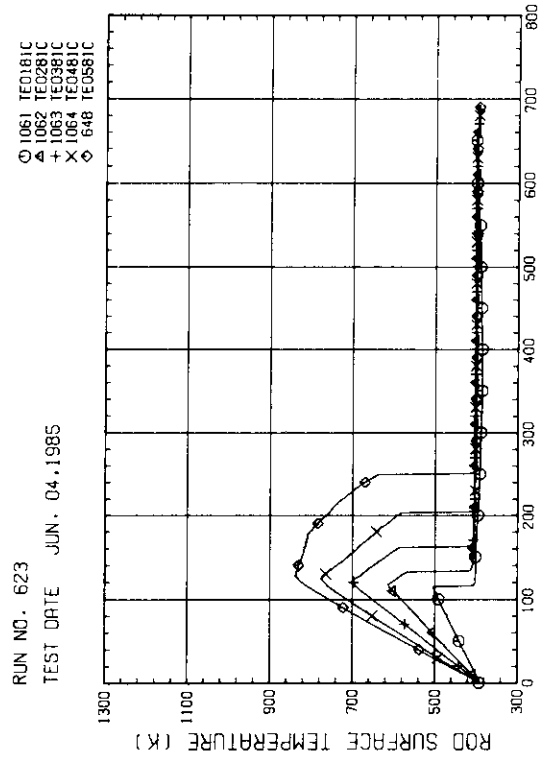

Fig. C-29 HEATER ROD TEMPERATURE (BUNDLE 8-1A, LOWER HALF)

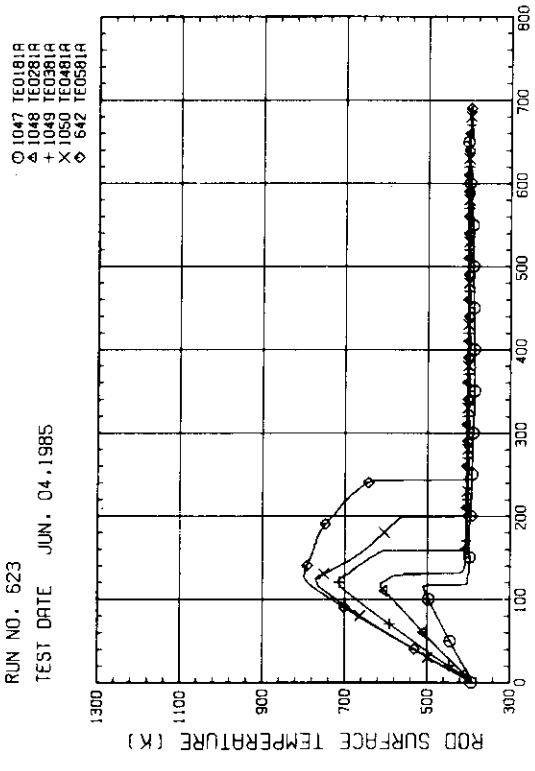

Fig. C-30 HEATER ROD TEMPERATURE (BUNDLE 8-1A, UPPER HALF)

Fig. C-31 HEATER ROD TEMPERATURE (BUNDLE 8-1C, LOWER HALF)

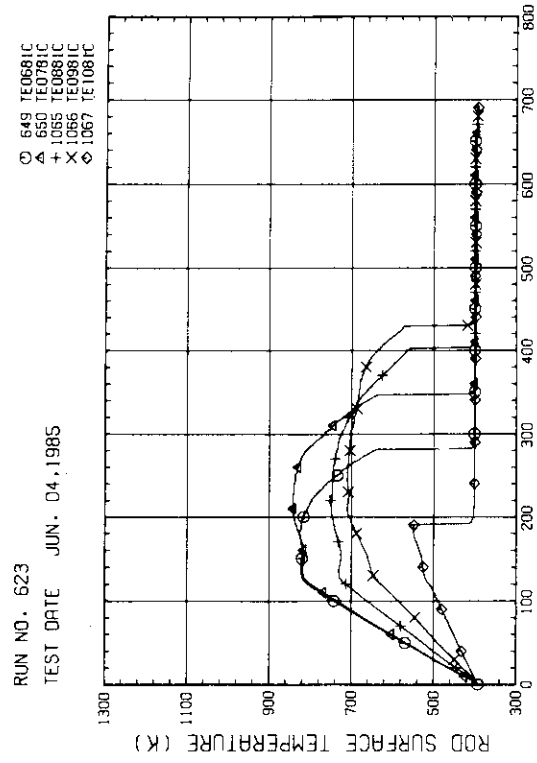

Fig. C-32 HEATER ROD TEMPERATURE (BUNDLE 8-1C, UPPER HALF)

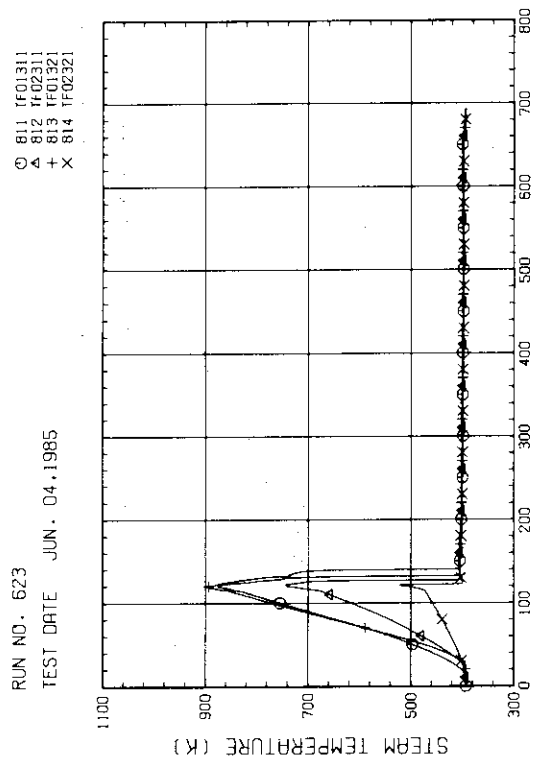

Fig. C-35 STEAM TEMPERATURE IN CORE, BUNDLE 3

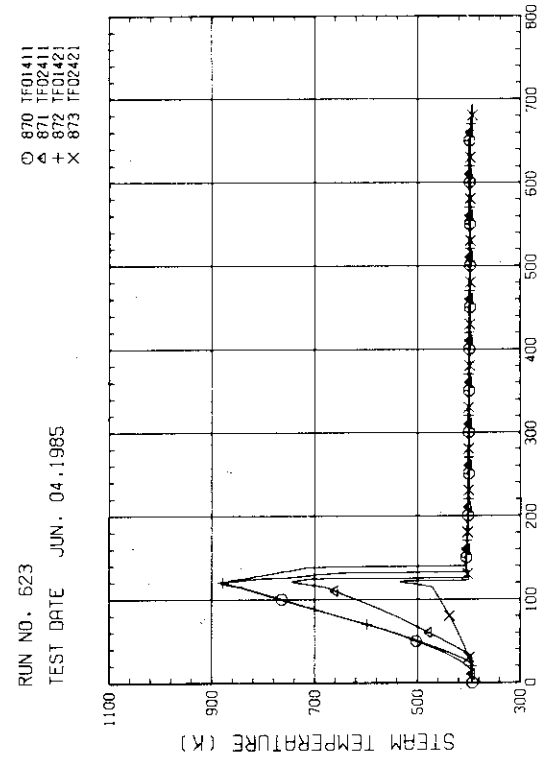

Fig. C-36 STEAM TEMPERATURE IN CORE, BUNDLE 4

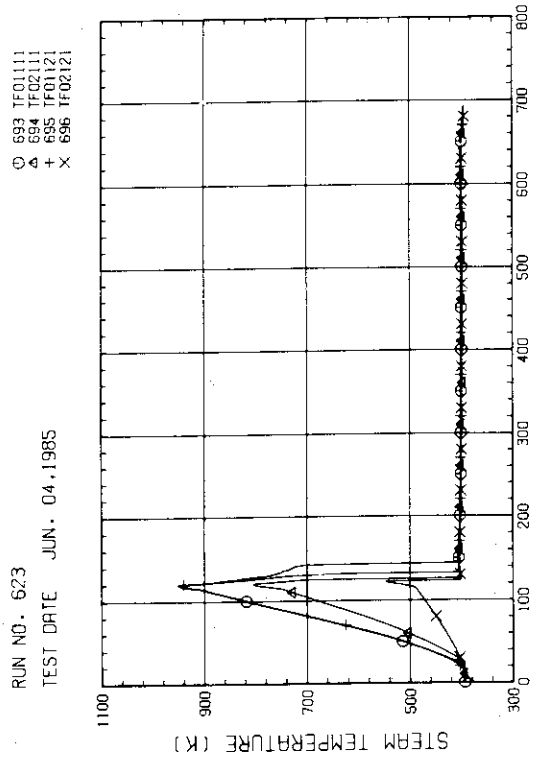

Fig. C-33 STEAM TEMPERATURE IN CORE, BUNDLE 1

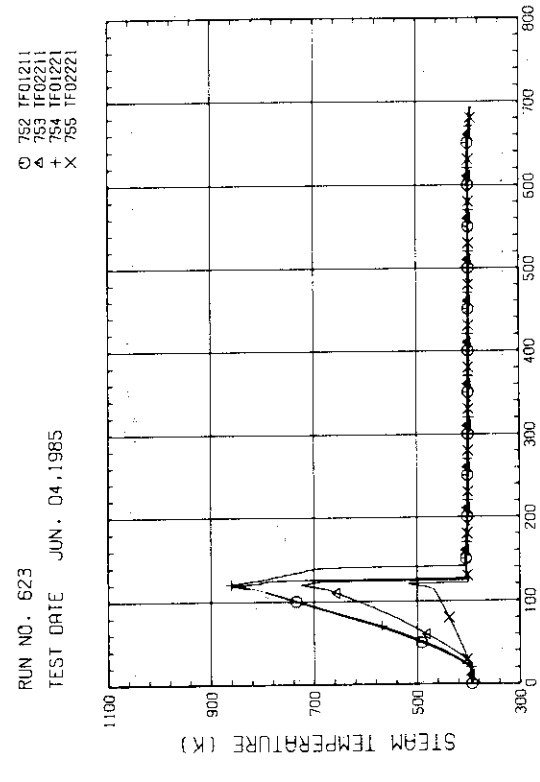

Fig. C-34 STEAM TEMPERATURE IN CORE, BUNDLE 2

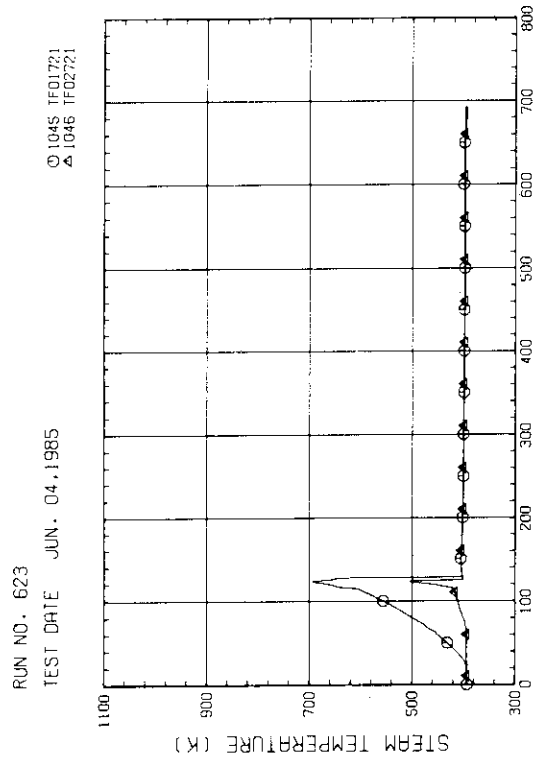

Fig. C-39 STEAM TEMPERATURE IN CORE, BUNDLE 7

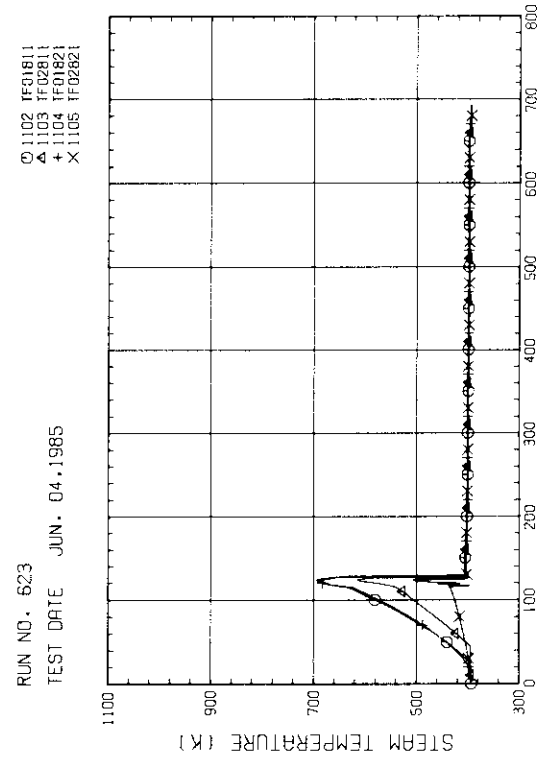

Fig. C-40 STEAM TEMPERATURE IN CORE, BUNDLE 8

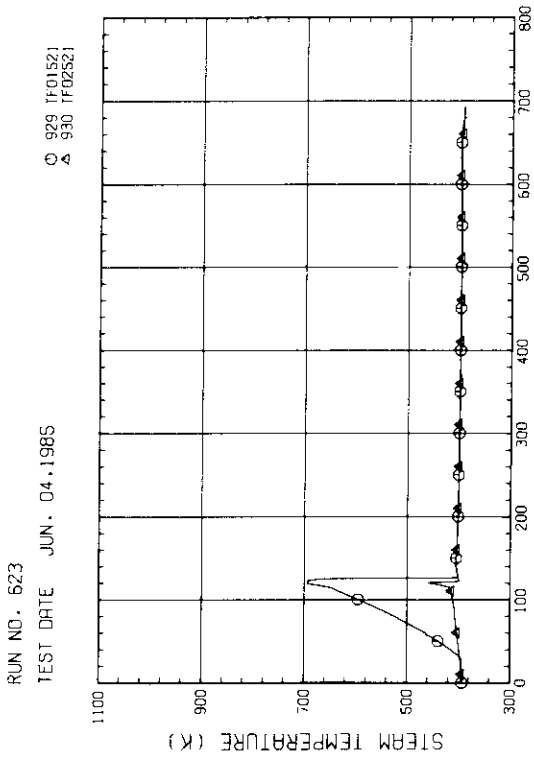

Fig. C-37 STEAM TEMPERATURE IN CORE, BUNDLE 5

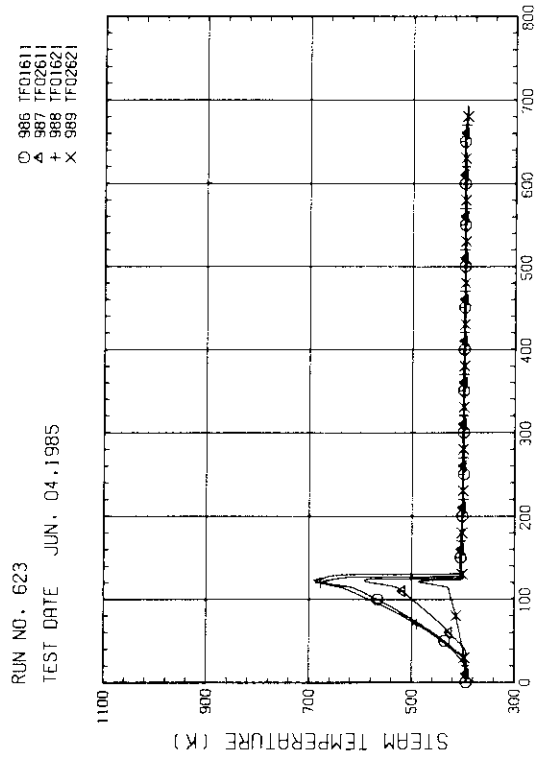

Fig. C-38 STEAM TEMPERATURE IN CORE, BUNDLE 6

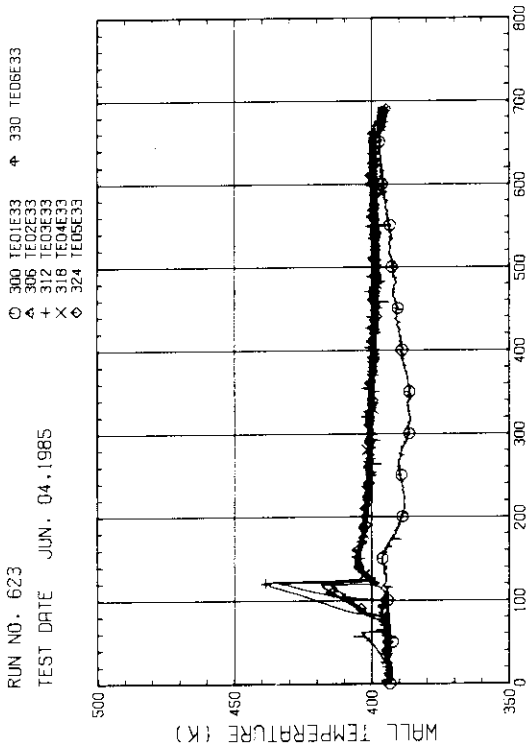

Fig. C-43 SURFACE TEMPERATURE OF CORE SIDE WALL (BUNDLE 3, COLD LEG SIDE, INNER SURFACE)

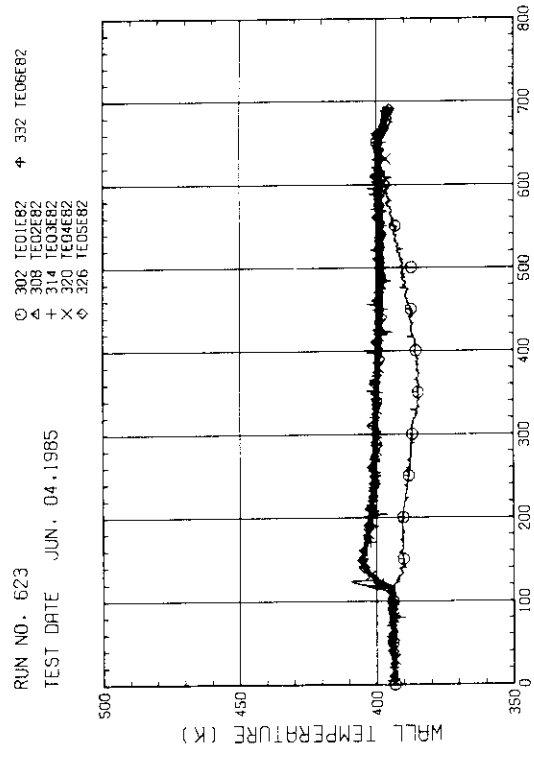

Fig. C-44 SURFACE TEMPERATURE OF CORE SIDE WALL (BUNDLE 8, COLD LEG SIDE, INNER SURFACE)

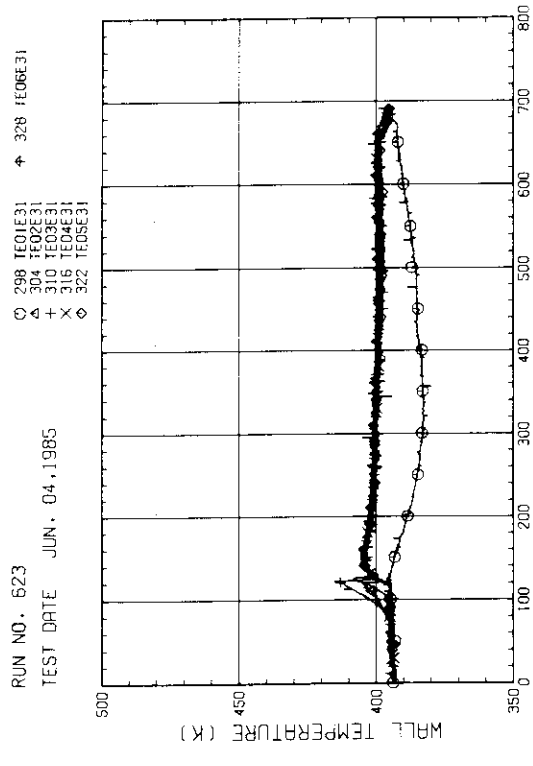

Fig. C-41 TEMPERATURE BETWEEN BARREL AND HONEYCOMB (BUNDLE 3, OPPOSITE SIDE OF COLD LEG)

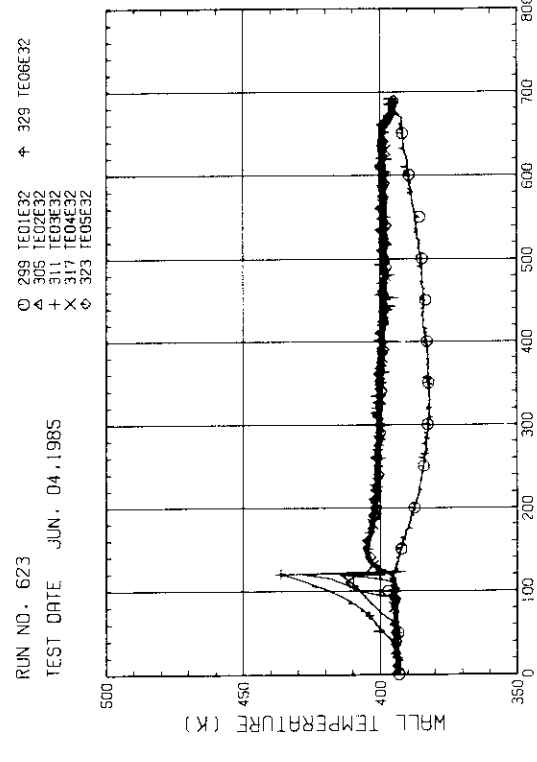

Fig. C-42 SURFACE TEMPERATURE OF CORE SIDE WALL (BUNDLE 3, OPPOSITE SIDE OF COLD LEG, INNER SURFACE)

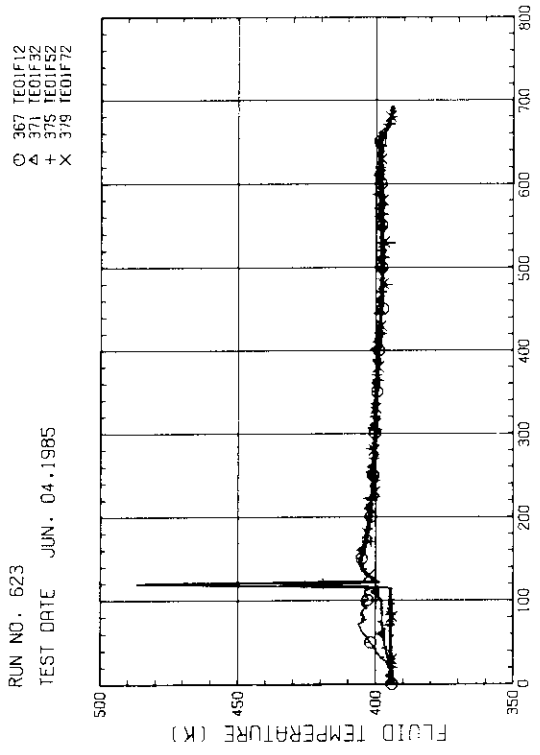

Fig. C-45 FLUID TEMPERATURE JUST BELOW END BOX TIE PLATE (BUNDLE 1,3,5,7, OPPOSITE SIDE OF COLD LEG, OUTER)

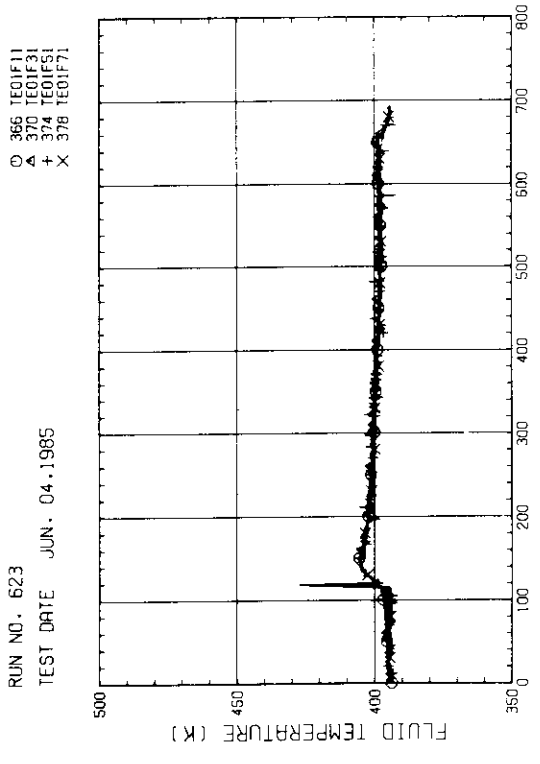

Fig. C-47 FLUID TEMPERATURE JUST BELOW END BOX TIE PLATE (BUNDLE 1,3,5,7, OPPSITE SIDE OF COLD LEG, INNER)

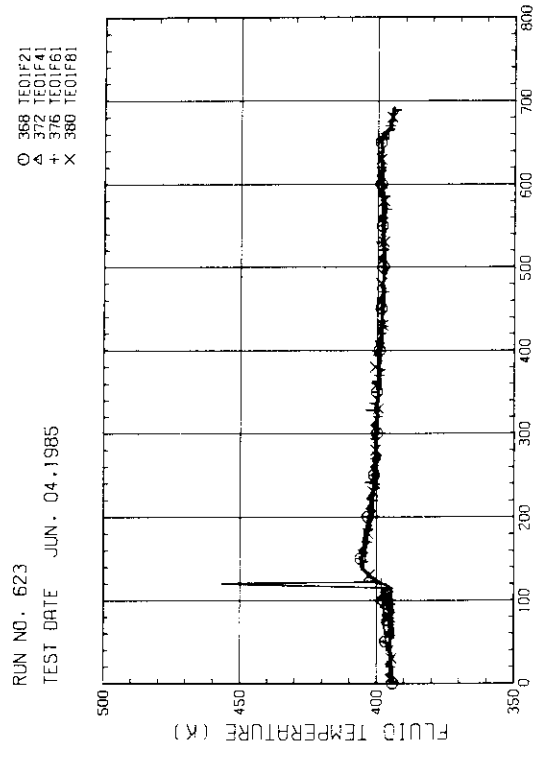

Fig. C-46 FLUID TEMPERATURE JUST BELOW END BOX TIE PLATE (BUNDLE 2,4,6,8, COLD LEG SIDE, INNER)

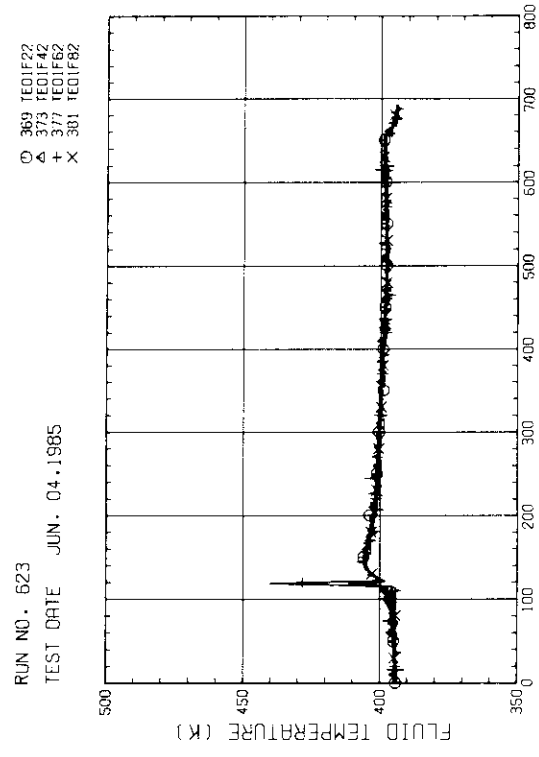

Fig. C-48 FLUID TEMPERATURE JUST BELOW END BOX TIE PLATE (BUNDLE 2,4,6,8, COLD LEG SIDE, OUTER)

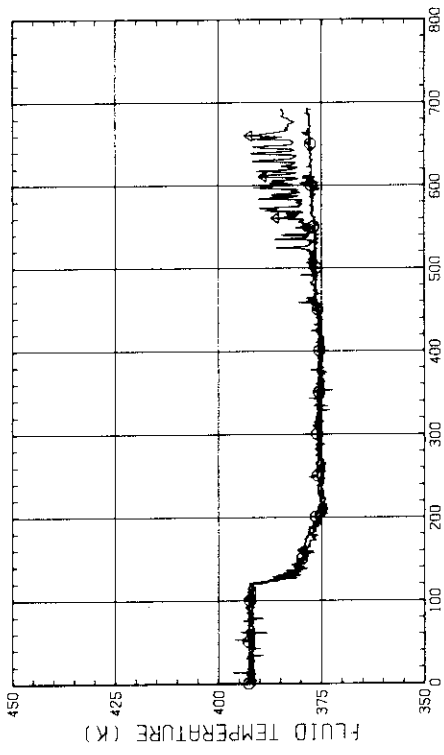

Fig. C-51 FLUID TEMPERATURE AT LOWER PLENUM INLET

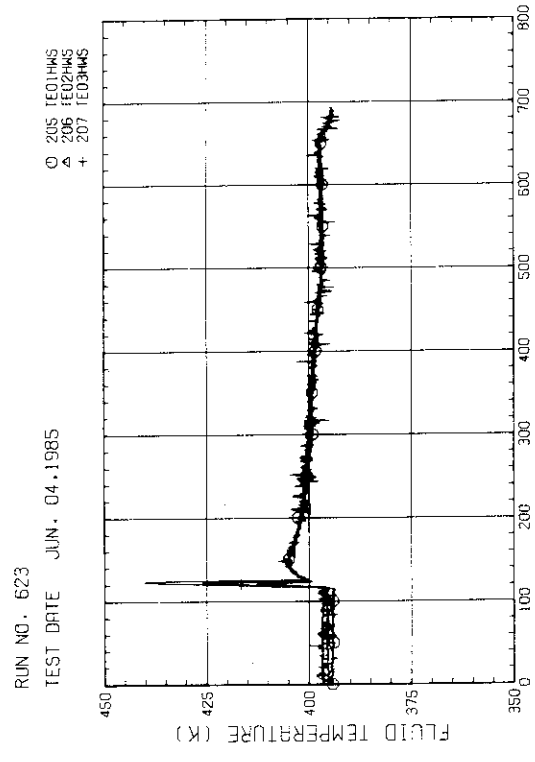

Fig. C-52 FLUID TEMPERATURE IN HOT LEG
(01,02,03 - FROM PV TO STEAM/WATER SEPARATOR)

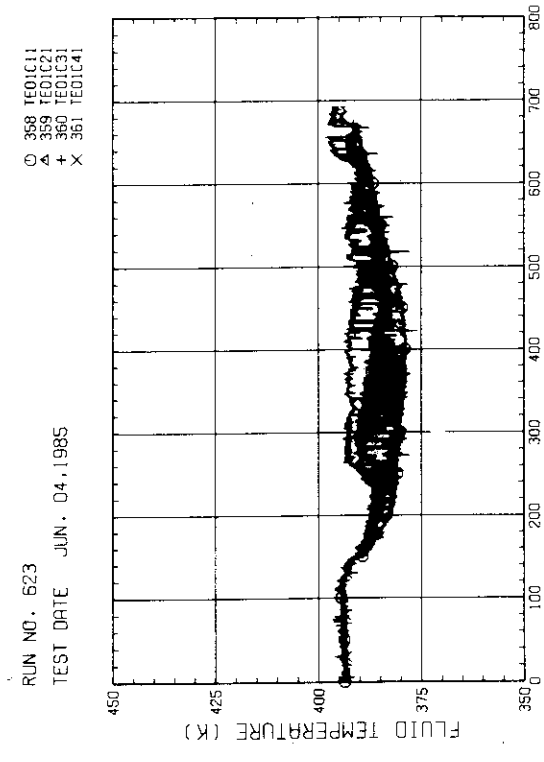

Fig. C-49 FLUID TEMPERATURE AT CORE INLET
(BUNDLE 1.2.3.4. 100MM BELOW HEATED PART)

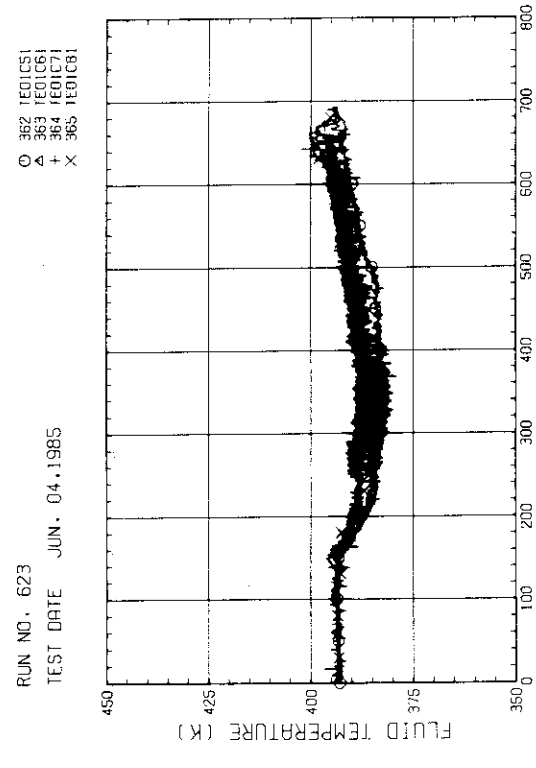

Fig. C-50 FLUID TEMPERATURE AT CORE INLET
(BUNDLE 5.6.7.8. 100MM BELOW HEATED PART)

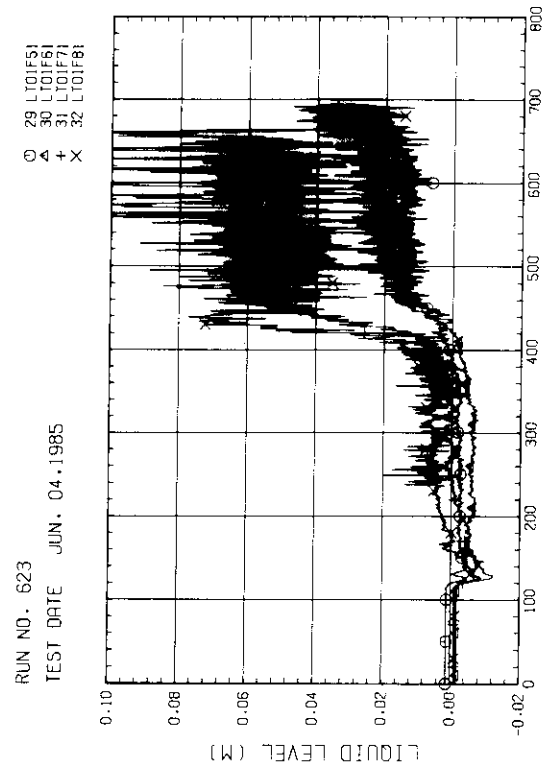

Fig. C-55 LIQUID LEVEL ABOVE END BOX TIE PLATE (BUNDLE 5,6,7,8)

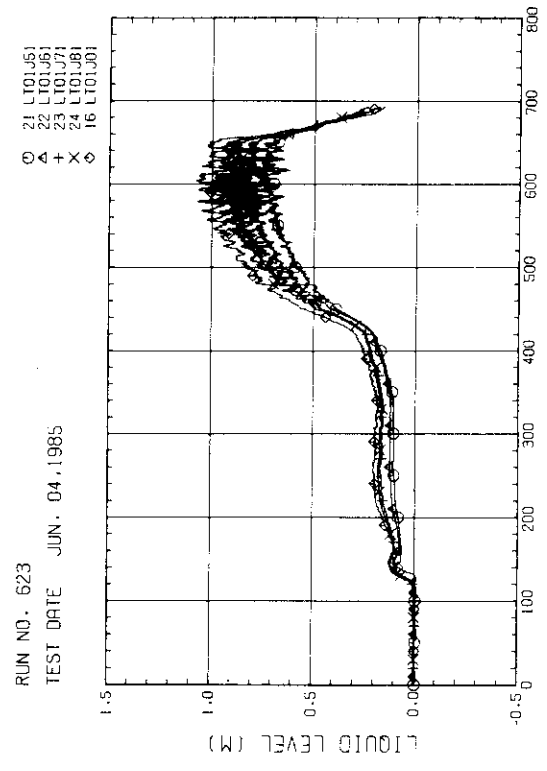

Fig. C-56 LIQUID LEVEL ABOVE UCSP (BUNDLE 5,6,7,8 AND CORE BAFFLE)

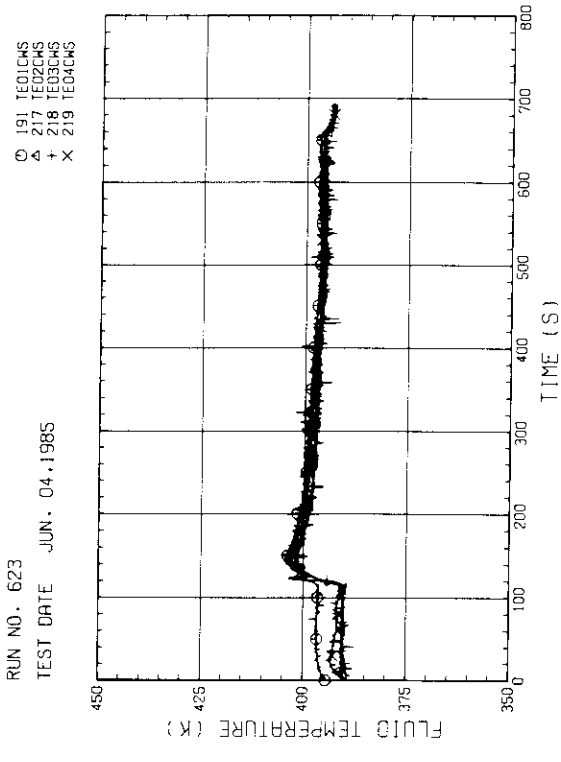

Fig. C-53 FLUID TEMPERATURE IN INTACT COLD LEG (BETWEEN PUMP SIMULATOR AND S/W SEPARATOR)

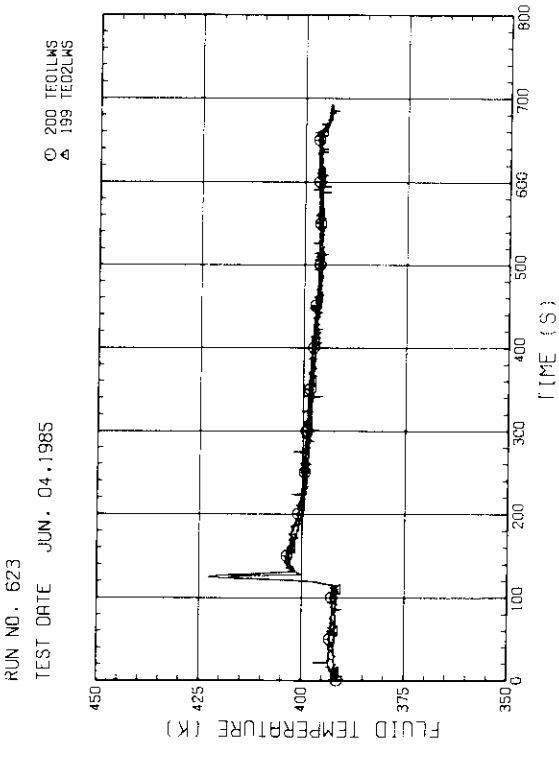

Fig. C-54 FLUID TEMPERATURE IN BROKEN COLD LEG

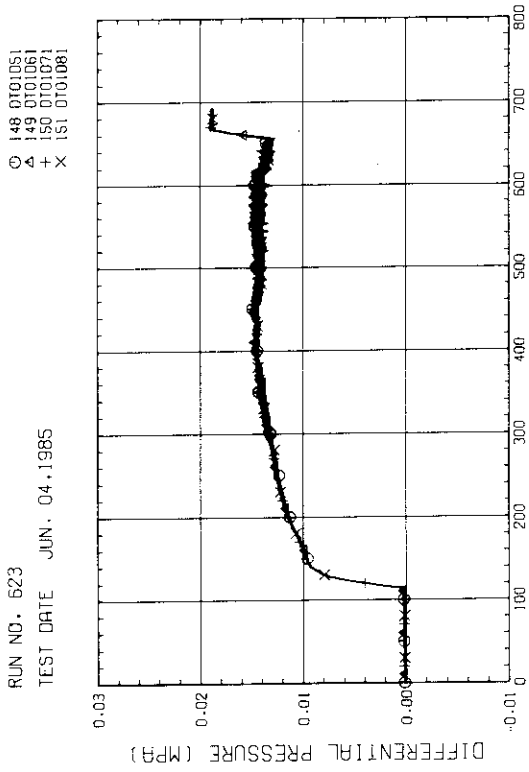

Fig. C-59 DIFFERENTIAL PRESSURE OF CORE LOWER HALF (BUNDLE 5.6.7.8)

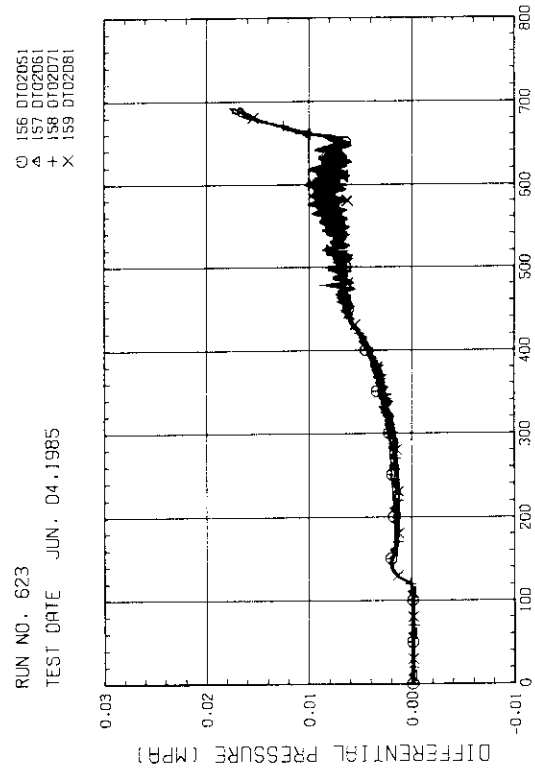

Fig. C-60 DIFFERENTIAL PRESSURE OF CORE UPPER HALF (BUNDLE 5.6.7.8)

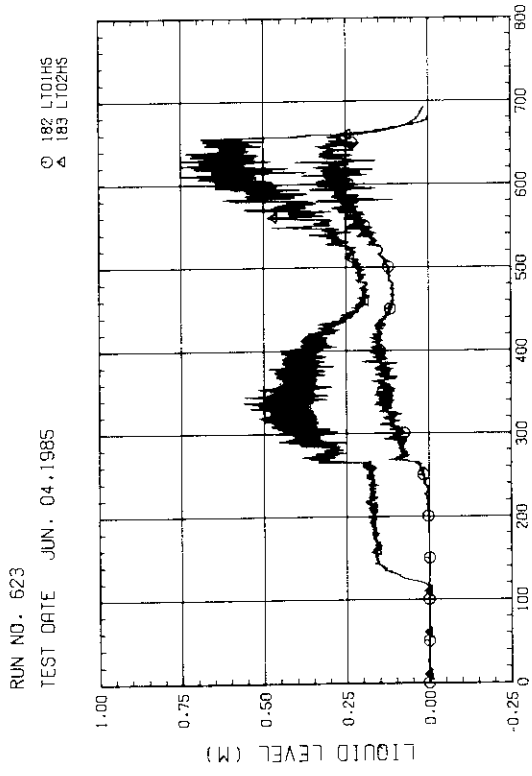

Fig. C-57 LIQUID LEVEL IN HOT LEG (01HS - PV SIDE, 02HS - STEAM/WATER SEPARATOR SIDE)

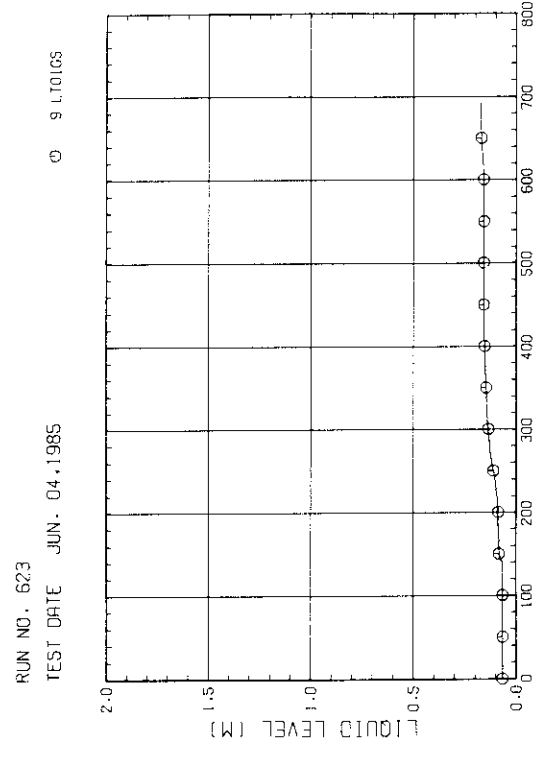

Fig. C-58 LIQUID LEVEL IN STEAM/WATER SEPARATOR

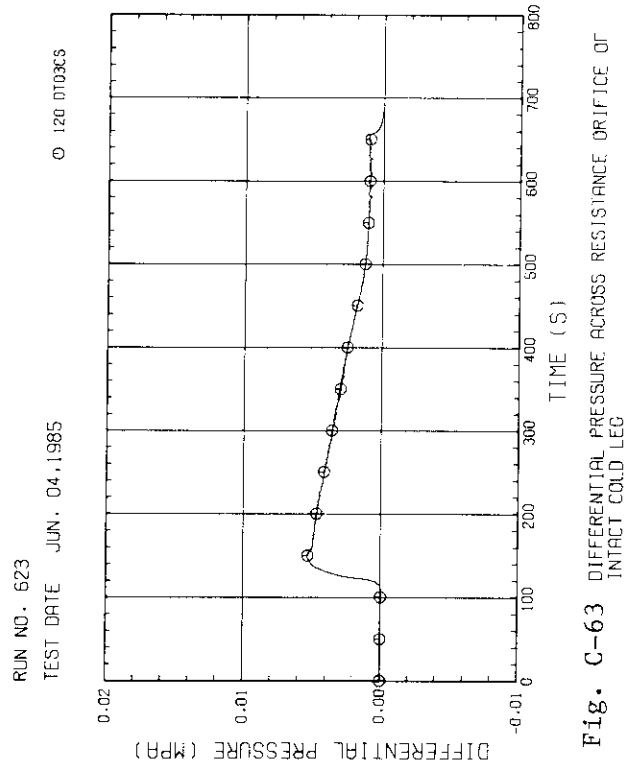

Fig. C-63 DIFFERENTIAL PRESSURE ACROSS RESISTANCE ORIFICE OF INTACT COLD LEG

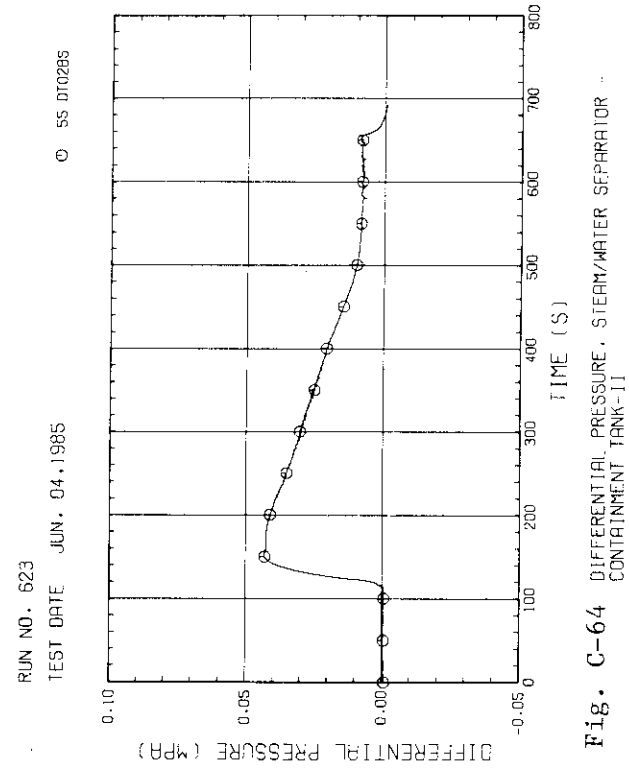

Fig. C-64 DIFFERENTIAL PRESSURE. STEAM/WATER SEPARATOR CONTAINMENT TANK-II

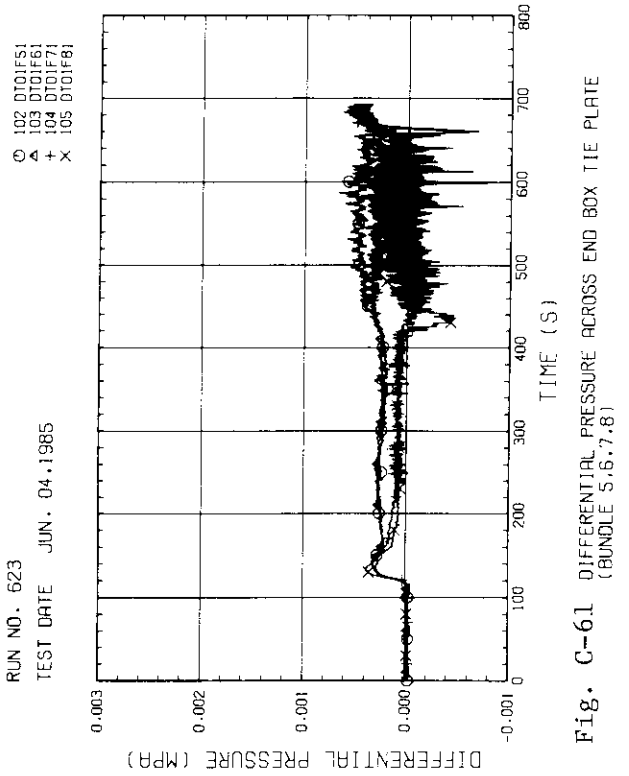

Fig. C-61 DIFFERENTIAL PRESSURE ACROSS END BOX TIE PLATE (BUNDLE 5,6,7,8)

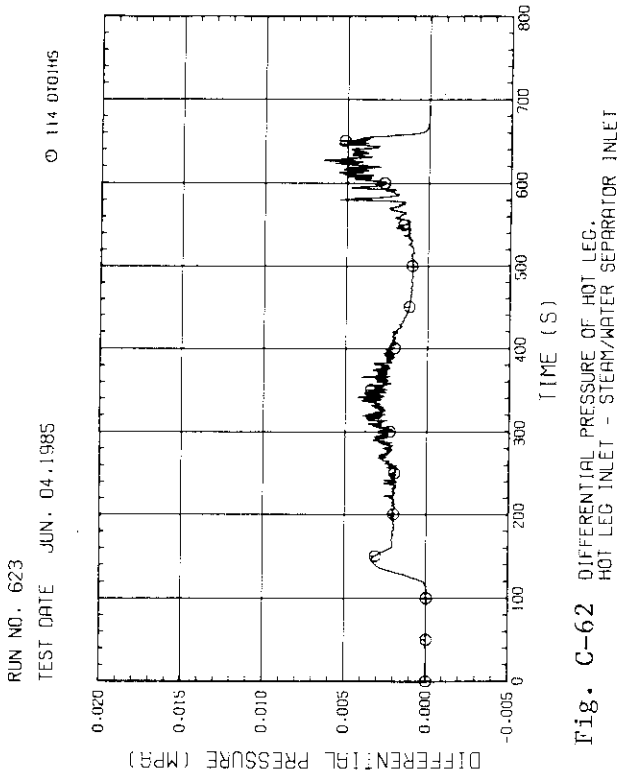

Fig. C-62 DIFFERENTIAL PRESSURE OF HOT LEG. HOT LEG INLET - STEAM/WATER SEPARATOR INLET

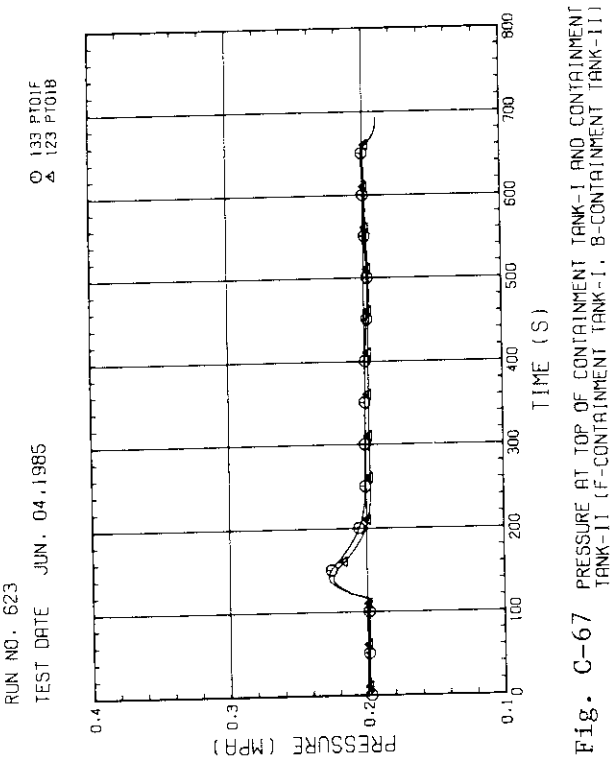

Fig. C-67 PRESSURE AT TOP OF CONTAINMENT TANK-I AND CONTAINMENT TANK-II (F-CONTAINMENT TANK-I, B-CONTAINMENT TANK-II)

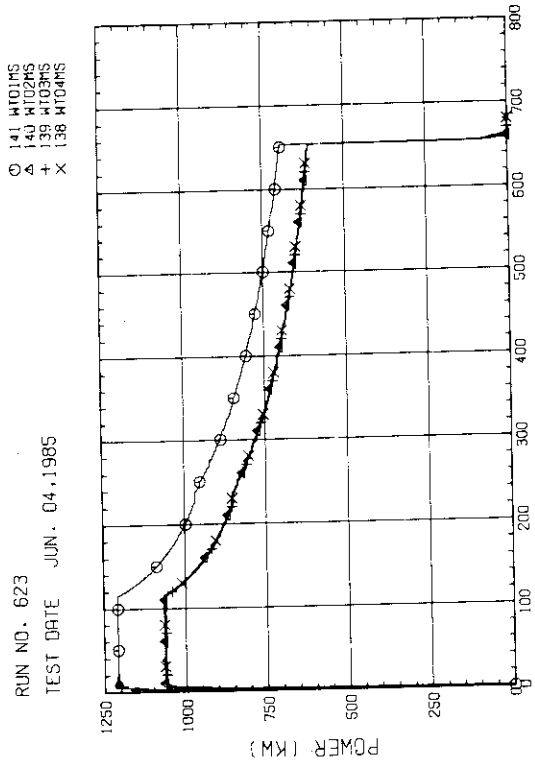

Fig. C-68 BUNDLE POWER (BUNDLE 1,2,3,4)

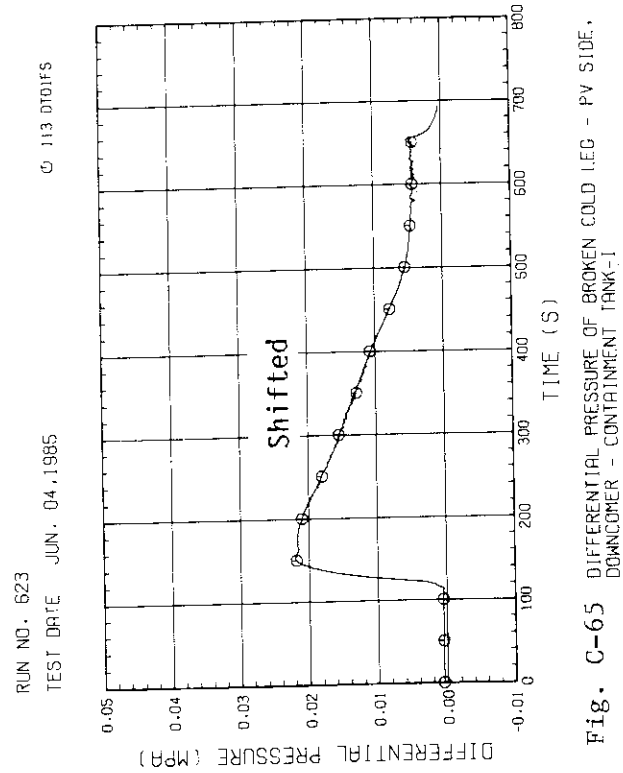

Fig. C-65 DIFFERENTIAL PRESSURE OF BROKEN COLD LEG - PV SIDE, DOWNCOMER - CONTAINMENT TANK-I

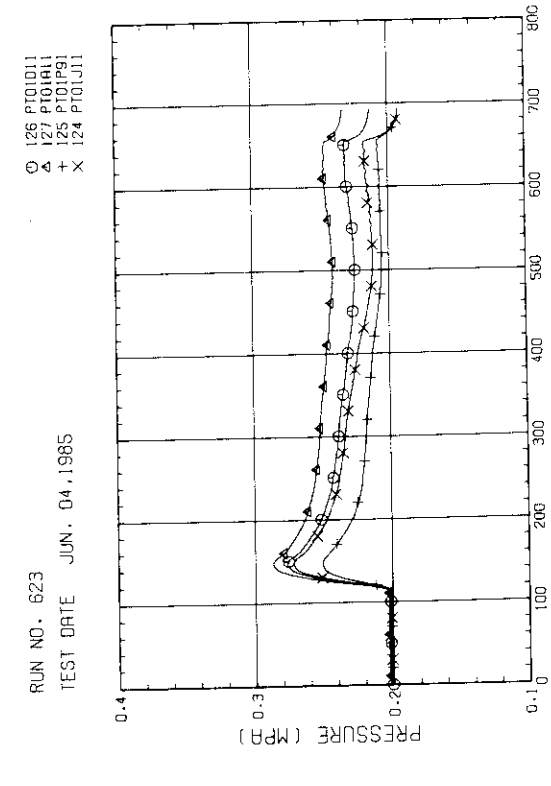

Fig. C-66 PRESSURE IN PV (J - TOP OF PV, D - CORE CENTER, A - CORE INLET, P - BELOW COLD LEG NOZZLE IN DOWNCOMER)

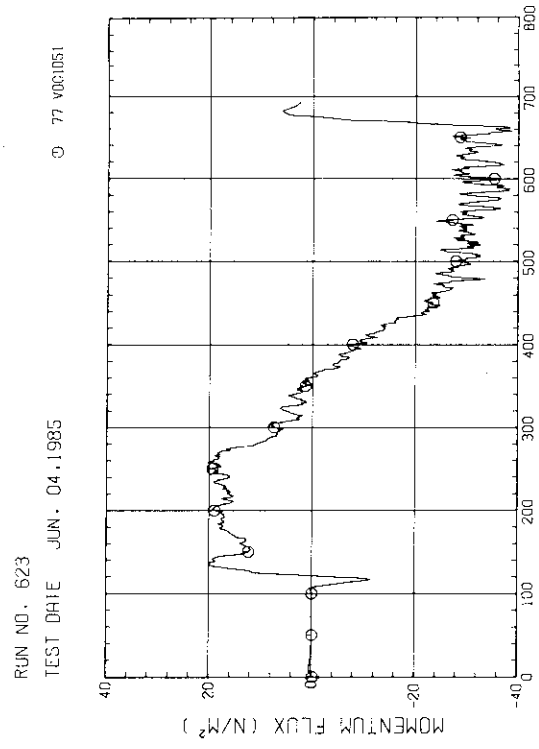

Fig. C-71 HORIZONTAL FLOW MOMENTUM FLUX DETECTED WITH DRAG DISK BETWEEN 5 AND 6 - ELEVATION 1.905M

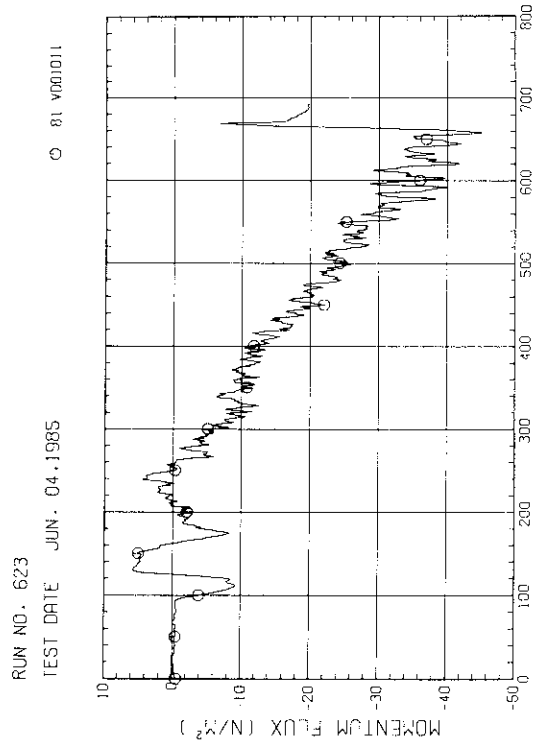

Fig. C-72 HORIZONTAL FLOW MOMENTUM FLUX DETECTED WITH DRAG DISK BETWEEN 1 AND 2 - ELEVATION 1.905M

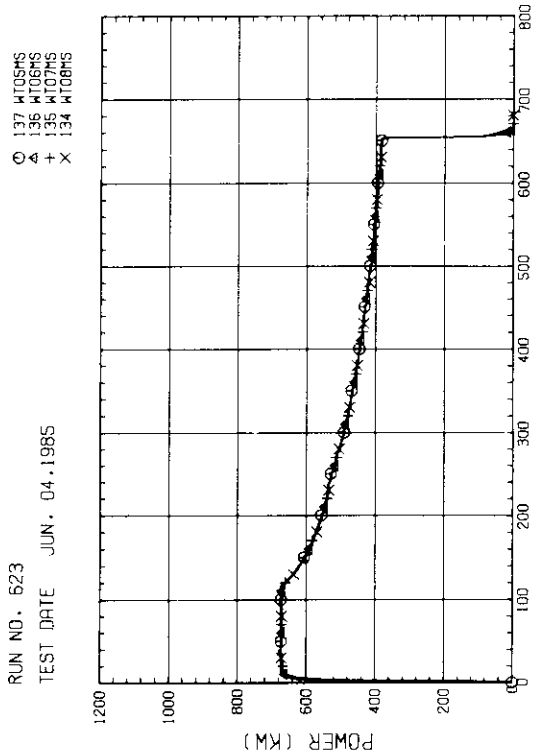

Fig. C-69 BUNDLE POWER (BUNDLE 5.6.7.8)

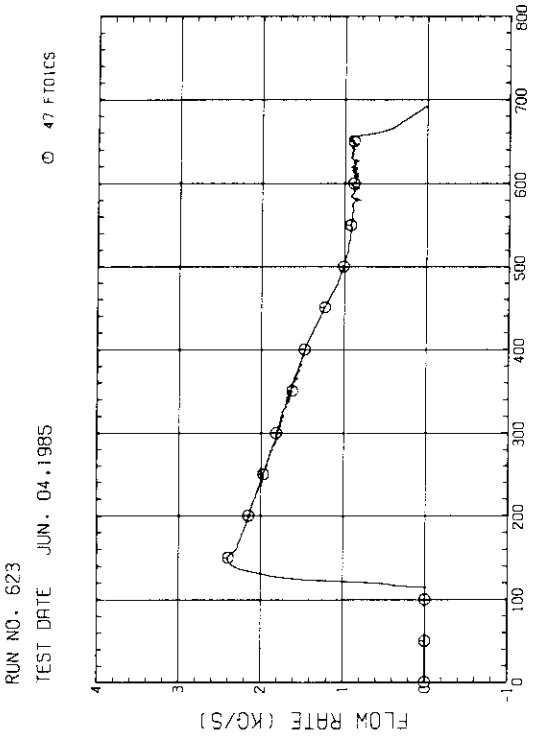

Fig. C-70 MASS FLOW RATE OF INTACT COLD LEG